Analysis of Artificial Chromosomes in Human Embryonic Stem Cells

A Thesis Submitted in Partial Fulfilment of the Requirements for the Degree of Doctor of Philosophy
Hilary Term 2011

Mohammad Ali Mandegar
Linacre College
Nuffield Department of Clinical Medicine
University of Oxford

Supervisor: Dr Zoia Larin Monaco
Wellcome Trust Centre for Human Genetics
Roosevelt Drive
Oxford
OX3 7BN

تقدیم به طلیعه ارباب و محمد حسین ماندگار

Declaration

Unless otherwise stated, the author conducted the work presented in this thesis. No part of this thesis has been submitted for another degree at this or any other university.

Acknowledgements

I thank Dr Zoia Larin Monaco for her support and supervision during my DPhil studies. I sincerely thank Dr Daniela Moralli who assisted me with almost every aspect of this thesis: from experimental design, data analysis and interpretation to editing this manuscript. My special thanks go to Professor William James and especially Dr Sally Cowley for their collaborative interest, technical guidance and constructive discussions in the human embryonic stem cell work. Drs Emanuela Volpi and Mohammed Yusuf collaborated in the analysis and karyotyping of the HUES-2 cell line at the cytogenetics core group at the Wellcome Trust Centre for Human Genetics, University of Oxford. Professor Adrian Thrasher, and Drs Sayandip Mukherjee and Michael Blundell performed the teratoma formation assay and analysis at the Institute of Child Health, University College London. I am grateful to other members of the Larin Monaco group: Dr David Chan and Suhail Khoja for their technical assistance with the hESc work and constructive discussions throughout the course of my DPhil studies. I would like to thank Azal Ahmadi for her helpful comments on the thesis. Improvements were made to the thesis based on helpful suggestions made by Drs Stephen Hyde and Joanna Bridger. Cathy Browne provided technical assistance in providing our lab with stem cell cultures and necessary reagents. Drs Richard Wade-Martins, Sara Ahmadi and Elizabeth Hartfield assisted in the RED/ET recombination reaction, neuronal differentiation and allowed access to sonicator for HSV-1 amplicon preparation. Professor William Earnshaw, Dr Ben Davies and Dr Alistair Pagnamenta provided our laboratory with anti-CENP C antibody, *Neo*^{R} MEFi and primers for Exon 18 of gene CNTNAP5, respectively. Linacre College provided me with the EPA Cephalosporin award in 2008-2009 and the Natural Sciences and Engineering Council of Canada (NSERC) granted me the NSERC Post Graduate Doctoral Studentship in 2010-2011.

Abstract

The development of safe and efficient gene delivery systems in pluripotent human embryonic stem cells (hESc) is essential to realising their full potential for basic and clinical research. The purpose of this study was to develop an efficient, non-integrating gene expression system in pluripotent hESc using human artificial chromosomes (HAC). Similar to endogenous chromosomes, HAC are capable of gene expression, replication and segregation during cell division. Unlike retroviral-mediated gene delivery vectors, HAC do not integrate into the host genome and can encompass large genomic regions for the delivery of multiple genes. Despite the advantages HAC offer, their use has been limited due to laborious cloning procedures and poor transfection efficiencies, and thus only studied in immortalised and tumour-derived human cell lines. In this study, the high transduction efficiency of herpes simplex virus type-1 (HSV-1) amplicons was utilised to overcome the described difficulties and delivered HAC vectors into pluripotent hESc. Analysis of stable hESc clones showed that *de novo* gene-expressing HAC were present at high frequencies ranging from 10-70% of metaphases analysed, without integrating into the genome. The established HAC contained an active centromere, and were stably maintained without integration or loss in the absence of selection for 90 days. Stable HAC-containing hESc clones retained their pluripotency as demonstrated by neuronal differentiation, *in vitro* germ layer and teratoma formation assays. HAC gene expression persisted, with some variation, post-differentiation in the various deriving cell types. This is the first report of successful *de novo* HAC formation in hESc for gene expression studies. These findings show potential for delivering high-capacity genomic constructs safely and efficiently into pluripotent cells for the purpose of genetic manipulation and ultimately patient-specific somatic gene therapy.

Table of Contents

List of Tables

List of Figures

Abbreviations

α	Alphoid/alpha DNA
AAV	Adeno Associated Virus
Amp^R	Ampicillin Resistance
ANOVA	Analysis of Variance
APC	Anaphase Promoting Complex
β-APP	β-Amyloid Precursor Protein
BAC	Bacterial Artificial Chromosome
bFGF	basic Fibroblast Growth Factor
BHS	Buffered Hypotonic Solution
BMP	Bone Morphogenetic Protein
bp	base pairs
ºC	degrees Centigrade
CCD	Charge-Coupled Device
Cdc20	Cell-division cycle protein 20
cDNA	complementary DNA
CENP	Centromere Protein
CFTR	Cystic Fibrosis Transmembrane Conductance Regulator
CHEF1α	Chinese Hamster Elongation Factor-1 α
CHO	Chinese Hamster Ovary
cHS4	chicken Hypersensitive Site-4
CMV	Cytomegalovirus
CpG	Cytosine-phosphatidy1l-Guanosine
C_T	Threshold Cycle
DABCO	1,4-Diazabicyclo(2,2,2)octane
DAPI	4,6-Diamidino-2-Phenylindole
DMD	Duchenne Muscular Dystrophy
DMEM	Dulbecco's Modified Eagle's Medium
DNA	Deoxyribonucleic Acid
DNMTs	DNA Methyltransferases
dNTPs	Deoxynucleotide Triphosphates
dUTP	2'-Deoxyuridine 5'-Triphosphate
E. coli	*Escherichia coli*
EB	Embryoid Body
EBNA-1	Epstein Barr Nuclear Antigen-1
EBV	Epstein Barr Virus
EC	Embryonal Carcinoma
EGFP	Enhanced Green Fluorescent Protein
FACS	Fluorescence-Activated Cell Sorting
FBS	Foetal Bovine Serum
FCS	Foetal Calf Serum
FISH	Fluorescence *in situ* Hybridisation
FITC	Fluorescein Isothiocyanate
FMR1	Human Fragile X Mental Retardation
GAPDH	Glyceraldehyde-3-Phosphate Dehydrogenase
GCH1	Guanosine Triphosphate Cyclohydrolase I
GFP	Green Fluorescent Protein
GMP	Good Manufacturing Practice
hAAT	human α1 anti-trypsin
HAC	Human Artificial Chromosomes

HDACs	Histone Deacetylase Enzymes
hEF1α	human Elongation Factor 1 α
HEPES	4-(2-hydroxyethyl)-1-piperazineethanesulfonic acid
hESc	human Embryonic Stem cells
HLA	Human Leukocyte Antigen
HPRT	Hypoxanthine Phosphoribosyltransferase
HSC	Hematopoietic Stem Cells
HSV-1	Herpes Simplex Virus Type 1
ICM	Inner Cell Mass
IFN	Interferons
INCENP	Inner Centromere Protein
iPSc	induced Pluripotent Stem cells
kb	kilo bases
LB	Luria–Bertani Broth
LMO2	LIM domain only 2
LTR	Long Terminal Repeat
µg	micrograms
µl	microlitres
µM	micromolar
M	Molar
M-FISH	Multicolour FISH
MAR	Matrix Attachment Regions
Mb	Mega base
MBD	Methylcytosine-Binding Domain
MEF	Mouse Embryonic Fibroblasts
mESc	mouse Embryonic Stem cells
mg	milligrams
ml	millilitres
mM	millimolar
MMCT	Microcell Mediated Chromosome Transfer
MOI	Multiplicity of Infection
mRNA	messenger RNA
MSC	Mesenchymal Stem Cells
NDM	Neuronal Differentiation Media
Neo^R	Neomycin Resistance
ng	nanograms
NIH	National Institutes of Health
nm	nanometres
nM	nanomolar
NSC	Neuronal Stem Cells
OHS	Optimal Hypotonic Solution
ORC	Origin of Recognition Complex
PAC	P1 Artificial Chromosome
PBS	Phosphate Buffered Saline
PCR	Polymerase Chain Reaction
PEI	Polyethylenimine
PFGE	Pulsed Field Gel Electrophoresis
PGK	Phosphoglycerate Kinase
R26	ROSA26
RNA	Ribonucleic Acid

ROCK	Rho-associated Coiled-coil Kinase
RSV	Rous Sarcoma Virus
SAR	Scaffold Attachment Regions
SCID	Severe Combined Immunodeficiency
SCNT	Somatic Cell Nuclear Transfer
SOB	Super Optimal Broth
SOC	Super Optimal Broth with Catabolite repression
SSC	Saline-Sodium Citrate
SSEA	Stage-Specific Embryonic Antigen
SV40	Simian Vacuolating virus 40
TAE	Tris-Acetate-EDTA
TBE	Tris-Borate-EDTA
TLR	Toll-Like Receptor
TNF	Tumour Necrosis Factor
TRITC	Tetramethyl Rhodamine Isothiocyanate
UbC	Ubiquitin C
YAC	Yeast Artificial Chromosome

Chapter 1. Introduction

1.1 Human Embryonic Stem Cells

Human embryonic stem cells (hESc) are pluripotent cells defined by their ability for indefinite self-renewal in the undifferentiated state, and potential to differentiate into the three embryonic germ layers. Due to their high replicative lifespan and differentiation capacity, hESc can be used for studying human developmental biology and hold potential for use in tissue regeneration, transplant therapies and drug discovery (Thomson et al. 1998; Reubinoff et al. 2000; Cowan et al. 2004). Thus, they are believed to hold great potential for use in basic and clinical research.

1.1.1 Derivation of Human Embryonic Stem Cells

After fertilisation of the secondary oocyte by the sperm, the zygote is formed. A day later, the impregnated oocyte initiates the first cleavage division. The cleavage divisions continue for four days until the formation of the morula (composed of ~30-40 cells named blastomeres). Up to this point, the blastomeres are still encapsulated inside the zona pellucida (the glycoprotein membrane that surrounds the plasma membrane of the oocyte). Four days after fertilisation, the outermost blastomeres of the morula join together and flatten to form the trophoblast layer of the blastocyst. The blastocyst is an early embryonic structure composed of ~100-150 cells, which forms after the morula stage during embryogenesis. Two to four of the innermost blastomeres within the morula form the inner cell mass (ICM) and a cavity (known as the blastocoele) emerges within the blastocyst. The inner cell mass is pluripotent

(capable of forming the three embryonic germ layers) and consequently forms the embryo, while the trophoblast forms the extra embryonic tissues such as the placenta. After the fifth day post-fertilisation, the blastocyst "hatches" from the zona pellucida, and is later implanted in the uterus wall (Vaillancourt and Lafond 2009).

Human embryonic stem cells are derived from the early, preimplantation embryo (reviewed in Strulovici et al. 2007); they were initially isolated from the pluripotent inner cell mass of embryos at the blastocyst stage (Thomson et al. 1998). The isolation of the inner cell mass from the blastocyst is performed through a process known as immuno-surgery, where acid Tyrode's solution is used to remove the zona pellucida. Subsequently, a primary antibody is used to bind to the trophectoderm, followed by a secondary complement serum that dissolves this layer, leaving the inner cell mass intact (Cowan et al. 2004; Chen et al. 2007). Recent studies have reported derivation of hESc from late morula (Strelchenko et al. 2004), arrested embryos (Zhang et al. 2006) and single blastomeres from 4 and 8-cell staged embryos (Klimanskaya et al. 2006; Geens et al. 2009). More recent methods use a combination of immuno-surgery in conjunction with mechanical dissection and isolation of the desired cells using glass pipettes (Chen et al. 2007).

Figure 1-1 shows a schematic diagram of the origin of human embryonic stem cells, their derivation and differentiation potential. As isolation of the ICM leads to the inevitable destruction of the human embryo, use of hESc for basic and clinical research has raised ethical concerns (Fischbach and Fischbach 2004; Jain 2005; Magnus and Cho 2005). To date, many of these ethical considerations have led to limitations in the field of hESc biology (Strulovici et al. 2007).

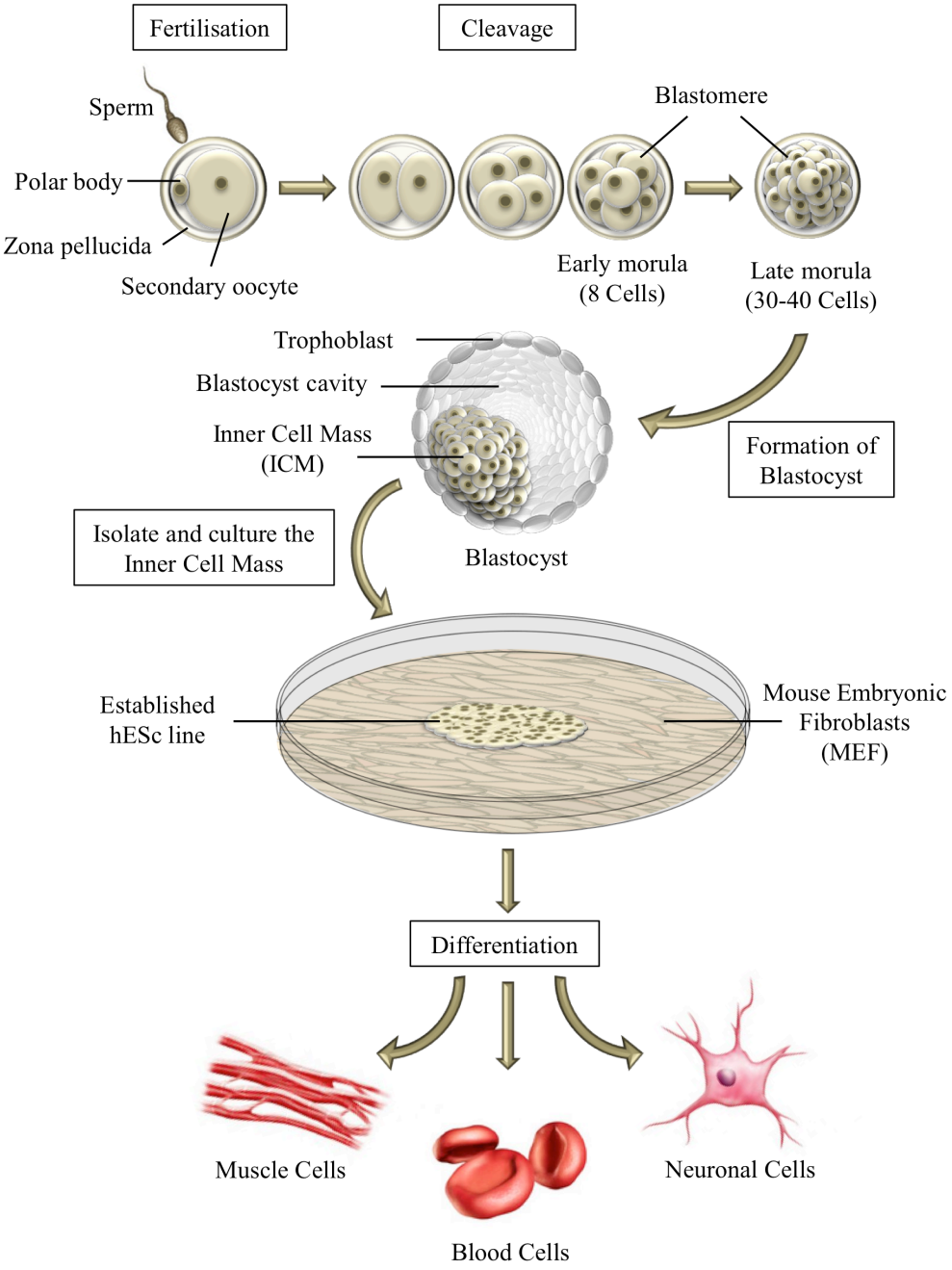

Figure 1-1 Schematic representation of the origin of human embryonic stem cells and their differentiation potential

The zygote is formed after fertilisation of the secondary oocyte by the sperm. The impregnated oocyte then undergoes cleavage divisions until the morula is formed. At the morula stage, the outermost blastomeres join up and flatten to shape the trophoblast layer of the blastocyst, while the innermost blastomeres form the inner cell mass. Human embryonic stem cells are most commonly isolated from the inner cell mass of the blastocyst. After *in vitro* establishment, hESc are capable of indefinite self-renewal and differentiation into all human cell types except for extra embryonic tissue (Strulovici et al. 2007).

1.1.2 Characteristics of Human Embryonic Stem Cells

Human embryonic stem cells grow in tightly packed colonies, have a high nuclear to cytoplasmic ratio, and while remaining undifferentiated, are theoretically capable of indefinite self-renewal. Furthermore, hESc differentiate into all human cell types except for extra embryonic tissue (Thomson et al. 1998; Reubinoff et al. 2000; Cowan et al. 2004). Other stem cell types such as hematopoietic stem cells are multipotent, only capable of forming a subset of cell lines such as blood cells (Muller-Sieburg et al. 2002). Unipotent stem cells, such as epithelial stem cells are capable of forming only one differentiated cell type (Slack 2000).

Human embryonic stem cells express high levels of telomerase, while most non-tumourigenic, non-ES cells do not exhibit this property. Similar to embryonal carcinoma cells (derived from teratocarcinoma; germ cell tumour) (Andrews et al. 2005), high levels of telomerase expression is one proposed method by which hESc may continue unlimited cell proliferation (Thomson et al. 1998). Transcription factors such as Oct4, Sox2 and Nanog are well-known proteins involved in the autoregulation of hESc pluripotency (Strulovici et al. 2007; Yu et al. 2007). The autoregulation of pluripotency in hESc takes place through a transcriptional regulatory circuitry, where Oct4, Sox2 and Nanog are known to co-occupy promoters and regulatory regions of a large population of genes involved in differentiation and developmental pathways. Autoregulation of hESc pluripotency is achieved through keeping an open chromatin state and positive regulation of genes involved in pluripotency (e.g. *Rex1*, *Dppa4*, *Tdgf1*, *Oct4*, *Nanog*, and *Lefty2*), and repression of genes involved in developmental

pathways (e.g. *Dlx5*, *HoxB1*, *Lhx5*, *Titf1* and *Lbx1*) (Boyer et al. 2005; Sims and Reinberg 2009).

Due to their pluripotent nature, hESc are capable of recapitulating embryogenesis *in vitro* by forming cell aggregates known as embryoid bodies (EBs). The formation and development of EBs, through forced cell aggregation of hESc, mimics rudimentary embryonic development of the inner cell mass of an embryo at the blastocyst stage (Itskovitz-Eldor et al. 2000). Cell surface marker antigens such as stage-specific embryonic antigen (SSEA)-3, SSEA-4, Tra-1-60 and Tra-1-80 are molecular indicators of pluripotency in human cells (Cowan et al. 2004). These markers are highly expressed on the surface of human pluripotent cells such as hESc (Strulovici et al. 2007; Yu et al. 2007) and induced pluripotent stem cells (iPSc) (Takahashi et al. 2007). Other pluripotent cells such as human embryonal carcinoma (EC) cells also express SSEA-3/4 and Tra-1-60/80 markers, while these markers are absent in mouse embryonic stem and mouse embryonal carcinoma cells (Laslett et al. 2003). Currently, the most rigorous and ethically permissible assessment of human cell pluripotency (Denker 2006) is through teratoma formation after subcutaneous injection of cells into severe combined immunodeficient (SCID) mice (Thomson et al. 1998; Cowan et al. 2004). A teratoma is a tumour containing tissue and cell components from all the three embryonic germ layers: endoderm, mesoderm and ectoderm (Prokhorova et al. 2009).

1.1.3 Culturing of Human Embryonic Stem Cells

Special culturing conditions are necessary for the successful maintenance of hESc self-renewal in an undifferentiated state. Currently, there are two mainstream methods

of *in vitro* culturing of hESc in a monolayer adhesion culture: using a feeder layer providing a base of cells (Cowan et al. 2004) and a feeder-free system (Ludwig et al. 2006). However, as culturing hESc in a monolayer severely limits cell yield for clinical and industrial applications, research on suspension growth of hESc is currently taking place. Recent studies have shown reasonable success at suspension culturing of hESc (Oh et al. 2009; Amit et al. 2010); however, it may take a number of years before this method of culturing hESc becomes commonplace.

The most common cell type used as a feeder layer for culturing hESc is mitotically inactivated primary mouse embryonic fibroblasts (MEFi). Due to their short replicative lifespan, MEFi need to be freshly prepared from low passage frozen MEF stocks, which are obtained by sacrificing pregnant female mice at 13-14 days post-coitum and harvesting the embryos (Nagy et al. 2003). Mitomycin C or gamma-irradiation is used to mitotically inactivate MEF by cross-linking their DNA and preventing cell proliferation. MEF secrete factors (e.g. basic fibroblast growth factor, leukemia inhibitory factor, transforming growth factor beta 1) that are necessary for proliferation of hESc in their undifferentiated state. However, due to possible contamination with animal pathogens, the use of MEF for culturing hESc compromises their suitability for clinical applications (Richards et al. 2002; Mallon et al. 2006). To avoid concerns regarding xeno contamination, some groups have used human adult marrow cells (Cheng et al. 2003), placental fibroblasts (Genbacev et al. 2005) and immortalised human skin fibroblasts (Unger et al. 2009) to culture hESc.

Recent advances in the field of hESc biology, in search for a xeno-free culturing system, have made it possible to culture hESc without a feeder layer, free of unknown

pathogens and in a serum-free, defined environment (Ludwig et al. 2006). Matrigel is a basement membrane matrix secreted by mouse sarcoma cells that provides a complex extracellular environment containing components such as laminin and collagen IV (Vukicevic et al. 1992). These conditions allow for the proliferation of hESc in a feeder-independent environment supplemented with MEF-conditioned media or commercially available media (e.g. mTeSR from STEMCELL Technologies). Development of feeder-free culturing systems for hESc has been a major step forward in realising their potential for clinical applications. Different hESc lines have been cultured on Matrigel for up to 20 passages without formation of karyotypic abnormalities, or loss of pluripotency (Ludwig et al. 2006). However, other hESc studies (Draper et al. 2004; Baker et al. 2007; Catalina et al. 2008; Spits et al. 2008) have reported the development of more frequent karyotypic abnormalities in the absence of a feeder layer, described in section 1.1.4.

Other than difficulties in culturing hESc, passaging the cells has been another challenge in the advancement of hESc research. As hESc prefer to grow in tightly packed colonies, they show poor survival rates when dissociated into a single cell suspension using enzymatic cell dissociators such as trypsin. Until 2006, mechanical passaging of hESc was the only viable option for their propagation and expansion in culture. The process consisted of dissecting colonies with a sharp, sterile scalpel and transferring the resulting pieces into a new dish. Mechanical passaging of hESc was not only extremely time consuming and laborious, but also risked tissue culture contamination (Ludwig et al. 2006). Recently, enzymatic passaging of hESc has been possible with the addition of p160-Rho-associated coiled-coil kinase (ROCK) inhibitor Y-27632 following trypsinisation. The mode of action of ROCK inhibitor Y-

27632 is not fully understood; however, it may prevent dissociation-induced apoptosis pathways, allowing for the survival of single hESc after enzymatic dissociation (Watanabe et al. 2007).

1.1.4 Karyotypic Abnormalities Developed in Human Embryonic Stem Cells

The use of hESc in a clinical setting requires continuous maintenance of undifferentiated cells under *in vitro* culture conditions. Thus, regular screening and quality control over the karyotype of these cells is necessary to avoid the development of fast-growing aneuploid cells, which would have detrimental effects if used in transplantation therapies. Draper et al. (2004) reported hESc chromosomal abnormalities could occur when grown under feeder-free conditions, while expressing hESc-specific markers and retaining their pluripotency. Trisomies of chromosomes 12 (specifically 12p), 17 (specifically 17q) and X have been the most commonly observed karyotypic abnormalities in hESc, suggesting that their presence provides hESc with a selective advantage for proliferation and prevention of apoptosis (Draper et al. 2004; Baker et al. 2007; Catalina et al. 2008; Spits et al. 2008). Candidate genes providing selective advantage on chromosome 17 are *Birc5* (an inhibitor of apoptosis), *Stat3* and *Grb2*, which are both involved in cell renewal. *Nanog* is the candidate gene on chromosome 12, as it is essential for the maintenance of pluripotency (Draper et al. 2004). Various laboratories have also reported other chromosomal aberrations, such trisomies of chromosome 1 and amplification of chromosomal regions such as 3q, 5q, 11q and 20q. Recent studies have suggested that enzymatic passaging (as opposed to mechanical passaging) of hESc has been associated with more chromosomal aberrations that promote cell self-renewal and hinder apoptosis (Baker et al. 2007; Spits et al. 2008). Enzymatic passaging is thus

thought to select for specific karyotypic abnormalities, which result in higher proliferation rates and prevent apoptosis. Furthermore, as enzymatic passaging dissociates hESc colonies into single cells, each individual cell is allowed more space to proliferate as opposed to mechanically passaged hESc colonies that are mostly proliferative at the outer periphery due to spatial restrictions.

1.1.5 Importance of Human Embryonic Stem Cells for Clinical Research

Owing to their self-renewal and pluripotent nature, the use of hESc has been proposed for drug toxicity and efficacy screenings in the relevant disease-specific hESc-derived cell types prior to animal testing. Furthermore, hESc allow the establishment of *in vitro* disease-specific models, for example, dopaminergic neurons in the case of Parkinson's disease. On the clinical side, the use of hESc has been proposed for tissue regeneration and transplant therapies for the prevention and treatment of conditions such as age-related macular degeneration, spinal cord injuries, cardiac failure, Parkinson's disease and juvenile-onset diabetes mellitus (Thomson et al. 1998; Reubinoff et al. 2000; Cowan et al. 2004; Singec et al. 2007; Takahashi et al. 2007; Li et al. 2008).

Since the isolation of hESc in 1998 by Thomson et al., a number of key advancements have been made in the field of hESc biology, which has brought the field closer to the clinic. It is now feasible to foresee a future where human leukocyte antigen (HLA) type-matched hESc could be expanded and differentiated *ex vivo* into the desired cell types and subsequently engrafted into patients for treatment. Indeed, mouse embryonic stem cells (mESc) have successfully treated a number of disease mouse models (Rosenthal 2003; Raikwar et al. 2006). mESc-derived motor neurons have

promoted motor function recovery of rats injured in their spinal cord (McDonald et al. 1999). Transplantation of mouse and human embryonic stem cell-derived dopaminergic neurons have improved symptoms in the Parkinson's rat model (Kim et al. 2002; Yang et al. 2008), and engraftment of mESc-derived retinal cells improved sight in blind mice (Lamba et al. 2009).

Other than ethical considerations facing the field of hESc biology (Fischbach and Fischbach 2004), difficulties in culturing hESc (Watanabe et al. 2007), genetic manipulation (Menendez et al. 2005; Strulovici et al. 2007), efficient differentiation of desired functional cell types (Anderson et al. 2007), efficacy and immune rejection (Vogel 2005; Parson 2006) and most importantly, safety of hESc-based therapies (Crook et al. 2007; Hentze et al. 2007; Hewitt et al. 2007; Li et al. 2008; Spits et al. 2008), have slowed the progress of the field. Despite such obstacles, the use of hESc has been proposed for cell and gene therapy treatments (Strulovici et al. 2007; StemCells&Diseases 2011).

1.2 Cell Therapy

Cell therapy is a procedure whereby healthy cells are injected into a specific location or tissue of a patient's body to restore damaged or diseased cell function. The source of injected cells can be either from the patient (autologous) or from a donor (allogeneic) (Anak et al. 2005; Naldini 2011). The first successful cell therapy treatment was a bone marrow transplantation performed in 1968 for the treatment of Wiskott–Aldrich syndrome (Bach et al. 1968). To date, hematopoietic stem cell transplantation (from the bone marrow) is still the most successful and ubiquitous form of cell therapy, where patients with leukemia are successfully treated following

chemotherapy (Zittoun et al. 1995). In this procedure, multipotent hematopoietic stem cells from the patient or a donor with similar HLA type (often a close relative) are extracted and stored for later administration. Hematopoietic stem cells are most commonly extracted from the bone marrow, generally the pelvis. However, as bone marrow extraction is highly invasive, recently peripheral blood has been used to extract blood stem cells especially from donors. After chemotherapy, cryopreserved cells are revitalised and injected into the patient to repopulate and restore the destructed hematopoietic cell population (Zittoun et al. 1995; Rocha et al. 2000; Buckley 2004).

Conceptually, cell, stem cell and hESc therapies follow the same hypothetical mode of function (Hochedlinger and Jaenisch 2003; Mimeault et al. 2007; Naldini 2011). Stem and embryonic stem cell therapies in their general form refer to injection or engraftment of multipotent or unipotent cells to restore function of a damaged tissue or organ. Stem cell therapies are based on the concept that engraftment of multipotent cells into a specific niche will allow signals from the surrounding environment to determine cell fate and functionality; thus, allowing the engrafted cells to restore the desired function (Vogel 1999). However, recent advancements in the field of cell therapy suggest that engraftment of the desired differentiated functional cell types, as opposed to undifferentiated progenitor cells, improves the efficacy and safety of stem cell based treatments (Mimeault et al. 2007).

1.2.1 Adult Stem Cells for Cell Therapy

Adult stem cells are self-renewing, multipotent cells that are found in different adult tissues (Naldini 2011). Adult stem cells are known to be a reservoir of cells

responsible for the maintenance and repair of damaged tissues. Unlike hESc, adult stem cells are not pluripotent; instead, they are multipotent, capable of producing a subset of cell types *in vivo* (Korbling and Estrov 2003). Furthermore, as adult stem cells are isolated from adult tissues, there are no ethical considerations when using them for basic and clinical research (Young et al. 2004). Examples of adult stem cells include hematopoietic stem cells (HSC) that are present in the bone marrow and produce blood derived cell types (Quesenberry and Levitt 1979), mesenchymal stem cells (MSC) that are capable of differentiation into bone, cartilage and adipose tissue (Caplan 2005), and neuronal stem cells (NSC) that are capable of differentiation into neurons and astrocytes (Reynolds and Weiss 1992).

Other than the commonly studied bone marrow transplantation treatment, the use of adult stem cells for replacement therapies is currently under way in a number of studies for the treatment of conditions such as: myocardial infarction (Chen et al. 2004a; Wollert et al. 2004; Assmus et al. 2006; Drexler et al. 2006), liver damage (Dan and Yeoh 2008), and development of bone and cartilage grafts for bone regeneration (Arvidson et al. 2011). However, further research and development is necessary to optimise identification and isolation of adult stem cells, and their efficient differentiation into specific functional cell types. Furthermore, as concerns have been raised regarding the safety and functionality of cells post-engraftment, further improvements need to be made to the transplantation approaches (Mimeault et al. 2007).

1.2.2 Human Embryonic Stem Cells for Cell Therapy

Currently, one of the challenges facing the field of hESc biology is poor characterisation of differentiation pathways toward a particular cell lineage. Furthermore, cell-specific surface markers that can be used for cell sorting and isolation are not fully characterised (Strulovici et al. 2007). Except for a few well-defined protocols for cell differentiation (e.g. neuronal) (Schulz et al. 2003; Itsykson et al. 2005; Yan et al. 2005; Iacovitti et al. 2007; Abranches et al. 2009), other forms of differentiation (e.g. lung, kidney, hepatocyte) are less defined (Forbes et al. 2002; Teramoto et al. 2005; Hay et al. 2008). Thus, to guarantee the safety and efficacy of hESc-based therapies, highly efficient differentiation and cell sorting protocols are required, ensuring derivation of a pure, differentiated and functional cell population.

In addition, studies have shown the possibility of teratoma formation after administration of hESc-derived target cells contaminated with a small fraction of undifferentiated or poorly differentiated hESc (Bjorklund et al. 2002; Robinson et al. 2005). To circumvent the tumourigenic hazards related to hESc therapy, the development of both highly efficient differentiation and purification assays, and ensuring rigorous quality control over the administrated cells is essential in achieving such a feat. However, other possibilities have been proposed such as the introduction of a suicide gene (such as herpes simplex virus thymidine kinase) under the regulation of a hESc-specific promoter (such as *Oct4* or *Rex1*) to destroy any remaining undifferentiated cells upon administration of ganciclovir (Yates and Daley 2006; Zhong et al. 2011). In addition, recent studies have suggested immunodepletion of cells expressing the SSEA-5 glycan, and two other pluripotency surface markers

(either CD9/CD90 or CD50/CD200) eliminates the entire teratoma-forming cell population (Tang et al. 2011).

As described, the most successful cell-based therapies have been in bone marrow transplantation from an autologous (from patient) or closely related allogenic sources (from a sibling). When the appropriate autologous or close allogenic sources are not available, HLA type matching can circumvent immune rejection upon cell injection. Similarly, the use of HLA typed hESc banks has been proposed for hESc-based therapies (Yates and Daley 2006; Strulovici et al. 2007) and is currently in use in clinical studies. To date, only three human embryonic stem cell trials have gained approval by the National Institutes of Health (NIH) in the United States (StemCells&Diseases 2011). The first hESc trial was initiated in 2009 and is currently being conducted by Geron Corporation to treat patients with spinal cord injuries. In 2010 and early 2011, the second and third hESc trials were commenced by Advanced Cell Technologies, Inc to treat patients with Stargardt disease and age-related macular degeneration using hESc derived retinal cells. The primary goal of the mentioned trials is to investigate the safety and tolerability of hESc therapies over their efficacy (StemCells&Diseases 2011). Once safety concerns have been addressed, more clinical trials will take place to improve efficacy of hESc-based therapies (Carpenter et al. 2009). Ensuring the safety of hESc therapies is absolutely essential, not only to ensure the wellbeing of the treated patients, but also to prevent similar setbacks that the field of gene therapy suffered during its early years of clinical studies (Marshall 1999; Hollon 2000; Hacein-Bey-Abina et al. 2003).

1.2.3 Induced Pluripotent Stem Cells

An alternative approach to using HLA-matched hESc has been the concept of reprogramming adult cells through somatic cell nuclear transfer (SCNT) to generate patient-specific cells in a pluripotent state (Hochedlinger and Jaenisch 2003). This approach not only circumvents ethical issues surrounding the destruction of embryos for the establishment of hESc lines, but more importantly, it addresses concerns regarding immune rejection of hESc in a clinical setting (Kastenberg and Odorico 2008). However, due to technical difficulties and poor efficiency of SCNT, the use of this technique has been limited (Blelloch et al. 2006). As of 2007, the focus of generating patient-specific pluripotent cells has been mostly directed toward the study of induced pluripotent stem cells (iPSc) (Nishikawa et al. 2008; Caulfield et al. 2010). This technology enables the use of as few as four transcription factors (*Oct4*, *Sox2*, *Klf4* and *c-Myc*) to induce a pluripotent state, at reasonable efficiencies (0.001% - 1%), in terminally differentiated fibroblast cells (Takahashi and Yamanaka 2006; Takahashi et al. 2007). Recent studies have used other reprogramming factors such as *Nanog*, *Lin28*, *l-Myc* and *Glis1* to induce a pluripotent state in terminally differentiated cell types (Yu et al. 2007; Nakagawa et al. 2010; Maekawa et al. 2011).

The first generation of iPSc was produced using retroviral-mediated transduction of transcription factors; however, multiple integrations of the transgenes were observed in the genome. Due to risk of insertional mutagenesis, the use of retroviral-generated iPSc has raised concerns regarding the safety of this technique in a clinical setting (Miura et al. 2009; Bock et al. 2011). Furthermore, the transcription factors necessary for reprogramming are known to promote oncogenesis, especially *c-Myc*, a well-

known oncogene (Nakagawa et al. 2010). Thus, recent studies have focused on the use of non-viral, integration-free methods, such as plasmids (Yu et al. 2009), small molecules (Lin et al. 2009), recombinant proteins (Kim et al. 2009a), minicircle plasmids (Jia et al. 2010) and miRNA (Li et al. 2011) to generate iPSc. Owing to the high tumourigenic nature of the transcription factors used for the induction of pluripotency, iPSc form teratomas more frequently than hESc in SCID mice (Gutierrez-Aranda et al. 2010). Due to such safety concerns, the iPSc technology is still in the research and development phase to improve safety and efficiency of derivation. Thus, further research is required before patient-specific iPSc may be used in a clinical setting (Fox 2011; Tang and Drukker 2011; Zhao et al. 2011).

1.3 Gene Therapy

The most common form of gene therapy is a procedure whereby a functional copy of a known gene is introduced into cells to replace or correct the function of a missing or mutated gene (Kay 2011). Gene therapy was first proposed in 1972 as a viable option for correcting single gene disorders such as cystic fibrosis, sickle cell anaemia, haemophilia and Duchenne muscular dystrophy (DMD) (Friedmann and Roblin 1972). Gene therapy can be performed either *in vivo* or *ex vivo* and the gene of interest can be delivered either through viral (e.g. adenovirus, adeno-associated virus, retrovirus, HSV-1) or non-viral (e.g. plasmid DNA) methods (Wells 2004; Edelstein et al. 2007; Sheridan 2011). To date, approximately 1700 gene therapy clinical trials have gained approval for the treatment of conditions such as cancer, cardiovascular and inherited monogenic diseases. The high prevalence and fatal outcome of cancer and cardiovascular diseases render them top targets for gene therapy studies. This is followed by the treatment of inherited monogenic diseases, as the notion of replacing

a defective or missing gene with a functional copy is intrinsic to the nature of gene therapy. Vectors along with their frequency of use in the gene therapy trials include adenovirus (~24%), retrovirus (~21%), naked/plasmid DNA (~18%), adeno-associated virus (~4.5%) and herpes simplex virus type-1 (~3.3%) (Edelstein et al. 2007; Sheridan 2011). Details of some of these gene delivery methods will be further discussed in section 1.3.2 in the context of *in vitro* hESc studies.

The first successful gene therapy trial was performed in 1990 on two patients suffering from severe combined immunodeficiency, caused by adenosine deaminase deficiency (ADA^- SCID) using retroviral delivery of the adenosine deaminase gene into their T cells (Blaese et al. 1995). In 1999, the first patient to have passed away as a direct consequence of gene therapy suffered a major immune response after receiving the adenoviral vector for the treatment of ornithine transcarbamylase deficiency (Marshall 1999; Hollon 2000). Following this case, in 2003, five patients (out of the treated twenty) were shown to have developed leukemia-like syndromes after mouse Moloney retroviral-mediated treatment of X-linked severe combined immunodeficiency disease (X-SCID). The symptoms involved uncontrolled proliferation of mature T lymphocytes due to retroviral-mediated insertional mutagenesis in the LIM domain only 2 (*LMO2*) proto-oncogene promoter (Hacein-Bey-Abina et al. 2003; Kohn 2010). Both cases resulted in a severe setback for the field of gene therapy (Kay 2011).

Nearly 40 years after gene therapy was first proposed as a viable form of clinical treatment and 20 years after the first gene therapy trial, the field still faces some obstacles (Edelstein et al. 2004; Edelstein et al. 2007; Aiuti and Roncarolo 2009). The

greatest concern with retroviral-mediated gene transfer is the risk of insertional mutagenesis from random integration of the transgene leading to either inactivation of tumour-suppressor genes (e.g. *p53*) or activation of proto-oncogenes (e.g. *LMO2*) (Hacein-Bey-Abina et al. 2003). Unless a multipotent stem cell progenitor population is the target of gene delivery (Schmidt et al. 2002; Hacein-Bey-Abina et al. 2003), the clinical effects of most gene therapy treatments is temporary and requires multiple rounds of re-administration (Kay 2011). Immune response and toxicity related to viral based therapies limit the dosage and frequency of re-administrations. Viral-induced immunogenic concerns have led to an increase in the use of naked/plasmid based gene transfer through either liposomes, dendrimers and lipofection or physical means of delivery such as electroporation, pressure-perfusion and ultrasound (Wells 2004). However, the efficiencies of delivery using non-viral methods are generally lower than viral methods (Strulovici et al. 2007).

1.3.1 Promoter Choice and Transgene Silencing

Many gene therapy studies have used viral promoters to drive transcription of the desired transgene in various tissues. In general, viral promoters such as the cytomegalovirus immediate early (CMV-IE) enhancer/promoter are known to drive transcription at higher levels when compared to eukaryotic promoters (Papadakis et al. 2004). Other commonly used viral promoters include Simian virus 40 (SV40), Rous sarcoma virus (RSV) and Moloney murine leukaemia virus long terminal repeat (MMLV-LTR) (Papadakis et al. 2004; Zheng and Baum 2005). A number of preclinical animal studies have shown success in utilisation of viral promoters. Examples include sustained MMLV-LTR driven factor VIII expression at physiological or higher levels for over a year in murine (VandenDriessche et al. 1999)

and in both murine and canine (Snyder et al. 1999) models from retroviral and AAV vectors, respectively. In another study, sustained CMV I/E driven factor IX expression was achieved for 17 months in dogs from an AAV vector (Herzog et al. 1999), and recently, *in utero* AAV delivery of a CMV-mini-dystrophin vector, in mice, demonstrated transgene persistence for at least 100 days after treatment (Koppanati et al. 2010).

Despite such examples, viral promoters have been shown to be susceptible to transcriptional silencing both *in vivo* and *in vitro* studies. *In vivo* suppression of viral-driven transgene expression is known to be due to inflammatory-mediated cytokines such as tumour necrosis factor (TNFα) and interferons (IFNγ) (Acsadi et al. 1998; Sung et al. 2001; Papadakis et al. 2004). Inhibition of viral-driven transgene expression is thought to be at the mRNA level and affects viral promoters more than constitutive cellular promoters (Qin et al. 1997; Chen et al. 2008). Thus, the use of mammalian promoters such as Ubiquitin C (UbC) and human elongation factor 1 α (hEF1α) promoters is becoming more common as they show sustained long-term transgene expression and suffer less from silencing events as compared to viral promoters (Gill et al. 2001; Papadakis et al. 2004; Zheng and Baum 2005; Strulovici et al. 2007; Hyde et al. 2008).

However, as constitutive viral and mammalian promoters generally do not drive transgene expression at physiological levels, some groups have engaged in the use of tissue-specific promoters. For example, long-term gene expression and phenotypic correction in the murine models has been achieved using tissue-specific promoters such as muscle-specific CK6 to drive dystrophin cDNA expression in the *dmx* mouse

model (Bertoni et al. 2006) and liver-specific human α1 anti-trypsin (hAAT) promoter to drive factor IX expression in factor IX knockout mice (Keravala et al. 2011). Furthermore, human artificial chromosome studies have utilised physiological promoters to drive transgene expression in cells. Examples include: guanosine triphosphate cyclohydrolase I (*GCH1*), globin (Ikeno et al. 2002; Suzuki et al. 2006b) and hypoxanthine-guanine phosphoribosyltransferase (*HPRT*) expression (Grimes et al. 2001; Mejía et al. 2001) in HT1080 cells, and dystrophin expression (Hoshiya et al. 2009; Kazuki et al. 2010) in human immortalised mesenchymal stem cells and transgenic HAC-containing mice. These HAC studies, along with others, will be discussed in further detail in section 1.5. Thus, the promoter of choice is of vital importance in the design of gene therapy vectors, and ultimately determines the success of the treatment.

Another issue that prevents long-term sustained transgene expression is the presence of bacterial sequences in the vector of interest. *In vivo* studies have demonstrated transgene silencing due to the presence of bacterial sequences enriched in cytosine-phosphatidyl guanosine (CpG) dinucleotides (Hemmi et al. 2000; Hyde et al. 2008). Bacterial DNA is known to stimulate the mammalian immune cells, which is thought to be attributed to the presence of highly unmethylated CpG dinucleotide motifs in the bacterial DNA sequences (Krieg 1996; Lipford et al. 1998; Hemmi et al. 2000). Hemmi et al. (2000) showed that a toll-like receptor (TLR9), a class of essential immune system proteins that recognise structurally conserved molecules from bacterial sources (Hansson and Edfeldt 2005), was responsible for the cellular immune response against CpG dinucleotides, which led to cellular injury and DNA loss. Reducing the number of CpG motifs in the vector design has shown to reduce

the immune response, thus leading to a more prolonged transgene expression (Yew et al. 2002; Chen et al. 2003; Hodges et al. 2004; Yew and Cheng 2004). In a more recent study by Hyde et al. (2008), it was shown that the presence of even a single CpG dinucleotide was sufficient to provoke an immune response. Thus, by removing CpG motifs from plasmid DNA, sustained *in vivo* expression was achieved, without causing inflammation, in the mouse lung.

To counter the effects of silencing, a new class of vectors (minicircle DNA) have emerged where the entire bacterial backbone has been removed through øC31-based recombination (Chen et al. 2003; Chen et al. 2008; Kay et al. 2010). Through the study of minicircle DNA, Chen et al. (2008) showed that transcriptional silencing in the liver was not primarily due to the presence of CpG dinucleotides, but instead due to the presence of bacterial sequences. These results may seem to be in contradiction to the findings by Hodge et al. (2004) and Yew et al. (2002 & 2004), mentioned above. However, Chen et al. (2008) suggest that the removal of CpG motifs in these studies was responsible for a reduced bacterial backbone content, which may have resulted in the extension of transgene expression. Chen et al. (2008) take their hypothesis one step further to suggest that even mammalian sequences that lack binding sites for regulatory factors could be subjected to silencing through heterochromatinisation.

Taken together, these findings suggest that for a gene therapy treatment to achieve sustained gene expression at physiological levels, it is necessary to design vectors with the transgene under the regulation of an appropriate promoter that is capable of escaping silencing and driving long-term expression. As described, the current

standing in the field indicates that ubiquitous mammalian or tissue-specific promoters are superior to viral promoters in facilitating sustained long-term expression at physiologically relevant levels. Furthermore, limiting the content of bacterial DNA (especially free of bacterial-derived CpG motifs) reduces *in vivo* immune response and DNA silencing, thus prolonging transgene expression. Some of these concepts, regarding promoter choice and sustained transgene expression, will be discussed next in the context of hESc studies.

1.3.2 Human Embryonic Stem Cells for Gene Therapy

Although the correction of most genetic deficiencies can hypothetically be achieved through gene therapy alone, simultaneous utilisation of gene therapy in combination with stem cell therapies can synergistically improve the efficacy of gene therapy treatments (Rideout et al. 2002; Kazuki et al. 2008; Oshimura and Katoh 2008; Kazuki et al. 2010). As described above, some gene therapy methods suffer from low efficiencies of gene delivery and short-lived transgene expression, thus necessitating multiple administrations of the treatment. Transient gene expression may be sufficient to provide the essential signals in treating some conditions such as bone regeneration, development of blood vessels and wound healing. However, long-term expression of the gene of interest at the appropriate physiological levels is necessary for sustainable correction of a genetic deficiency (Yates and Daley 2006; Strulovici et al. 2007; Oshimura and Katoh 2008).

The clonogenic, self-renewal and pluripotent nature of hESc, have made them an ideal target for *ex vivo* gene therapy studies (Rideout et al. 2002; Kazuki et al. 2008; Oshimura and Katoh 2008; Kazuki et al. 2010; Kay 2011). The clonogenic nature of

hESc circumvents problems due to short-lived transient gene expression, as it enables isolation and characterisation of clones expressing ideal levels of the gene of interest. In the case where retroviral delivery methods are used, the genetically modified hESc clones can be screened ensuring the site of integration is not likely to cause mutagenic effects. The self-renewal ability of hESc enables utilisation of a hypothetically unlimited source of cells, thus allowing for storage of cells if readministration is necessary. Finally, pluripotency of hESc enables the derivation of various functional cell types expressing the gene of interest that can be administered to the desired site.

As mentioned, there are two modes of gene delivery into cells: viral and non-viral. With the exception of some physical gene delivery methods such as focused laser, microinjection, ballistic delivery, magnetofection and sonoporation (Wells 2004), most other methods have been implemented for gene delivery in hESc, and have not resulted in loss of their pluripotency and self-renewal properties. With the exception of helper-dependent adenoviruses (Palmer and Ng 2005) and herpes simplex virus type-1 (Martin et al. 1991), the delivery load of most commonly used viral vectors is limited to ~5-10kb (Wu et al. 2009). While non-viral methods can deliver larger sized vectors, the efficiency of delivery is generally reduced as the size of the transgene increases. Table 1-1 summarises different DNA delivery modes into hESc along with their corresponding efficiency of delivery.

Table 1-1 Various modes of gene delivery into human embryonic stem cells

Mode of Delivery	Method	Efficiency	Notes	Reference
Non-viral Transfection	Electroporation	~5-40%	Generally high cell mortality observed post-treatment	(Eiges et al. 2001; Siemen et al. 2005; Costa et al. 2007; Braam et al. 2008b)
	Nucleofection	~30-65%	Combines both electroporation and use of a transfection agent (Nucleofector)	(Siemen et al. 2005; Moore et al. 2011)
	Lipofectamine	~5-30%	Generally low transfection efficiencies are obtained for most vectors, especially larger vectors High efficiencies obtained only when delivering small, highly optimised commercial vectors	(Eiges et al. 2001; Siemen et al. 2005; Tan and Droge 2005)
	ExGen 500	~10%		(Eiges et al. 2001)
	FuGENE	~5-80%		(Eiges et al. 2001; Lebkowski et al. 2001; Tan and Droge 2005)
	GeneJammer	~80%		(Braam et al. 2008b)
Viral Transduction	γ-Retrovirus	~50-65%	Highly efficient at delivery of small vectors Transgene integrates into host genome Packaging capacity 8kb	(Lebkowski et al. 2001)
	Lentivirus	~5-90%		(Gropp et al. 2003; Ma et al. 2003; Xiong et al. 2005; Jang et al. 2006; Braam et al. 2008b)
	Foamy Virus	~15-50%		(Gharwan et al. 2007)
	Adenovirus	~58-80%	Highly efficient at delivery of non-integrating transgenes Packaging capacity 7.5kb	(Braam et al. 2008b; Brokhman et al. 2009)
	Helper-dependent Adenoviruses	~10-100%	Non-integrating Packaging capacity 36kb	(Suzuki et al. 2008)
	Rep$^-$ Adeno Associated Virus	~5-25%	Very high MOIs (in the order of 1000s) necessary to reach reasonable transduction efficiencies Packaging capacity 4.5kb	(Mitsui et al. 2009)
	Herpes Simplex Virus Type 1 Amplicons	~15-85%	Non-integrating Packaging capacity 152kb	This report

Table adapted and updated from Strulovici et al. 2007.

Non-viral gene delivery methods in hESc include the use of commercially available chemical reagents such as Lipofectamine, ExGen 500, FuGENE and GeneJammer (Eiges et al. 2001; Braam et al. 2008b), electroporation (Costa et al. 2007) or Nucleofection which combines both electroporation and use of a transfection agent (Nucleofector) (Siemen et al. 2005; Moore et al. 2011). Reported viral transduction in hESc includes use of retroviruses (γ-retrovirus, lentivirus, foamy virus) (Lebkowski et al. 2001; Gharwan et al. 2007; Braam et al. 2008b), adenovirus (Braam et al. 2008b), helper-dependent adenovirus (Suzuki et al. 2008), *Rep*$^{-}$ adeno associated virus (Mitsui et al. 2009) and recently herpes simplex virus type-1 amplicons (Mandegar et al. 2011). There is a huge variation reported in the efficiencies of transgene delivery into hESc using different methods. These discrepancies may partly be attributed to the use of different promoters, hESc lines, vector size and transduction conditions (e.g. MOI). However, it is generally believed that in hESc, viral gene delivery methods are more effective at transgene delivery as compared to non-viral methods (Strulovici et al. 2007).

Retroviruses are RNA viruses that use reverse transcriptase to convert their RNA genome to DNA, which then randomly integrates into the host genome. They are capable of transducing non-dividing cells at high efficiencies, however their packaging capacity is limited to approximately 8kb (Lebkowski et al. 2001; Logan et al. 2002). Another class of retroviruses are known as lentiviruses, which are capable of transducing both dividing and non-dividing cells (Pfeifer and Verma 2001). Lenti/retroviruses have successfully been used to transduce hESc at maximal efficiencies ranging from 65-90% (Lebkowski et al. 2001; Braam et al. 2008b). The adeno associated virus (AAV) contains a single stranded DNA genome and is capable

of transducing both dividing and non-dividing cells. Wild-type AAV vectors are known to have a preferential integration site on chromosome 19 (Kotin et al. 1990). However, currently used AAV (*Rep*-negative recombinant rAAV) vectors are devoid of integration machinery and thus considered as non-integrating. Due to their low immunogenicity, AAV vectors have been successfully used in a number of gene therapy trials, for example the treatment of Leber's congenital amaurosis (Maguire et al. 2008). However, the major disadvantage of AAV vectors is their limited packaging capacity of ~4.5kb, and extremely high MOIs are required to achieve moderate transduction efficiencies in hESc (Mitsui et al. 2009).

Adenoviral (Ad) vectors are non-integrating double-stranded DNA viruses known to be one of the most efficient viral systems for transgene delivery, with transduction efficiencies close to 80% in hESc (Brokhman et al. 2009). Out of over 50 known adenoviral serotypes, Ad2 and Ad5 are the most commonly used for gene therapy purposes (Wang and Huang 2000; Palmer and Ng 2005; Kay 2011). Adenoviral vectors are capable of transducing both dividing and non-dividing human cells such as osteoblasts, hepatocytes, myocardium, skeletal muscle, epithelial and neuronal cells at high efficiencies; however, in general, transgene expression decreases rapidly after treatment (Mountain 2000; Palmer and Ng 2005; Ross et al. 2011). The main drawback of Ad vectors as a gene therapy system has been their high toxicity at dosage levels required for efficacy (Kay 2011) as exemplified by the tragic death of a gene therapy patient in 1999 (Marshall 1999; Hollon 2000).

Recent developments in adenoviral vector technology has allowed for the removal of nearly all viral genes, yet retention of elements essential for its propagation and

packaging. This class of viral vectors is known as helper-dependent adenoviruses (HdAd) (Palmer and Ng 2005; Ross et al. 2011). In addition to reduced toxicity and immunogenicity, relative to classical E1-deleted replication-deficient adenoviral vectors (Reddy et al. 2002), HdAd provide efficient long-lasting gene expression that has shown to last for several months in animal models (Maione et al. 2001; Reddy et al. 2002; Brunetti-Pierri et al. 2005). Furthermore, HdAd vectors have a large carrying capacity of up to ~36kb (Palmer and Ng 2005; Ross et al. 2011), which enables the incorporation of genes that are larger than the carrying capacity of adenoviral vectors such as dystrophin cDNA (14kb) (Wang et al. 2000) and factor VIII cDNA (9kb) (Murphy and High 2008). Helper-dependent adenoviruses have been used to genetically modify hESc at transduction efficiencies reaching approximately 100% at MOI 1000 (Suzuki et al. 2008).

Herpes simplex virus type 1 (HSV-1) amplicon vectors contain minimal *cis*-acting sequences necessary for replication and packaging in the presence of helper elements in *trans*. HSV-1 amplicons are capable of delivering a non-integrating double stranded DNA of up to 152kb into a wide range of cell types across different species. HSV-1 amplicons infect both dividing and non-dividing cells at high efficiencies with minimal immunogenic and cytotoxic side effects post-infection (Sena-Esteves et al. 2000; Hibbitt and Wade-Martins 2006; Suzuki et al. 2007). The details of this vector will be discussed further in section 1.5.5.

In addition to the efficiency of transgene delivery, another problem hindering stable genetic modification of hESc is that these cells, similarly to other mammalian cells, have the innate ability to silence foreign DNA, thus limiting transgene expression to a

few days only (Yates and Daley 2006; Liew et al. 2007). Similarly to mouse embryonic stem cells, hESc express high levels of *de novo* methyltransferases DNMT3a and DNMT3b (Kameda et al. 2006). Epigenetic silencing has been reported in hESc for both integrating (Poleshko et al. 2008; Poleshko et al. 2010) and episomal (Chen et al. 2004b; Riu et al. 2005; Suzuki et al. 2006a) vectors, which may be an evolutionary defence mechanism that resists expression of foreign DNA (Matzke et al. 1999; Matzke et al. 2000).

In eukaryotic cells, gene expression is tightly regulated through DNA methylation/ demethylation and histone tail acetylation/deacetylation, phosphorylation, methylation and ubiquitination, which have important implications in developmental biology (Grassi et al. 2003; Shen et al. 2006; Bergbauer et al. 2010). A well-known mechanism of transcriptional silencing is via cytosine-phosphatidyl guanosine (CpG) methylation of the promoter region of the transgene by DNA methyltransferases (DNMTs) (Grassi et al. 2003; Liew et al. 2007; Bergbauer et al. 2010). Following CpG methylation, methylcytosine-binding domain (MBD) proteins co-localise with the methylated DNA, blocking access of transcription factors to the promoter region, resulting in epigenetic silencing (Grassi et al. 2003; Bergbauer et al. 2010). In addition, MBD binding leads to the recruitment of histone deacetylase enzymes (HDACs) resulting in tighter chromatin packaging and heterochromatin formation, further reducing transcription by blocking access of transcription factors to promoter regions (Grassi et al. 2003; Turek-Plewa and Jagodzinski 2005; Klose and Bird 2006).

Similar to the described *in vivo* studies, viral promoters have also been widely used *in vitro* hESc research, specifically the CMV promoter (Eiges et al. 2001; Lebkowski et

al. 2001; Lakshmipathy et al. 2004; Tan and Droge 2005; Chan et al. 2008; Siemen et al. 2008). Other viral promoters such as the RSV-LTR (Smith-Arica et al. 2003), SV40 (Chan et al. 2008) and HSV-1 I/E have also been used to drive transgene expression in various hESc lines. However, short-term transgene expression under viral promoters such as the CMV has been commonly reported in various hESc studies (Eiges et al. 2001; Kameda et al. 2006; Liew et al. 2007; Chan et al. 2008; Macarthur et al. 2011). Instead, long-term transgene expression from mammalian promoters such as the human elongation factor 1 α (hEF1α) (Ma et al. 2003; Liu et al. 2004b; Xiong et al. 2005; Chan et al. 2008; Macarthur et al. 2011), Chinese hamster elongation factor-1 α (CHEF1α) (Chan et al. 2008), human ROSA26 (R26) and Ubiquitin C (UbC) (Liew et al. 2007) has been reported in hESc.

Promoter activity in hESc has shown to vary markedly from one line to another. For example, Liew et al. (2007) showed that UbC was not able to drive reporter expression in two out of the four studied hESc lines (H1 and H14). Using mammalian promoters (UbC and R26), they recovered *GFP*-positive stable clones, while using CMV no *GFP*-positive stable clones were obtained. In another study, Kameda et al. (2006) reported that the delivery of episomal DNA sequences using Epstein-Barr EBNA based vectors in hESc resulted in heavy methylation of transduced sequences. Rapid loss of transgene expression occurred within 1-2 weeks post-treatment, however, such an effect was not observed in the control 293 cell line. Moreover, generation and selection of stable hESc clones has proved difficult due to low cloning rates (Ludwig et al. 2006; Yates and Daley 2006; Kazuki et al. 2010; Ardehali et al. 2011; Moore et al. 2011). These findings have potential consequences for effective genetic modification of hESc and their stable clone selection.

1.3.3 An Alternative Gene Expression Vector: Human Artificial Chromosomes

Human artificial chromosomes (HAC) are genetic molecules, containing a functional centromere that behaves similarly to endogenous chromosomes, capable of gene expression, replication and segregation during cell division. Different studies have shown the ability of HAC to successfully express the gene of interest and complement genetic deficiencies in various cell lines (Mejía et al. 2001; Grimes et al. 2002; Kazuki et al. 2008; Hoshiya et al. 2009; Kazuki et al. 2010; Kurosaki et al. 2011). Thus, HAC have been proposed as potential gene carrying candidate vectors for use in therapeutic medicine. The use of HAC in gene therapy has theoretical advantages over conventional gene therapy methods, as HAC do not require integration into the host genome and can encompass large DNA fragments, including multiple genes and associated regulatory elements for tissue-specific gene expression. The presence of repetitive centromeric sequences allows HAC to be stably maintained in the nucleus with low loss rates during mitotic divisions (<1% per cell division). HAC also avoid problems associated with positional effects and thus silencing of the desired therapeutic gene. Research on HAC is not only significant because of their potential therapeutic applications, but also because they provide a useful model system to study normal chromosome structure and function, genomic instability and possible causes of cancer (Larin and Mejía 2002; Grimes and Monaco 2005; Basu and Willard 2006; Oshimura and Katoh 2008). Details of HAC studies will be further explored in section 1.5, after describing the structure and function of endogenous chromosomes.

1.4 Chromosomes

1.4.1 Chromosome Structure and Function

The eukaryotic chromosome is a single stretch of coiled DNA molecule with associated proteins. The DNA carries genetic information, while proteins associated with the chromosome govern its structure, gene expression and function (Miller and Therman 2001). Most eukaryotic cells contain large linear chromosomes, while prokaryotic cells often contain small circular chromosomes (Bendich and Drlica 2000). In most eukaryotes, the chromosomes become condensed during cell division, allowing them to be visualised under the microscope. Chromosome condensation is initiated during prophase where the ~2m long stretch of DNA becomes tightly condensed by 10,000 to 20,000 fold through association with proteins. It is believed that chromosome condensation is achieved through at least 3 levels of chromatin folding (Belmont 2002).

The first level of chromosome compaction takes place through the formation of nucleosomes, where 146bp of DNA wraps 1.7 times around the histone octamer, containing two molecules each of histones: H2A, H2B, H3 and H4. The nucleosome forms the basic unit of chromatin (Kornberg 1974; Luger et al. 1997). The nucleosome compacts the DNA (~2nm) to produce a chromatin fibre that is ~10nm in diameter. There are approximately 20-80bp of linker DNA between each nucleosome and histone H1 binds at the site where the DNA wraps the octamer core. One model suggests that in the second level of compaction, the nucleosome fibre wraps around a regular helix structure composing of ~6 nucleosomes per turn allowing for further compaction through formation of a 30nm solenoid chromatin fibre structure (Miller

and Therman 2001; Sumner 2003; Robinson and Rhodes 2006). The first two levels of chromatin condensation accounts for only ~40-fold compaction of the DNA length. The model by which the other ~500-fold compaction is achieved has been poorly characterised and consequently has been a source of controversy (Belmont 2002).

Traditionally, a radial loop model of chromosome condensation has been proposed where the 30nm fibres radiate from a proteinaceous chromosome scaffold that runs through the entire length of the chromosome (Miller and Therman 2001; Stack and Anderson 2001). However, Poirier and Marko (2002) show that the structural integrity of the chromosome relied on chromatin itself and was not depedent on scaffold proteins. Thus, an alternative model of the chromosome assumes a network of 30nm chromatin fibre that is cross-linked at approximately every 15kb, and does not include a continuous scaffold at its core (Belmont 2002; Poirier and Marko 2002).

As chromosomes carry the genetic information necessary for maintenance and survival of a cell, it is necessary that this structure is accurately replicated and passed onto its daughter cells. In eukaryotic cells, the essential chromosomal elements required for accurate replication and segregation during cell division consist of the centromere, origins of replication and telomeres (Stinchcomb et al. 1979; Clarke and Carbon 1980; Cleveland et al. 2003; Baird and Farr 2006). The normal human karyotype consists of 46 chromosomes: 22 autosomal pairs and two sex chromosomes (either XX or XY). Variation to the structure and number of chromosomes typically leads to developmental abnormalities or the development of cancer. Even balanced chromosomal aberrations, where no genetic material is gained or lost, often results in impaired fertility, due to segregation problems in meiosis. The presence of structural

aberrations include deletions (e.g. Cri du Chat syndrome: deletion of the short arm of chromosome 5: 5p15.2 locus), duplications (Charcot-Marie-Tooth disease, demyelinating, Type 1a: duplication of 17p12 locus), translocations (Philadelphia translocation, between chromosomes 9 and 22: t(9;22)(q34;q11)), inversions (in some cases asymptomatic, as in the inversion of the pericentromeric region of chromosome 9, 9p12 or 9q13-21.1) and ring chromosomes (ring chromosome 20 syndrome). The most frequently described numerical aberrations in live births include monosomies such as the Turner syndrome (XO) and trisomies such as the Down syndrome (trisomy 21), Edwards syndrome (triosomy 18), Klinefelter's syndrome (XXY) and triple X syndrome (XXX) (OMIM 2011).

1.4.2 The Centromere and Associated Proteins

In most eukaryotic organisms, the centromere consists of stretches of repetitive DNA sequences that associate with the kinetochore, a complex protein structure that is the site for spindle attachment and movement during cell division. Electron microscopy analysis reveals that the kinetochore is a trilaminar protein structure composed of the inner plate, outer plate and fibrous corona (Figure 1-2) (Chan et al. 2005; Musacchio and Salmon 2007). The kinetochore is essential to chromosome inheritance as it enables the capture of spindle microtubules, verifies kinetochore-microtubule anchoring and activates the spindle assembly checkpoint (Cleveland et al. 2003). The inner plate of the kinetochore is the closest to the centromere and binds both DNA and centromere proteins such as CENP-A and CENP-C (Saitoh et al. 1992). The outer plate is the site of microtubule attachment and hosts many of the microtubule-interacting proteins (e.g CENP-E, CENP-F) and checkpoint proteins (e.g BubR1, Bub1, Mad1) that control the integrity of microtubule attachments to the kinetochore.

When microtubules are not attached to the kinetochore, a network of fibres (fibrous corona) can be seen on the surface of the outer plate. The fibrous corona directly interacts with the spindle microtubules and hosts proteins involved in the spindle checkpoint and microtubule anchoring (e.g. CENP-E, Dynein, BubR1) (Chan et al. 2005; Musacchio and Salmon 2007). The inner and outer plates are separated through a space known as the interzone where phosphorylated 3F3/2 antigen localises to regulate spindle assembly checkpoint by associating with kinetochores not under tension (Campbell and Gorbsky 1995). The details of these centromeric proteins will be further discussed in section 1.4.4.

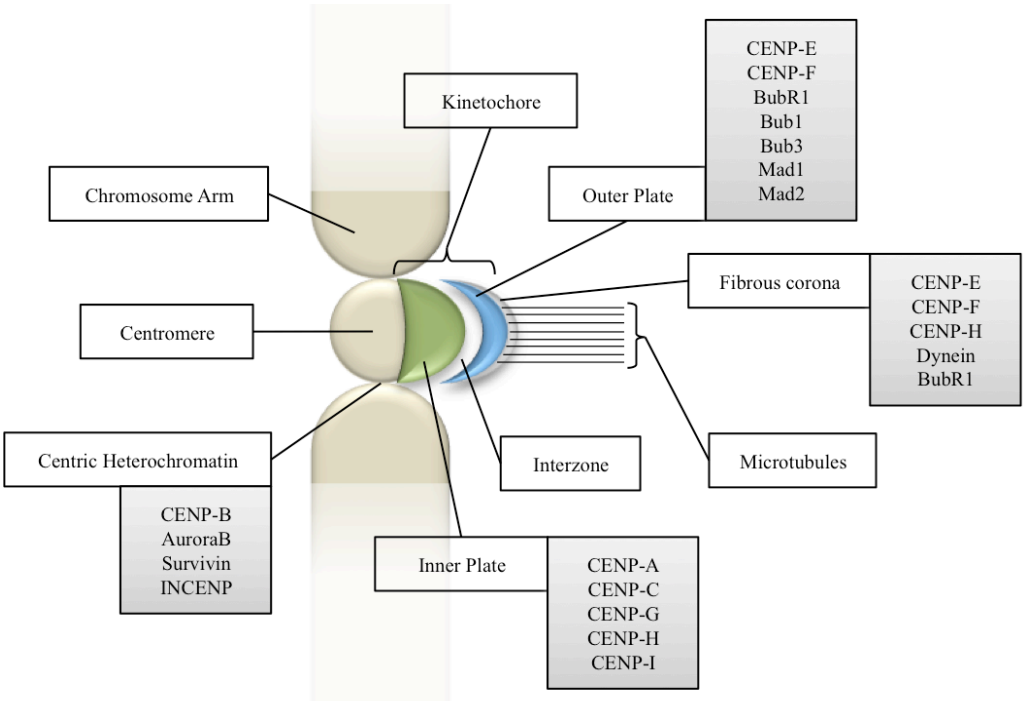

Figure 1-2 Schematic diagram of the centromere, kinetochore and associated proteins

The kinetochore is a trilaminar protein structure that associates with active centromeres, and is composed of the inner plate, outer plate and fibrous corona. The inner plate of the kinetochore directly interacts with the centromere and binds both the DNA and centromere proteins. The outer plate hosts many of the microtubule-interacting and checkpoint proteins, which control the integrity of microtubule attachment to the kinetochore. The fibrous corona is the outermost layer of the kinetochore and interacts with spindle microtubules and hosts proteins involved in the spindle checkpoint and microtubule anchoring. The grey boxes list a number of the main protein components that associate with each layer of the kinetochore (Chan et al. 2005; Musacchio and Salmon 2007).

The position of the centromere on the chromosome determines the shape and length of its arms as seen at metaphase. The short and long arms of the chromosome are denoted by “p” and “q” respectively. Chromosomes with their centromere near the middle of the chromosome are known as metacentric (e.g. human chromosomes 1 & 3). Acrocentric chromosomes have their centromere close to one end, resulting in a very short p arm and a much larger q arm (e.g. human chromosomes 13-15, 21 & 22), and telocentric chromosomes have their centromere at terminal ends. Chromosomes that fall in between metacentric (p≈q) and acrocentric (q>>p) categories are referred to as sub-metacentric or sub-acrocentric (Miller and Therman 2001; Sumner 2003).

Centromeric regions are generally gene-poor and associate with transcriptionally inactive and late-replication heterochromatin regions. Heterochromatin is the tightly condensed form of chromatin whose components (nucleosomes, as previously described) associate with heterochromatin protein 1 (HP1). Two forms of heterochromatin have been defined: constitutive and facultative heterochromatin. Constitutive heterochromatin remains tightly packed during different cell developmental stages. It is found on the same location on both homologous chromosomes, mostly present in centromeric and terminal regions of chromosomes. On the other hand, facultative heterochromatin occurs during certain developmental stages when specific genes need to be repressed through epigenetic silencing (Grewal and Jia 2007). A well-known example of facultative heterochromatin establishes on the inactive X chromosome. In female mammals, where two copies of the X chromosome are present, a dosage control machinery is present to balance the difference in expression levels of genes expressed from the X chromosome between males (XY) and females (XX). This dosage control machinery takes place through the

random inactivation of one of the X chromosomes. The X-inactive specific transcript (*Xist*) gene, located on the X chromosome, is transcribed into a non-coding RNA that coats the inactive X chromosome in *cis*, which ultimately results in the transcriptional inactivation of the X chromosome through heterochromatinisation (Penny et al. 1996; Ng et al. 2007; Hoki et al. 2009).

Genetic and epigenetic factors are believed to be involved in active centromere formation. In human cells, the genetic factors include repetitive DNA sequences consisting of 171bp repeat units known as alpha satellite DNA (Waye and Willard 1986; Carroll and Straight 2006; Dawe and Henikoff 2006). The alpha satellite DNA repeats can be divided into two classes: type-I alphoid DNA consists of highly homologous repeats, while type-II alphoid DNA consists of divergent alphoid subfamilies. Centromeric proteins are mostly known to associate with type-I alphoid DNA sequences (Ikeno et al. 1994; Chan et al. 2005). Variation in the monomeric nucleotide sequence and higher order assembly of tandem alpha satellite DNA repeats contributes to chromosome-specific differences (Carroll and Straight 2006). Higher order alpha satellite tandem repeats may be composed of either a heterogeneous mix of monomeric repeats, where the monomeric units are up to 70% identical, or a homogenous mix of monomeric repeats, where monomeric units are up to 100% identical (Rudd and Willard 2004). Centromere-specific proteins such as CENP-A and CENP-C assemble on higher order alpha satellite repeats, thus indicating that alphoid DNA is necessary for centromere formation and function (Schueler et al. 2001). The epigenetic factors involved in centromere function are less well-defined; however, it is thought that pericentric heterochromatin formation through methylation of H3 on lysine 9 and non-coding and interfering RNA may be involved (Grewal and

Moazed 2003). Some studies have reported neocentromere formation in the absence of alpha satellite DNA and CENP-B binding on marker chromosomes that were detected in patient cell lines (Depinet et al. 1997; Barry et al. 1999).

1.4.3 Neocentromeres

Neocentromeres are ectopic centromeres that can occasionally occur on new sites along the chromosome length. In humans, 90 neocentromeres have been identified on 20 different chromosomes. Neocentromeres commonly lack alpha satellite DNA sequences and do not form constitutive heterochromatin (C-band negative), however bind essential centromeric proteins (with the exception of CENP-B), and form functional kinetochores. Marker chromosomes containing neocentromeres are mitotically stable. As neocentromeres lack sequence similarities to alpha satellite DNA, epigenetic factors are known to be essential to neocentromere formation and function (Saffery et al. 2000; Warburton 2004; Marshall et al. 2008a; Marshall and Choo 2009). It is thought that through neocentromere formation, the centromere can be relocated, which could result in speciation events (Henikoff et al. 2001; Amor et al. 2004; Marshall and Choo 2009).

The most common method of neocentromere formation occurs as a result of an inverted duplication of the distal portion of a chromosome arm often leading to an unbalanced karyotype. Distal euchromatic regions of the chromosome seem to be the most common sites for neocentromere formation, in particular 3q, 8p, 9p, 13q and 15q. However, as heterochromatin-specific proteins such as HP1 have been recovered from neocentromeres, it is possible that a transition from a euchromatic to a heterochromatic state is essential for neocentromere formation (Amor and Choo 2002;

Marshall and Choo 2009). Some studies have suggested that neocentromeres and alpha satellite DNA may share some sequence characteristics (such as high AT content), which leads to preferential CENP-A deposition (Lo et al. 2001a; Lo et al. 2001b). Thus alpha satellite sequences are not absolutely essential for centromere formation on these types of chromosomes, but function in the recruitment of centromeric proteins such as CENP-A. After the recruitment of centromeric proteins, other epigenetic factors engage in the establishment and maintenance of the centromere (Carroll and Straight 2006).

1.4.4 Centromeric Proteins

During centromere formation, a histone H3 variant known as centromere protein A (CENP-A), replaces some of the H3 histones in alpha satellite DNA nucleosomes. CENP-A associates with active centromeres and neocentromeres and is localised in the inner kinetochore plate (Palmer et al. 1991; Warburton et al. 1997). CENP A nucleosomes alternate with nucleosomes containing H3, dimethylated in lysine 4 (Sullivan et al. 2001). According to one of the proposed models, this interspersed arrangement of CENP-A and H3 nucleosomes is organised into a cylindrical configuration where CENP-A faces outwards for kinetochore assembly (Blower et al. 2002; Marshall et al. 2008b). The presence of CENP-A is a strong epigenetic marker for kinetochore recruitment and active centromere formation (Marshall et al. 2008b). Inactivating CENP-A leads to disruption of mitosis and misplacement of the kinetochore and centromere-specific proteins such as CENP-C (Howman et al. 2000). However, CENP-A is not the only factor necessary for successful kinetochore assembly. Overexpression of CENP-A leads to its incorporation throughout the

chromosome and signals localisation of kinetochore assembly proteins, however does not result in a fully functional kinetochore (Van Hooser et al. 2001).

Human type-I alpha satellite DNA contains a 17pb motif, known as the CENP-B box, that is found at regular intervals within the linker DNA region, which signals CENP-B recruitment (Ikeno et al. 1994; Harrington et al. 1997; Chan et al. 2005). The centromere of the Y chromosome is devoid of type-I alpha satellite DNA and neocentromeric regions lack alphoid DNA altogether, consequently both lack CENP-B boxes (Gimelli et al. 2000). CENP-B is a highly conserved protein that is present under the kinetochore plates within the inner heterochromatin region of human autosomal and X chromosomes (Masumoto et al. 1989; Cooke et al. 1990). CENP-B contains a helix-loop-helix DNA binding domain at its N-terminus and a dimerisation domain at its C-terminus (Chan et al. 2005). Adjacent DNA-bound CENP-B proteins form dimers with one another, which brings neighbouring nucleosomes within close proximity and facilitates their condensation (Yoda et al. 1998). The presence of CENP-B is not absolutely essential for centromere function, as studies in CENP-B knockout mice, have not revealed an obvious phenotype other than a slight decrease in body weight and testis size (Hudson et al. 1998; Fowler et al. 2004). Despite this, the presence of CENP-B boxes and higher order alphoid DNA sequences are necessary for *de novo* human artificial chromosome formation and recruitment of functional centromeric proteins (Mejía et al. 2002; Masumoto et al. 2004). It is believed that CENP-B boxes signal recruitment of CENP-A, C and E, which in turn results in kinetochore assembly (Ohzeki et al. 2002; Irvine et al. 2004; Basu et al. 2005).

CENP-C is a constitutive protein that binds directly to the DNA through a DNA-binding domain which is necessary for recognition of and targeting to the centromeric region (Sugimoto et al. 1994; Yang et al. 1996; Politi et al. 2002). Studies have shown that CENP-B and CENP-C associate with the same types of alpha-satellite sequences, but in separate non-overlapping regions (Politi et al. 2002). CENP-C associates with active centromeres during the cell cycle through localisation at the inner kinetochore on mitotic chromosomes (Earnshaw et al. 1989; Saitoh et al. 1992; Sullivan and Schwartz 1995). It is thought that CENP-C cross-links CENP-A blocks together and through this mechanism, CENP-C plays a fundamental role in stabilising the kinetochore chromatin (Ribeiro et al. 2010). CENP-C alone is not sufficient for centromere formation, but is necessary for mitotic segregation and cell survival, and its disruption leads to irregular cellular and nuclear morphologies, delays in mitosis and formation of kinetochores, defective chromosome segregation and eventually mitotic arrest (Tomkiel et al. 1994; Gassmann et al. 2007; Ribeiro et al. 2010).

CENP-E accumulates during G2 and localises to active centromeres, specifically to the outermost fibrous corona region of the kinetochore and is discarded at the end of mitosis (Yen et al. 1992; Sullivan and Schwartz 1995). It is thought that CENP-E simultaneously binds microtubules and kinetochore bound checkpoint components and as such acts as a kinetochore attachment sensor (Mao et al. 2003). Depletion of CENP-E results in the misalignment of chromosomes during metaphase, leading to mitotic arrest (McEwen et al. 2001). CENP-F is a facultative kinetochore protein of the nuclear matrix; it peaks during G2 and mitosis and subsequently degrades after completion of mitosis. During G2, CENP-F is detected on the pre-kinetochore complex and during mitosis it associates with the kinetochores (Rattner et al. 1993;

Liao et al. 1995). CENP-F is known to interact with CENP-E to form a complex that is then targeted to the centromere through CENP-C. Studies have shown CENP-F depletion, results in a phenotype similar to CENP-E depletion: premature chromosome condensation, misalignment of chromosomes followed by cell death (Yang et al. 2005; Feng et al. 2006).

CENP-G is a constitutive centromeric protein that is present at the centromere during the cell cycle and associates with the nuclear matrix (He et al. 1998). Unlike CENP-A, C, E and F that localise only to active centromeres and neocentromeres, and CENP-B that localises only to regions containing CENP-B boxes, CENP-G localises to alpha satellite DNA sequences at inactive centromeres, and also to neocentromeres and the Y chromosome alpha satellite (which lack CENP-B boxes) (Gimelli et al. 2000). At active centromeres, CENP-H is found to colocalise with CENP-A and CENP-C both during interphase and metaphase (Sugata et al. 2000). CENP-H is also found outside the periphery of centromeric heterochromatin where CENP-B is present and on the outermost fibrous corona region of the kinetochore where CENP-E is located (Sugata et al. 2000). CENP-H is necessary for targeting CENP-C to the centromere and its disruption results in misaligned chromosomes, multipolar spindles and metaphase arrest (Fukagawa et al. 2001; Orthaus et al. 2006). CENP-I is a constitutive protein that is known to colocalise with CENP-A, C and H during the cell cycle. When absent, chromosomes become misaligned, the cell arrests at metaphase, and eventually exists mitosis without undergoing cytokinesis (Nishihashi et al. 2002).

Chromosomal passenger proteins localise at the centromeric region of the chromosome during metaphase, then dissociate from the centromere when the cell

enters anaphase and eventually localise to the midbody during cytokinesis (Mackay et al. 1998; Pohl and Jentsch 2008). Chromosomal passenger proteins are involved in the spindle assembly checkpoint, correction of microtubule-kinetochore attachment errors and the completion of cytokinesis (Vagnarelli and Earnshaw 2004). Examples of chromosomal passenger proteins include inner centromere protein (INCENP), Aurora B kinase, survivin, borealin and spindle checkpoint proteins (Chan et al. 2005; Musacchio and Salmon 2007).

INCENP localises to the inner centromere and spindle midzone during metaphase and anaphase, respectively. INCENP directly interacts with another passenger protein known as Aurora B kinase, enhancing its activity and targeting it to the centromere and spindle midzone (Vagnarelli and Earnshaw 2004). Aurora B kinase phosphorylates both CENP-A and H3 and is involved in spindle assembly checkpoint and cytokinesis. Silencing of Aurora B using RNA interference disrupts the kinetochore-microtubule attachment and spindle assembly checkpoint, thus dramatically reducing cell proliferation and viability (Girdler et al. 2006). Survivin and borealin are other chromosomal passenger proteins that associate with the kinetochore in metaphase, spindle midzone in anaphase and midbody during cytokinesis (Chan et al. 2005; Musacchio and Salmon 2007). Spindle checkpoint proteins include BubR1, Bub1, Bub3, Mad1 and Mad2 (Pidoux and Allshire 2000). These proteins ensure the integrity of kinetochore-microtubule attachment prior to proceeding to anaphase. In the absence of microtubule attachment, high concentrations of spindle checkpoint proteins localise to the kinetochore and block the function of cell-division cycle protein 20 (Cdc20). The attachment of microtubules to the kinetochore results in the disassembly of spindle checkpoint proteins, enabling

Cdc20 to activate the anaphase promoting complex (APC), which subsequently leads to sister chromatid separation, through cleavage of cohesion proteins (Uhlmann et al. 1999), and transition to anaphase (Musacchio and Salmon 2007).

1.4.5 Origins of Replication

The origins of replication are sequences where DNA replication is initiated. Some of these sequences are well characterised in prokaryotes and unicellular eukaryotes. For example, origins of replication in *Saccharomyces cerevisiae* are composed of ~150bp of AT rich units of autonomously replicating sequences that contain an essential 11bp consensus sequence that initiate the binding of the origin of recognition complex (ORC) for the commencement of replication (Gilbert 2001; Gerbi and Bielinsky 2002). However, the identification of origins of replication in multicellular eukaryotes has been more difficult, and less defined. In some organisms it is believed that any sequence of DNA can initiate replication (Gilbert 2001). It has been suggested that many potential initiation sites may exist in the multicellular eukaryotic genome, however the exact structure and sequence has not been well defined (Yu et al. 1998; Norio 2006). Recent studies show the presence of multiple origins of replication in different genomic loci as exemplified by the chicken *β-globin*, the mouse *HoxB* and the human fragile X mental retardation (*FMR1*) loci, suggesting that the replication of a particular region can be initiated by different origins of replication (Norio 2006; Gray et al. 2007). Although the locations and sequence specificity of the origins of replication remain controversial, many of the proteins involved in the initiation of replication are highly conserved from yeast to higher eukaryotes (e.g. single-strand binding proteins and DNA primase) (Gilbert 2001; Gerbi and Bielinsky 2002).

The origins of replication are generally thought to be evenly spaced along the chromosome to avoid incomplete DNA synthesis during the S phase of the cell cycle. For example, in *Xenopus laevis* eggs, origins of replication are spaced on average approximately every 9-12kb (Blow et al. 2001). Replication is initiated at sites distributed regularly along the DNA that do not display a consistent sequence similarity and appear to be random with regards to the DNA sequence (Gerbi and Bielinsky 2002). Studies have shown that human DNA fragments greater than ~15kb promote autonomous replication, suggesting that replication signals must occur on average every 10-15kb in the human genome (Heinzel et al. 1991). Another study revealed that a 2.7kb fragment of alpha DNA consensus was capable of autonomous replication, albeit at low efficiencies. Instead concatameric DNA sequences consisting of six repeat units of this 2.7kb consensus resulted in high efficiency of replication (Krysan et al. 1993). Thus, efficient autonomous replication may be directed by a higher order of DNA sequence architecture (Blow et al. 2001; Gilbert 2001).

1.4.6 Telomeres

Telomeres are short, tandem repeat units of TTAGGG noncoding DNA sequences maintained as a loop-like structure (ranging from ~2-10kb) at the ends of linear chromosomes that are essential for maintaining genomic integrity by protecting chromosome shortening during cell division. The telomere forms a loop structure of ~200bp that associates with telomere-binding proteins and forms a quadruplex structure (Shay 1999; Burge et al. 2006). This structure acts as a molecular cap to protect chromosome ends from exonuclease degradation, recombination and end-end fusion with other chromosomes (Moyzis et al. 1988; Farr et al. 1991; Neidle and Parkinson 2003). However, circular chromosomes such as prokaryotic chromosomes

(Bendich and Drlica 2000), ring chromosomes (Miller and Therman 2001) and *de novo* circular human artificial chromosomes (Ebersole et al. 2000) do not require telomeres for function and mitotic stability.

During DNA synthesis, DNA polymerase requires the binding of RNA primers to single stranded DNA to initiate the synthesis in the 5' to 3' direction. The unidirectional 5' to 3' DNA synthesis results in a leading strand and a lagging strand. On the leading strand, an RNA primer is only required at the start of the origin of replication and DNA synthesis takes place uninterrupted in the 5' to 3' direction. However, on the lagging strand, DNA synthesis takes place in a discontinuous fashion where Okazaki fragments are formed enabling synthesis in the 5' to 3' direction. The RNA primers bound to the newly synthesised complementary template to the lagging strand are then removed by RNA nuclease and replaced by DNA fragments by repair DNA polymerase, using the neighbouring Okazaki fragment DNA as a primer. Finally, DNA ligase seals the gaps between the DNA fragments by joining the 5' phosphate end to the 3' hydroxyl end of the next fragment. The "end-replication" problem occurs at the absolute 3' end of the lagging strand where the RNA primer is removed and no neighbouring Okazaki fragment is present to enable repair DNA polymerase to fill in the necessary DNA fragment. Thus, during each replication cycle, a portion of the telomere is shortened at the 5' end of the complementary strand to the lagging strand (Levy et al. 1992; Allsopp et al. 1995; Cerni 2000). To overcome this problem, the enzyme telomerase (a reverse transcriptase containing a central RNA component) is responsible for maintaining telomere lengths by appending units of TTAGGG to the telomeric linear ends of the lagging strand of chromosomes in a 5' to 3' direction. The telomerase is not present in all normal cell types, instead its

activity is mostly restricted to germ, stem and cancerous cells. In non-stem and non-cancerous somatic cells, telomere lengths are shortened during each DNA replication cycle, which is thought to be associated with replicative senescence or apoptosis (Moyzis et al. 1988; Neidle and Parkinson 2003; Gilson and Geli 2007). In contrast, stem cells such as pluripotent hESc and iPSc (Thomson et al. 1998; Takahashi et al. 2007) and cancerous cells such as embryonal carcinoma (Andrews et al. 2005) express high levels of telomerase. Telomerase activity has been proposed as one mechanism through which such cell types are capable of theoretical indefinite self-renewal.

1.4.7 Scaffold/Matrix Attachment Regions

Specific regions in the genome generally found close to promoters, enhancers and origins of replication that bind to the nuclear matrix are known as matrix attachment regions (MAR); sometimes also referred to as scaffold attachment regions (SAR). These sequences commonly referred to as S/MAR lack sequence conservation, however are usually ~70% AT rich and are thought to organise the genome into spatially distinct transcriptional regions by bringing regulatory regions within close proximity of matrix-bound DNA and RNA enzymatic complexes (Bode et al. 2000; Argyros et al. 2008; Wong et al. 2010). As S/MAR sequences are non-viral episomal retention elements, they have been proposed for use in designing non-integrating vectors. Indeed, studies have shown sustained long-term transgene expression through episomal vectors containing S/MAR elements (Argyros et al. 2008; Wong et al. 2010; Argyros et al. 2011). However, the exact mechanism by which they function is not fully understood.

1.5 Generation of Human Artificial Chromosomes

The eukaryotic artificial chromosome technology was first introduced when yeast artificial chromosomes (YAC) were constructed. In initial experiments, yeast genomic sequences were cloned onto a circular vector and tested to determine if they conferred to the deriving construct the capacity to segregate correctly. This approach allowed for the identification of *S. cereviasiae* centromeric sequences, and led to the assembly of YAC vectors, utilised for genome and sequencing analysis (Murray and Szostak 1983). Several human YAC libraries were successfully developed and used for genome mapping (Larin et al. 1991). However, YAC were known to be highly unstable and rearranged frequently. Bacterial and P1 artificial chromosomes (BAC and PAC) were later developed and allowed for establishment of stable genomic libraries for cloning and sequencing purposes in *E. coli* (Shizuya et al. 1992; Ioannou et al. 1994). There are two methods for constructing human artificial chromosomes: the "top-down" (engineered chromosomes) and "bottom-up" (*de novo* chromosomes) approach (Saffery and Choo 2002).

1.5.1 Top-Down Human Artificial Chromosomes

The top-down approach takes advantage of pre-existing chromosomes maintained in cells, whose size is reduced to a minimal unit that still guarantees correct replication and segregation (Farr et al. 1991; Barnett et al. 1993). Using homologous recombination and telomere associated chromosome fragmentation (TACF), mammalian chromosomes can be truncated using cloned telomeric DNA. Using a linear vector containing a selectable marker and few hundred base pairs of short tandem repeats of telomeric DNA sequences $(TTAGGG)_n$, fragmentation of

chromosome arms can be achieved following integration and generation of a new telomeric end (Farr et al. 1991; Farr et al. 1992; Itzhaki et al. 1992; Farr et al. 1995). TACF is the most commonly used method by which top-down artificial chromosomes are engineered. Using this technique, human X-derived (Farr et al. 1995; Mills et al. 1999), Y-derived (Heller et al. 1996) and 21-derived minichromosomes (Katoh et al. 2004), have been successfully engineered and transferred to mouse and immortalised human cells using microcell mediated chromosome transfer (MMCT). These minichromosomes show prolonged mitotic and transgene stability in both human and mouse backgrounds. More recent mouse and human studies on the 21-derived minichromosome (Katoh et al. 2004) will be discussed further in section 1.5.3.

Another method of top-down chromosome engineering utilises radiation-induced chromosome fragmentation. Examples of radiation-induced chromosome fragmentation include the isolation of a 5.5Mb minichromosome derived from chromosome 1 (Guiducci et al. 1999), and a circular marker chromosome formed by the fusion of chromosome 20 and p arm of chromosome 1 (Voet et al. 2001). Additionally, chromosome breakage by targeting heterologous DNA to pericentromeric regions has been used to form large derivative satellite-rich artificial chromosomes (SATAC). SATAC tend to be relatively large in size (~50-400Mb) (Basu and Willard 2005), such that they can be purified through fluorescence-activated cell sorting (FACS) (deJong et al. 1999; Csonka et al. 2000). They have been generated in both mouse and human cells and have shown up to 95% mitotic stability and transgene expression after 50 generations in culture (Csonka et al. 2000). Other groups have transferred SATAC into human mesenchymal stem cells, where

stable *RFP* reporter expression and correct segregation was achieved, without compromising the multipotent nature of the cells (Vanderbyl et al. 2004).

1.5.2 Bottom-Up Human Artificial Chromosomes

Contrary to the top-down method of chromosome engineering, the bottom-up approach brings together critical chromosomal elements required for the formation of a functional and stable *de novo* HAC in the cell (Harrington et al. 1997). The main requirement for *de novo* HAC formation is the presence of a large array of alpha satellite DNA sequences, which can be cloned into YAC, BAC or PAC vectors, which enables the formation of an active centromere (Saffery and Choo 2002). As *de novo* HAC are generally large (~1-10 Mb), circular and stable, telomeres are dispensable (Ebersole et al. 2000), and origins of replication occur naturally in any DNA fragment larger than ~10kb (Heinzel et al. 1991). The focus of this thesis (chapters 3 to 7) will be on *de novo* HAC generation using the bottom-up assembly approach.

The first-generation of bottom-up HAC was reported in human fibrosarcoma HT1080 cells by transfecting long synthetic arrays of alpha satellite DNA, telomeric repeats and sheared genomic DNA sequences. The resulting artificial minichromosomes were ~6-10Mb in size, bound centromere-specific proteins, and were mitotically stable for up to 6 months in the absence of selection (Harrington et al. 1997). Later studies established HAC by incorporating alpha satellite DNA sequences into YAC (Ikeno et al. 1998; Henning et al. 1999), BAC (Mejía et al. 2001) and PAC (Ebersole et al. 2000) followed by transfection into HT1080 cells (reviewed in Saffery and Choo 2002). Established HAC were composed of multimeric repeat units of input DNA, ranged from ~1-10Mb in size, contained an active centromere with functional

kinetochore and did not acquire host genomic sequences (Harrington et al. 1997; Ikeno et al. 1998; Henning et al. 1999; Ebersole et al. 2000; Mejía et al. 2001). Figure 1-3 shows a schematic diagram illustrating strategies for *de novo* HAC generation (image adapted from Saffery and Choo 2002).

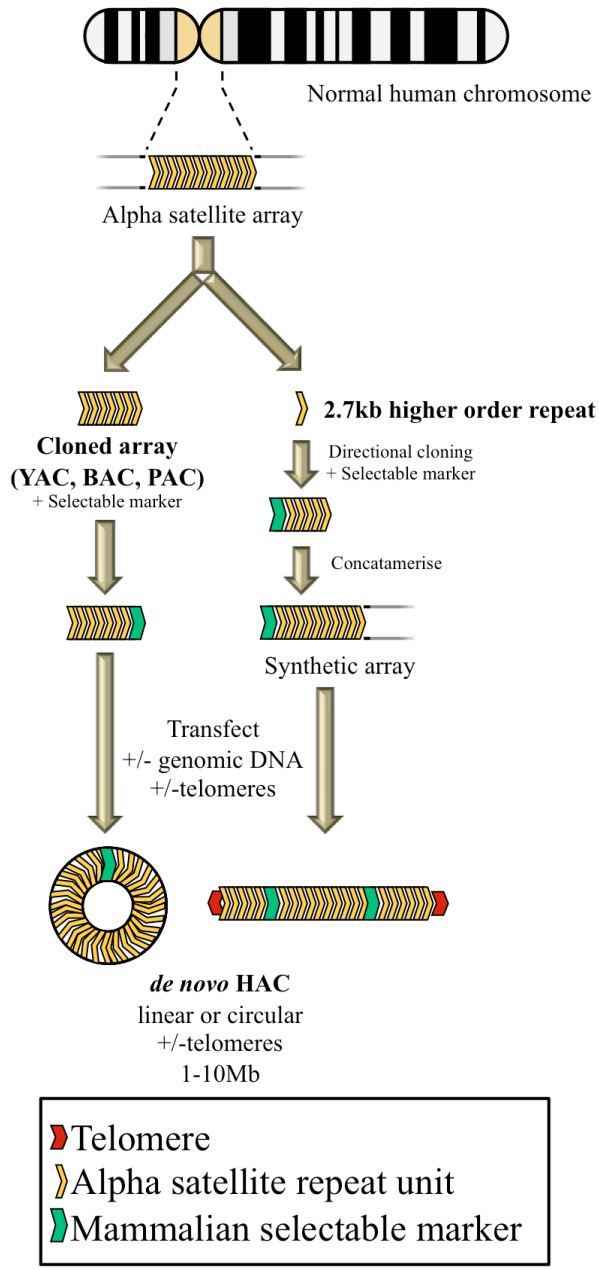

Figure 1-3 *De novo* human artificial chromosome formation
There are two strategies for producing HAC vectors: alpha satellite DNA can be cloned into YAC, BAC or PAC to form a circular HAC vector. As an alternative strategy, alphoid DNA can be synthesised using PCR to produce large concatemers forming a large linear HAC vector. The resulting HAC vector can carry telomeric regions and genomic DNA (image adapted from Saffery and Choo 2002).

As mentioned, the main requirement for bottom-up *de novo* HAC formation is the presence of an array of higher order alpha satellite DNA sequences (Harrington et al. 1997; Ikeno et al. 1998; Ebersole et al. 2000; Grimes et al. 2002; Mejía et al. 2002). The length and type of alphoid DNA influences the HAC formation efficiency. HAC have been formed in cells, following delivery, using input vectors containing as little as ~30kb of alphoid DNA with comparable stability to HAC with larger sized (>40kb) alphoid DNA. On the other hand, alphoid DNA stretches of ~10kb in size, within an input vector, were unable to form HAC following introduction into cells (Okamoto et al. 2007). Another study has shown that decreasing the size of alpha satellite DNA from ~80 to ~35kb in a PAC vector, reduced the HAC formation efficiency (Grimes et al. 2002). Furthermore, different alpha satellite sequences have been shown to have different HAC formation efficiencies. In general, 17α satellite DNA has shown to have a higher *de novo* HAC formation potential, as compared to other alpha satellite arrays. HAC constructs containing 17α satellite DNA have shown 20 times higher *de novo* formation efficiency when compared to constructs holding Yα satellite DNA (Grimes et al. 2002; Mejía et al. 2002).

The presence of CENP-B boxes in the sequence of 17α satellite DNA, while absent in Yα satellite DNA (Warburton et al. 1993), may be a contributing factor resulting in the difference in HAC formation efficiency. In accordance to these findings, "bottom-up" *de novo* HAC cannot be generated from neocentromeric DNA, as they lack alphoid DNA sequences and CENP-B boxes. This indicates that at the DNA level, neocentromeric DNA are not equivalent to alpha satellite DNA, as they do not support *de novo* centromere formation (Saffery et al. 2001; Willard 2001). Studies have shown that YAC containing 21α satellite DNA arrays, which lack CENP-B boxes, fail

to establish *de novo* HAC (Ikeno et al. 1998). Also, vectors containing mutations in CENP-B box sequences in the 21α satellite DNA fail to establish HAC (Ohzeki et al. 2002). Other studies have shown that the addition of extra CENP-B boxes into alpha satellite sequences improved HAC formation efficiency (Basu et al. 2005), while decreasing the frequency of CENP-B boxes reduced HAC formation efficiency (Okamoto et al. 2007). Others have shown HAC formation, albeit at low frequencies, using Yα (Grimes et al. 2002) and 22α (Kouprina et al. 2003) satellite sequences (which lack CENP-B boxes), suggesting that while CENP-B boxes improve HAC formation efficiency, they are not absolutely essential for *de novo* HAC formation. As most *de novo* HAC are most likely circular (Mejía et al. 2001), telomeric sequences are dispensable (Ebersole et al. 2000; Grimes et al. 2002; Mejía et al. 2002). However, removal of telomeric repeats from linear artificial constructs results in a significant reduction in the efficiency of artificial chromosome formation (Ebersole et al. 2000).

1.5.3 Gene Expression in Human Artificial Chromosome Studies

Various groups have demonstrated successful gene expression under the regulation of endogenous promoters in different HAC studies. For example, studies have used YAC (~320kb) and BAC (~275-300kb) vectors containing the cystic fibrosis transmembrane conductance regulator (*CFTR*) gene, including upstream regulatory elements, to establish gene-expressing minichromosomes in CHO (Chinese hamster ovary) and Fisher rat thyroid cells respectively (Auriche et al. 2002; Auriche et al. 2010). *De novo* HAC vectors containing ~220kb of 17 alpha satellite DNA carrying the hypoxanthine-guanine phosphoribosyltransferase (*HPRT*) locus (~140kb) have successfully shown genetic complementation of human *HPRT* deficient HT1080 cells

(Mejía et al. 2001). In another study, co-transfection of two PAC vectors, one containing ~70kb of 21 alpha satellite DNA and the other carrying the *HPRT* locus was successful at forming a single, gene-expressing HAC, and complemented the deficiency in human *HPRT* deficient HT1080 cells (Grimes et al. 2001). In more recent studies, Kotzamanis et al. (2005) and Moralli et al. (2006) have demonstrated complementation of *HPRT* deficiency in HT1080 cells. These studies successfully utilised the high mitotic stability and gene expression of *de novo* HAC to complement genetic deficiency in tumour-derived HT1080 cells, suggesting the potential use of *de novo* HAC for use in gene therapy studies.

Using the bottom-up approach, Ikeno et al. (2002) constructed a HAC vector in HT1080 cells containing ~90kb of alpha satellite DNA (α21- type I) and ~180kb of genomic DNA carrying the guanosine triphosphate cyclohydrolase 1 (*GCH1*), and its endogenous regulatory elements (*GCH1*-HAC). In another study by the same group, Suzuki et al. (2006) constructed a bottom-up linear HAC in HT1080 cells containing ~80kb of alpha satellite DNA (α21- type I), ~150kb of the human globin cluster and telomeric sequences (globin-HAC). Both the *GCH1*-HAC and globin-HAC expressed the gene of interest and were highly stable in the absence of selection in HT1080 cells, showing 0.5% and 0.3% daily HAC loss respectively. Both the circular *GCH1*-HAC and linear globin-HAC were transferred into mESc using MMCT. In the mouse background, the circular HAC showed 0.4-0.6% daily loss, while the linear HAC showed a higher daily loss rate of 1.0-3.6%. Chimeric HAC-containing mice were successfully produced from both the *GCH1*-HAC and globin-HAC; in addition, germline transmission of the globin-HAC was demonstrated (Suzuki et al. 2006b).

As previously mentioned, Katoh et al. (2004) engineered a top-down HAC derived from human chromosome 21 containing a functional centromere, telomeres and minimal DNA elements for selection and recombination. In separate studies, the *EGFP* reporter (Katoh et al. 2004) and Erythropoietin (*EPO*) expression cassette (Kakeda et al. 2005) were targeted into the *loxP* site on the 21-derived minichromosome and delivered into human cells using MMCT. The resulting minichromosome was capable of stable transgene expression in human HT1080 (Katoh et al. 2004), primary fibroblasts (Kakeda et al. 2005), immortalised mesenchymal stem cells (Ren et al. 2005) and haematopoietic cells (Yamada et al. 2006). Using the same 21-derived minichromosome, their group has more recently constructed two additional minichromosomes, one containing the tumour suppressor *p53* gene (*p53*-HAC) (Kazuki et al. 2008) and the other containing the entire 2.4Mb human dystrophin gene (DYS-HAC) (Hoshiya et al. 2009; Kazuki et al. 2010).

Using MMCT, the *p53*-HAC was introduced into wild-type mouse embryonic and germ stem cells where chimeras were successfully produced showing tissue-specific transcription of human *p53*. Functional restoration of *p53* deficiency was achieved in *p53*-/- mouse germ cells, however inert rearrangements had occurred in the HAC structure, which did not affect *p53* expression. The HAC-containing *p53*-/- mouse germ cells were able to differentiate into various cell types through teratoma formation; however, coat colour chimeras were not able to form, possibly due to the presence of chromosomal abnormalities in the starting *p53*-/- mouse germ stem cell line (Kazuki et al. 2008).

A discussed condition potentially suitable for HAC-based gene therapy is the treatment of Duchenne muscular dystrophy (DMD), which is caused by recessive mutations and deletions in the dystrophin gene located on the X chromosome at Xp21.2. As the dystrophin gene is the largest known gene in the human genome (2.4Mb total size; 14kb of cDNA), the delivery of the dystrophin genomic locus into cells is unattainable unless delivered as part of a HAC vector (Wang et al. 2000; Murakami et al. 2003; Ren et al. 2006; Kazuki et al. 2010). As mentioned previously, Hoshiya et al. (2009) constructed a human artificial chromosome carrying the entire human dystrophin gene (DYS-HAC). The DYS-HAC was generated using Cre-*loxP* chromosomal translocation. First, a *loxP* site was targeted to the proximal locus of the dystrophin gene on the short arm of human chromosome X carried by the recombination-proficient chicken DT40 cells. Next, the rest of the genes distal to the dystophin gene were removed using telomere associated chromosome truncation. The truncated *loxP*-containing chromosome X was then moved into Chinese hamster ovary (CHO) cells containing the 21-derived minichromosome (Katoh et al. 2004) using MMCT. Through Cre-*loxP* recombination, the entire dystrophin gene (2.4Mb) was translocated onto the 21-derived minichromosome, which also contained a *loxP* site. The resulting DYS-HAC was then transferred into mouse ES and human immortalised mesenchymal stem cells using MMCT (Hoshiya et al. 2009). Chimeric mice were successfully produced from the DYS-HAC-containing mouse ES cells and expressed tissue-specific human dystrophin isoforms in the intestine, heart and skeletal muscle. However, germline transmission of the DYS-HAC was not observed. The human immortalised mesenchymal stem cells containing the DYS-HAC were passaged in culture for 100 generations and showed no signs of HAC loss, gene silencing or rearrangements during this period (Hoshiya et al. 2009).

In a more recent study, the DYS-HAC was successfully transferred into mouse iPSc derived from the *mdx* dystrophic mouse model and human fibroblasts derived from a DMD patient with a large deletion (exons 4-43) in the dystrophin gene. The patient-derived DMD fibroblasts containing the DYS-HAC were subsequently reprogrammed using lentiviral vectors carrying *Klf4*, *Sox2*, *Oct4* and *c-Myc* transcription factors. The chimeric mice showed the presence of the DYS-HAC in ~50% of the analysed cells, as expected by the pattern of coat colour chimerism. Similar to the Hoshiya et al. (2009) study, tissue-specific expression of human dystrophin isoforms were detected in chimeric heart, skeletal muscle and the brain. In the human fibroblast-derived iPSc, the DYS-HAC was maintained as an independent chromosome without loss or integration after 4 months of culturing under no selection pressure. Teratomas were formed from the HAC-containing iPSc where dystrophin expression was detected in muscle-like tissues (Kazuki et al. 2010). However, it must be noted that Kazuki et al. (2010) were unsuccessful at transferring their HAC construct into hESc and hiPSc due to low efficiencies of MMCT-mediated HAC delivery and difficulties in selecting stable clones (Park 2010).

Taken together, these results highlighted that HAC remain stable for extended periods in both mouse and human cells, show teratoma-derived "tissue-specific" expression of the desired transgene, and do not interfere with developmental processes, as demonstrated by chimera and teratoma formation. Furthermore, HAC can successfully complement dystrophin deficiency in patient-derived fibroblast cells, which can then be reprogrammed into a pluripotent state. Thus, these studies suggested that synergistic utilisation of gene-expressing HAC in stem and pluripotent cells can be used for combined cell and gene therapy applications (Park 2010).

1.5.4 Human Artificial Chromosome Delivery into Cells

Until recently, large DNA vectors, containing alpha satellite centromeric sequences, have been introduced into different cell lines through lipofection. Lipofection is generally inefficient in the delivery of large naked DNA (~10^{-6}), and often results in the shearing and degradation of the input HAC DNA vector (Marschall et al. 1999; Moralli et al. 2006). As such, successful HAC generation in human studies has been mostly limited to the tumour-derived human fibrosarcoma HT1080 cell line (Heller et al. 1996; Harrington et al. 1997; Ikeno et al. 1998; Ebersole et al. 2000; Grimes et al. 2002; Mejía et al. 2002; Katoh et al. 2004). The reason for this is not fully understood, but it may be attributed to the relative ease with which HT1080 cells can be transfected and high efficiency of stable clone selection (Harrington et al. 1997). Furthermore, as HT1080 cells contain an activated *N-ras* oncogene (Paterson et al. 1987), the presence of extra-chromosomal elements may be more permissible when compared to other cell lines. At low passages, pseudodiploidy is observed in HT1080 cells (its modal karyotype is 46 and ranges from 44 to 48) (Rasheed et al. 1974), while at higher passages further chromosomal abnormalities can accumulate (Katoh et al. 2004).

As mentioned, whole chromosomes (including established HAC) can be transferred to different cell lines via microcell mediated chromosome transfer (MMCT). However, this procedure also suffers from extremely low delivery efficiencies (~10^{-7}) and can lead to rearrangements in the HAC structure (Marschall et al. 1999; Kazuki et al. 2008). As discussed above, recent studies have been successful at establishing MMCT delivered HAC in mouse embryonic stem cells (Shen et al. 1997; Shen et al. 2000;

Paulis et al. 2007; Kazuki et al. 2008), mouse germ stem cells (Kazuki et al. 2008), human immortalised mesenchymal stem cells (Ren et al. 2005; Hoshiya et al. 2009) and patient-specific fibroblasts, which were subsequently reprogrammed into a pluripotent state (Kazuki et al. 2010). However, previous to this study, HAC establishment in human primary cell lines, specifically in human pluripotent cells (hESc and hiPSc) has been unsuccessful due to poor DNA delivery efficiency and difficulties in stable clone selection (Ludwig et al. 2006; Yates and Daley 2006; Kazuki et al. 2010; Ardehali et al. 2011; Moore et al. 2011).

In a study by our group, Moralli et al. (2006) took advantage of the ability of the herpes simplex virus type 1 (HSV-1) amplicons to deliver large DNA constructs (up to 152kb) at high frequencies (up to 100%) into a range of different human cell types including HT1080, G16-9 (glioma), 293 (kidney), BeFA (primary keratinocyte), MRC-5V2 (lung fibroblast) and MRC5 (primary cells, derived from foetal lung). HAC vectors containing a large stretch of alpha satellite DNA and the necessary HSV-1 elements were packaged into HSV-1 amplicons and different cultured cell types were transduced by the infectious particles. FISH with HAC-specific and alpha satellite probes and anti-centromeric indirect-immunostaining revealed HAC formation and the presence of an active centromere on the *de novo* HSV-HAC in several different human cell lines (Moralli et al. 2006). The development of the HSV-HAC technology was a significant step forward in *de novo* HAC studies, which subsequently paved the way for implementation of this technology in pluripotent hESc.

1.5.5 Herpes Simplex Virus Type 1 (HSV-1) Amplicon System

The herpes simplex virus type 1 (HSV-1) is a member of *Herpesviridae*, a family of DNA viruses. HSV-1 has tropism to the peripheral nervous system where it establishes latent infection, and is most commonly known for causing cold sores (Jacobs et al. 1999a, b). HSV-1 has a linear double stranded DNA genome size of 152kb (Martin et al. 1991), consisting of 94 putative open reading frames (Rajcani et al. 2004). There are two types of HSV-1 vectors: recombinant and amplicon. Recombinant vectors contain all the viral genes and can accommodate only few genes of interest. While, the amplicon vectors contain minimal *cis*-acting sequences that are necessary for replication (origin of replication; *OriS*) and packaging (packaging/ cleavage signal; *Pac*) in the presence of helper elements in *trans* (Saeki et al. 2001; Wade-Martins et al. 2001; Saeki et al. 2003). Only the helper virus-free HSV-1 amplicon vector system will be described and utilised in this thesis.

HSV-1 amplicons are produced by co-transfecting the helper BAC fHSVΔpacΔ27 0+ (containing the HSV-1 genome) and pEBHICP27 (containing the essential transcriptional regulator for viral replication *ICP27*) vectors, along with the desired amplicon vector (containing *OriS* and *Pac*) (e.g. HSV-HAC vector) into African green monkey cells (Vero 2-2) (Figure 1-5). The HSV-1 genome (fHSVΔpacΔ27 0+) cannot be packaged into HSV-1 amplicons to produce wild-type HSV-1 viruses as it lacks the packaging/cleaving signal (*Pac*), the origin of replication (*OriS*) and the essential immediate early gene for viral replication (*ICP27*). Moreover, the total size of fHSVΔpacΔ27 0+ has been increased using "stuffer" (*ICP0*) elements, so that its size (178kb) is larger than the maximum capacity of the viral capsid (Saeki et al.

2001; Saeki et al. 2003). Thus, fHSVΔpacΔ27 0+ and pEBHICP27 vectors provide all the necessary genes that are required for packaging of the desired amplicon vector in *trans*, while ensuring that no wild-type viral particles are packaged into the HSV-1 virions. During packaging, the amplicon vector undergoes a concatamerisation process through a head-to-tail rolling-circle DNA replication, after which, the final concatemeric DNA (~152kb in size) is cleaved and packed into HSV-1 virions (Figure 1-4) (Saeki et al. 2001; Saeki et al. 2003). The genome in the HSV-1 virion is known to be linear, however after infection, end joining is believed to occur to form a circular genome (Garber et al. 1993; Deshmane et al. 1995; Sandri-Goldin 2003).

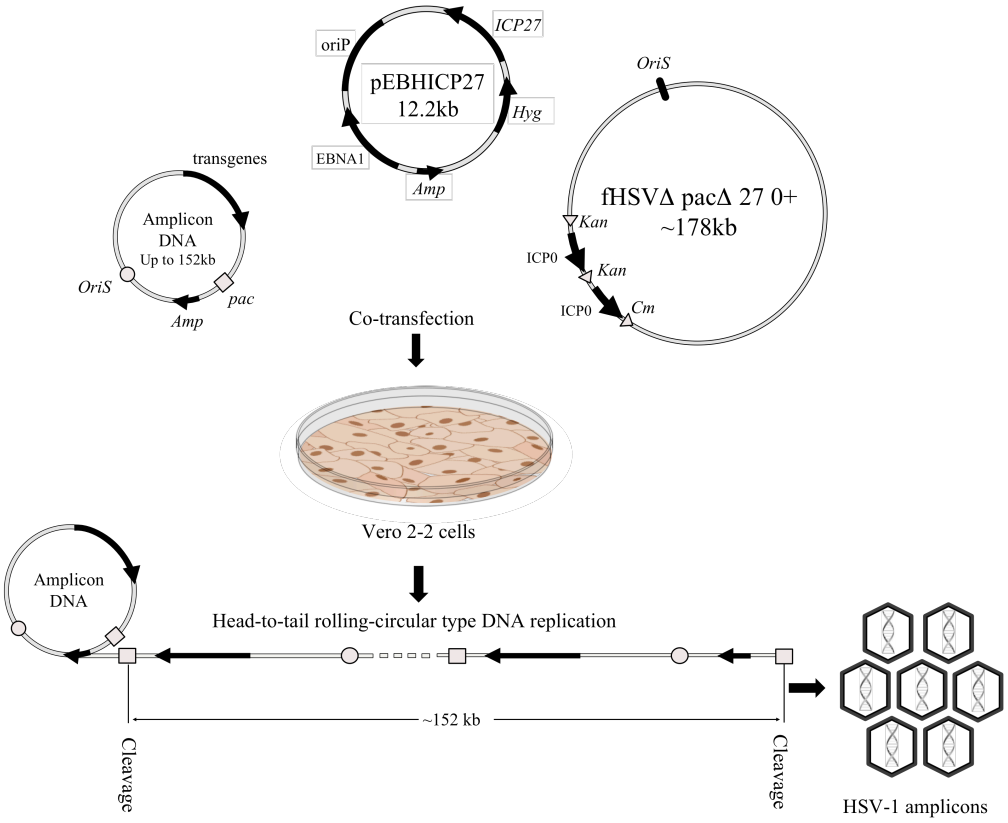

Figure 1-4 Schematic diagram of HSV-1 amplicon packaging system
For amplicon preparation, Vero 2-2 cells are co-transfected with the desired amplicon vector and two other helper constructs (fHSVΔpacΔ27 0+ and pEBHICP27). The amplicon vector (up to 152kb in size) contains the necessary minimal *cis*-acting sequences that are necessary for replication (origin of replication; *OriS*) and packaging (packaging/ cleavage signal; *Pac*). In *trans*, the fHSVΔpacΔ27 0+ (178kb) and pEBHICP27 (12.2kb) provide the essential HSV-1 genes and the viral replication gene *ICP27*, respectively. The amplicon vector undergoes a head-to-tail rolling-circle

DNA replication concatamerisation, after which, the final concatemeric DNA is cleaved and packed into HSV-1 virions (image adapted from Saeki et al. 2003).

After the packaging of the desired construct (e.g HAC vector) is completed, the Vero 2-2 cells are sonicated to release the containing amplicons. The amplicons are then concentrated and subsequently titrated using the glioma cell line (G16-9) to determine the number of infectious units per set volume. The appropriate amount of amplicon (expressed in units of multiplicity of infection, MOI) is then used to transduce the desired cell types (HT1080 and HUES-2 cells in this thesis). Stable clones carrying the transgene of interest are then obtained by applying drug selection, and finally screened using fluorescence *in situ* hybridisation (FISH) (Figure 1-5).

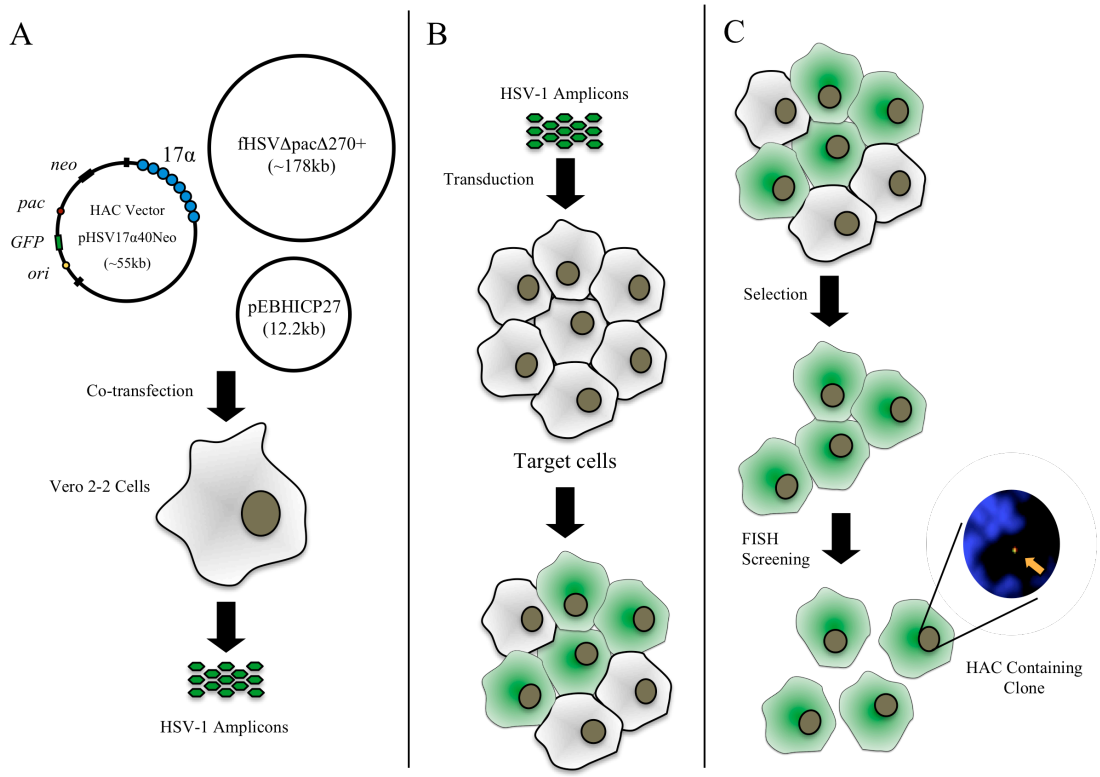

Figure 1-5 Generation of *de novo* HAC using HSV-1 amplicons
The desired HAC vector (e.g. pHSV17α40Neo) is co-transfected with fHSVΔpacΔ27 0+ and pEBHICP27 into Vero 2-2 cells to produce HSV-1 amplicons (A). HSV-1 amplicons are then used to transduce target cells (B). Through drug selection, stable clones are isolated and screened using FISH to identify HAC (C).

Due to lack of viral genes, HSV-1 amplicons cause minimal immunogenic and cytotoxic side effects post-infection (Costantini et al. 1999; Olschowka et al. 2003; Suzuki et al. 2007). HSV-1 amplicons have the ability to transduce a wide range of cell types across different species and can infect both dividing and non-dividing cells at high efficiencies. Furthermore, HSV-1 amplicons have a large transgene capacity of up to 152kb, which enables the accommodation of nearly 95% of the human genomic loci. Thus, the versatility and high transduction efficiency of HSV-1 amplicons, in conjunction with its large genome size, has made it a promising gene delivery tool for transgenic, and especially gene therapy studies (Sena-Esteves et al. 2000; Hibbitt and Wade-Martins 2006; Suzuki et al. 2007).

Indeed, HSV-1 amplicons have been used in a number of animal gene therapy studies in the case of Parkinson's disease (Burton et al. 2003), chronic pain (Goss et al. 2001; Srinivasan et al. 2008) and spinal cord injury pain (Liu et al. 2004a). Out of approximately 1700 gene therapy clinical trials, 56 involve the use of HSV-1 amplicons (Edelstein et al. 2007; Sheridan 2011). Examples include the treatment of chronic pain (Glorioso and Fink 2009; Yeomans and Wilson 2009) and use of oncolytic HSV-1 amplicons for the treatment of brain tumours (Kohno et al. 2007; Nawa et al. 2008). Furthermore, HSV-1 amplicons have been utilised *in vitro* to deliver complete genomic loci along with associated endogenous regulatory elements into human and mouse cells. Wade-Martins et al. (2001) used the HSV-1 DNA delivery system to deliver the complete hypoxanthine phosphoribosyltransferase (*HPRT*) locus in *HPRT* deficient mouse and human cells using a BAC backbone. The same system was later used to complement low-density lipoprotein receptor (*LDLR*) deficiency in both *LDLR* deficient mouse cells and human fibroblasts obtained from

patients with mutations in the *LDLR* gene (Wade-Martins et al. 2001; Wade-Martins et al. 2003). The HSV-BAC systems in both these studies were mitotically retained by episomal retention sequences, Epstein-Barr nuclear antigen-1 (*EBNA-1*), a candidate oncogene (Schulz and Cordes 2009). Substituting the EBNA episomal retention elements with an array of alpha satellite sequences, Moralli et al. (2006) were able to obtain a mitotically stable, *HPRT*-expressing human artificial chromosome, which was able to complement *HPRT* deficiency in *HPRT* deficient HT1080 cells.

1.6 Project Outline

The development of a safe and stable gene-expressing vector is of importance for the field of gene therapy. As previously described, human artificial chromosomes (HAC) have shown potential as an alternative non-integrating gene therapy system in tumour-derived cell lines. The objective of this thesis was to investigate the feasibility of establishing HAC in pluripotent human embryonic stem cells, analyse their stability and gene expression in culture. HAC studies in hESc were undertaken with the aim of using the HAC gene expression system for genetic manipulation of pluripotent cells, and potentially translating this technology toward patient-specific *ex vivo* gene therapy applications. This report is the first study to have studied the efficacy of HAC as a gene expression system in hESc.

This work initially involved investigating the size and type of alphoid DNA template incorporated into the HAC vector, which would be required for efficient generation of HAC in human cells, together with identification of cellular factors affecting HAC stability. With this aim, three candidate HAC vectors, containing different sized 17α satellite DNA templates, were constructed for introduction into hESc. The ability of

these vectors to form HAC was initially verified by introducing each of the vectors into the control cell line HT1080 and screening stable clones by FISH for the presence of HAC. The optimal conditions for HSV-1 mediated delivery of input HAC vector DNA to hESc were determined, as well as selection of stable clones. Each HAC vector was introduced into HUES-2 hESc line, and several putative stable clones were isolated. Approximately half of the isolated clones were shown to contain HAC in ~10-70% of the analysed metaphases. The HAC contained an active centromere, were mitotically stable and showed stable gene expression for 90 days in the absence of selection. The HAC-containing hESc clones were pluripotent and capable of formation of the three embryonic germ layers, neuronal differentiation and teratoma formation.

Chapter 2. Materials and Methods

2.1 Suppliers

Unless otherwise stated, all chemicals were purchased from Sigma-Aldrich, all tissue culture reagents from Invitrogen (Gibco), all tissue culture dishes from VWR. Restriction enzymes were obtained from New England Biolabs (NEB). Oligonucleotides were synthesised by Eurofins MWG Operon. Phosphate buffered saline (PBS) solution was purchased from PAA.

2.2 Solutions and Media

KCM Buffer

120 mM KCl, 0.02 M NaCl, 0.01 M Tris-HCl (pH 8.0), 0.5 M EDTA (pH 8.0), 0.1% (v/v) Triton X-100.

Luria – Bertani Broth (LB)

LB medium and agar were both prepared using Sigma capsules in accordance with the manufacturer's protocol.

Super Optimal Broth with Catabolite Repression (SOC)

Super optimal broth (SOB) medium (Hanahan's Broth) (Sigma) was prepared according to the manufacturer's instructions and then glucose was added to a final concentration of 20 mM.

20×Saline-Sodium Citrate (SSC)

3 M NaCl, 0.3 M $C_6H_5Na_3O*2H_2O$ (trisodium citrate 2 hydrate).

50×Tris-Acetate-EDTA (TAE)

40 mM Tris base, 20 mM glacial acetic acid, 1 mM EDTA (pH 8.0).

5×Tris-Borate-EDTA (TBE)

450 mM Tris base, 450 mM Orthoboric Acid, 10 mM EDTA (pH 8.0).

2.3 Bacterial Culture and Plasmid Preparation

Vectors of interest were introduced into DH10B electrocompetent *E. coli* (Invitrogen) (unless otherwise stated) using electroporation at 2.0kV, 200Ω and 25μF in a gene pulser cuvette with 0.1cm electrode gap (Bio-Rad), and streaked onto Luria-Bertani (LB) agar plates containing the appropriate antibiotic. Antibiotic selection was carried out at 100μg/ml of ampicillin, 33μg/ml of kanamycin and 20μg/ml of chloramphenicol. Bacterial colonies were picked and grown in LB broth, containing the appropriate antibiotics, overnight at 37ºC. Plasmid DNA was extracted using the Qiagen miniprep or Qiagen maxiprep kits, according to the manufacturer's instructions, and resuspended in TE (10mM Tris-HCl, 1mM EDTA) buffer. The plasmids were characterised by diagnostic digestion with appropriate restriction enzymes (NEB), following the supplier's instructions.

2.4 Restriction Enzyme Digestion

PAC, BAC and plasmid DNA was digested in a total volume of 10-20µl containing 1× of the appropriate digestion buffer, and if necessary 1× BSA, as described by the manufacturer. For each µg of DNA, 2-5 units of the desired enzyme was added to the mix. In cases where the NaCl concentration in the buffer was in excess of 50mM, then 5mM spermidine (Sigma) was added to the reaction mix, otherwise 2mM spermidine was used. Samples were incubated for at least 1 and up to 16 hours at the optimal digestion temperature as described by the manufacturer's instructions.

2.5 Linearised Vector Dephosphorylation and Ligation

50ng of the desired linearised vector DNA was dephosphorylated using 1 unit of shrimp alkaline phosphatase (Roche) in 1× dephosphorylation buffer for 1 hour at 37ºC, followed by heat inactivation at 65ºC for 15 minutes. 150ng of the desired insert was ligated to the dephosphorylated vector using T4 DNA ligase (NEB) and 1× T4 DNA ligase reaction buffer and incubated overnight at 16°C.

2.6 Agarose Gel Electrophoresis

DNA fragments were run on a 1% (w/v) agarose gel in 1×TAE. Samples were loaded with 6× loading buffer (NEB) and a 1kb ladder (NEB) was used as a DNA size marker. Gels were run at ~9-10 V/cm, and depending on the size of expected bands for 20-60 minutes. Gels were stained for 20 minutes in water containing 0.5µg/ml ethidium bromide and then visualised on a UV transilluminator (Bio Rad). Images were acquired using the AlphaView software version 3.0 (Alpha Innotech).

2.7 Pulsed Field Gel Electrophoresis (PFGE)

Pulsed field gel electrophoresis (PFGE) was performed on a CHEF Mapper machine (Bio-Rad) using 1% (w/v) SeaKem GTG agarose (Lonza) gels and run in 0.5×TBE at 14ºC. The gels were run for 15 hours at ~6 V/cm, and used an initial pulse time of 0.2s and a final pulse time of 22s. The λ concatemer ladder (48.5kb to 1018.5kb) (NEB) was used to determine the size of fragments. Gels were stained for 60 minutes in water containing 0.5µg/ml ethidium bromide and then visualised on a UV transilluminator (Bio Rad). Images were acquired using the AlphaView software version 3.0 (Alpha Innotech).

2.8 DNA Purification from Agarose Gels

DNA purification from Agarose gels was performed using QIAquick gel extraction Kit (Qiagen) according to the manufacturer's instructions. Extracted gel fragments were melted at 55ºC and the DNA was eluted in 30µl of elution buffer.

2.9 HAC and HSV-HAC Vectors

In this thesis, vectors containing an array of alpha satellite DNA will be referred to as HAC vectors. While vectors containing essential *cis*-acting HSV-1 elements (HSV-1 origin of replication and packaging signal) in addition to the alpha satellite DNA, will be referred to as HSV-HAC vectors. The vectors constructed and used for transduction/transfection analysis and HAC formation in HT1080 and HUES-2 cells are listed in Table 2-1. pHGNeo4, pHGBsd and pHGPuro are HSV-1 vectors that were mostly used as controls and are approximately 8kb in size. pHSV21αNeo,

pHSV17α40Neo, pHSV17α60Neo, pHSV17α100Neo are HSV-HAC vectors that contain both alpha satellite DNA and essential HSV-1 elements ranging from ~55 to 115kb in size. The hBAC495J24 and pJM2256 are HAC vectors that contain 17α satellite DNA but lack HSV-1 elements.

Table 2-1 List of vectors and corresponding features used in this study

Vector	Type of Vector	Size	Reporter Gene (Promoter)	Mammalian Resistance Gene (Promoter)	Bacterial Resistance Gene
pHGNeo4	HSV -1 amplicon, pSG80A-HG plasmid backbone	8.0kb	*GFP* (HSV-1 I/E)	*Neo* (SV40)	*Amp, Kan*
pHGBsd (Chan 2011)	HSV-1 amplicon, pSG80A-HG plasmid backbone	7.8kb	*RFP* (HSV-1 I/E)	*Bsr* (UbC)	*Amp*
pHGPuro (Chan 2011)	HSV-1 amplicon, pSG80A-HG plasmid backbone	7.7kb	*GFP* (HSV-1 I/E)	*Pac (Puro)* (SV40)	*Amp*
pHSV21αNeo (Moralli et al. 2006)	HSV-HAC Vector; pBeloBAC11 backbone	~73kb (~60kb of 21α satellite DNA)	*GFP* (HSV-1 I/E)	*Neo* (SV40)	*Amp, Kan*
pHSV17α40Neo	HSV-HAC Vector; pBeloBAC11 backbone	~ 55kb (~40kb of 17α satellite DNA)	*GFP* (HSV-1 I/E)	*Neo* (SV40)	*Amp, Kan*
pHSV17α60Neo	HSV-HAC Vector; pCYPAC2 backbone	~77kb (~60kb of 17α satellite DNA)	*GFP* (HSV-1 I/E)	*Neo* (SV40)	*Amp, Kan*
pHSV17α100Neo	HSV-HAC Vector; pBeloBAC11 backbone	~115kb (~100kb of 17α satellite DNA)	*GFP* (HSV-1 I/E)	*Neo* (SV40)	*Amp, Kan*
pJM2256-GFP (Mejía et al. 2002, modified by Dr Daniela Moralli)	HAC Vector; pBeloBAC11 backbone	~240kb (~220kb of 17α satellite DNA)	*GFP* (PGK)	*Neo* (SV40)	*Amp, Kan, Cm*
hBAC495J24 (Kim et al. 1996)	HAC Vector; pBeloBAC11 backbone	~227kb (~220kb of 17α satellite DNA)	-	-	*Cm*
fHSVΔpac Δ27 0+ (Saeki et al. 2001)	Modified HSV-1 genome for producing HSV-1 amplicons	~178kb	-	-	*Cm, Kan*
pEBHICP27 (Saeki et al. 2001)	For producing HSV-1 amplicons	12.2kb	-	-	*Amp*
pBeloBAC11 (Kim et al. 1996)	For BAC construction	7.5kb	-	-	*Amp*
pCYPAC2 (Pierce et al. 1992)	For PAC construction	18.8kb	-	-	*Kan*

2.10 Vector Construction and Maps

Figure 2-1 shows schematic vector maps of pBeloBAC11 (A) and hBAC495J24 (B). The vector pBeloBAC11 is an *E. coli* cloning plasmid devised for use in the construction of bacterial artificial chromosomes (BAC) (Kim et al. 1996). Up to ~300kb of DNA can be cloned into pBeloBAC11 and is maintained as a single copy. The vector contains an Ori2 (OriS) origin of replication and also encodes the SopA and SopB, which act at SopC ensuring after cell division, each daughter cell receives a copy of the plasmid (Mori et al. 1986). RepE is the initiation factor that mediates the assembly of the replication complex at Ori2 (Imber et al. 1983). A *loxP* site is also present on the vector for Cre mediated *loxP* recombination. hBAC495J24 is a BAC vector (pBeloBAC11 backbone) containing approximately 220kb of genomic 17α satellite DNA. pJM2256 is a HAC vector derived from hBAC495J4 that has been modified to accommodate a retrofitting cassette, containing a CMV-*lacZ* reporter, selectable markers (*Neo* and *Puro* resistance genes), telomere and stuffer sequences (Figure 2-2) (Mejía et al. 2002). A second derivative vector, pJM2256-GFP, has been further modified by adding a cassette for the constitutive expression of the green fluorescent protein (*GFP*) gene under control of the phosphoglycerate kinase (PGK) promoter (vector construction by Dr Daniela Moralli).

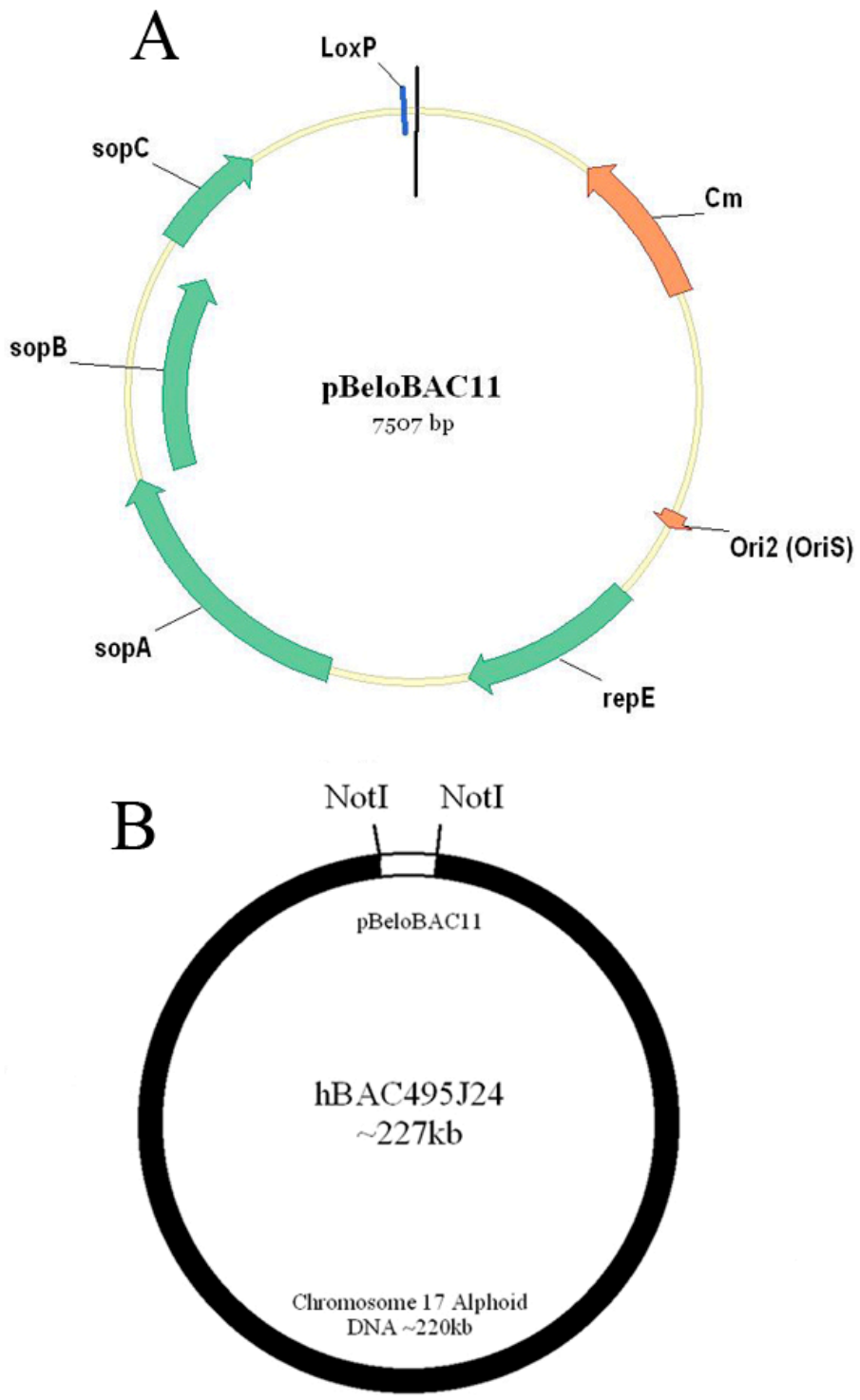

Figure 2-1 Schematic vector maps of pBeloBAC11 and hBAC495J24
Vector map of pBeloBAC11 (A) contains the Ori2 (OriS) origin of replication, chloramphenicol resistance gene (*Cm*), SopA/B/C sequences to ensure each daughter cell receives a copy of the plasmid after cell division. RepE is the initiation factor that mediates the assembly of the replication complex at Ori2. A *loxP* site is also present on the vector for Cre mediated *loxP* recombination. hBAC495J24 (B) consists of ~220kb of 17α satellite DNA carried by pBeloBAC11 vector, which is released by NotI digestion.

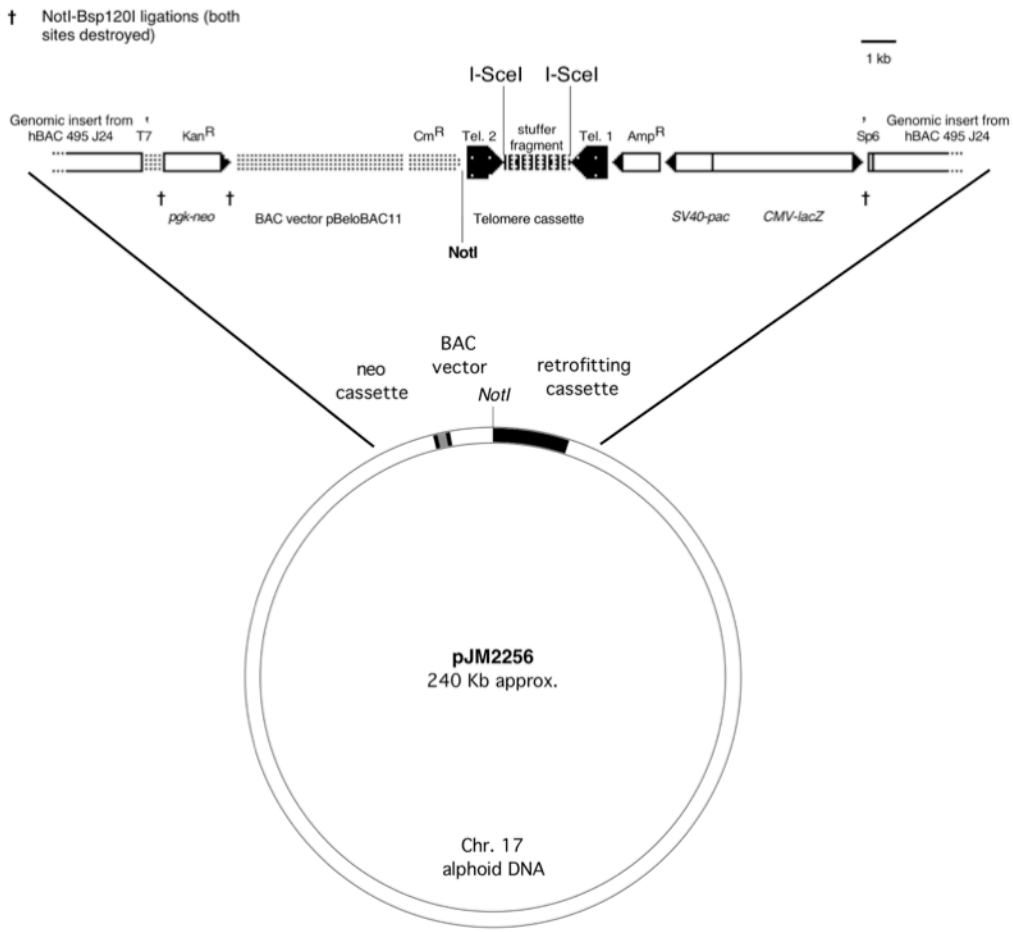

Figure 2-2 Vector map of pJM2256
pJM2256 is a BAC vector (pBeloBAC11 backbone) containing ~220kb of 17α satellite DNA which has been derived from hBAC495J24 by incorporating a *Neo* resistance cassette and a retrofitting cassette containing a CMV-*lacZ* reporter, telomere and stuffer sequences. The vector contains ampicillin (*Amp*), kanamycin (*Kan*) and chloramphenicol (*Cm*) bacterial selectable markers (Mejía et al. 2002).

Except for hBAC495J24 and pJM2256, all the other vectors in this thesis are HSV-HAC vectors that can be packaged into HSV-1 amplicons. Figure 2-3 shows the vector map of pSG80A-HG (pHG) vector described by (Saeki et al. 2001). The pSG80A-HG vector (a gift from Dr Richard Wade-Martins) contains the R6K-gamma origin of replication, which requires the R6K initiator protein p, which is sometimes referred to as pi (coded by the *pir* gene) for replication (Wu et al. 1995). pSG80A-HG was modified to include the puromycin and blasticidin resistance open reading frames

and associated promoter sequences; these vectors were consequently labelled pHGPuro and pHGBsd (cloning performed by Dr David Chan (Figure 2-4)).

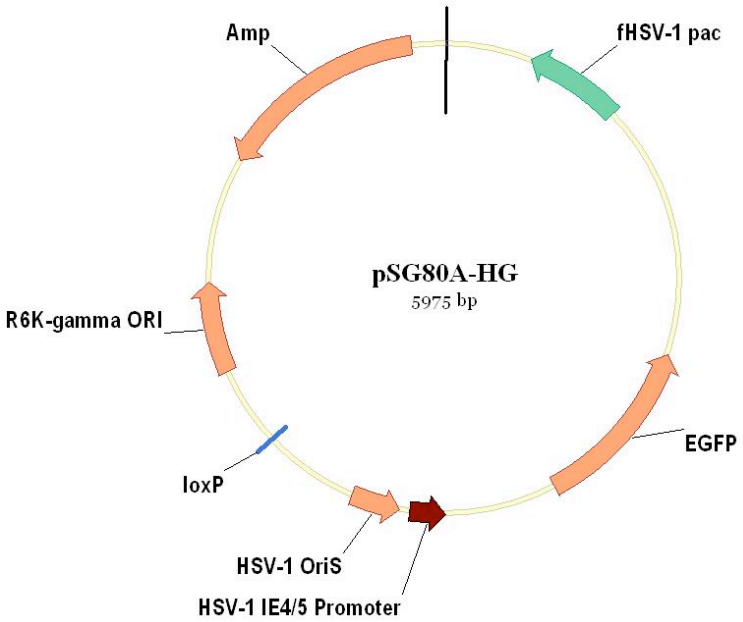

Figure 2-3 Vector map of pSG80A-HG
Vector map of the HSV-1 vector pSG80A-HG, abbreviated as "pHG" for short. The vector contains the bacterial R6K-gamma origin of replication, ampicillin (*Amp*) bacterial selectable marker, HSV-1 *OriS* origin of replication, HSV-1 packaging sequence, *GFP* reporter gene and a *loxP* site (vector a gift from Dr Richard Wade-Martins) (Saeki et al. 2001).

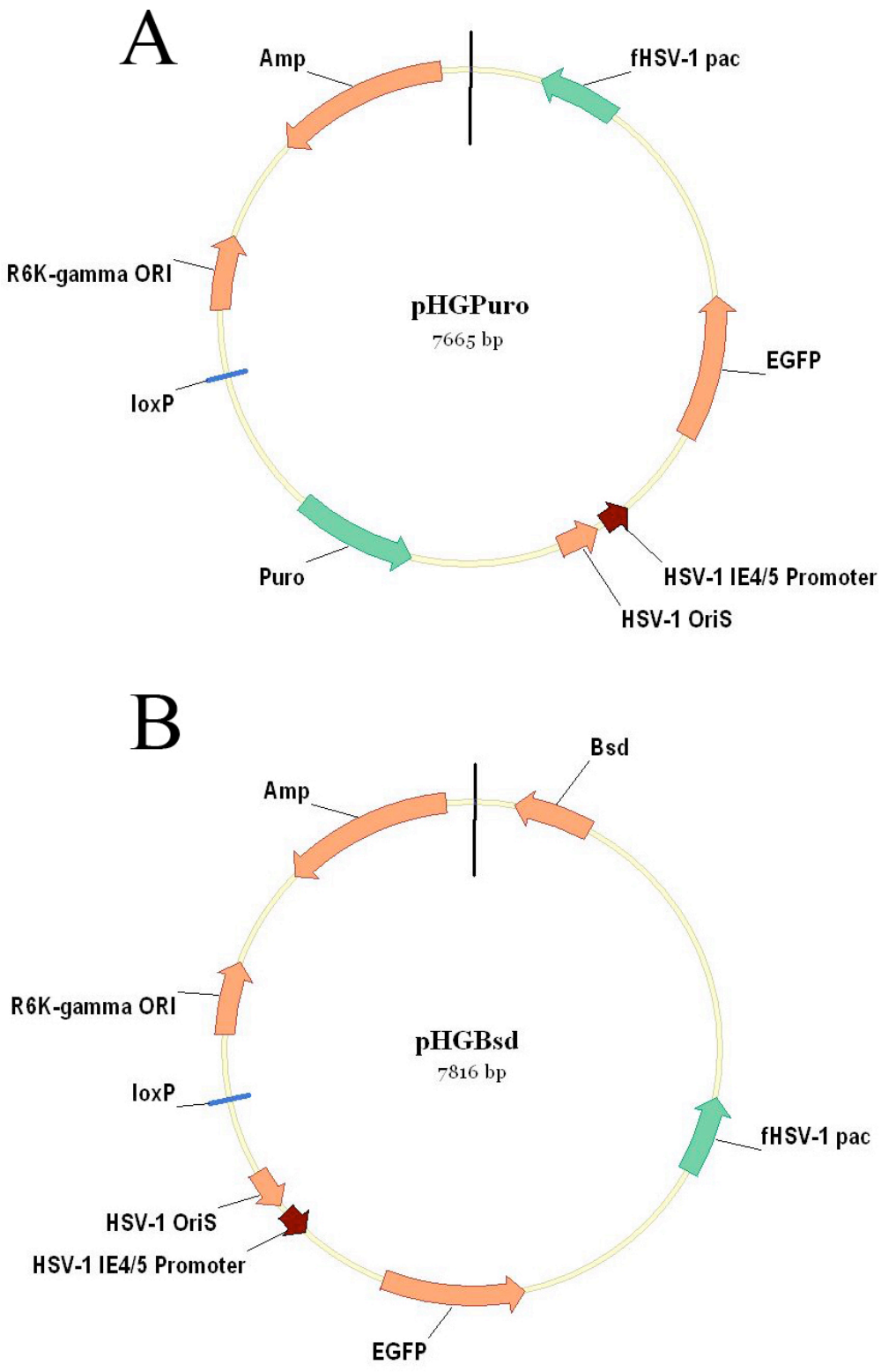

Figure 2-4 Vector maps of pHGPuro and pHGBsd
pHGPuro (A) contains the puromycin (*puro*) selectable marker and pHGBsd (B) contains the blasticidin (*Bsd*) selectable marker. Both vectors contain the bacterial R6K-gamma origin of replication, ampicillin (*Amp*) bacterial selectable marker, HSV-1 *OriS* origin of replication, HSV-1 packaging sequence (*Pac*), *GFP* reporter gene and a *loxP* site. Both vectors were constructed by Dr David Chan (Chan 2011).

The HSV-HAC vector pHSV21αNeo, containing ~60kb of 21α satellite DNA, was assembled by Moralli et al. (2006). pHSV21αNeo was digested at BstBI sites and religated to release a smaller plasmid, pHGNeo4, by removing all the 21α satellite DNA sequences. pHGNeo4 carries the HSV-1 origin of replication and packaging signals, *GFP* reporter and *Neo* resistance gene (Figure 2-5).

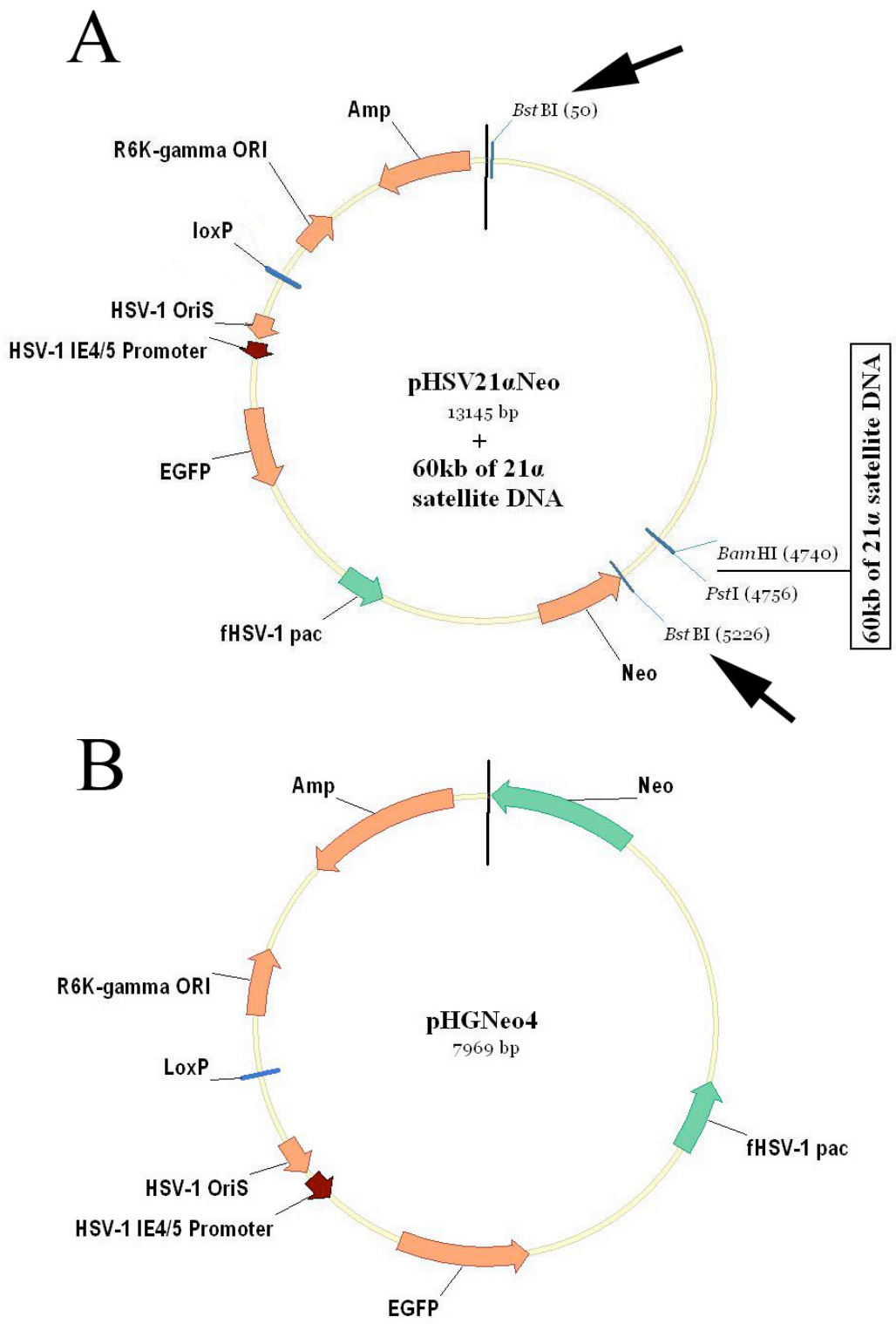

Figure 2-5 Vector maps of pHSV21αNeo and pHGNeo4
pHSV21αNeo (A) was constructed by Moralli et al. (2006). pHGNeo4 (B) was derived from pHSV21αNeo using a BstBI digestion (position of BstBI sites highlighted by arrows) and religation to remove ~60kb of 21α satellite DNA. Both vectors contain the bacterial R6K-gamma origin of replication, ampicillin (*Amp*) bacterial selectable marker, HSV-1 *OriS* origin of replication, HSV-1 packaging sequence (*Pac*), *Neo* selectable marker, *GFP* reporter gene and a *loxP* site.

Through spontaneous recombination and insert deletion of a large portion of hBAC495J24, two reduced vector versions were generated (BACα40 and BACα100), these vectors were then recombined with pHGNeo4 through Cre mediated *loxP* recombination to generate the pHSV17α40Neo and pHSV17α100Neo vectors (Figure 2-6).

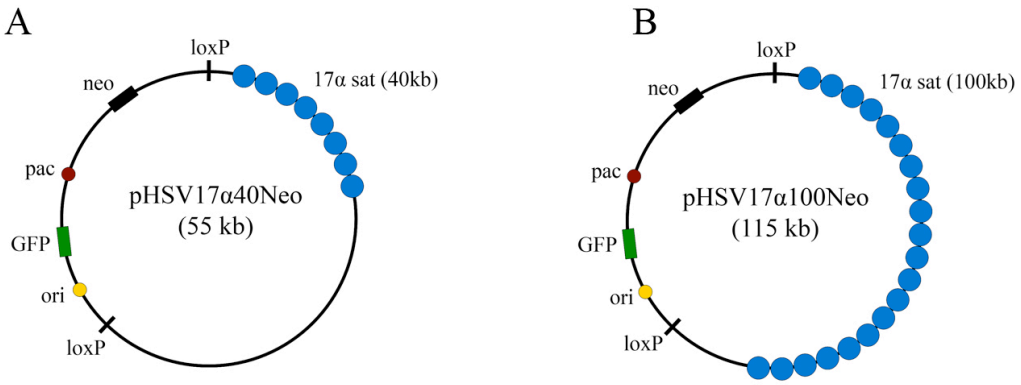

Figure 2-6 Schematic maps of pHSV17α40Neo and pHSV17α100Neo
pHSV17α40Neo (A) and pHSV17α100Neo (B) were derived from hBAC495J24 through spontaneous recombination. The vectors contain ~40kb and ~100kb of 17α satellite DNA respectively. Both vectors contain the HSV-1 origin of replication (*OriS*), HSV-1 packaging sequence (*Pac*), *Neo* selectable marker, *GFP* reporter gene and two *loxP* sites.

Through RED/ET recombination (discussed in section 2.12) (Rivero-Muller et al. 2007), ~60kb of 17α satellite DNA from hBAC495J24 was transferred onto a PAC (pCYPAC2) vector backbone (Figure 2-7) (a gift from Dr Richard Wade-Martins). The pCYPAC2 is a PAC vector containing the P1 plasmid replicon, which maintains recombinant vectors at a single copy per cell. The induction of the P1 lytic replicon using the IPTG *lac* inducer results in higher copy numbers of the PAC vector. The *sacBII* gene, under the regulation of its promoter, converts sucrose into a toxic metabolite. A stuffer insert (pUC-link) is flanked by two multiple cloning sites on either end that inactivates the *sacBII* gene. This system can be used to successfully select for recombinant clones by growing cells on plates containing kanamycin and

sucrose (Ioannou et al. 1994); however, such a system was not used in the RED/ET recombination reaction.

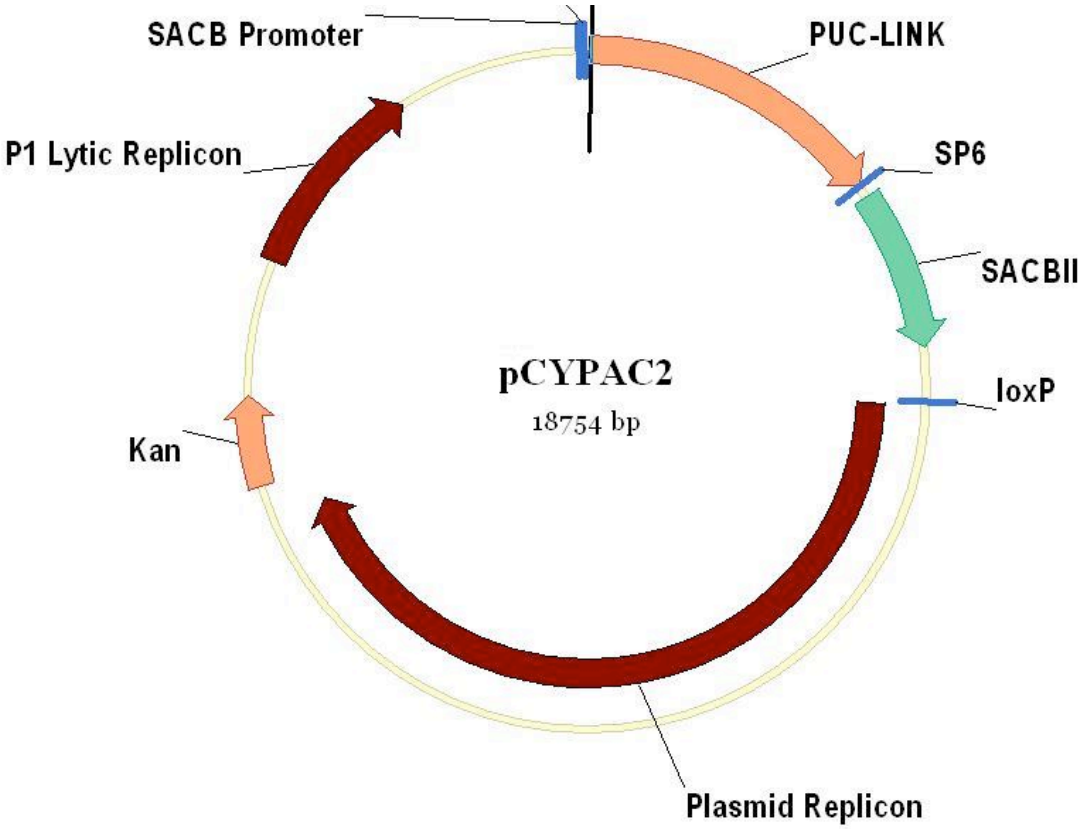

Figure 2-7 Vector map of pCYPAC2
pCYPAC2 was used to transfer a large cloned fragment from a BAC vector onto a PAC vector using RED/ET recombination. The P1 plasmid replicon maintains recombinant vectors at a single copy per cell. The induction of the P1 lytic replicon using the IPTG *lac* inducer results in higher copy numbers of the PAC vector. *sacBII* gene under the regulation of its promoter, converts sucrose into a toxic metabolite. A stuffer insert (pUC-link) is flanked by two multiple cloning sites on either end that inactive the *sacBII* gene (Ioannou et al. 1994).

The resulting reduced vector from the RED/ET recombination was labelled as PACα60 and was subsequently retrofitted with pHGNeo4 using Cre mediated *loxP* recombination to generate the pHSV17α60Neo vector (Figure 2-8).

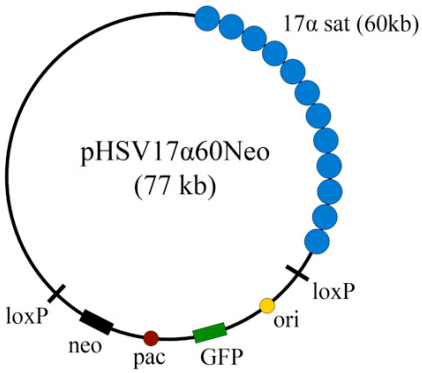

Figure 2-8 Schematic map of pHSV17α60Neo
pHSV17α60Neo was derived from hBAC495J24 using RED/ET recombination. The vector contains ~60kb of 17α satellite DNA, HSV-1 origin of replication (*OriS*), HSV-1 packaging sequence (*Pac*), *Neo* selectable marker, *GFP* reporter gene and two *loxP* sites.

2.11 Preparation of Electrocompetent Cells

A single freshly grown bacterial colony was picked and transferred to a 2.0 ml LB culture containing the appropriate antibiotic. The sample was incubated overnight at 37ºC on a shaker. The next day, 1.0 ml of the bacterial starter culture was inoculated into 100 ml of LB plus antibiotic and grown at 37ºC for approximately 3-4 hours until the OD_{600} ranged between 0.4 and 0.5. The culture was then centrifuged at ~2000g for 15 minutes at 4ºC. The supernatant was discarded and the pellet washed with 100 ml of sterile ice-cold 10% (v/v) glycerol (Sigma) for 3 times. The pellet was finally resuspended in 500µl of 10% (v/v) glycerol, aliquoted and stored at -80ºC.

2.12 RED/ET Recombination

Bacterial cells containing the hBAC495J24 vector were initially electroporated with 100ng of the RED/ET vector (pSC101-BAD-gbaA-tetra/pRed/ET), carrying a temperature sensitive origin of replication, the ampicillin resistance gene and the

RED/ET genes for homologous recombination, under control of a tetracycline inducible promoter (Rivero-Muller et al. 2007). Bacterial colonies were selected in ampicillin/ chloramphenicol, and analysed by digestion to verify that intact hBAC495J24 and RED/ET vectors were present.

The Oligo Perfect software (Invitrogen) was used to design primers based on pCYPAC2 sequence, containing 50bp homology to 17α satellite DNA (Table 2-2). pCYPAC2 was linearised by NotI digestion and the linear product was gel purified using QIAquick gel extraction kit (Qiagen). This DNA fragment was then used as a DNA template in a long PCR reaction using the Bio-X-Act kit (BioLine) according to the manufacturer's instructions. The 9.8kb PCR fragment was purified by QIAquick PCR purification kit (Qiagen), and electroporated into electrocompetent hBAC495J24/RED/ET cells. The cells were initially grown at 37ºC in the presence of tetracycline, to allow the recombination step to occur, and were then transferred to a medium containing kanamycin and grown at 42ºC. Under these conditions, only the cells where the recombination had occurred can survive. The RED/ET plasmid is lost, as it cannot be replicated at 42ºC.

2.13 Cre Mediated *LoxP* Recombination

100µl of electrocompetent ElectroMAX Stbl4 *E. coli* (Invitrogen) containing BACα40, BACα100 (both *Cm* resistant) or PACα60 (*Kan* resistant) vector, which all include a *loxP* site, were transformed as described with 50ng of the pCTP-T plasmid (carrying Cre recombinase under control of a tetracycline inducible promoter) and 100ng of pHGNeo4 (containing a *loxP* site and *Amp* resistance gene). 500µl of SOC containing 20µg/ml of heat-inactivated chlorotetracycline (cTc) was then added to

initiate Cre expression from pCPT-T and incubated at 30ºC for 1 hour. After this incubation period, the cells were diluted into 4.5ml of LB (1:10 dilution), containing ampicillin and kanamycin or ampicillin and chloramphenicol and incubated at 30ºC for further 3 hours. The cells were then centrifuged for 2 minutes at ~500g to pellet the cells and finally plated onto ampicillin and kanamycin or ampicillin and chloramphenicol LB-Agar plates and incubated at 42ºC overnight. Under these conditions, only the cells where recombination had occurred could survive. The pCP-T plasmid cannot replicate at 42ºC and is subsequently lost ensuring no further recombination events occur. Furthermore, due to the absence of the *pir* gene from the Stbl4 bacterial host, the R6K gamma origin of replication on pHGNeo4 becomes inactive, thus the plasmid is no longer able to replicate and is subsequently lost, unless it recombines with the BAC/PAC constructs.

2.14 Polymerase Chain Reaction (PCR)

Primers used for PCR amplification are listed in Table 2-2. Standard PCR conditions were used: 60ºC annealing temperature and 30 seconds of extension at 72ºC per 1kb of product. PCR reactions took place in a total volume of 25µl using BioMix Red 2× PCR kit (Quanta Biosciences). Real-Time qPCR reactions took place in a 25µl volume using the SYBR Green supermix IQ kit (Quanta Biosciences) on a Bio-Rad iCycler machine.

Table 2-2 Primers used for PCR amplification

Primer	Sequence
pCYPAC2 Long F1	5' - ATTCGTTGGAAACGGGATAATTTCAGCTGACTAAACAGAAGCAGT CTCAGGATCCATTGACCCGGAACCCTTAATATAAC-3'
pCYPAC2 Long R1	5' – ATATGCAATTGCAGATTCTGCAGAAAGTGTGTTTCTAAACTGCTAC ATCGGATCCAAAATCATTTAATTGGTGGTGCTGC-3'
Vect 1F	5'-TGGTTTGTCCAAACTCATCAA-3'
Vect 1R	5'-AGCAAAAACAGGAAGGCAAA-3'
Neo8 F	5'-CGTTGGCTACCCGTGATATT-3'
Neo8 R	5'-GCCCAGTCATAGCCGAATAG-3'
Ex18 CNTNAP5 F	5'-AGACCTTCATGACAACAGAGAACT-3'
Ex18 CNTNAP5 R	5'-AAACAGCGGGAGAGTAGATGA-3'
Oct4 F	5'-AGTGAGAGGCAACCTGGAGA-3'
Oct4 R	5'-GCCGGTTACAGAACCACACT-3'
Nanog F	5'-TTCCTTCCTCCATGGATCTG-3'
Nanog R	5'-ATCTGCTGGAGGCTGAGGTA-3'
Sox2 F	5'-ACTTTTGTCGGAGACGGAGA-3'
Sox2 R	5'-CATGAGCGTCTTGGTTTTCC-3'

Table 2-3 Primers used for Real-Time qPCR

Neo7 F	5'-GAGTACGTGCTCGCTCGATG-3'
Neo7 R	5'-CTTGCTCCTGCCGAGAAAGT-3'
EGFP F	5'-TGCTCAGGTAGTGGTTGTCG-3'
EGFP R	5'-AGAACGGCATCAAGGTGAAC-3'
GAPDH F	5'-TGTTGCCATCAATGACCCCTT-3'
GAPDH R	5'-CTCCACGACGTACTCAGCG-3'

2.15 Genomic DNA Preparation from Cells

Approximately 10^6 cells were washed in PBS, trypsinised and collected by centrifugation at ~750g. The cells were then resuspended in lysis buffer (50 mM KCl, 10 mM Tris-HCl, 1% (v/v) Tween 20 and 10µg/ml Proteinase K) and incubated at 55˚C for 1 hour followed by 95˚C for 10 minutes. An equal volume of phenol:chloroform:isoamylic alcohol (25:24:1) was added to the sample and gently inverted for 2 minutes. The sample was then centrifuged for 10 minutes at ~5,000g. The aqueous phase was then moved to a fresh tube and finally ethanol precipitation was used to precipitate the DNA. Samples were left to air-dry for 10 minutes and resuspended in 50µl of dH_2O.

2.16 Cell Culture

The HT1080 (ATCC-CCL-121) cells (Rasheed et al. 1974) were grown using standard techniques in Dulbecco's Modified Eagle's Medium (DMEM), supplemented with 10% (v/v) foetal bovine serum (FBS). HUES-2 cells were grown as described by (Cowan et al. 2004), on inactivated mouse embryonic fibroblasts (MEFi). 10mg/ml of Mitomycin C (Sigma) was used for 4 hours to mitotically inactivate MEF. When using MEFi as a feeder layer, hES media was used with the following composition: DMEM F/12 (Invitrogen) supplemented with 20% (v/v) KnockOut serum replacement (Invitrogen), 0.1mM non-essential amino acids (Sigma), 1× GlutamaxTM-1 (Invitrogen), 0.1mM β-mercaptoethanol (Invitrogen), 10ng/ml basic fibroblast growth factor (bFGF) (R&D Systems) and 1% (v/v) penicillin and streptomycin (Invitrogen). Feeder independent culturing of hESc took place on Matrigel (BD Biosciences) and using the mTeSR medium (STEMCELL Technologies) (Braam et al. 2008a). TrypLE Express was used to enzymatically passage hESc. Cells were maintained and passaged at high densities: a minimum of 2.5×10^5 cells was seeded in 24-well plates, while 10^6 cells were seeded in 6-well plates. To promote single cell survival, p160-Rho-associated coiled-coil kinase (ROCK) inhibitor Y-27632 (Merck Biosciences) was used at a concentration of 10μM each time hESc were passaged.

2.17 Cell Transfection

Lipofection and electroporation of HT1080 cells was carried out as described by (Mejía et al. 2002) and (Costa et al. 2007), respectively to deliver control plasmids pHSV21αNeo and pHGNeo4. For lipofection, 2μg of DNA was delivered to 10^7 cells

using 12µl of Lipofectamine 2000 (Invitrogen). Electroporation was carried out in a gene pulser cuvette with a 0.4cm electrode gap (Bio-Rad) using 10µg of DNA and 10^7 cells with the following settings: 250V, 200Ω and 500µF (Costa et al. 2007). The efficiency of transfection was determined by counting the number of *GFP*/*RFP* positive cells 24 hours after transfection. For HUES-2, ExGen 500 (Fermentas) was used as a commercial transfection agent as described by the manufacturer's instructions (Eiges et al. 2001). 1µg of plasmid plus 3.3µl of ExGen 500 was added to 2.5×10^5, in 24-well plates, cells in a final volume of 200µl of media (transfection experiments performed by Dr Daniela Moralli).

2.18 HSV-1 Amplicon Preparation

The Vero 2-2 packaging cells were seeded in 6cm dishes at ~90% confluency (10^6 cells). To each 6cm dish, 1.8µg of the desired BAC/PAC vector to be packaged, 2µg of fHSVΔpacΔ27 0+ and 0.2µg of pEBHICP27 was added in 250µl of OptiMEM (Invitrogen) containing 23µl of Lipofectamine (Invitrogen) and 10µl Plus Reagent (Invitrogen), and incubated for 4 hours at 37ºC. fHSVΔpacΔ27 0+ and pEBHICP27 are both used for generation of HSV-1 amplicons (Table 2-1) by furnishing *in trans* the necessary proteins for packaging. fHSVΔpacΔ27 0+ (178kb) consists of the HSV-1 genome, however due to safety considerations the *Ori*, *Pac* and *ICP27* sequences have been deleted. Stuffer sequences of ICP0 have been added to fHSVΔpacΔ27 0+ to ensure the size of this vector exceeds the packaging capacity of HSV-1 amplicons (~152kb). pEBHICP27 carries the *ICP27* sequences that are necessary for production of HSV-1 amplicons (Saeki et al. 2001). After 4 hours of incubation, the medium was replaced by DMEM containing 6% (v/v) FBS and 25mM HEPES pH 7.0. After further ~66 hours of incubation, the cells were harvested, pooled, sonicated and

centrifuged at ~3500g at 4ºC to remove cell debris. To concentrate the amplicons, the supernatant was then placed on a 25% (w/v) sucrose cushion and centrifuged at ~90,000g, 4ºC for 3 hours in an SW41 rotor, in a Beckman ultracentrifuge. The pellet deriving from 9×10cm tissue cultured dishes was resuspended in 500µl of DMEM containing 10% (v/v) FBS, aliquoted and stored at -80ºC.

2.19 Calculating Amplicon Preparation Titre Using G16.9 Cells

The glioma derived G16.9 cells (Kubo et al. 2003), highly susceptible to HSV-1 infection, were seeded at 2.5×10^5 cells per 24-well plate. The next day, the wells were incubated in a total volume of 250µl of media containing 1µl, 2µl and 5µl of HSV-1 amplicon suspension and incubated for 24 hours at 37°C and 5% CO_2. After 24 hours, the cells were analysed using a Nikon TE2000U inverted microscope with a Nikon Plan Fluor 10×/0.30 ph1 DL ∞/1.2 WD 15.2 objective and CFI 10×/22 eyepiece lens equipped with epifluorescence, and the number of *GFP* or *RFP* positive cells (i.e. transduced) was scored. The titre (expressed as amplicons/µl) of an HSV-1 amplicon preparation was thus calculated by plotting the number of transduced G16.9 cells as a function of the volume of amplicon used (typically 1µl, 2µl and 5µl) and calculating the slope of this graph. Titres of ~10^4 amplicons/µl were routinely obtained.

2.20 HSV-1 Amplicon Transduction

The transduction of HT1080 and HUES-2 cells with HSV-1 amplicons, carrying different vectors, was carried out as described by (Wade-Martins et al. 2001; Moralli et al. 2006). HUES-2 cells were grown under feeder-free conditions on Matrigel. The day before transduction, 2.5×10^5 HUES-2 or HT1080 cells were seeded per 24-well

plate. On the day of transduction, HSV-1 amplicons were inoculated at multiplicity of infection (MOI) of 1, 2 or 5 in a total volume of 250µl of media and were incubated for 24 hours. Transient expression was measured at 24 hours post-transduction as described in section 2.19.

2.21 Spinoculation

For spinoculation, after the HSV-1 amplicons were added to the cells, the plates were carefully covered with sterile adhesive PCR films, to avoid aerosol escape during centrifugation. The plate was centrifuged at ~750g for 30 minutes (O'Doherty et al. 2000).

2.22 Selection and Colony Picking

For HT1080 cells, selection was applied 48 hours post-treatment at 350µg/ml G418, or 0.5µg/ml puromycin or 10µg/ml blasticidin and maintained for 7-10 days. Selection of HUES-2 cells was carried out 5 days post-treatment using 50µg/ml G418 on *Neo*^{R} MEFi and maintained for 7 days. Following selection of cells with the appropriate antibiotic, stable HT1080 and HUES-2 clones were picked using a 20µl pipette tip under a Motic SMZ 168 Trinocular stereomicroscope using a 2× objective and W10×/23 eyepiece lens. Picked HT1080 clones were trypsinised briefly to dissociate cells and transferred to individual wells of a 96-well plate. HUES-2 clones were transferred onto MEFi coated plates without trypsinisation with the addition of 10µM ROCK inhibitor Y-27632.

2.23 Chromosome Harvesting

HT1080 cells were blocked in metaphase by incubation in 30μg/ml Colcemid for ~4 hours. HUES-2 cells were treated with 0.1μg/ml nocodazole overnight. For HT1080 cells, chromosomes were harvested using standard protocols: following a 10 minute incubation period in 75mM KCl hypotonic solution at room temperature, the cells were fixed twice in cold Carnoy's fixative (3:1 (v/v) methanol to acetic acid) (Mejía et al. 2002). For HUES-2, cells were incubated in buffered hypotonic solution (0.4% (w/v) KCl with 4-(2-hydroxyethyl)-1-piperazineethanesulfonic acid (HEPES) at pH 7.4; Genial Genetics) for 30 minutes at 37ºC, followed by two fixations in cold Carnoy's solution. The pellet was resuspended in 500μl of cold Carnoy's solution and stored at -20ºC.

2.24 Preparation of FISH Probes

FISH probes were prepared by nick translation using a commercially available nick translation system kit (Invitrogen). 1μg of DNA was labelled with either biotin-16-dUTP or digoxigenin-11-dUTP (Roche) according to the manufacturer's instructions. For consistency throughout this study, 17α and 21α satellite DNA were labelled with biotin, and vector DNA (pBeloBAC11 and pCYPAC2) were labelled with digoxigenin. Samples were incubated at 16ºC overnight for the nick translation reaction to take place. Labelled probes were next precipitated using 10× excess of CotI DNA (10μg) (Roche), 3M ammonium acetate, 2 volumes of ethanol and 0.2% (w/v) dextran blue (Sigma) for 15 minutes at room temperature, followed by centrifugation at ~10,000g for 10 minutes. The probes were resuspended in

hybridisation buffer (2× SSC, 50% (v/v) formamide, 10% (w/v) dextran sulphate) at a final concentration of 10ng/µl.

2.25 Fluorescence *in situ* Hybridisation (FISH)

30-50µl of fixed metaphase spreads were dropped onto a slide and immediately air-dried and left overnight. The next day, chromosomes were denatured on a heat block at 95°C for 10 minutes in 10mM Tris-HCl, pH 8.0, 50mM KCl and 5% (v/v) glycerol. The slide was then washed in 0.1× SSC for 1 minute and then dehydrated in 70%, 90% and 100% (all v/v) ethanol for 3 minutes each. During the dehydration step, the probes were denatured at 85ºC for 10 minutes. For each slide, 10-15µl of labelled probe (~100-150ng) was used, the slide was covered using a coverslip and incubated in a humid box at 37ºC overnight. The next day, the slides were washed 3 times, 5 minutes each in 0.1× SSC at 60°C. DNA probes labelled with biotin were detected using AlexaFluor 488 conjugated avidin (Molecular Probes, Invitrogen; [Stock]=1.0mg/ml), followed by biotinylated goat anti-avidin antibody (Vector Laboratories; [Stock]=0.5mg/ml), and a second layer of AlexaFluor 488 conjugated avidin. DNA probes labelled with digoxigenin were detected using rhodamine conjugated sheep anti-digoxigenin antibody (Roche; [Stock]=0.2mg/ml), followed by rhodamine anti-sheep antibody (Chemicon Europe; [Stock]=0.2mg/ml). For each slide, 100µl of antibody or avidin was used at a 1/100 dilution factor in 4×SSC, 0.1% (v/v) Tween20 (Sigma) and 3% (w/v) BSA (Sigma) and incubated at 37°C for 30 minutes. Slides were then washed 3 times, 5 minutes each in 4×SSC, 0.1% (v/v) Tween20 at 42°C. A final wash was performed in 4×SSC at room temperature. The chromosomes were counterstained with 3ng/ml DAPI (4',6-Diamidino-2-Phenylindole) for 5 minutes, rinsed in PBS and mounted in DABCO (1,4-

Diazabicyclo(2,2,2)octane) (Sigma) antifade solution. Wherever stated, FISH experiments were performed by Dr Daniela Moralli.

The HUES-2 karyotype analysis was performed by Dr Mohammed Yusuf and analysed by Dr Emanuela Volpi at the Molecular and Cytogenetics Core, Wellcome Trust Centre for Human Genetics (WTCHG) at the University of Oxford. Metaphase spreads were subjected to FISH with whole chromosomes paint probes for chromosomes 12 and 17 (Aquarius Whole Chromosome Paint Probes, Cytocell), according to the manufacturer's instructions. Images were acquired with an Olympus BX-51 upright epifluorescence microscope using an Olympus UPlanF1 60×1.25 oil ∞/0.17 objective and Olympus widefield WHN10×/22 eyepiece lens equipped with a JAI CVM4+ progressive-scan 24 fps B&W fluorescence charge-coupled device (CCD) camera. Images were analysed using the Genetix CytoVision Genus 4.5.1 software.

2.26 Immuno-FISH

Cells arrested in metaphase were cytospunned at ~1000g for 5 minutes onto slides using a Labofuge 400 (Heraeus Instruments). The cells were fixed in 2% (v/v) formalin in PBS, and permeabilised in KCM buffer (120mM KCl, 20mM NaCl, 10mM Tris pH 8, 0.5mM EDTA, 0.1% (v/v) Triton X-100) for 10 minutes. Non-specific binding was reduced by incubating the slides in 3% (w/v) BSA, 0.1% (v/v) Triton X-100 in PBS for 30 minutes. Primary antibody detection was carried out using rabbit anti-human CENP C antibody (a gift from Professor William Earnshaw) at 1/100 dilution in 3% (w/v) BSA, 0.1% (v/v) Triton X-100 in PBS and left overnight at 4ºC. The slides were then washed 3 times, for 5 minutes each in KCM buffer

followed by secondary antibody detection for 30 minutes at 37ºC. Goat anti-rabbit FITC conjugated antibody (Sigma; [Stock]=1.0mg/ml) was used as the secondary at a 1/100 dilution in 3% (w/v) BSA, 0.1% (v/v) Triton X-100 in PBS. Slides were then washed 3 times, for 5 minutes each in 0.1% (v/v) Triton-X100 in PBS followed by fixation in 2% (v/v) formalin in PBS for 10 minutes. FISH was subsequently performed on these slides and images were acquired as described in section 2.25.

2.27 Fibre-FISH

Cells were trypsinised and resuspended in PBS in a concentration of 10^6 cells/ml. 10µl of cell suspension was spread on the slide and dried. Slides were then placed in plastic coverplate holder and 150µl of lysis solution (0.05M NaOH, 30% (v/v) ethanol) was added and allowed to drain. Next, 200µl of methanol was added and allowed to drain. The slide was then removed from the coverplate and slide holder and was allowed to air-dry. The preparations were then dehydrated for 2 minutes each in 70%, 90% and 100% (all v/v) ethanol. FISH was then performed on these slides and images acquired as described in section 2.25. Fibre-FISH experiments were performed by Dr Daniela Moralli.

2.28 Multicolour FISH (M-FISH)

M-FISH was performed by Dr Mohammed Yusuf and analysed by Dr Emanuela Volpi at the Molecular and Cytogenetics Core, Wellcome Trust Centre for Human Genetics (WTCHG) at the University of Oxford. Chromosome spreads were hybridised with 24XCyte Human Multicolour FISH probe kit (Metasystems)

according to the manufacturer's instructions. Images were acquired as described in section 2.25.

2.29 Indirect-Immunofluorescence Staining

Cells were initially fixed for 10 minutes in 2% (v/v) formaldehyde in PBS, followed by a 10 minute permeabilisation step using 0.1% (v/v) Triton X-100. The cells were then blocked in 3% (w/v) BSA, 0.1% (v/v) Triton X-100 in PBS for 30 minutes. The following primary antibodies were used at 1/100 dilution in 3% (w/v) BSA, 0.1% (v/v) Triton X-100 in PBS for 1 hour at room temperature: mouse anti-Tra-1-60 ([stock]=2.0mg/ml); rabbit anti-Oct4 ([stock]=0.5mg/ml); rabbit anti-Nanog ([stock]=0.2mg/ml); rabbit anti-Sox2 ([stock]=1.0mg/ml); mouse anti-β-III tubulin ([stock]=1.0mg/ml) (all from Abcam). After treatment with the primary antibody, the cells were washed three times in PBS for 15 minutes each. For the secondary antibody, goat anti-mouse TRITC conjugated ([Stock]=3.0mg/ml) or goat anti-rabbit FITC conjugated ([Stock]=1.0mg/ml) (both from Sigma) were used at 1/100 dilution in 3% (w/v) BSA, 0.1% (v/v) Triton X-100 in PBS for 30 minutes at room temperature. The cells were again washed three times in PBS for 15 minutes each. Finally, the nuclei were counterstained using DAPI. Images were captured using a Nikon TE2000U inverted microscope with a Nikon Plan Fluor 4×/0.13 phL DL ∞/1.2 WD 16.4 objective and CFI 10×/22 eyepiece lens, and analysed using the IPLab 3.7 software and pseudo-coloured in Adobe Photoshop 8.0.

2.30 Fluorescence-Activated Cell Sorting (FACS)

hESc were trypsinised using TrypLE Express and fixed in 4% (v/v) formaldehyde in PBS. Samples were then run through a 4-colour FACSCalibur machine (BD) using the following settings: FL1 449, FL2 499, FL3 500. At least 10,000 events were captured for each preparation. The data were acquired in CellQuest Pro and analysed using FlowJo 7.6. The fraction of *GFP*-expressing cell population was calculated by setting the *GFP* gate at 0.5% for the negative control sample. FACS runs and data analysis performed with the assistance of Dr Sally Cowley, Dunn School of Pathology at the University of Oxford.

2.31 RNA Preparation and Real-Time qPCR Analysis

RNA was extracted from approximately 6×10^6 cells with the RNeasy kit (Qiagen), using on-column DNaseI digestion, following the manufacturer's instructions. Approximately 1μg of RNA was then reverse transcribed into cDNA, using the RETROScript system (Ambion), with random decamer primers, according to the manufacturer's instructions. Gene expression levels were quantified using Real-Time qPCR on cDNA using SYBR Green supermix IQ kit (Quanta Biosciences) on an ICycler (Bio-Rad) machine. Quantification of HAC gene expression was carried out in independent experiments using primers against *GFP* or *Neo* and normalised against a ubiquitously expressed endogenous control *GAPDH* (primers listed in Table 2-3). The fold enrichment of the gene of interest was normalised against *GAPDH* by using the difference in threshold cycle (Ct) values between the gene of interest (*GFP* or *Neo*) and control (*GAPDH*) using the following equation (Livak and Schmittgen 2001):

$$\text{Fold Enrichment} = 2^{-\Delta\Delta Ct},$$

$$\text{where } \Delta\Delta Ct = \Delta Ct_{(\text{Time Point 0})} - \Delta Ct_{(\text{Time Point T})},$$

$$\Delta Ct_{(\text{Time Point 0})} = Ct_{\text{GFP/Neo }(\text{Time Point 0})} - Ct_{\text{GAPDH }(\text{Time Point 0})},$$

$$\text{and } \Delta Ct_{(\text{Time Point T})} = Ct_{\text{GFP/Neo }(\text{Time Point T})} - Ct_{\text{GAPDH }(\text{Time Point T})}.$$

2.32 Statistical Analysis

Statistical analyses including two-tailed Pearson correlation, two-tailed two-sample t-test and analysis of variance (ANOVA) were carried out using the IBM SPSS statistics software version 19.0. When applicable, the data were tested for equal variances using the Levene's test, and normal distribution was assessed using normal Q-Q plots. For one-way ANOVA, equal variances were assumed, and the Tukey post-hoc test was used after initially obtaining a significant ANOVA. Statistical significance was assigned for a value of $p<0.05$. ArcSine transformation of the mitotic index data were performed using the following equation: ArcSine $(MI+0.5)^{1/2}$, where MI is the mitotic index presented as a fraction. When applicable, a best-fit linear regression line was fit through the data using Microsoft Excel version 12.2.5. The data are presented as the arithmetic mean ± standard error to the mean.

2.33 Calculating Average Daily Growth Rate

The intrinsic daily growth rate, *r*, was calculated by assuming a logistic growth model using the equation $p(t) = p_0 e^{rt}$, where *e* is the Euler's mathematical constant, *P(t)* is the population size at time *t*, and P_0 is the starting population size (Otto and Day

2007). Using Microsoft Excel version 12.2.5, a best-fit exponential regression line was fit through the population density data as a function of time. The doubling time was calculated as *Ln(2)/r*.

2.34 Embryoid Body Formation

Embryoid bodies (EBs) were made using cell-aggregation methods. Small EBs were made using AggreWell plates for EBs of maximum size ~4000 cells/EB. While for large EBs, non-adherent 96-well V-bottom (Nunc) were used to make EBs of size ~150,000 cells/EB. The EBs were left in the appropriate wells in mTeSR supplemented with 10μM ROCK inhibitor Y-27632 for 2-3 days for complete formation. Images were acquired as described in section 2.29.

2.35 Germ Layer Differentiation

For germ layer differentiation, approximately 200 large embryoid bodies (EB) of size ~1.5×10^5 cells/EB were used. After 2-3 days of EB formation, EBs were released onto non-adherent plates and left in suspension for 8-10 days in DMEM containing 20% (v/v) FBS, 1% (v/v) P/S. EBs were then placed on Matrigel-coated plates to adhere and expand for further 15-20 days. Images were acquired as described in section 2.29. At the end of the differentiation period, cells were harvested using TrypLE Express trypsin for subsequent studies.

2.36 Neuronal Differentiation

Neuronal differentiation was carried out as described by Iacovitti et al. (2007) with minor adjustments. Small EBs of size ~4000 cells/EB were formed using AggreWell^{TM}400 plates (STEMCELL Technologies) as described by the manufacturer. After 2 days of EB formation in AggreWell^{TM}400 plates, EBs were released from the wells and left in suspension in non-adherent plates for 5 days under neuronal differentiation media- I (NDM-I) containing DMEM F/12, 1% (v/v) P/S, 1% (v/v) N2 supplement (Invitrogen), 5μg/ml human plasma fibronectin (Sigma) and 200μg/ml recombinant human noggin (RDI/Fitzgerald Industries). After the suspension period, EBs were then transferred onto Matrigel-coated plates under NDM-I for further 8 days. The medium was then changed to NDM-II (DMEM F/12, 1% (v/v) P/S, 1% (v/v) N2 supplement, 20ng/ml bFGF (BD Biosciences) and left for further 8-10 days for expansion of neuronal rosettes. After a period of ~25 days of directed differentiation, neuronal rosettes were finally lifted using TrypLE Express and plated on Matrigel-coated slides. ROCK inhibitor Y-27632 was added to promote single cell survival after passaging. Indirect-immunostaining using β-III-tubulin and Immuno-FISH were carried out shortly after.

2.37 Teratoma Formation Assay

The teratoma formation assay was carried out in collaboration with Professor Adrian Thrasher (Institute of Child Health, University College London). Approximately 10^6 cells from HUES-2 40.2 clone grown on Matrigel were injected subcutaneously into the scruff of neck of immunodeficient mice (*IL2rg* -/-, *Rag2* -/-, *C5* -/-). Approximately 5-7 weeks post-injection, tumours became visible as a small bump

from under the mouse skin; at this point, the mice were sacrificed to extract the developed tumours. The tumours were dissected and sections analysed using haematoxylin/eosin staining for histological analysis. To study the presence of three embryonic germ layers, indirect-immunostaining with the following primary antibodies were used at a 1/500 dilution: rabbit-anti-β-III-tubulin isoform (Tuj1) ([Stock]=0.4mg/ml) for ectodermal derivatives, mouse-anti-alpha-actinin ([Stock]=0.2mg/ml) for mesodermal derivatives and mouse-anti-alpha fetoprotein ([Stock]=0.5mg/ml) for endodermal derivatives (all from Millipore). For the secondary antibody, goat anti-rabbit FITC conjugated (Sigma; [Stock]=1.0mg/ml) or goat anti-mouse TRITC conjugated (Sigma; [Stock]=3.0mg/ml) was used at 1/250 dilution for 30 minutes at room temperature. Confocal analysis was carried out at the confocal microscopy core facility at University College London using a Zeiss LSM 710 inverted confocal microscope using a 20× Carl Zeiss objective and 10× eyepiece lens.

2.38 Establishment of *in vitro* Teratoma-Derived Cells

Half of the teratoma mass was sectioned and mashed in a sterile cell strainer. Loose cells were then washed in PBS, spun and the supernatant discarded. Cells were resuspended in DMEM supplemented with 10% (v/v) FBS, 1% (v/v) P/S, 10μM ROCK inhibitor Y-27632 and plated on a 10cm dish coated with Matrigel. After 4 hours, cells were washed with PBS and media filtered to remove excess cell debris from the mashing process.

Chapter 3. Results and Discussion I: Construction and Analysis of Candidate HSV-HAC Vectors

With the aim of generating a vector highly proficient at forming HAC in target cells, and of suitable size for delivery by HSV-1 amplicons, a construct (hBAC495J24) that had previously shown success in HAC generation at high frequencies was reduced in size. The BAC vector, hBAC495J24 (Mejía et al. 2002) contains approximately 220kb of 17α satellite DNA cloned on the pBeloBAC11 vector (7.5kb) (Figure 2-1). Mejía et al. (2002) showed that HAC vectors derived from hBAC495J24 (pJM2256) had a relatively high HAC forming potential compared to other HAC vectors. Following lipofection of pJM2256 in HT1080 cells, 32% of the screened clones contained HAC (Mejía et al. 2002). As the size of hBAC495J24 is approximately 70kb larger than the packaging capacity of HSV-1 amplicons, its size was reduced to enable its incorporation into the HSV-1 amplicon delivery system, while potentially retaining the HAC forming properties.

3.1 Isolation of BACα40 and BACα100

As it is known that large stretches of repetitive DNA incur rearrangements in *E. coli* (Bzymek and Lovett 2001), purified hBAC495J24 DNA was analysed by NotI digestion. The expected pattern of NotI DNA fragments was approximately 220kb fragment of 17α satellite DNA and 7.5kb of pBeloBAC11 vector. It was noted that while most of the colonies contained an intact vector, spontaneously arising BAC derivatives of hBAC495J24 were also present among the isolated colonies (Figure 3-1 indicated by an asterisk).

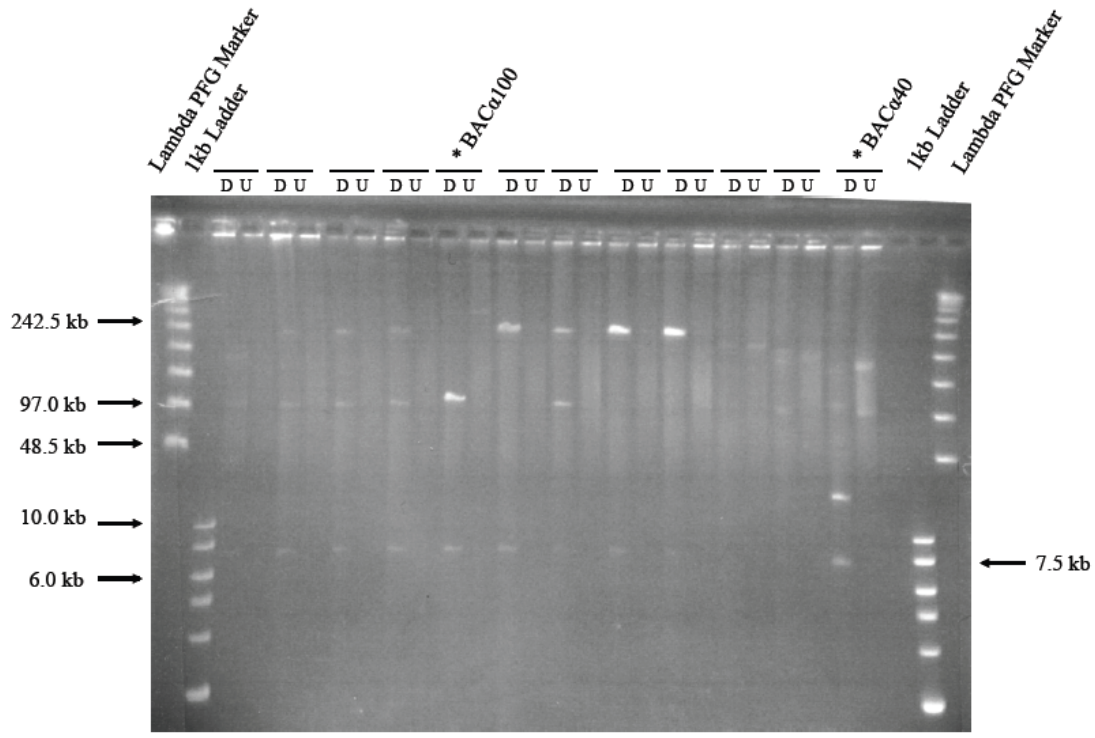

Figure 3-1 Analytical NotI digest of DNA prepared from 12 colonies obtained from transformation of the hBAC495J24
The hBAC495J24 was introduced into *E. coli* following electroporation. DNA from 12 colonies was prepared and analysed using NotI enzyme digestion. Both digested (D) and undigested (U) DNA were run on a 1% pulsed field gel electrophoresis (PFGE). Two fragments were expected: one containing ~220kb of 17α satellite DNA and the other 7.5kb of pBeloBAC11. Analysis of the screened colonies showed that two vectors were reduced in size: ~40kb and ~100kb, marked with an asterisk. There were other clones showing a mixed population of ~220kb and ~100kb BAC vectors, which may have resulted due to cross-contamination. Lambda PFG Marker was used as a ladder.

In two of the BAC derivatives, the 17α satellite DNA inserts were reduced in size: ~40kb and ~100kb BAC (labelled BACα40 and BACα100, respectively; marked with an asterisk in Figure 3-1), compared to the ~220kb intact form of hBAC495J24. These reduced BAC derivatives were isolated for further analysis. As BACα40 and BACα100 vectors were presumably obtained through spontaneous recombination, resulting in a size reduction of their parental vector insert, the retention of the structural integrity of each clone was subsequently determined. Using electroporation, the BACα40 and BACα100 vectors were introduced into ElectroMAX Stbl4 *E. coli*, and 10 subclones were obtained from each construct. DNA vectors from each of the

subclones were then digested with NotI to release the 7.5kb pBeloBAC11 vector fragment. The results showed that the alphoid DNA from each of the analysable clones did not exhibit any further size rearrangements (see Figure 3-2).

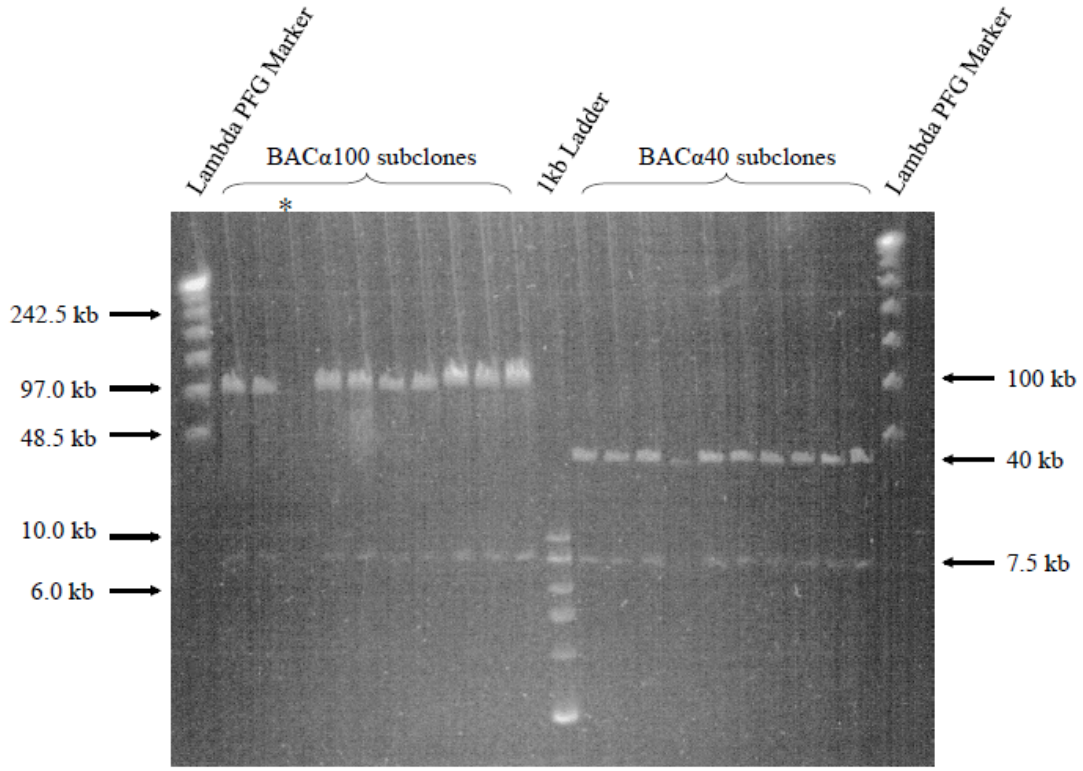

Figure 3-2 Analytical NotI digest of BACα40 and BACα100 DNA subclones
The BACα40 and BACα100 DNA prepared from 10 subclones showed structural integrity following recovery from electroporation into ElectroMAX Stbl4 electrocompetent cells. The analysis showed that both vectors released the expected 7.5kb pBeloBAC11, and either a fragment containing ~40kb or ~100kb stretch of 17α satellite DNA backbones, respectively. Note that the 4th lane from the left (marked with an asterisk) appears empty due to an error in the DNA preparation resulting in low concentration of DNA being loaded. Lambda PFG Marker and 1kb ladder were used as a size reference.

3.2 Generation of PACα60 Using RED/ET Recombination

Another reduced derivative of hBAC495J24 was obtained using the RED/ET recombination system as described by Rivero-Muller et al. (2007), which allowed the transfer of specific sequences from a BAC onto a PAC vector (Figure 3-3). P1-derived artificial chromosomes (PAC) are cloning vectors designed for introducing

recombinant DNA into *E. coli* using electroporation for genomic analysis (Ioannou et al. 1994). Through this system, a PAC vector containing a reduced 17α satellite DNA insert was derived from hBAC495J24 using a two-step process. The first step involved generation of a linear 9.8kb PCR fragment from pCYPAC2 vector with the addition of 50bp homologous tails to the 17α satellite DNA consensus. The second step consisted of *in vivo* homologous recombination of the 50bp homologous tails of the PCR product with the 17α satellite DNA sequences of hBAC495J24, in the *E. coli* host (Figure 3-3).

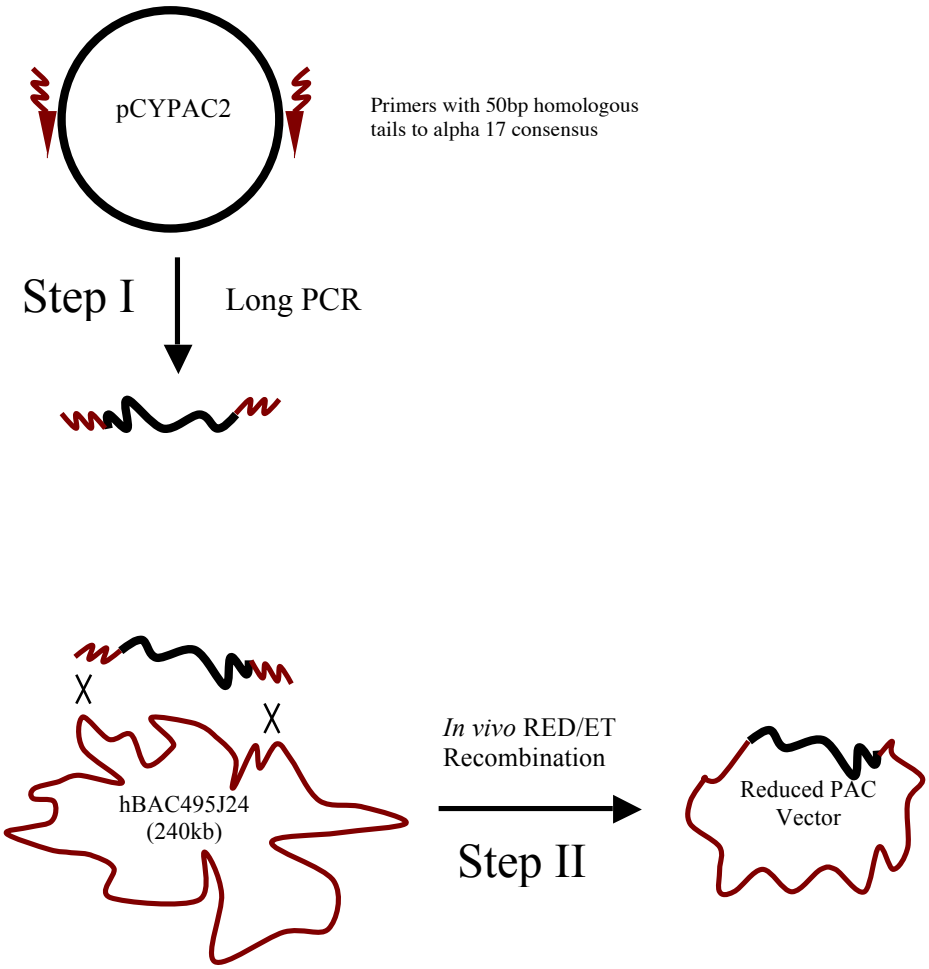

Figure 3-3 RED/ET recombination was used to generate a reduced version of hBAC495J24.
A PAC vector containing a reduced 17α satellite DNA insert was derived from hBAC495J24 using a two-step process. The first step involved the generation of a long PCR pCYPAC2 fragment containing 50bp homologous tails to the 17α consensus. The second step consisted of homologous recombination of the 50bp tails of the PCR fragment with hBAC495J24 in *E. coli*, expressing the RED/ET system proteins.

For the long PCR reaction (step I), initially 30bp primers (Figure 3-4 in blue) were designed on the pCYPAC2 vector sequence to amplify a 9.8kb PAC fragment containing the essential vector components (e.g. origin of replication and kanamycin selectable marker). Then, 50bp tails homologous to the 17α satellite DNA consensus were added to the 5' end of each primer sequence (Figure 3-4, in red). To facilitate downstream analysis of derivative clones, a BamHI restriction site was added between the 30bp primer fraction and the 50bp tail (Figure 3-4 in grey; see materials and methods section 2.14 for sequence). The resulting primer set (~85bp each) was used to amplify a 9.8kb fragment from the pCYPAC2 vector.

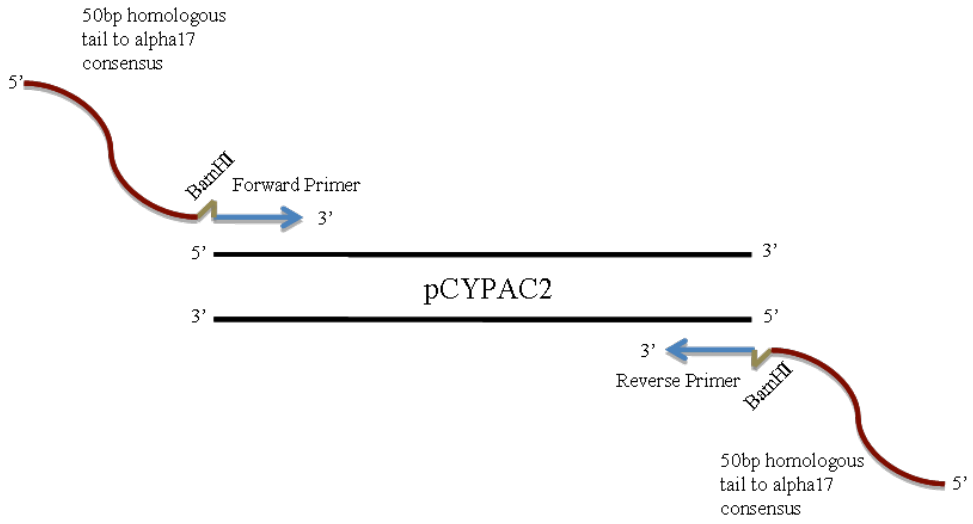

Figure 3-4 Design of primers containing 50bp of homologous tails to the 17α satellite DNA consensus to amplify a 9.8kb fragment of pCYPAC2.
Primers from the pCYPAC2 vector (in blue) were designed with 50bp tails homologous to the 17α satellite DNA consensus (in red). BamHI restriction sites were added to facilitate the identification of desired derivative clones (in grey).

The described pCYPAC2 primers were used to amplify 10ng of pCYPAC2 template as described in the materials and methods sections 2.12 and 2.14. The linear pCYPAC2 PCR product was fractionated on a 1% agarose gel (Figure 3-5), purified through gel extraction and then introduced by electroporation into *E. coli* cells containing hBAC495J24, and expressing the RED/ET system proteins.

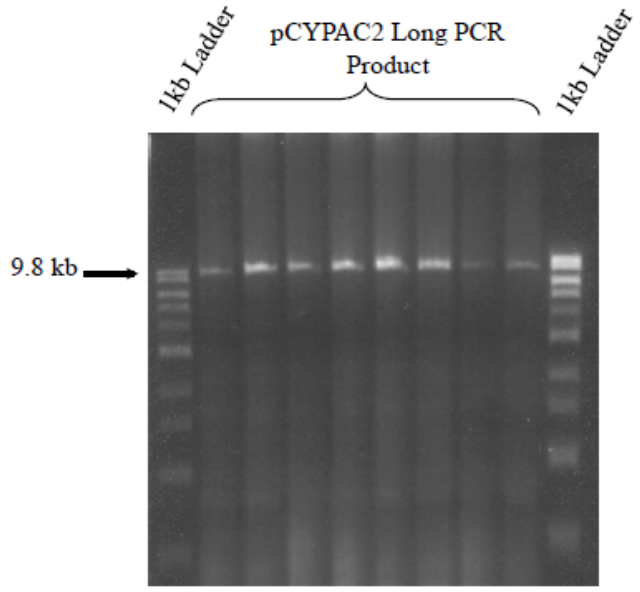

Figure 3-5 pCYPAC2 long PCR product run on a 1% agarose gel.
8 parallel 25µl PCR reactions were performed to scale up the yield of the long PCR product (9.8kb). The products were run on a 1% agarose gel and purified through gel extraction. 1kb ladder was used as a size reference.

Subsequent to the RED/ET recombination reaction, 8 clones were isolated and analysed. Because of the repetitive nature of the alpha satellite array, the *in vivo* RED/ET recombination produced a library of PAC containing an array of different sized 17α satellite DNA sequences. The DNA prepared from colonies was screened using the BamHI enzyme, which released the 9.8kb pCYPAC2 and 17α satellite DNA fragment shorter than the parental hBAC495J24 clone ranging from ~40kb to ~220kb (Figure 3-6). A PAC clone containing approximately 50-60kb of 17α satellite DNA was chosen for further studies and labelled as PACα60 (marked with an asterisk in Figure 3-6). Due to problems with the electrode of the PFGE apparatus in the laboratory, runs were skewed, and thus identification of the exact size of this vector proved difficult (size ranged from ~50-60kb). As a consequence an estimated size of 60kb of 17α satellite DNA was chosen as an approximation.

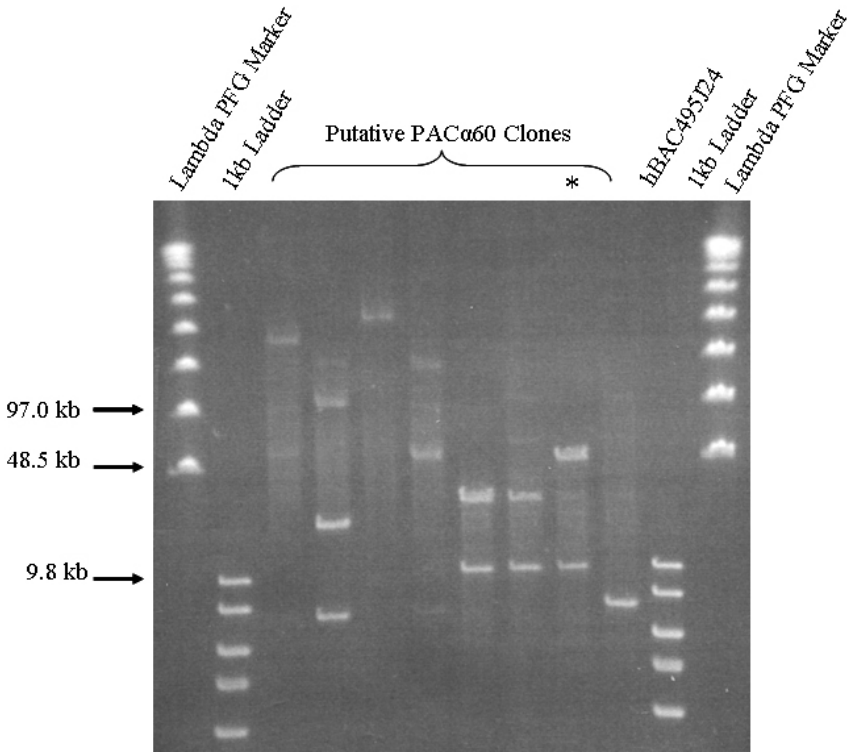

Figure 3-6 Analytical BamHI digest of colonies recovered post RED/ET recombination.
Putative PAC colonies were recovered post RED/ET recombination, and screened using BamHI and run on a 1% PFGE. PACα60 has been marked with an asterisk showing the release of a 9.8kb linear fragment and an approximately 50-60kb of alpha satellite DNA. Lambda PFG Marker and 1kb ladder were used as a size reference.

3.3 Generation of pHSV17αNeo HAC Vectors Using Cre Mediated *loxP* Recombination

To retrofit the hBAC495J24-reduced variants with the HSV-1 origin of replication and packaging signal, BACα40, PACα60 and BACα100 constructs were then recombined with the HSV-1 pHGNeo4 vector using Cre mediated *loxP* recombination as described in materials and methods section 2.13 (Figure 3-7). The BACα40, PACα60 and BACα100 vectors were also recombined further with the pHGBsd and pHGPuro vectors.

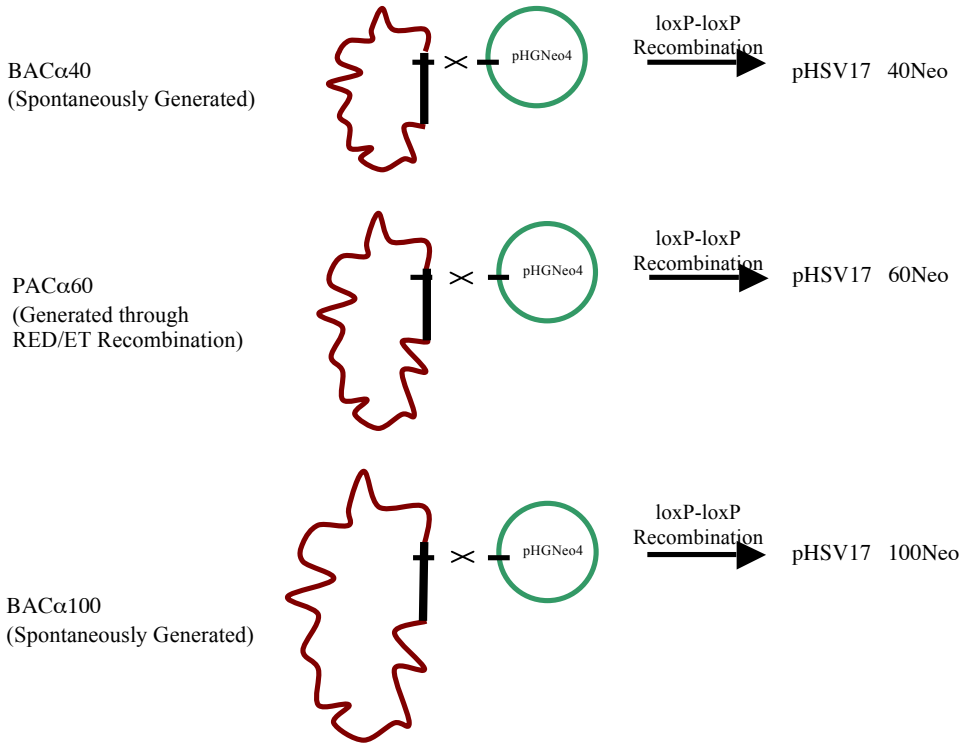

Figure 3-7 Cre mediated *loxP* recombination of pHGNeo4 with BACα40, PACα60 and BACα100.
The hBAC495J24 reduced derivatives (BACα40, PACα60 and BACα100) were recombined with pHGNeo4 using Cre mediated *loxP* recombination, producing HSV-HAC vectors pHSV17α40Neo, pHSV17α60Neo and pHSV17α100Neo.

Following recombination in *E. coli*, five colonies generated from each recombined alpha satellite vector were isolated and the DNA from each vector was analysed using NotI, BamHI and EcoRI enzymes to identify colonies containing the correct construct. The hBAC495J24 and pJM2256 (a derivative of hBAC495J25 and highly efficient at forming HAC) (Mejía et al. 2002) vectors were used as controls. As expected, NotI digestion of pJM2256 resulted in a single product of size ~240kb, while NotI digestion of hBAC495J24, BACα100 and BACα40 released a 7.5kb fragment corresponding to pBeloBAC11, and ~220kb, ~100kb and ~40kb of alpha satellite DNA, respectively. BamHI digestion of PACα60 released the 9.8kb linear fragment from pCYPAC2 and ~60kb of alpha satellite DNA. The pHSV17α40Neo,

pHSV17α60Neo and pHSV17α100Neo vectors showed the correct pattern when digested with NotI and BamHI as they contain the pHGNeo4 (Figure 3-8 A).

The integrity of the core 17α satellite DNA was investigated by EcoRI digestion. In addition to the candidate HAC vectors pHSV17α40Neo, pHSV17α60Neo and pHSV17α100Neo vectors, pJM2256 and hBAC495J25 were also included in the analysis as controls. The expected band size released after EcoRI digest is a 2.7kb 17α satellite DNA consensus; all the described vectors released the expected 2.7kb fragment (Figure 3-8 B).

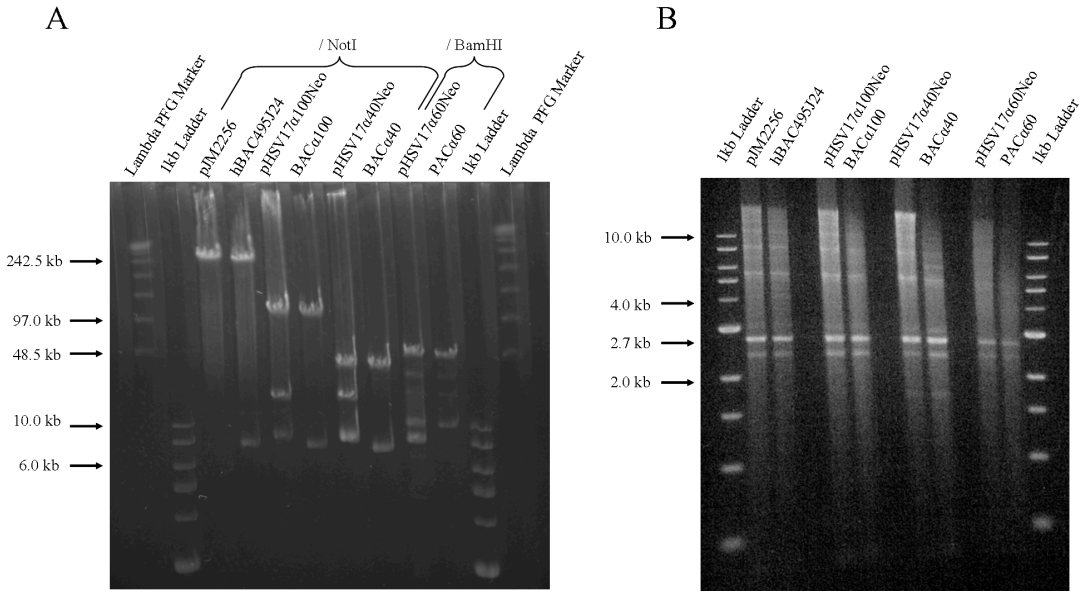

Figure 3-8 Analytical digests of pJM2256, hBAC495J24, pHSV17α100Neo, BACα100, pHSV17α40Neo, BACα40, pHSV17α60Neo and PACα60 using either NotI or BamHI (A) and EcoRI (B) digest.
The pJM2256 was linearised when digested with NotI (~240kb). NotI digest of hBAC495J24, BACα100 and BACα40 released a 7.5kb fragment of pBeloBAC11, and ~220kb, ~100kb and ~40kb of alpha satellite DNA, respectively. BamHI digest of PACα60 released the 9.8kb pCYPAC2 and ~50-60kb of alpha satellite DNA. The pHSV17α40Neo, pHSV17α60Neo and pHSV17α100Neo vectors show the correct pattern when digested with NotI, as they contain the pHGNeo4 vector. The products were run on a 1% PFGE. Lambda PFG Marker was used as a size reference (A). As expected, pJM2256, hBAC495J24 and all the hBAC495J24 reduced derivatives contained the core 2.7kb 17α satellite DNA fragment when digested with EcoRI. The products were run on a 1% agarose gel and a 1kb marker was used as a size reference (B).

Thus, using both spontaneously occurring rearrangement events and RED/ET mediated recombination three candidate HSV-HAC vectors were generated. These vectors differed in size, yet shared the same core 17α satellite DNA sequences. To test the HAC formation capabilities of the candidate HSV-HAC vectors (pHSV17α40Neo, pHSV17α60Neo and pHSV17α100Neo), control experiments were performed on HT1080 cells using both HSV-1 amplicon transduction and transfection.

3.4 HSV-1 Amplicon Transduction versus Transfection in HT1080 Cells

To compare different DNA delivery methods, two vectors differing in size were delivered into HT1080 cells using HSV-1 amplicon mediated transduction, lipofection or electroporation. The HAC vector pHSV21αNeo (containing ~60kb of 21α satellite DNA; total size ~73kb) (Moralli et al. 2006) and a derivative vector pHGNeo4 (8.0kb) were used in this experiment. The pHGNeo4 vector was released from pHSV21αNeo by BstBI digestion to remove the 21α satellite DNA sequences, while retaining the HSV-1 elements, and *GFP* and *Neo* genes (described in materials and methods sections 2.9 and 2.10). These two vectors contained identical promoters on the *GFP* reporter (HSV-1 I/E) and *Neo* selectable marker (SV40). Thus, pHSV21αNeo and pHGNeo4 were comparable vectors when analysing the differences in stable clone formation efficiency.

Table 3-1 presents a comparative analysis of the efficiency of stable clone formation in HT1080 cells using the following DNA delivery methods: HSV-1 amplicon transduction (MOI 5), lipofection and electroporation. The efficiency of stable clone formation was measured as the number of stable clones divided by the number of

target cells (2.5×10^5 for HSV-1 amplicon transduction and 10^7 for lipofection and electroporation). For the smaller vector (pHGNeo4; 8.0kb), HSV-1 transduction was approximately 40 to 200 times more efficient at producing stable clones when compared to electroporation and lipofection, respectively (both $p<0.01$; one-way ANOVA). While, for the larger vector (pHSV21αNeo; ~73kb) HSV-1 transduction was approximately 60 to 400 times more efficient at producing stable clones when compared to electroporation and lipofection, respectively (both $p<0.02$; one-way ANOVA). The fold increase in stable clone formation efficiency was measured by dividing the number of stable clones from each treatment by the number of stable clones obtained through lipofection. These results suggested that HSV-1 amplicons were more efficient at stable clone formation in HT1080 cells compared to both lipofection and electroporation. The difference in efficiency of stable clone formation was further pronounced when a large DNA vector (size ~73kb) was used.

Table 3-1 Comparison of efficiency of stable clone formation using different modes of DNA delivery into HT1080 cells.

Vector	Mode of DNA Delivery	Efficiency of Stable Clone Formation ± SE (%)	Fold Increase in Stable Clone Formation Efficiency Compared to Lipofection
pHGNeo4 (8.0kb)	HSV-1	0.21 ± 0.03	194
	Electroporation	0.0053 ± 0.0008	4.8
	Lipofection	0.0011 ± 0.0004	1.0
pHSV21αNeo (73kb)	HSV-1	0.10 ± 0.02	382
	Electroporation	0.0018 ± 0.0003	6.7
	Lipofection	0.0003 ± 0.0002	1.0

The efficiency of stable clone formation was measured as the number of stable clones divided by the number of target cells. Experiments based on 2 replications per group. MOI 5 was used for HSV-1 amplicon transduction. SE, standard error of the mean.

3.5 HSV-1 Amplicon Transduction of HT1080 Cells

The efficiency of HSV-1 amplicon transduction of new candidate vectors was investigated in HT1080 cells. The candidate vectors pHSV17α40Neo, pHSV17α60Neo and pHSV17α100Neo were used to prepare HSV-1 amplicons. Together with control DNA including pHGNeo4, pHGBsd, pHGPuro and pHSV21αNeo, HSV-1 amplicons were used to transduce 2.5×10^5 HT1080 cells seeded in 24-well plates at MOI 1, 2 and 5. Figure 3-9 shows HT1080 cells expressing *GFP*/*RFP*, 24 hours post HSV-1 transduction with the indicated vector at MOI 2.

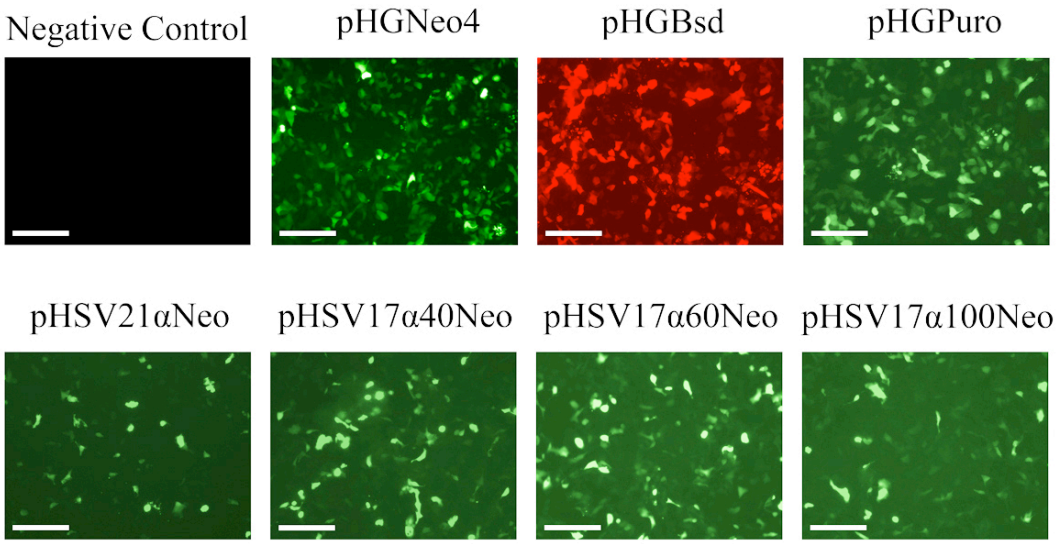

Figure 3-9 HT1080 cells 24 hours post HSV-1 amplicon transduction at MOI 2. HT1080 cells were transduced with the indicated HSV-1 amplicon at MOI 2. Images were taken using an epifluorescence microscope, 24 hours post HSV-1 transduction. Green and red signals show transduced cells expressing *GFP* and *RFP* respectively. Scale bar = 200μm.

From each MOI, the percentage of *GFP*/*RFP* positive cells was determined using an epifluorescence microscope, 24 hours post HSV-1 transduction. The results of HSV-1 amplicon transduction in HT1080 cells are summarised in Table 3-2. For comparative purposes, HT1080 cells were also transfected with each vector using Lipofectamine

2000 as illustrated in materials and methods section 2.17. Furthermore, the pJM2256-GFP vector, highly efficient at HAC formation, was transfected into HT1080 cells as control. As the size of pJM2256-GFP vector was ~90kb larger than the packaging capacity of HSV-1 amplicons, the vector was only delivered to cells by transfection. Transduced and transfected HT1080 cells were placed under the appropriate antibiotic selection and after 7-10 days, the number of stable clones was recorded (Table 3-3).

Table 3-2 HSV-1 transduction and transfection efficiencies of various vectors in HT1080 cells.

Vector	HSV-1 Amplicon Transduction (%)			Transfection (%)*
	MOI 1	MOI	MOI 5	
pHGNeo4	17.7	27.6	40.3	6.7 ± 3.7 [a]
pHGBsd	18.5	32.1	45.0	7.9 ± 1.7 [a]
pHGPuro	14.8	23.6	31.9	6.2 ± 2.1 [a]
pHSV21αNeo	5.5 ± 0.4 [a]	8.4 ± 0.7 [a]	11.7 ± 2.2 [a]	1.38 ± 0.6 [a]
pHSV17α40Neo	13.8	18.9	22.1	0.06
pHSV17α60Neo	23.5	33.7	40.0	0.001
pHSV17α100Neo	17.0	24.7	29.0	0.28
pJM2256-GFP	NA	NA	NA	0.005

Experiments labelled with (a) were based on 2 replications and the remainder was based on 1 replication. Other than transfection with pHGBsd and pHGPuro, the remaining transfection experiments and analyses were performed by Dr Daniela Moralli (marked with an asterisk). NA, not applicable.

Table 3-3 Number of stable HT1080 clones after HSV-1 amplicon transduction or transfection with various vectors.

Vector	HSV-1 Amplicon Transduction			Transfection*
	MOI 1	MOI 2	MOI 5	
pHGNeo4	130	286	532	20
pHGBsd	184	306	666	-
pHGPuro	206	368	738	-
pHSV21αNeo	92	172	248	30
pHSV17α40Neo	134	278	404	4
pHSV17α60Neo	174	308	602	1
pHSV17α100Neo	126	224	390	17
pJM2256-GFP	NA	NA	NA	4

Transfection experiments and analysis were performed by Dr Daniela Moralli (marked with an asterisk). NA, not applicable.

The stable clone formation efficiency was calculated as the number of stable clones after selection and normalised against the initial number of transduced (2.5×10^5) or transfected (10^5) cells. Correlation analysis on samples from each MOI indicated that the number of stable clones was directly correlated with HSV-1 transduction efficiency ($p_{MOI\ 1} = 0.009$, $p_{MOI\ 2} = 0.007$, $p_{MOI\ 5} = 0.002$; analysis includes data point [0, 0] for each MOI. p values calculated using two-tailed Pearson correlation analysis). Based on the best-fit linear regression model, the data suggested that approximately 0.5% of transduced cells formed stable clones (Figure 3-10).

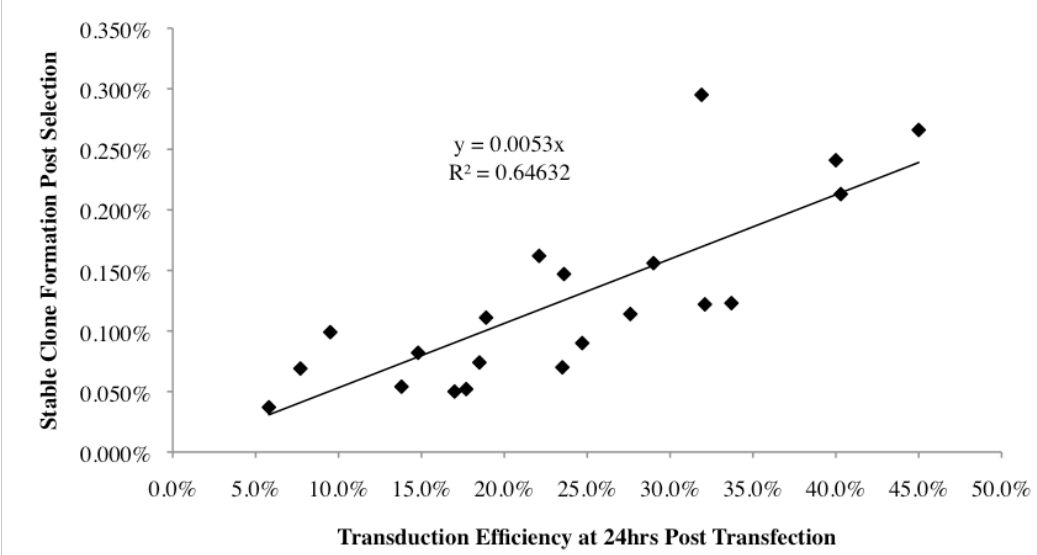

Figure 3-10 Stable clone formation as a function of HSV-1 transduction efficiency in HT1080 cells.
HSV-1 transduction efficiency was measured 24 hours post-treatment and plotted against the stable clone formation efficiency. The best fit linear equation suggests that approximately 0.5% of the transduced cells formed stable clones. R^2 is the coefficient of determination, which implies that 65% of the variation is explained by the linear model (y=0.0053x).

Similar to HSV-1 amplicon transduction, analysis was carried out on the efficiency of stable clone formation as a function of the number of transfected HT1080 cells. There are relatively limited data available to conclusively understand the relationship between the stable clone formation and transfection efficiency. However, correlation

analysis on this limited dataset suggested that the number of stable clones was also directly correlated with the number of transfected cells (p=0.022; analysis includes data point [0, 0]. p value calculated using two-tailed Pearson correlation analysis). Thus, assuming a linear fit model, approximately 1.5% of the transfected cells developed stable clones.

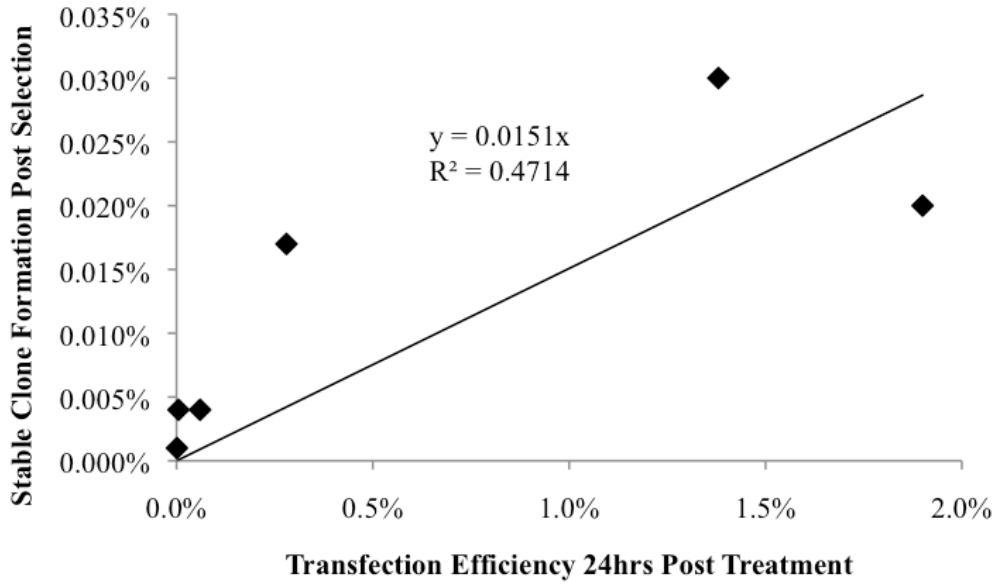

Figure 3-11 Stable clone formation as a function of transfection efficiency in HT1080 cells.
Transfection efficiency was measured 24 hours post-treatment and plotted against the stable clone formation efficiency. The best fit linear equation suggests that approximately 1.5% of the transfected cells developed stable clones. R^2 is the coefficient of determination, which implies that 47% of the variation is explained by the linear model (y=0.0151x).

Regardless of the stable clone formation efficiency in HT1080 cells, HSV-1 amplicon transduction produced a greater number of stable clones when compared to transfection. As a result, the HSV-1 amplicons were preferentially used to deliver large HAC vectors into HT1080 and subsequently hESc (as described in Chapter 5), and were successful at generating a number of stable clones.

3.6 *De novo* HAC Formation in HT1080 Cells

Prior to proceeding to HAC studies in hESc, it was necessary to investigate the HAC forming potential of the candidate HAC vectors in the HT1080 cell line, which is highly efficient at HAC formation (Harrington et al. 1997; Ikeno et al. 1998; Ebersole et al. 2000; Grimes et al. 2002; Mejía et al. 2002). Stable HT1080 clones derived from the HSV-1 transduction of pHSV17α40Neo, pHSV17α60Neo and pHSV17α100Neo vectors were isolated and expanded to study *de novo* HAC formation. Chromosome harvests were obtained from each clone. FISH was carried out as described in materials and methods section 2.25, using two DNA probes: one specific for 17α satellite DNA (detected with FITC conjugated avidin) and one specific for vector DNA (either pBeloBAC11 or pCYPAC2; detected with a TRITC conjugated antibody). Figure 3-12 shows examples of FISH on metaphase spreads on HAC-containing HT1080 stable clones. Putative episomes were scored as HAC only when they were labelled by both 17α satellite DNA and vector probes, and a DAPI signal was present.

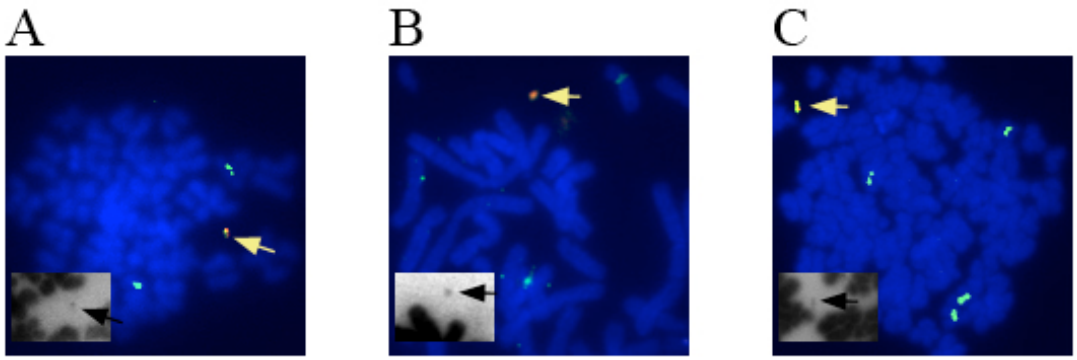

Figure 3-12 FISH analysis of stable HT1080 clones.
Metaphase spreads from stable HT1080 clones containing the pHSV17α40Neo (A), pHSV17α60Neo (B) and pHSV17α100Neo (C) HAC. Probes specific to 17α DNA sequence (in green) and vector DNA (either pBeloBAC11 or pCYPAC2; in red) were used to detect the presence of *de novo* HAC. The 17α satellite DNA probe also recognises the homologous endogenous chromosome 17. The inset shows the inverted DAPI staining for visualisation of the HAC.

In parallel experiments, the stable clones obtained after transfection were similarly analysed by FISH to detect the HAC formation frequency (analysis carried out by Dr Daniela Moralli). Table 3-4 shows the HAC analysis of HT1080 stable clones obtained either through HSV-1 amplicon transduction or transfection. The percentage of HAC present in metaphase spreads is presented as a range (the transfection experiments and HAC analysis of obtained stable clones were performed by Dr Daniela Moralli).

Table 3-4 HAC analysis of HT1080 stable clones.

	HSV-1 Amplicon Transduction			Transfection*		
HAC Vector	**No. of Clones Analysed**	**HAC Positive Clones**	**% of HAC**	**No. of Clones Analysed**	**HAC Positive Clones**	**% of HAC**
pHSV21αNeo	-	-	-	8	4	20-35
pHSV17α40Neo	10	6	5-30	3	3	15-30
pHSV17α60Neo	3	1	20	1	0	-
pHSV17α100Neo	4	1	15	6	1	25
pJM2256	NA	NA	NA	4	3	27-75

Percentage of HAC-positive metaphases scored in the HAC-containing HT1080 clones. Stable clones were screened by FISH, 15-25 metaphases were scored for each clone. Transfection experiments were performed and analysed by Dr Daniela Moralli, marked with an asterisk. NA, not applicable.

In HT1080 cells, using both HSV-1 transduction and transfection, HAC were observed using pHSV17α40Neo and pHSV17α100Neo in ~5-30% of the metaphases in the HAC-containing HT1080 clones. However, in some clones obtained by either method, the HAC DNA had also integrated into the host genome. Figure 3-13 shows examples of integration events in HT1080 cells when delivering the pHSV17α40Neo, pHSV17α60Neo, and pHSV17α100Neo vectors via HSV-1 amplicons.

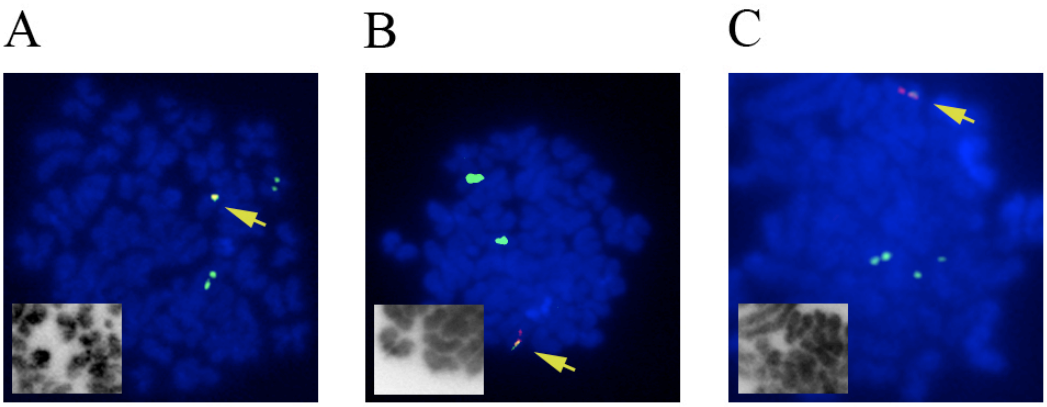

Figure 3-13 Integration events on metaphase spreads of stable HT1080 clones. Metaphase spreads from stable HT1080 clones showing the presence of integration events when using pHSV17α40Neo (A), pHSV17α60Neo (B) and pHSV17α100Neo (C) HSV-1 amplicons. Probes specific to 17α satellite DNA sequence (in green) and vector (either pBeloBAC11 or pCYPAC2; in red) were used to detect the presence of HAC DNA integrations. The 17α satellite DNA probe also recognises the endogenous chromosome 17. The inset shows the inverted DAPI staining.

The HAC vector pHSV17α40Neo appeared to be the most efficient at HAC formation: 6 out of 10 stable HSV-1 clones contained HAC, and all 3 transfected stable clones contained HAC. Using HSV-1 amplicon transduction of pHSV17α60Neo, 1 clone (out of total 3) showed the presence of HAC in ~20% of the metaphases, while due to low transfection efficiencies, only 1 stable clone was recovered through transfection of pHSV17α60Neo, which did not contain HAC. As the results following HSV-1 amplicon transduction of pHSV21αNeo in HT1080 cells were already published (Moralli et al. 2006), only transfection of pHSV21αNeo was carried out in HT1080 cells: 4 out of 8 stable clones contained HAC in ~20-35% of the metaphases. The HAC vector pJM2256 was approximately 90kb larger than the packaging capacity of HSV-1 amplicons, thus it was only introduced into HT1080 cells through transfection. 3 out of 4 stable clones contained HAC in ~27-75% of the metaphases. All stable HT1080 clones, even in the absence of HAC, contained integration events in ~10-35% of the metaphases scored.

3.7 Summary

In this chapter, the construction of three candidate HAC vectors, containing reduced stretches of 17α satellite DNA backbone (~40kb, ~60kb and ~100kb) from the previously studied HAC vector hBAC495J24 (Mejía et al. 2002), was described. These vectors were then joined by Cre mediated *loxP* recombination with pHGNeo4, which contained the *GFP* reporter gene, the *Neo* selectable marker and HSV-1 sequences necessary for packaging and replication. Initially, different methods of DNA delivery (HSV-1 amplicon transduction, electroporation and lipofection) were compared in HT1080 cells. HSV-1 amplicon transduction (at MOI 5) was more efficient at stable clone formation when compared to lipofection and electroporation; such a difference appeared to be more pronounced when using a larger vector (~73kb).

The candidate HAC vectors (pHSV17α40Neo, pHSV17α60Neo and pHSV17α100Neo) along with control vectors (pHGNeo4, pHGBsd, pHGPuro and pHSV21αNeo) were introduced into HT1080 cells via HSV-1 transduction and transfection. Transduction efficiency following vector delivery and stable clone formation appeared to be higher when using HSV-1 transduction as compared to transfection. Depending on the vector type, HSV-1 transduction efficiency at MOI 5 ranged from 11.7±2.2% (pHSV21αNeo; 73kb) to 45.0% (pHGBsd; 7.8kb). By contrast, the transfection efficiency of the delivered vectors appeared to be lower than that of HSV-1 transduction, especially for the larger vectors. The transfection efficiency of small vectors (~8kb) ranged from 6.2±2.1% to 7.9±1.7%; while that of the larger vectors (>55kb) appeared to be even lower, ranging from 0.001% to

1.38±0.6%. Detailed FISH analysis on stable HT0180 clones revealed the presence of HAC in 8 out of 17 clones, with HAC frequencies ranging from ~5-30%; however, genomic integrations were also present. The candidate HSV-HAC vectors were subsequently used in transduction experiments in hESc and will be discussed in the following chapters.

Chapter 4. Results and Discussion II: Optimisation of hESc Growth and Chromosome Harvest Conditions

With the aim of determining the optimal conditions for HSV-1 amplicon transduction, drug selection, stable clone formation and chromosome harvest preparations of hESc, the growth pattern of HUES-2 line was examined in detail.

4.1 HUES-2 Growth Dynamics

Human embryonic stem cells (hESc) require maintenance at high densities, as they need sufficient cell-cell contact to support their viability and retain their pluripotency (Watt and Hogan 2000). However, hESc can also be plated at lower densities; this strategy is generally not recommended as it reduces their proliferation rate and can favour karyotypic abnormalities that result in higher proliferation rates (Ludwig et al. 2006). Thorough qualitative observations, it was noted that when HUES-2 cells were seeded on Matrigel and cultured under mTeSR medium, the cells actively moved on the surface of the dish in an attempt to make new connections with adjacent cells and colonies. This neighbour-seeking behaviour was more apparent when HUES-2 cells were seeded at lower densities on Matrigel, however this phenomenon was not observed with HUES-2 cells grown on inactivated mouse embryonic fibroblasts (MEFi) (data not shown). This reduction in cell mobility could be attributed to the presence of MEFi that provided extra cell support for HUES-2 cells, thus reducing their need to establish further cell-cell contact with neighbouring hESc. These observations are in accordance with recently published studies on the dynamics of hESc growth in culture, where it has been shown that high cell motility at low

densities on Matrigel is an inherent property of hESc, which is essential for their clonogenicity and self-renewal (Li et al. 2010b; Xu et al. 2010).

4.2 Drug Selection of HUES-2 Cells

Initially, broad drug selection conditions were employed using three different commonly used mammalian antibiotics (G418, blasticidin and puromycin) to determine the ideal concentration range for HUES-2 selection. Consequently, the screening identified the necessary selection conditions for further study. Table 4-1 lists the range of antibiotic concentrations used on HUES-2 cells seeded at 2.5×10^5 cells per 24-well on Matrigel, and grown under mTeSR medium. Selection was applied 24 hours after seeding and only maintained for 24 hours, after which, selection was removed and observations were recorded. Two replicate experiments were performed at each concentration. Any treatment that did not kill all the cells was studied for further 3-7 days to monitor the condition and morphology of the surviving cells. The concentrations in the red zone in Table 4-1 were sufficient to kill the entire cell population within 24 hours. The concentrations in the orange zone killed ~95% of the population within the first 24 hours; however, the remaining ~5% were able to recover once selection was removed. The concentrations in the green zone were not sufficient to cause noticeable cell death within the first 24 hours (cell survival>95%).

Table 4-1 Range of different antibiotic concentrations used on HUES-2 cells seeded at 2.5×10^5 cells per 24-well on Matrigel.

Antibiotic	Concentration (µg/ml)									
G418	50		25	10			5	2.5	1.0	
Blasticidin	10	5	2.5	1.0	0.5	0.4	0.2	0.1	0.04	0.02
Puromycin	1.0	0.5	0.25	0.10	0.05	0.04	0.02	0.01	0.004	

Data based on 2 replications per group. The concentrations in red killed the entire cell population within 24 hours. The concentrations in the orange zone killed approximately 95% of the population within the first 24 hours, while the concentrations in the green zone did not cause noticeable cell death within the first 24 hours.

Based on the preliminary experiments described above, provisional concentrations for HUES-2 drug selection were determined, and are listed in Table 4-2. For comparative purposes, the concentrations used for HT1080 cells are also listed in this table. It appeared that HUES-2 cells were ~10-100× more sensitive to drug selection when compared to HT1080 cells.

Table 4-2 Established antibiotic concentrations used for HUES-2 selection.

Antibiotic	Cell Line	
	HUES-2	HT1080
G418	5-25 µg/ml	350 µg/ml
Blasticidin	0.1-0.4 µg/ml	10 µg/ml
Puromycin	0.01-0.04 µg/ml	0.5 µg/ml

To confirm the efficacy of the antibiotic concentrations described in Table 4-2, two independent sets of experiments were carried out to select HUES-2 cells transduced with pHGNeo4, pHGBsd and pHGPuro using G418 (5, 10, 25µg/ml), blasticidin (0.1, 0.2, 0.4µg/ml) and puromycin (0.01, 0.02, 0.04µg/ml), respectively. However, all these experiments were unsuccessful at recovering stable clones. The G418 selection resulted in a steady cell death of the transduced HUES-2 population that lasted 7-10 days; however, at the end of this period no clones were recovered. Blasticidin was inefficient at selecting stable clones at all applied concentrations; even after 10 days

of selection, there was no significant cell death. On the other hand, puromycin rapidly killed the transduced HUES-2 population, leaving no cells after 4-5 days. The reasons behind these unsuccessful attempts at recovering stable clones were not clear. However, possible reasons could be due to the heat sensitivity of blasticidin that made selection ineffective, and the fast mode of action of puromycin that reduced the cell population too rapidly to allow survival of stable colonies. As G418 selection resulted in a steady, yet consistent cell death, and the majority of the HSV-HAC vectors used in this study contained the *Neo* resistance gene, additional experiments were carried out to further refine the optimal G418 selection conditions, before proceeding with any additional stable clone selection experiments.

Titration experiments were carried out on untransduced HUES-2 cells on Matrigel using different seeding cell densities (2.5×10^5, 4.5×10^5 and 5.0×10^5 cells per 24-well dishes) and different G418 concentrations (1.0-50μg/ml). A cell density of 5.0×10^5 cells per 24-well corresponded to a confluency level of approximately 60%. Selection was added 24 hours post cell seeding. These results are summarised in Table 4-3, and suggested that G418 drug selection of HUES-2 cells was density dependent. For example, 50μg/ml of G418 resulted in ~99% cell death within 1 day when selection was applied to 2.5×10^5 cells. However, using the same G418 concentration, it took 3-4 days to result in ~99% cell death when applied to 5.0×10^5 cells seeded per 24-well dish. Similarly, at 10μg/ml of G418, doubling the cell density (from 2.5×10^5 to 5.0×10^5 cells per 24-well) delayed the duration until ~99% population cell death from 1 day to more than 4-5 days. Density dependence of HUES-2 cell selection was most possibly due to the support provided by neighbouring cells as a result of cell-cell

interactions; at higher cell densities, there was more cell-cell support, thus prolonging the period of selection.

Table 4-3 Titration of G418 at different cell densities on HUES-2 cells.

[G418]	Cell Density per 24-well	Days Until Observed ~99% Cell Death
50μg/ml	2.5×10^5	1 day [a]
	5.0×10^5	3-4 days [a]
25μg/ml	2.5×10^5	1 day [b]
20μg/ml	5.0×10^5	5-6 days [b]
15μg/ml	5.0×10^5	No significant signs of cell death within 6 days [a]
10μg/ml	2.5×10^5	1 day [b]
	4.5×10^5	4-5 days [a]
	5.0×10^5	No significant signs of cell death within 6 days [a]
5μg/ml	2.5×10^5	No significant signs of cell death within 24 hours [a]
	4.5×10^5	6-7 days [a]
2.5μg/ml	2.5×10^5	No significant signs of cell death within 24 hours [a]
1.0μg/ml	2.5×10^5	No significant signs of cell death within 24 hours [a]

Selection was performed 24 hours post cell seeding. Experiments labelled by (a) and (b) were based on 2 and 4 replications respectively.

The selection conditions determined thus far were tested in a new set of HSV-1 transduction experiments. Approximately 2.5×10^5 HUES-2 cells were transduced with pHSV21αNeo and pHGNeo4 at MOI 5. Stable clone selection was carried out using 5, 10, 25, and 50μg/ml of G418 on Matrigel, and maintained for 10 days. Out of these selection conditions, only using 25μg/ml of G418 resulted in a small number of putative stable clones, which were observed around the 6^{th} day of selection: 3 colonies following pHSV21αNeo, and 2 from pHGNeo4 HSV-1 transduction. DNA extracted from these putative stable clones was analysed by PCR with primers specific for the vector sequences. As a positive control, DNA from HUES-2 and HT1080 cell pools transduced with pHSV21αNeo was used. PCR analysis of these putative clones revealed that they were false positive colonies. In contrast to the positive controls

(transduced pools), the three isolated "HUES-2 α21" clones (pHSV21αNeo transduced), and the two isolated "HUES-2 Neo" clones (pHGNeo4 transduced), did not amplify the desired vector fragment (Figure 4-1). Primers for Exon 18 of *CNTNAP5* gene (a gift from Dr Alistair Pagnamenta) were used to control for the presence of DNA in each sample.

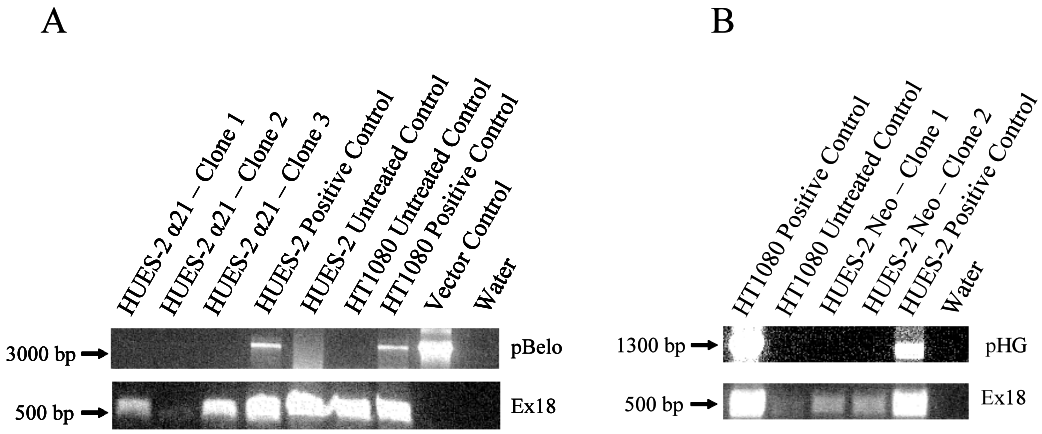

Figure 4-1 PCR analysis of the isolated HUES-2 clones.
Isolated HUES-2 clones transduced with pHSV21αNeo and pHGNeo4 were analysed using "pBelo" (A) and "pHG" (B) primers, respectively. Primers for Exon 18 of *CNTNAP5* gene ("Ex18") were used as DNA loading control. The HT1080 and HUES-2 positive controls were pHSV21αNeo transduced cell pools. 1ng of pHSV21αNeo was used as the vector control.

After several unsuccessful attempts to recover stable HUES-2 clones on Matrigel, an alternative strategy was employed: selection was carried out on Neo^R MEFi using a higher concentration of G418 (50μg/ml). A higher concentration of G418 was used to improve selection stringency to reduce the possibility of recovering false positive colonies, while Neo^R MEFi were used to provide maximal support and growth conditions for the survival of stable HUES-2 clones (Costa et al. 2007). As it will be discussed later in Chapter 6, this approach proved successful as it enabled the isolation of a number of stable HUES-2 clones.

4.3 Maximizing the Number of HUES-2 Metaphase Spreads in Chromosome Preparations

To demonstrate successful *de novo* HAC formation, it is necessary to visualise the HAC through metaphase FISH on high quality, well-spread chromosome spreads. To determine the quality of chromosome preparations, metaphases were harvested using standard protocols, counterstained with DAPI and analysed using an epifluorescence microscope. Initially, ~1.0-2.0×10^6 HUES-2 cells were seeded per 6-well dish on Matrigel and grown under mTeSR media. 24 hours post cell seeding, 0.1 and 100 μg/ml of Colcemid (incubated for 2-4 hours) were used to prepare chromosome harvests from HUES-2 cells (Heng et al. 2006; Catalina et al. 2008). However these conditions were not efficient at arresting sufficient number of cells in metaphase. Overnight incubation of HUES-2 cells in low concentrations of Colcemid (0.1μg/ml) resulted in a moderate percentage of cells arrested in metaphase (9.9±0.9%). However, as chromosome lengths were shortened during extended exposure to Colcemid (Moralli et al. 2011), an alternative mitotic arrest reagent was tested. Nocodazole is a mitotic arrest reagent that disrupts spindle formation during mitosis; however, chromosome length shortening has not been reported using this agent (Jordan et al. 1992; Hirota et al. 2004). Initially, a range of different nocodazole concentrations and incubation periods (listed in Table 4-4) were tested based on literature search (Samson et al. 1979; Vasquez et al. 1997; Cooper et al. 2006; Catalina et al. 2008). Initial qualitative screens of metaphase spreads suggested that an overnight incubation with 0.1μg/ml of nocodazole consistently resulted in the highest number of cells arrested in metaphase.

Table 4-4 Nocodazole concentrations and incubation periods initially tested on HUES-2 cells.

Nocodazole Concentration (µg/ml)	Incubation Period (hours)
3.0	2
3.0	4
1.5	3
0.1	8
0.1	16

To initiate a comparative study on the number of cells arrested in metaphase, 2-6 replicate cultures of HUES-2 seeded at ~2.0×10^6 cells per 6-well dish on Matrigel and grown under mTeSR media were set up 24 hours prior to treatment. The cells were then incubated in various concentrations of Colcemid and nocodazole and incubated for various time periods as outlined in Table 4-5. Incubation of HUES-2 in a concentration lower than 0.1µg/ml of Colcemid or nocodazole resulted in very low number of cells arrested in metaphases. The highest percentage of cells arrested in metaphase was obtained from overnight incubation of cells in 0.1 µg/ml of nocodazole (19.2±1.1%). The percentage of cells arrested in metaphase (mitotic index) was calculated as the number of metaphases over the total number of cells present in 10 randomly selected microscope fields using a 10× objective; these results are summarised in Table 4-5.

Table 4-5 Mitotic Index of HUES-2 cells after incubation with various concentrations of Colcemid and nocodazole.

Mitotic Arrest Reagent	Concentration (µg/ml)	Incubation Period	Number of Replicates	Mitotic Index ± SE (%)
Colcemid	100	4hrs	2	1.8 ± 0.2
	0.1	4hrs	6	2.4 ± 0.7
	100	Overnight	2	5.7 ± 1.2
	0.1	Overnight	3	9.9 ± 0.9
	<0.1	Overnight	2	ND (values too low)
Nocodazole	0.1	4hrs	3	4.3 ± 1.3
	0.1	Overnight	6	19.2 ± 1.1
	<0.1	Overnight	2	ND (values too low)

The mitotic index was calculated as the number of metaphases over the total number of scored cells. ND, not determined. SE, standard error of the mean.

The mitotic index data were analysed using one-way ANOVA after ArcSine transformation, as described in materials and methods section 2.32 and are tabulated in Table 4-6. Overnight incubation in 0.1 µg/ml of Nocodazole was identified as the condition that significantly maximised the number of metaphase spreads (19.2±1.1%) when compared to all other treatments. Next, experiments were carried out to improve the quality of the metaphase spreads for reliable HAC analysis.

Table 4-6 Statistical comparisons of the mitotic index of various treatments

	Col 0.1µg/ml 4hrs	Col 100µg/ml O/N	Col 0.1µg/ml O/N	Noc 0.1µg/ml 4hrs	Noc 0.1µg/ml O/N
Col 100µg/ml 4hrs	p=0.999	p=0.492	p=0.007	p=0.785	p<0.001
Col 0.1µg/ml 4hrs		p=0.449	p=0.001	p=0.786	p<0.001
Col 100µg/ml O/N			p=0.269	p=0.982	p<0.001
Col 0.1µg/ml O/N				p=0.045	p<0.001
Noc 0.1µg/ml 4hrs					p<0.001

One-way ANOVA was used to calculate statistical significance after ArcSine transformation of the mitotic index data. Col, Colcemid. Noc, nocodazole. O/N, Overnight.

4.4 Improving the Quality of HUES-2 Metaphase Spreads

Initially, the chromosome spreads of HUES-2 cells were prepared using standard (75mM KCl) hypotonic solution. Using standard KCl hypotonic solution, the majority of the recovered metaphases were tightly packed and consisted of predominantly unidentifiable chromosomes. The large number of chromosomal overlaps per metaphase complicated downstream karyotypic and HAC analysis. To improve the quality of chromosome spreads, lower concentrations of KCl hypotonic solution (as low as 30mM) and extended incubation periods in hypotonic solution (up to 40 minutes) at 37ºC were tested. Furthermore, different methods of dropping cells onto slides were tested either on slides dipped in ice-cold dH_2O, or slides placed over a humid chamber. Neither of these modifications resulted in any noticeable improvement to the quality of the spreads (data not shown).

Next, two commercially available hypotonic solutions from Genial Genetics were tested as an alternative to the standard KCl hypotonic: buffered hypotonic solution (BHS) and optimal hypotonic solution (OHS). Incubation of chromosome harvests in BHS (0.4% (w/v) KCl with HEPES, pH 7.4) for 30 minutes at 37ºC showed a dramatic improvement to the quality of the chromosome spreads when compared to 75mM KCl (Figure 4-2). The chromosomes in the majority of the metaphases were spread over a larger area, thus significantly reducing the number of chromosomal overlaps (listed in Table 4-7; data analysis using two sample t-test). The effects of OHS on the quality of the spreads were not significantly different from standard KCl (data not shown).

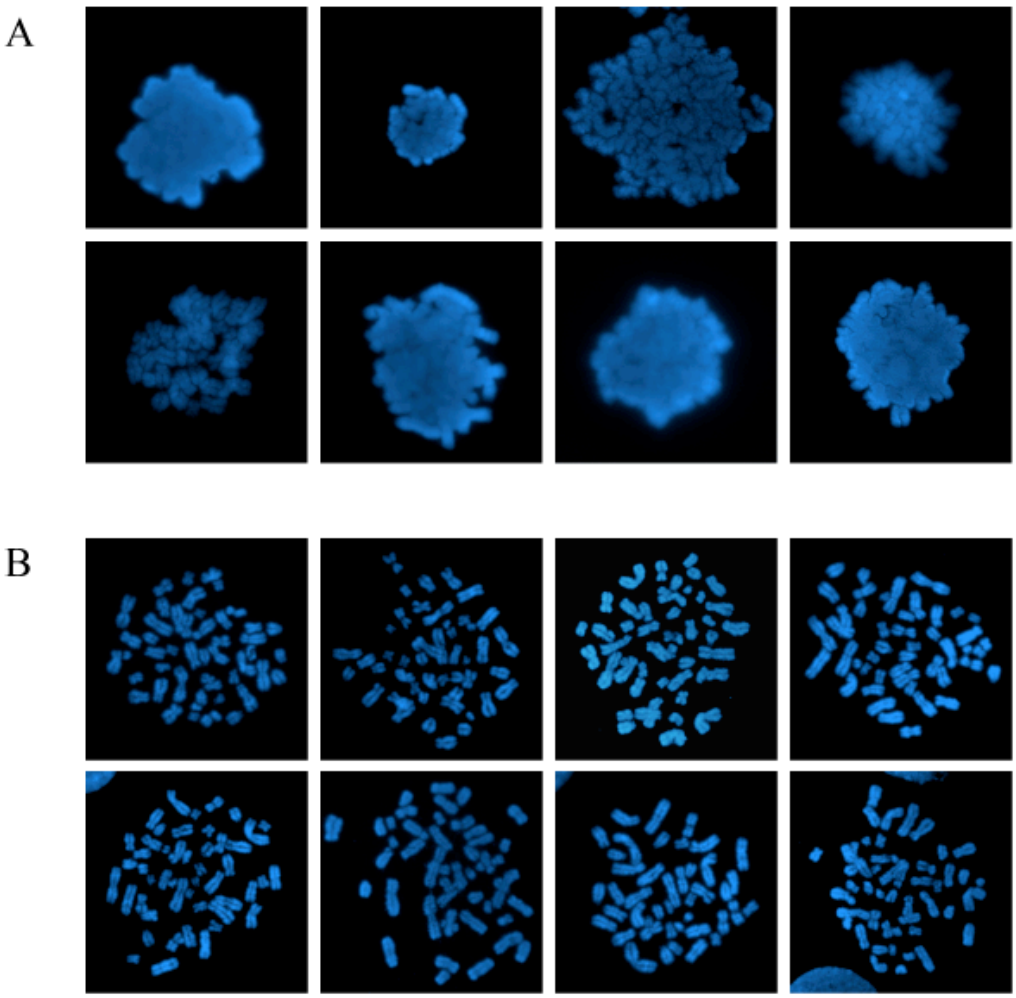

Figure 4-2 HUES-2 chromosome harvests prepared using either 75mM KCl (A) or buffered hypotonic solution (B).
HUES-2 chromosome harvests prepared in suspension after overnight treatment with 0.1µg/ml of nocodazole using either standard 75mM KCl (A) or buffered hypotonic solution (B).

Table 4-7 Mean number of chromosome overlaps per metaphase using 75mM KCl hypotonic compared to the buffered hypotonic solution (BHS).

Mitotic Arrest Reagent	Hypotonic	Mean Number of Chromosome Overlaps/Metaphase ± SE	Range of Overlaps	Significance of the Difference (Two Sample t-test)
Colcemid	75mM KCl	12.6 ± 1.3	4-23	p<0.001
	BHS	4.3 ± 0.8	0-10	
Nocodazole	75mM KCl	12.8 ± 1.2	5-23	p<0.001
	BHS	4.8 ± 0.9	0-16	

25 metaphases were scored for each treatment. Data scored and analysed by Dr Daniela Moralli. BHS, buffered hypotonic solution. SE, standard error of the mean.

The number of overlaps per metaphase using BHS ranged from 0-16, while for 75mM KCl this value ranged from 4-23. An overlap value of 23 indicated that all the chromosomes were involved in at least one overlapping event. Treatments with buffered hypotonic solution resulted in approximately a 3-fold reduction in the mean number of chromosomal overlaps compared to 75mM KCl in both Colcemid and nocodazole treated samples (both $p<0.001$; two-sample t-test). The results clearly indicated that preparing HUES-2 chromosome harvests using the buffered hypotonic solution consistently resulted in better chromosome spreads compared to 75mM KCl hypotonic solution. The use of BHS in preparing chromosome spreads was not only instrumental in improving the quality of the spreads for improved and accurate HAC detection through FISH, it also paved the way for detailed karyotypic analysis using chromosome paints and M-FISH.

4.5 Summary

In this chapter, the growth pattern of HUES-2 cells, conditions for feeder and feeder-free drug selection and preparation of high quality chromosome spreads were described. Use of 50μg/ml of G418 and *Neo*^{R} MEFi as a feeder layer were determined as the ideal selection conditions for obtaining stable HUES-2 clones. Using an improved chromosome harvest protocol, both the quantity and quality of metaphase spreads in chromosome harvests were improved for subsequent FISH analysis. Overnight incubation using 0.1μg/ml of nocodazole resulted in a substantial improvement to the number of cells arrested in metaphase over conventional protocols (4 hours of incubation in 100μg/ml of Colcemid). Furthermore, use of the commercially available buffered hypotonic solution over 75mM KCl, dramatically reduced the number of overlapping chromosomes in metaphase spreads.

Chapter 5. Results and Discussion III: HSV-1 Amplicon Transduction of hESc

In this section, the previously described candidate HSV-HAC vectors were used in the HSV-1 transduction of the HUES-2 cells to investigate *de novo* HAC formation in hESc.

5.1 Optimisation of HSV-1 Amplicon Transduction of HUES-2 Cells

Pilot experiments were undertaken to establish ideal conditions for HSV-1 amplicon transduction of HUES-2 cells. Initially, two seeding cell densities (2.5×10^5 and 5.0×10^5 cells per 24-well) and three different multiplicities of infection (MOIs 1, 5 and 10) were tested using pHSV21αNeo HSV-1 amplicons to maximise the transduction efficiency. HSV-1 transduction was then carried out 24 hours post cell seeding, and the transduction efficiency was measured 24 hours post-treatment. Through qualitative observations, it was noticed that HSV-1 transduction efficiency of HUES-2 was reduced at higher cell densities (data not shown). Table 5-1 shows the HSV-1 transduction efficiency of HUES-2 cells 24 hours post-treatment using 2.5×10^5 cells per 24-well dish. The transduction efficiencies at MOIs 5 and 10 were significantly higher than that of MOI 1 (both $p<0.05$; one-way ANOVA). However, as there was no significant difference between the HSV-1 transduction efficiency at MOIs 5 and 10 ($p=0.660$; one-way ANOVA), the results suggested that at approximately MOI 5 to 10, the cells had probably reached their maximal transduction threshold.

Table 5-1 HSV-1 transduction efficiency of HUES-2 cells using pHSV21αNeo HSV-1 amplicons at different multiplicities of Infection.

MOI	HSV-1 Transduction Efficiency (% ± SE)
1	20.7 ± 1.7
5	30.3 ± 2.8
10	33.7 ± 3.2

Data based on 3 replications per group. SE, standard error of the mean.

Thus, similar to HT1080 cells, 2.5×10^5 HUES-2 cells seeded in 24-well plates on Matrigel were used as an ideal cell density for HUES-2 transduction. Furthermore, MOIs ranging from 1 to 5 were assumed ideal for the HSV-1 transduction of hESc. In an attempt to maximise the HSV-1 amplicon transduction efficiency of hESc, while minimising the amount of amplicons used (due to their potential toxic effects, as observed by significant cell loss in HSV-1 transduced mesenchymal stem cells (El-Sherbini 2010 and unpublished data from our laboratory)), following addition of HSV-1 amplicons, the cells were centrifuged under a low gravitational force (~750g), a process known as spinoculation (O'Doherty et al. 2000).

Figure 5-1 shows spinoculated versus non-spinoculated HUES-2 cells transduced with pHGNeo4 and pHGBsd at MOIs 1, 2 and 5. Spinoculation increased the HSV-1 transduction efficiency, especially at lower MOIs prior to reaching the HSV-1 transduction saturation threshold. The mechanism through which spinoculation increases HSV-1 transduction efficiency is not well defined (O'Doherty et al. 2000). However, as HSV-1 amplicons are too small, ~150-200nm in diameter (Boddingius et al. 1987; Jacobs et al. 1999a; Sena-Esteves et al. 2000), to be settled to the bottom of the well by the applied weak gravitational force, it is unlikely that such a force is directly acting upon the amplicon particles. Instead, it is hypothesised that the applied

gravitational force acts on HSV-1 amplicons that are attached to residual cell debris from the amplicon preparation process (El-Sherbini 2010).

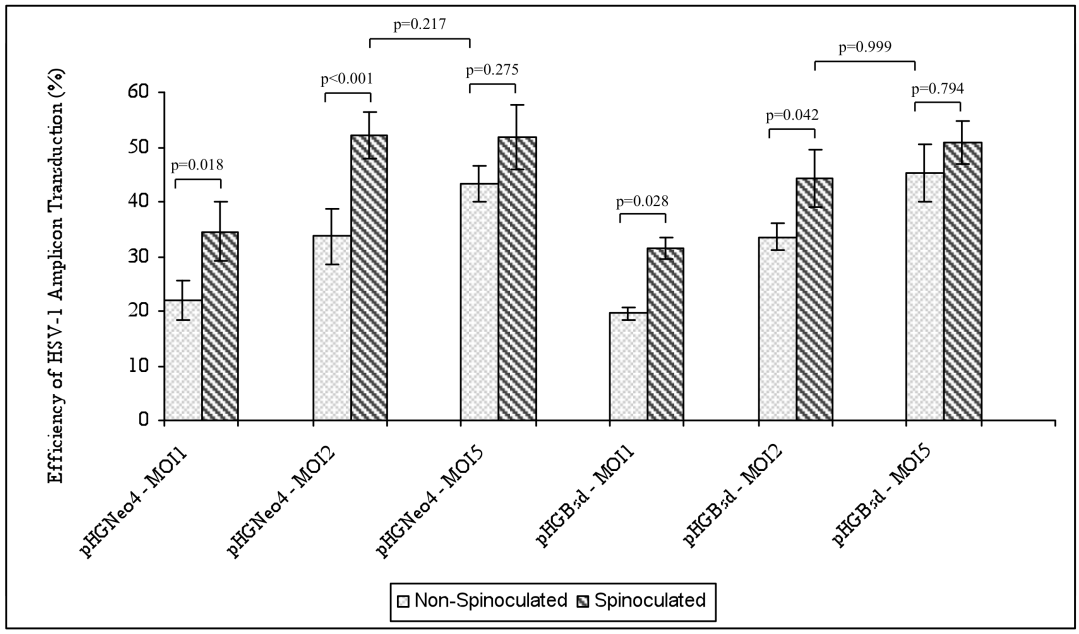

Figure 5-1 HSV-1 transduction efficiency of spinoculated versus non-spinoculated samples.
Data based on 3 replications per group. At each MOI, the HSV-1 transduction efficiency was measured as the number of *GFP* or *RFP* positive cells scored 24 hours post-treatment (with either pHGNeo4 or pHGBsd HSV-1 amplicons) divided by the total number of treated cells. Solid and dashed bars represent the transduction efficiency for non-spinoculated and spinoculated samples, respectively. Error bars represent standard error of the mean. The statistical significance between each group is indicated by the p value and calculated using one-way ANOVA.

There was a statistically significant increase in the transduction efficiency of the spinoculated samples when compared to non-spinoculated samples at MOIs 1 and 2. The average improvement to the HSV-1 amplicon transduction efficiency after spinoculation was ~60% at MOI 1 and ~45% at MOI 2 (all $p<0.05$; one-way ANOVA). While, at MOI 5, the difference between the spinoculated and non-spinoculated samples was not statistically significant (one-way ANOVA). Furthermore, as there was no statistically significant difference between the transduction efficiency of the spinoculated MOI 2 and the non-spinoculated MOI 5 samples (one-way ANOVA), it was decided to predominantly use MOI 2 in

combination with spinoculation in the transduction of HUES-2 cells, in order to reduce the amount of amplicons used per experiment.

Reducing the amount of HSV-1 amplicons per transduction was initially carried out due to concerns regarding potential toxic effects as mentioned previously. However, as will be described in sections 5.3 and 5.4, no adverse effects were observed as a result of the HSV-1 amplicon transduction of HUES-2 cells; therefore, spinoculation only served to improve the transduction efficiency to amplicon ratio. Due to genetic variation, other pluripotent or multipotent cell lines (Allegrucci and Young 2007; Bock et al. 2011) may be more sensitive to HSV-1 amplicon transduction. In such instances, spinoculation might provide an added advantage in reducing potentially undesirable toxic effects, while maintaining satisfactory efficiencies of transgene delivery into cells.

5.2 HSV-1 Amplicon Transduction of HUES-2 Cells

After performing preliminary experiments to establish the ideal conditions for HSV-1 amplicon transduction of HUES-2 cells (2.5×10^5 cells seeded per 24-well dish on Matrigel, using MOI 2 and spinoculation), experiments were carried out to introduce HAC vectors (pHSV21αNeo, pHSV17α40Neo, pHSV17α60Neo, pHSV17α100Neo) and control vectors (pHGNeo4, pHGBsd, pHGPuro) into HUES-2 cells to obtain stable clones. As shown in Figure 5-2, a high proportion of the HUES-2 cells expressed *GFP*/*RFP*, 24 hours post HSV-1 transduction at MOI 2.

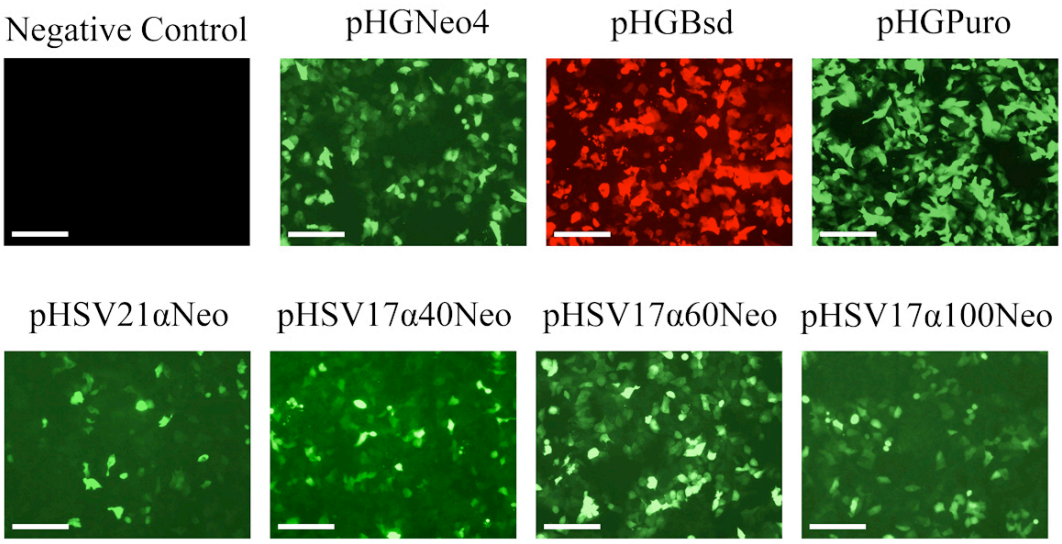

Figure 5-2 HSV-1 amplicon transduced HUES-2 cells expressing *GFP*/*RFP* 24 hours post-treatment.
HUES-2 cells were transduced with various HSV-1 amplicons at MOI 2. Images were taken using an epifluorescence microscope, 24 hours post HSV-1 transduction. Green and red signals show transduced cells expressing *GFP* and *RFP* respectively. Scale bar = 200μm.

Table 5-2 presents HSV-1 amplicon transduction of HUES-2 cells using various vectors at different MOIs and their corresponding HSV-1 transduction efficiencies at 24 hours post-treatment. HSV-1 transduction efficiency was measured by calculating the percentage of *GFP*/*RFP* positive cells using an epifluorescence microscope. The HSV-1 transduction efficiency of HSV-1 amplicon vectors in HUES-2 cells appeared to be comparable to, or even higher than that of HT1080 cells (see Table 3-2). In particular, pHGPuro demonstrated very high HSV-1 transduction efficiencies; up to 84% of HUES-2 cells were transduced at MOI 5. Treatments marked with Δ (under the MOI 2 column) led to stable clone formation following selection (described in Chapter 6). In parallel experiments, the same vectors were also used to transfect HUES-2 cells as a control using ExGen 500 (experiments and data analysis performed by Dr Daniela Moralli, marked with an asterisk). Transfection experiments to HUES-2 cells also included the delivery of pJM2256-GFP, which as previously mentioned,

can only be delivered by transfection due to its size being larger than the HSV-1 amplicon capacity.

Table 5-2 HSV-1 transduction and transfection efficiencies of various vectors in HUES-2 cells.

Vector	HSV-1 Amplicon Transduction (%)			Transfection* (%)
	MOI 1	MOI 2	MOI 5	
pHGNeo4	27.3 ± 1.7 [b]	41.4 ± 3.1 [b Δ]	48.8 ± 2.8 [b]	6.00
pHGBsd	25.5 ± 3.4 [a]	38.9 ± 2.3 [a]	47.7 ± 3.7 [a]	ND
pHGPuro	55.7	62.4	84.3	ND
pHSV21αNeo	14.5 ± 5.7 [a]	16.9 ± 2.3 [b Δ]	22.5 ± 7.1 [a]	0.01
pHSV17α40Neo	ND	40.4 ± 4.2 [b Δ]	ND	0.17
pHSV17α60Neo	ND	20.1 ± 3.6 [b Δ]	ND	0.01
pHSV17α100Neo	ND	16.2 ± 4.9 [b Δ]	ND	0.11
pJM2256-GFP	NA	NA	NA	0.01

Experiments labelled with (a) and (b) were based on 2 and 4 replications respectively, and the remainder was based on 1 replication. All HSV-1 transduced samples were spinoculated. Treatments marked with Δ (under the MOI 2 column) were selected using G418 on *Neo*^{R} MEFi and formed stable clones. Transfection experiments and data analysis performed by Dr Daniela Moralli, marked with an asterisk. NA, not applicable. ND, not determined.

As mentioned, due to the potential toxic effects of HSV-1 amplicons on stem cells (as observed in mesenchymal stem cells), it was necessary to investigate whether there were any potential adverse toxic and morphogenic effects of HSV-1 amplicons on hESc. Thus, the growth rate and morphology of HSV-1 transduced HUES-2 cells was measured and monitored following HSV-1 transduction.

5.3 Viability of HUES-2 Cells Post HSV-1 Amplicon Transduction

Following qualitative observations based on numerous HSV-1 amplicon transduction experiments performed on HUES-2 cells, neither reductions in cell viability, nor morphological changes were observed. To quantitatively assess these observations, 2.5×10^5 HUES-2 cells were transduced on Matrigel using either pHGNeo4 or pHGBsd HSV-1 amplicons at MOIs 1, 2 and 5 and their growth was followed in

culture in the absence of selection for up to 6 days. Figure 5-3 summarises the population size at 0, 3 and 6 days post HSV-1 transduction. Half of the samples were spinoculated to also study the impact of spinoculation on cell survival.

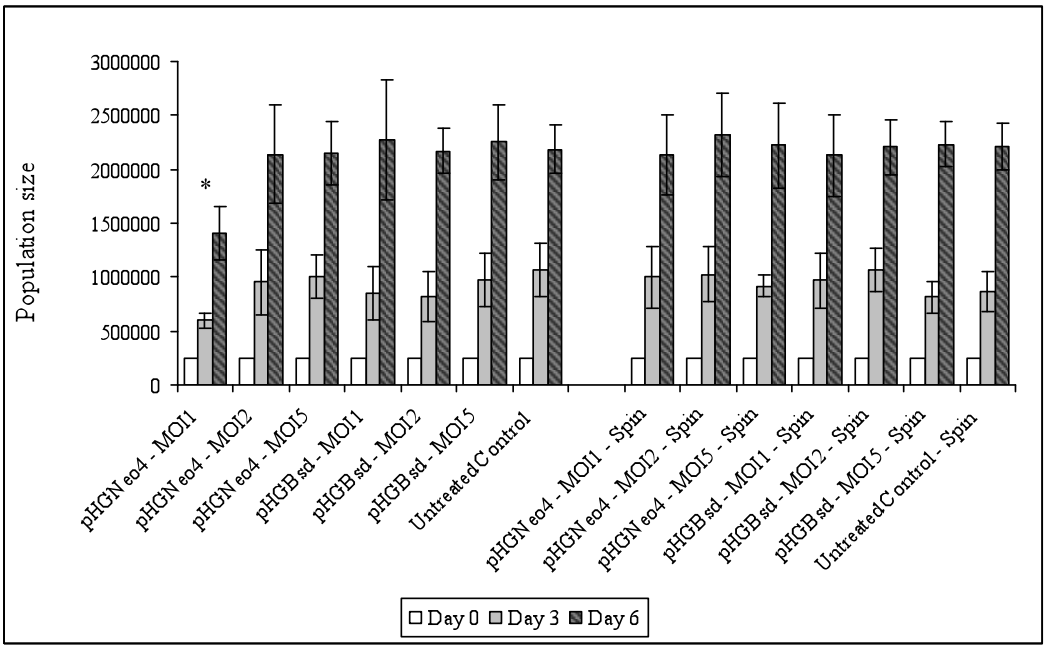

Figure 5-3 HUES-2 cell density at 0, 3 and 6 days post HSV-1 amplicon transduction.
The HUES-2 cells were transduced with pHGNeo4 and pHGBsd amplicons at MOI 1, 2 and 5. Half the samples were spinoculated, as labelled by "spin." White bars represent the population size on the day of HSV-1 transduction (day 0). Solid bars represent population size on day 3, while dashed bars represent population size on day 6 post HSV-1 transduction. During passaging of the pHGNeo4 MOI 1 treatment (marked with an asterisk), a significant number of cells were lost due to error. Data based on 6 replications per group. Error bars represent standard error of the mean.

Using these data, the average doubling time of the various treatment groups was calculated, as described in materials and methods section 2.33, and is listed in Table 5-3. There was no significant difference between the average daily growth rates of spinoculated versus non-spinoculated samples ($p=0.886$; two-sample t-test, analysis excludes pHGNeo4 MOI 1 non-spinoculated treatment marked with an asterisk). Furthermore, using one-way ANOVA, no significant difference was detected in the average daily growth rate of any of the treatment groups (analysis excludes pHGNeo4

MOI 1 non-spinoculated treatment marked with an asterisk). Thus, neither increasing the amount of HSV-1 amplicons, nor spinoculation had a measurable effect on the growth rate of HUES-2 cells.

Table 5-3 Average doubling time (days) of HUES-2 cells post HSV-1 amplicon transduction.

Treatment		Average Doubling Time (Days) ± SE	
Vector	**MOI**	**Non- Spinoculated**	**Spinoculated**
pHGNeo4	1	3.47* ± 0.59	2.80 ± 0.40
	2	2.79 ± 0.49	2.69 ± 0.33
	5	2.79 ± 0.31	2.75 ± 0.38
pHGBsd	1	2.72 ± 0.51	2.80 ± 0.40
	2	2.78 ± 0.20	2.76 ± 0.25
	5	2.73 ± 0.31	2.74 ± 0.19
Untreated Control	-	2.77 ± 0.21	2.75 ± 0.21

Data based on 6 replications per group. During passaging of the pHGNeo4 MOI 1 treatment (marked with an asterisk), a significant number of cells were lost due to error. SE, standard error of the mean.

5.4 Morphology of HUES-2 Cells Post HSV-1 Amplicon Transduction

Qualitative observations of HUES-2 cells post HSV-1 amplicon transduction indicated that transduced cells did not demonstrate immediate morphological alterations. This observation indicated that neither HSV-1 amplicons, nor other less defined factors present in the amplicon preparation (such as cell debris) caused morphological changes in HUES-2 cells. Figure 5-4 compares the morphology of HSV-1 amplicon-transduced HUES-2 cells, 24 hours post-treatment against untreated HUES-2 cells on Matrigel. No immediate noticeable morphological changes were observed between transduced and untreated cells. The HSV-1 transduced cells were

closely monitored for 7 days post-treatment; *GFP* and non-*GFP*-expressing cells showed no observable signs of morphological change (Figure 5-5). As will be described in chapters 6 and 7, detailed follow up studies on a subset of stable HSV-1 transduced HUES-2 clones showed no further evidence of morphological change or loss of pluripotency. Thus, to date, there is no evidence demonstrating that HSV-1 amplicon transduction has any immediate or long-term effect on either morphology or pluripotency of hESc.

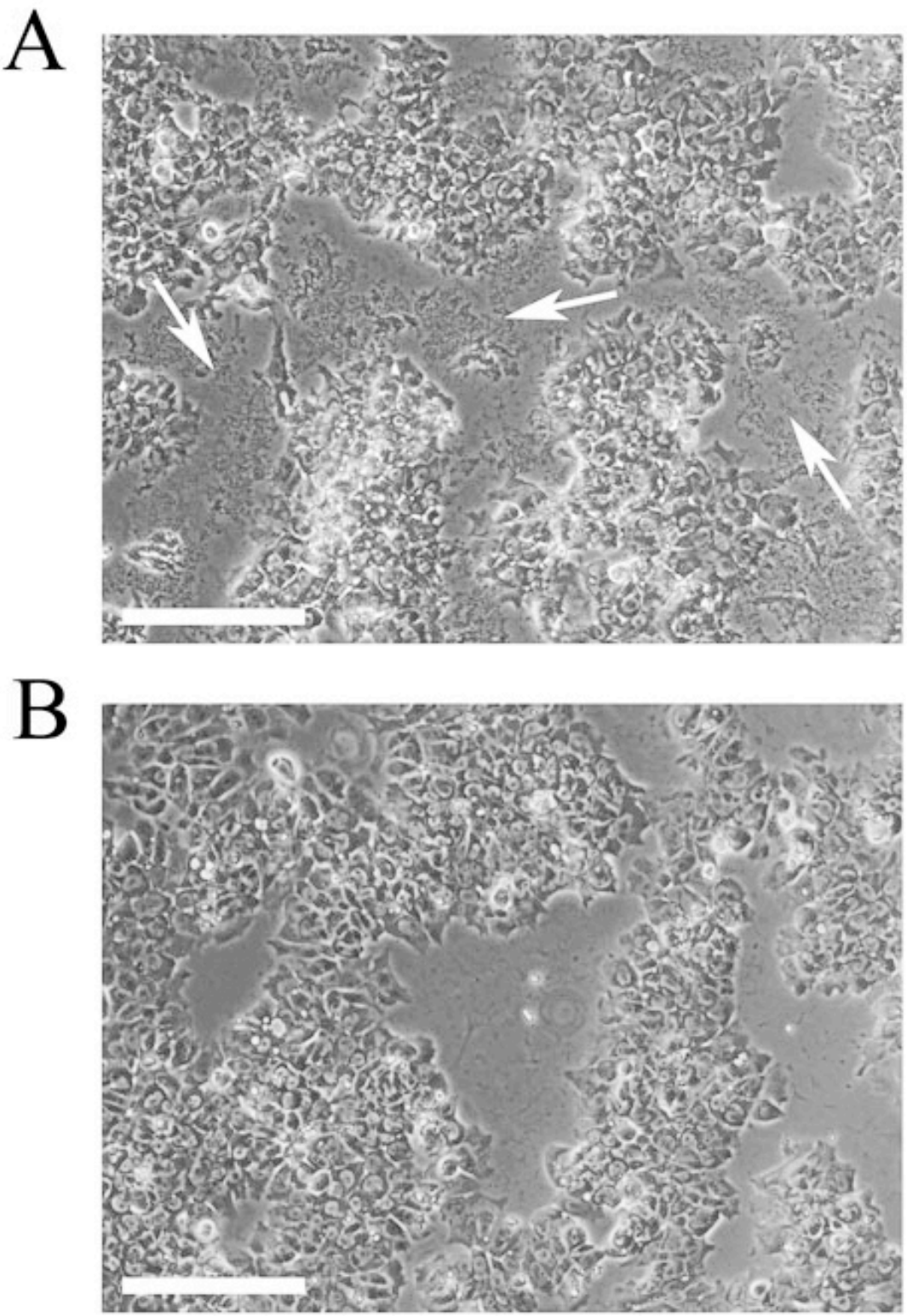

Figure 5-4 HSV-1 amplicon transduced versus untreated HUES-2 cells, 24 hours post-treatment.

No observable morphological differences were detected between HSV-1 amplicon-transduced HUES-2 (A) and untreated HUES-2 (B) cells the day following HSV-1 transduction. In A, arrows point to cell debris from the HSV-1 amplicon preparation that had adhered to the surface of the well. The cell debris was removed after a few washes with PBS. Scale bar = 200μm.

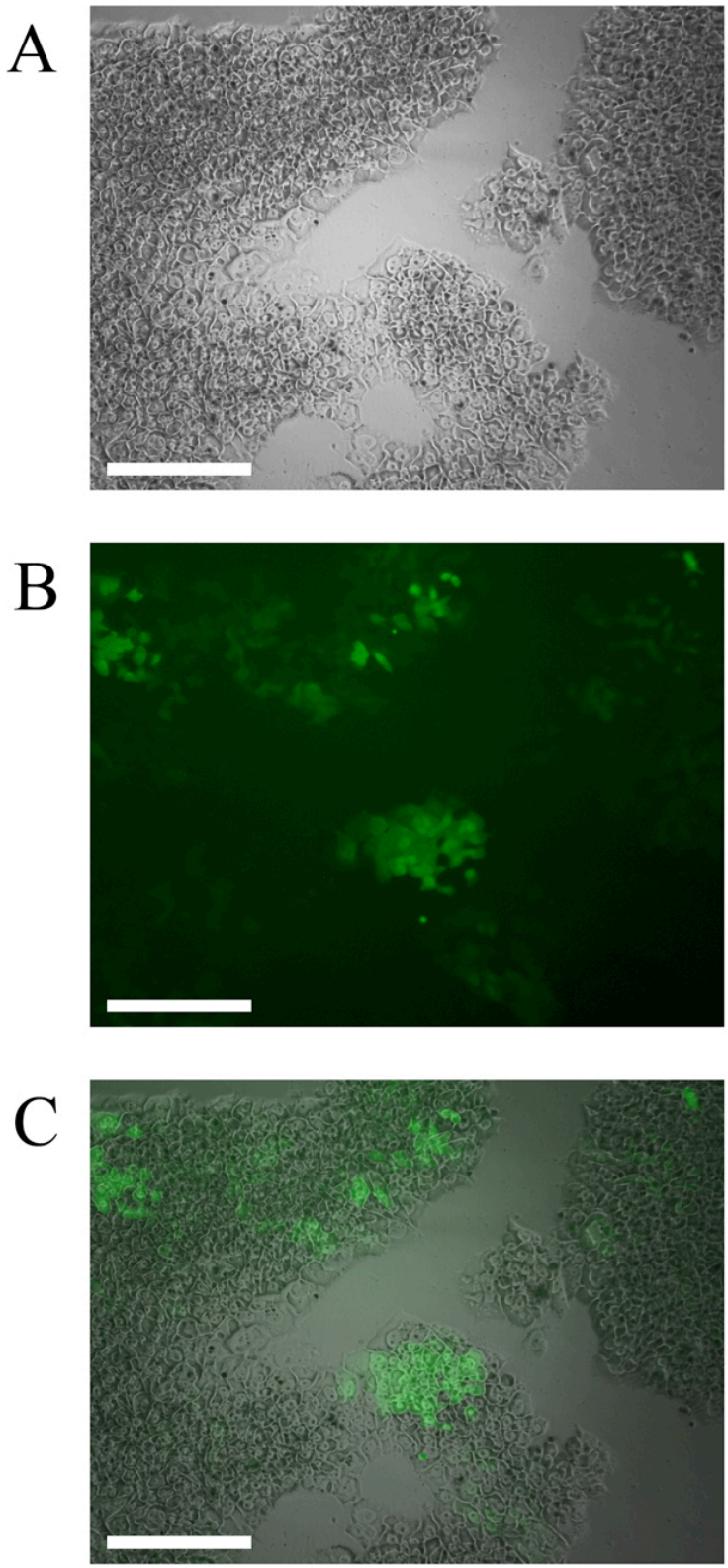

Figure 5-5 HSV-1 amplicon transduced HUES-2 cells 7 days post-treatment. HUES-2 cells 7 days post HSV-1 amplicon transduction using pHGNeo4 at MOI2. Images show the bright field view of transduced HUES-2 cells (A), the same field showing *GFP*-expressing cells (B) and merged fields (C). As suggested here, there are no visible signs of morphological difference between *GFP* and non-*GFP*-expressing HUES-2 cells. Scale bar = 200μm.

5.5 Summary

In this chapter, HSV-HAC vector amplicons were used to transduce HUES-2 cells to obtain stable clones. Ideal conditions for HSV-1 amplicon transduction of HUES-2 cells were determined at approximately 2.5×10^5 cells seeded per 24-well dish on Matrigel. MOI 2 in conjunction with subjecting cells to low gravitational forces (~750g) for 30 minutes resulted in optimal HSV-1 transduction conditions for the amount of amplicon used. Depending on the vector type, HSV-1 amplicon transduction efficiency ranged from 14.5±5.7% (pHSV21αNeo; 73kb at MOI 1) to 84.3% (pHGPuro; 7.7kb at MOI 5). By comparison, the transfection delivery appeared to be less efficient: for pHGNeo4 (8.0kb) was 6.0%, while that of the larger vectors (>55kb) appeared to be even lower, ranging from 0.01% to 0.17%. The results suggested that the high transduction efficiency of HSV-1 amplicons overcame the challenge of introducing large vectors into hESc. Furthermore, there were no noticeable immediate or long-term reductions in cell viability or morphological changes observed in the HUES-2 line post HSV-1 transduction.

Chapter 6. Results and Discussion IV: Generation of *de novo* HAC in hESc

After successful HSV-1 amplicon transduction of HUES-2 cells, they were plated onto *Neo*^{R} MEFi where drug selection was applied. After approximately 3 weeks, stable HUES-2 clones were isolated, expanded and screened initially by PCR. Positive clones were then analysed by FISH to confirm the presence of HAC. The established HAC were characterised using immuno-FISH and fibre-FISH, and their mitotic stability and gene expression was monitored for 90 days in the presence and absence of selection.

6.1 Isolation of Stable HUES-2 Clones on *Neo* Resistant MEFi

As previously described in Chapter 4, a number of failed attempts were undertaken to select stable HUES-2 clones transduced with pHGNeo4, pHSV21αNeo, pHGBsd and pHGPuro amplicons on Matrigel using G418 (5, 10, 25, 50μg/ml), blasticidin (0.1, 0.2, 0.4μg/ml) and puromycin (0.01, 0.02, 0.04μg/ml), respectively. As hESc show low survival rates when growing at low cell densities, it was postulated that because the selection process was killing off the non-resistant cells at a fast rate, small stable clones would have a low probability of survival under such conditions. As an alternative strategy, selection was performed on a feeder layer to reduce the rate of selection-induced cell death, and to provide the small surviving stable clones with maximal support during the selection period. The *Neo* resistant mouse embryonic fibroblasts (*Neo*^{R} MEFi; a gift from Dr Ben Davies) were used as a feeder layer to

provide maximal surviving conditions for the stable hESc clones while at low cell densities.

Three days post HSV-1 amplicon transduction of HUES-2 cells with pHGNeo4, pHSV21αNeo pHSV17α40Neo, pHSV17α60Neo and pHSV17α100Neo, the cells were trypsinised and plated onto mitomycin inactivated *Neo*^{R} MEFi in hES media (see composition in materials and methods section 2.16). Two days later, the cells were placed under 50μg/ml of G418 selection. To enhance the recovery of stable hESc clones, and to avoid removing important growth factors secreted by the cells, only half of the hES media was changed daily. Selection was maintained for 7 days until the untreated control cells were dead, after which small putative stable hESc colonies were identified. Drug selection was then withdrawn and putative stable HUES-2 clones were maintained for further 14 days on *Neo*^{R} MEFi allowing them to expand (Figure 6-1). Putative stable clones were then picked and moved to individual wells of a 96-well plate on MEFi. Upon reaching confluency, the cells were trypsinised and moved onto a 24-well plate on MEFi, and subsequently passaged onto Matrigel-coated 24-well plates and expanded in mTeSR media for further analysis. Figure 6-2 represents the time-line of the process of HUES-2 stable clone selection.

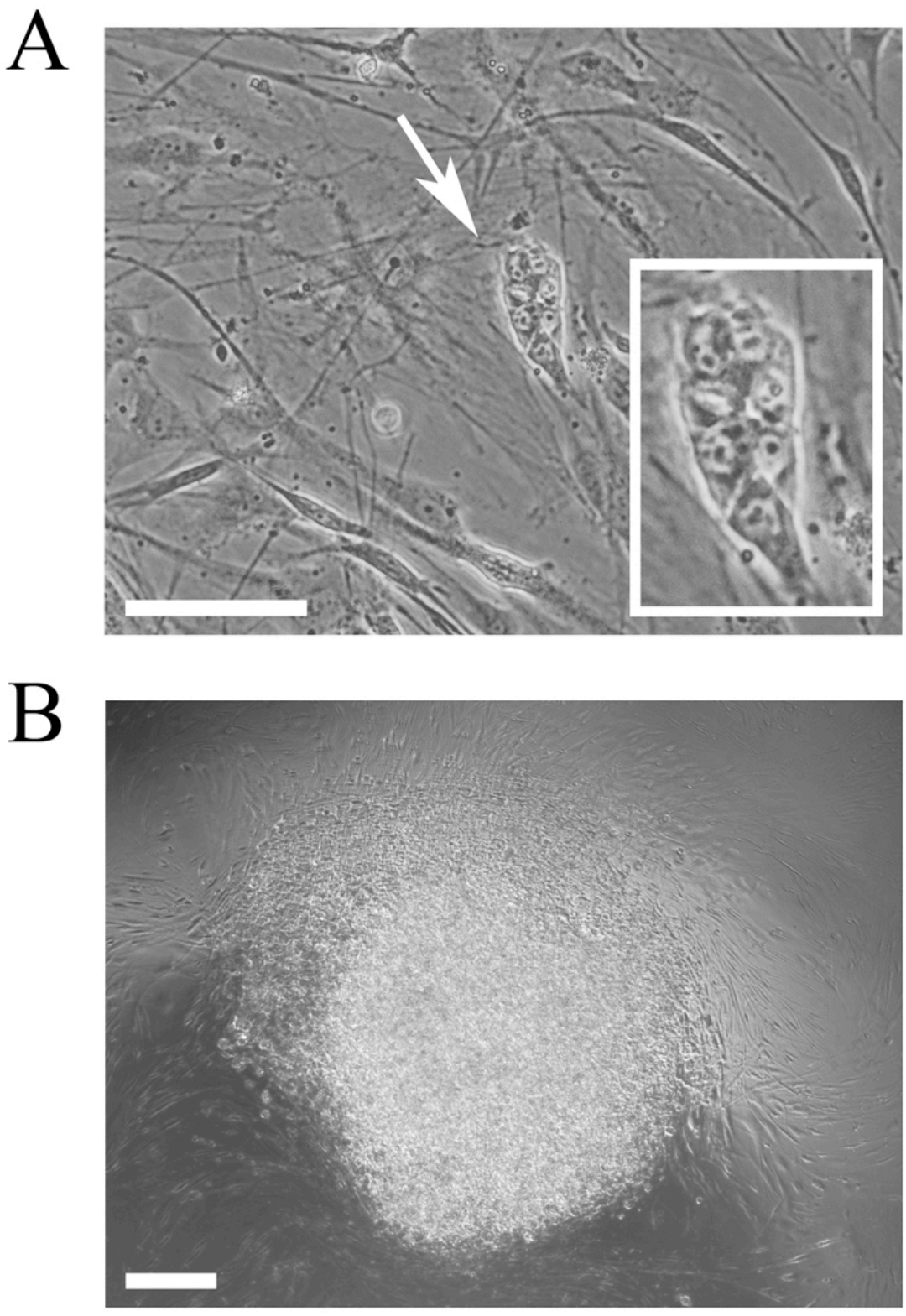

Figure 6-1 Putative stable HUES-2 clones post G418 selection on *Neo*^{R} MEFi
Representative putative stable HUES-2 clone selected on *Neo*^{R} MEFi after 7 days of continuous selection, highlighted by an arrow. The inset shows a 2× magnification of the clone containing ~8 cells (A). A different putative clone after 14 days of further growth (B). Scale bar = 200μm.

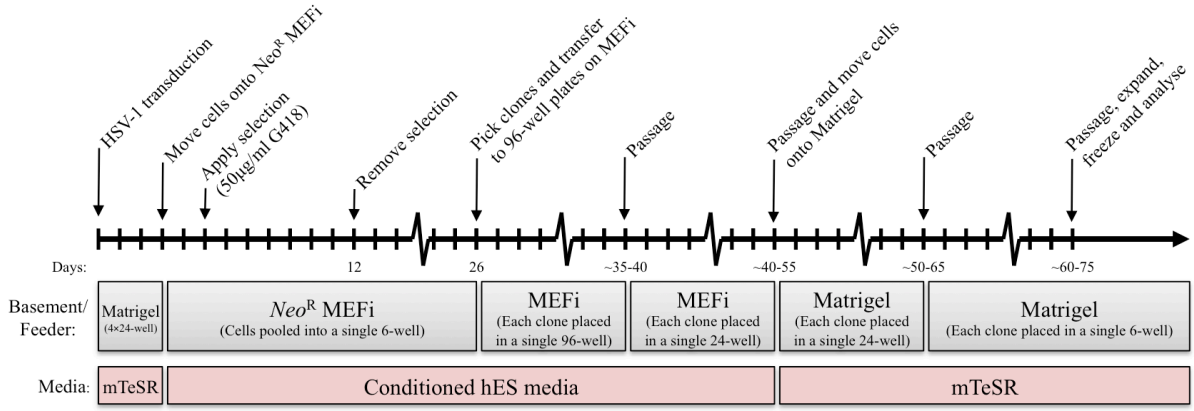

Figure 6-2 Time-line of the process of HUES-2 stable clone selection.
Three days post HSV-1 amplicon transduction of HUES-2 cells, they were plated onto *Neo*^{R} MEFi in hES media. Two days later, the cells were placed under 50µg/ml of G418 selection for 7 days. Putative stable HUES-2 clones were maintained for further 14 days on *Neo*^{R} MEFi allowing them to expand. Stable clones were then picked and moved to individual wells of a 96-well plate on MEFi. Upon reaching confluency, the cells were moved onto a 24-well plate on MEFi, and subsequently passaged onto Matrigel-coated 24-well plates and expanded in mTeSR media for further analysis.

Table 6-1 presents the number of stable HUES-2 clones initially picked from each transduction experiment, and the number of surviving clones. Approximately 80% of the picked clones survived and maintained their hESc morphology during clone isolation and passaging.

Table 6-1 Putative stable HUES-2 clones selected on *Neo*^{R} MEFi

Vector	No. Picked hESc Clones	No. Surviving hESc Clones
pHGNeo4	11	9
pHSV21αNeo	2	2
pHSV17α40Neo	10	10
pHSV17α60Neo	12	9
pHSV17α100Neo	12	7
Total	47	37

In parallel experiments, using similar selection conditions, stable clone isolation was attempted on HUES-2 cells using ExGen 500-mediated transfection with pHGNeo4, pHSV21αNeo, pHSV17α40Neo, pHSV17α60Neo, pHSV17α100Neo, and pJM2256-GFP vectors. Possibly due to the poor delivery efficiency, the transfection procedure

did not generate any stable clones from pHSV17α40Neo, pHSV17α60Neo, and pHSV17α100Neo. A small number of resistant cells were recovered upon delivery of pJM2256-GFP and pHSV21αNeo, which were replated and allowed to grow as pools of transfected cells (experiments conducted by Dr Daniela Moralli).

6.2 Initial Screening of Stable HUES-2 Clones

As previously described, due to the sensitive nature of HUES-2 cells to drug selection, isolated clones were only subjected to 50μg/ml of G418 selection for 7 days on *Neo*^{R} MEFi. The clones were maintained off selection for the majority of the time in culture (approximately 2-2.5 months) before they were sufficiently grown for chromosome harvesting and HAC analysis. To eliminate any false positive clones from further studies, they were first screened using PCR before proceeding to detailed FISH analysis.

Genomic DNA was extracted from ~1.0×10^{6} cells from each isolated stable HUES-2 clone as described in materials and methods section 2.15. Because of the small amount of DNA recovered, PCR screening was performed on all clones using a two-round PCR reaction. Two assays were used to validate the presence of the vector of interest in the isolated clones. In the first assay, the same primer set (Neo8F/Neo8R) was used in both rounds of PCR. Neo8 primer set amplifies part of the *Neo* gene on pHGNeo4 that is present in all the HSV-HAC vectors described in Chapter 3. In the second assay, a nested PCR was used with the initial round amplifying a region outside the *Neo* gene (Vect1F/Vect1R) and the second round amplifying the same part of the *Neo* gene as in the first assay (Figure 6-3).

A

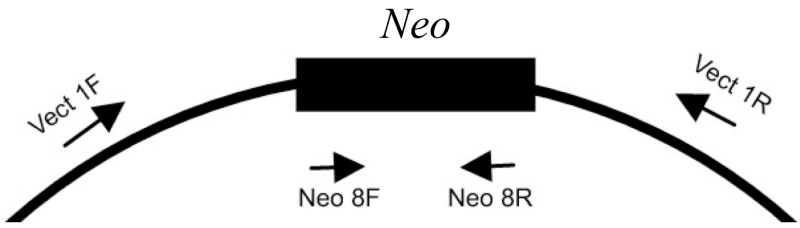

B

Assay	Primers Used	
	First Round	Second Round
I	Neo 8F – Neo 8R	Neo8F – Neo8R
II	Vect 1F – Vect 1R	Neo8F – Neo8R

Figure 6-3 Two-step PCR reaction assays for screening of putative HUES-2 colonies
Schematic presentation of the location of PCR primers on pHGNeo4 (A). Vect1F/ Vect1R primer pair amplifies a 2080bp region outside the *Neo* gene, while Neo8F/Neo8R primer pair amplifies a 630bp product within the *Neo* gene. In the first assay, the Neo8F/Neo8R primer pair was used in both rounds of PCR. In the second assay, a nested PCR was used: in the first reaction a region outside the *Neo* gene was amplified using the Vect1F/Vect1R primer pair, and in the second round the Neo8F/Neo8R primer pair was used (B). Primer sequences listed in Table 2-2.

In both assays, 1µl (out of total 25µl reaction volume) from the first round of PCR was used as product template for the second round of PCR. Primers for exon 18 of the *CNTNAP5* gene (a gift from Dr Alistair Pagnamenta) were used as an internal control, and confirmed the presence of genomic DNA in all samples (data not shown). *Neo*^{R} MEFi are mitotically inactive and have a short lifespan of approximately 2 weeks. Given that the stable hESc clones took approximately 2-2.5 months to expand in culture and were passaged at least 4 times in the absence of *Neo*^{R} MEFi at the point of DNA extraction, there should not have been any contaminating DNA from *Neo*^{R} MEFi in the prepared DNA samples. However, any concern over contaminating *Neo*^{R} MEFi was addressed by the second (nested) PCR assay, as the Vect1F/R primer set did not amplify a product from *Neo*^{R} MEFi (data not shown).

Figure 6-4 shows the gel products of both PCR detection assays. Both assays confirmed the presence of vector DNA in the putative hESc clones (marked with an asterisk). Following the prolonged period in culture that was necessary to isolate and expand each of the HUES-2 clones, three of the pHSV17α100Neo clones lost their hESc morphology and differentiated into fibroblast-like cells (clones 3, 4 and 7 as marked with Δ in Figure 6-4). These clones were consequently excluded from further analysis. Over half of the hESc clones amplified the HAC-specific DNA product; these results are summarised in Table 6-2. Both of the pHSV21αNeo clones were negative for the PCR assay.

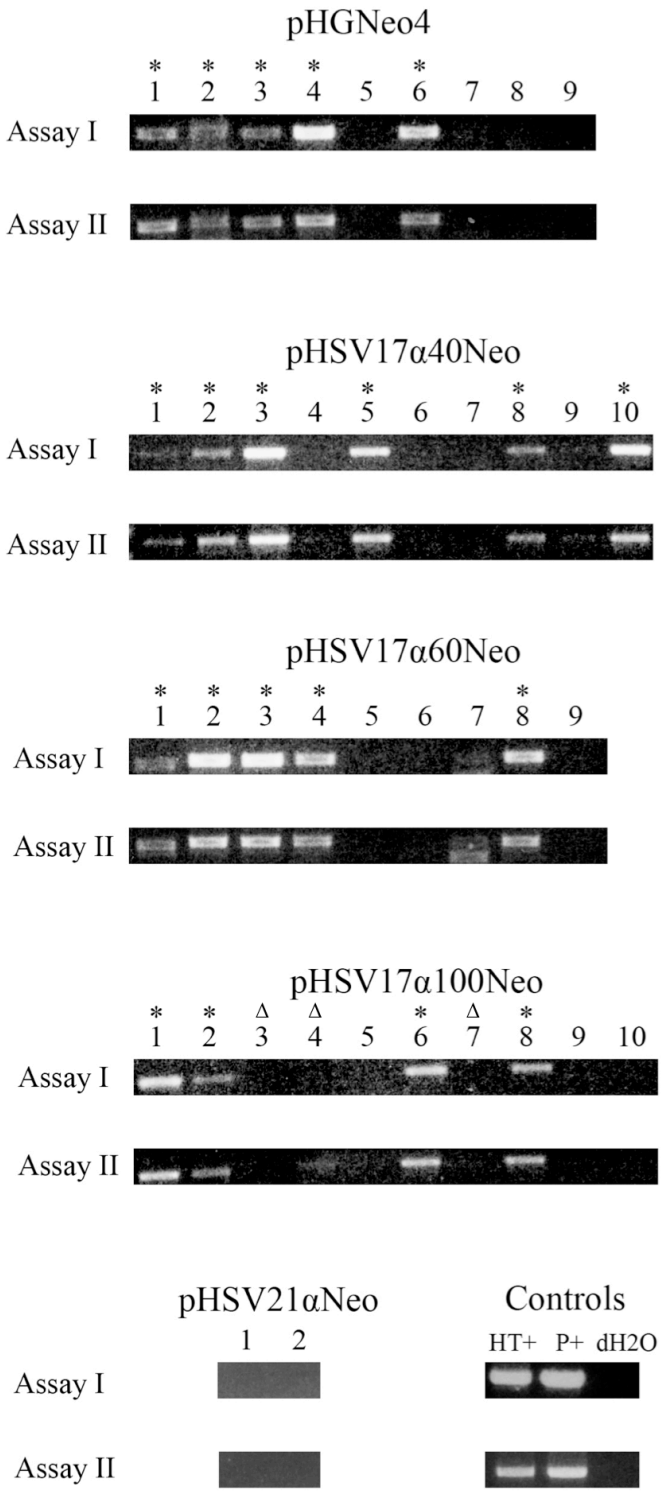

Figure 6-4 Two-step PCR reactions on putative stable HUES-2 clones
Two-round PCR reactions were carried out on HUES-2 clones. The figure shows the results of the second round of PCR for both assays I and II. The expected product size is 630bp. Genomic DNA prepared from HT1080 cells transfected with pHGNeo4 was used as a positive control (indicated by HT+). 1ng of pHGNeo4 was used as plasmid control (indicated by P+), while dH_2O was used as negative control. 3 of the clones had differentiated into fibroblast-like cells as marked with Δ. Putative clones amplifying the desired product are marked with an asterisk. Some of the putative stable clones were negative and did not amplify the desired PCR product.

Table 6-2 PCR analysis of putative stable HUES-2 clones selected on *Neo*^{R} MEFi

Vector	No. Surviving hESc Clones	No. PCR Positive hESc Clones
pHGNeo4	9	5
pHSV21αNeo	2	0
pHSV17α40Neo	10	6
pHSV17α60Neo	9	5
pHSV17α100Neo	7	4
Total	37	20

6.3 FISH Analysis of HUES-2 Stable Clones

Stable HUES-2 clones that were positive for both PCR assays were subjected to further analysis using fluorescence *in situ* hybridisation (FISH). FISH was carried out as outlined in materials and methods section 2.25. Figure 6-5 presents metaphase spreads of HAC-containing HUES-2 stable clones obtained from pHSV17α40Neo (A), pHSV17α60Neo (B) and pHSV17α100Neo (C) HSV-1 transduction. In parallel experiments conducted by Dr Daniela Moralli, the HAC frequency in HUES-2 cells following ExGen 500-mediated transfection of the HAC vectors was analysed by FISH on chromosome metaphase spreads. These results are summarised in Table 6-3.

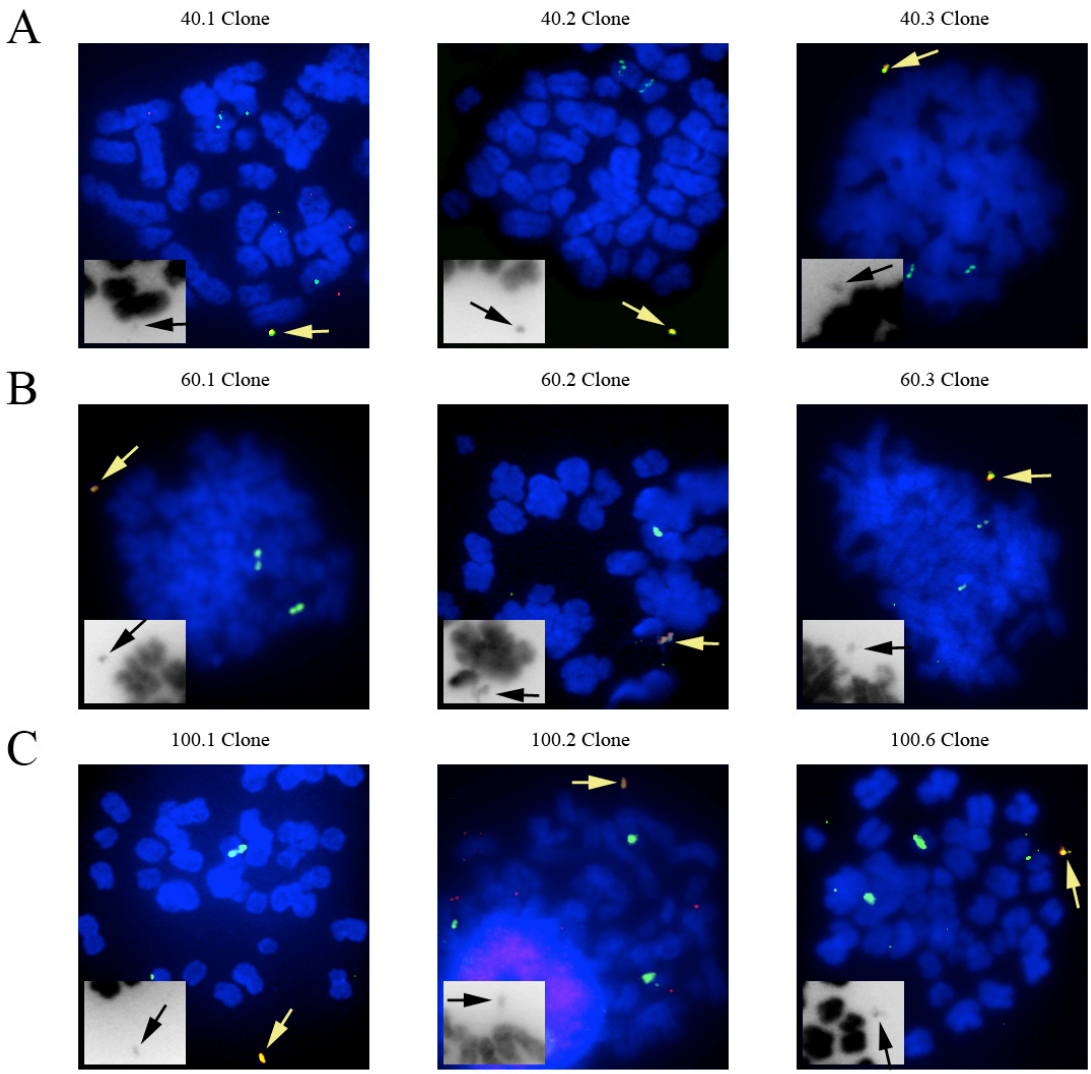

Figure 6-5 FISH analysis of HUES-2 metaphase spreads
Metaphase spreads showing the presence of HAC, indicated by an arrow, in HUES-2 stable clones obtained by HSV-1 amplicon delivery of pHSV17α40Neo (A), pHSV17α60Neo (B), pHSV17α100Neo (C) vectors. Probes against the 17α satellite DNA (in green) bind the HAC and endogenous chromosome 17. Probes against pBeloBAC11 or pCYPAC2 vectors (in red) bind HAC only. One representative metaphase from a number of the HAC-containing clones is presented here. The inset shows the inverted DAPI staining for visualisation of the HAC.

Table 6-3 HAC Analysis in stable HUES-2 clones

	HSV-1 Transduction			Transfection*		
HAC Vector	**No. of Clones Analysed**	**HAC Positive Clones**	**% of HAC**	**No. of Clones Analysed**	**HAC Positive Clones**	**% of HAC**
pHSV21αNeo	2	0	-	Pool	NA	16
pHSV17α40Neo	10	5	10-70	-	-	-
pHSV17α60Neo	9	5	10-25	-	-	-
pHSV17α100Neo	7	3	10-20	-	-	-
pJM2256	NA	NA	NA	Pool	NA	11

Percentage of HAC-positive metaphases scored in the HAC-containing HUES-2 clones. Stable HUES-2 clones were screened by FISH, 20-40 metaphases were scored for each clone. No stable clones were obtained following transfection of pHSV17α40Neo, pHSV17α60Neo and pHSV17α100Neo, hence only cell "pools" were analysed. Transfection experiments and data analysis performed by Dr Daniela Moralli, marked with an asterisk. NA, not applicable.

In comparison to the HT1080 results, where integrated DNA were observed in all the stable clones generated, no integration events were observed in any of the stable HSV-1 derived HUES-2 clones. Even clones that failed to show the presence of HAC after FISH studies, did not contain any integration events. Given that these HUES-2 stable clones were PCR positive for the introduced HAC vector, but showed no signs of integration, this result raised the possibility that small HAC, cytologically undetectable, may be present in these clones. To test this hypothesis more sensitive FISH assays could be carried out, however no further experiments were performed to validate such a hypothesis. Two derivative clones from the pHSV17α40Neo vector that had the highest prevalence of HAC were chosen for further analysis. These two clones will be referred to as HUES-2 40.2 (containing ~70% HAC) and HUES-2 40.3 (containing ~30% HAC) from here onwards.

6.4 Centromere Protein C Analysis

The presence of an active centromere on the HAC in HUES-2 40.2 and HUES-2 40.3 clones was analysed by staining with an antibody against the essential centromeric protein CENP C, which is only found at functional centromeres and kinetochores (Tomkiel et al. 1994; Przewloka et al. 2011). Samples were prepared as described in materials and methods section 2.26. The HAC were identified using a HAC-specific vector probe (pBeloBAC11). In the analysed metaphases, the HAC FISH signal in HUES-2 40.2 and HUES-2 40.3 cells co-localised with anti-CENP C antibody, indicating the presence of an active centromere on the established HAC.

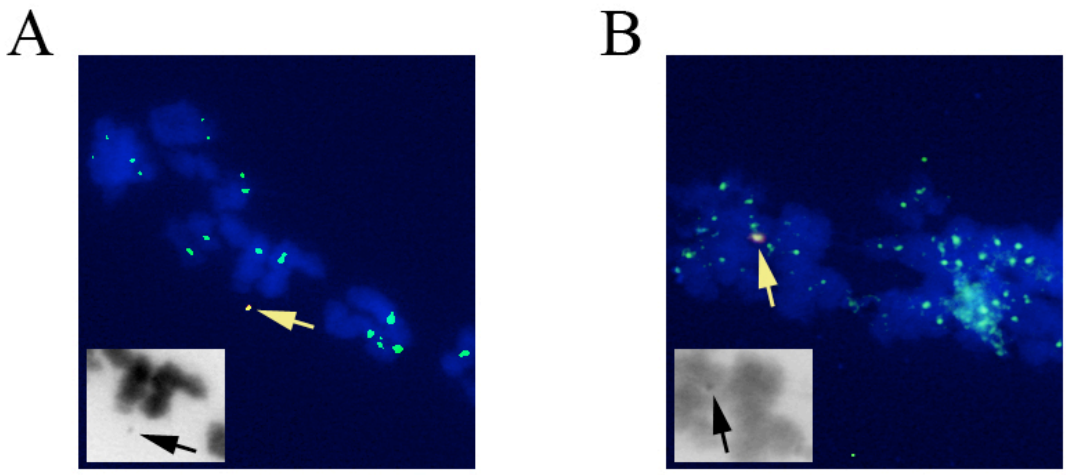

Figure 6-6 CENP C staining of chromosome metaphase spreads prepared from HUES-2 40.2 and HUES-2 40.3 cells
Immuno-FISH analysis of chromosome metaphase spreads, using an anti-CENP C antibody (in green) and pBebloBAC11 vector probe (in red). The HAC present in clones HUES-2 40.2 (A) and HUES-2 40.3 (B) are stained with both the HAC-specific vector probe and anti-CENP C antibody (identified by an arrow). The inset shows the inverted DAPI staining for visualisation of the HAC.

6.5 Characterisation of the HAC Structure

As the HUES-2 40.2 clone contained HAC at the highest frequency amongst the other stable clones, its HAC composition was studied using fibre-FISH with 17α satellite

and vector (pBeloBAC11 and pHGNeo4) DNA probes (Figure 6-7). As expected, endogenous chromosome 17 fibres were only labelled with the 17α satellite DNA probe. Fibre-FISH results on the HUES-2 40.2 HAC suggested that the HAC were composed of several alternating units of 17α satellite and vector (pBeloBAC11 and pHGNeo4) DNA sequences. Similar to previous studies in HT1080 cells (Mejía et al. 2001; Grimes et al. 2002), the established HAC in HUES-2 cells consisted of repeat units of the input DNA suggesting that the vector DNA amplified during HAC formation (fibre-FISH and analysis performed by Dr Daniela Moralli).

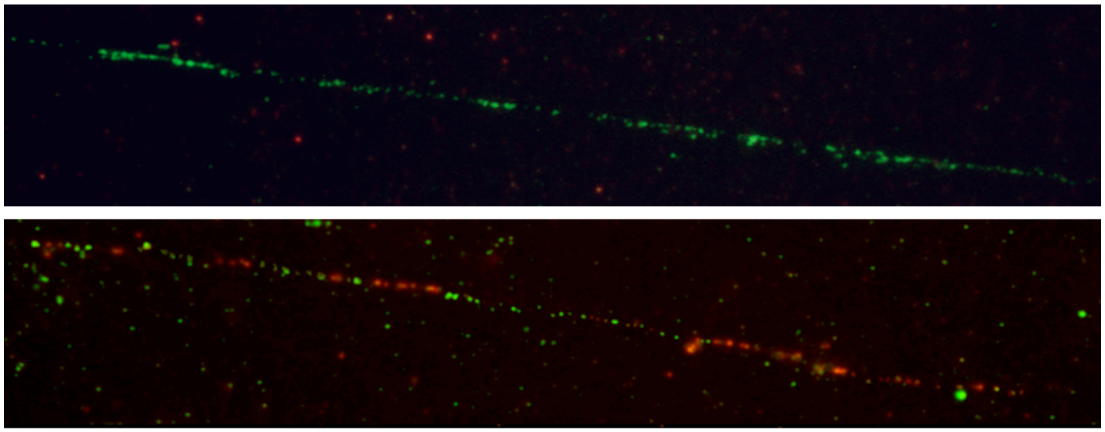

Figure 6-7 Fibre-FISH analysis on endogenous chromosome 17 and HAC
FISH on released chromatin fibres with a 17α satellite DNA probe (in green) and a vector probe (pBeloBAC11 and pHGNeo4, in red). The top panel shows the endogenous chromosome 17, while the bottom panel shows HAC from HUES-2 40.2 clone. The alternating pattern of red and green suggested the HAC is composed of several repeat units of input DNA (fibre-FISH and analysis performed by Dr Daniela Moralli).

6.6 HAC Stability and Gene Expression

In vitro HAC stability and gene expression was characterised next. The HUES-2 40.2 and HUES-2 40.3 clones were placed in culture for a 90-day period (~30 passages) either in the presence or absence of drug selection. The cells were passaged at a 1:2 split approximately every 3 days and drug selection was carried out at 25μg/ml of G418. At 30-day intervals, the HUES-2 40.2 and HUES-2 40.3 cells (on and off

selection) were fixed in 4% formaldehyde and analysed by FACS as outlined in materials and methods section 2.30 (FACS runs and data analysis performed with the assistance of Dr Sally Cowley, Dunn School of Pathology at the University of Oxford). Throughout the analysis, the same gates were used to quantify *GFP* expression from each time point. The results, summarised in Table 6-4, suggested that *GFP* expression remained stable for the HUES-2 40.2 clone during this 90-day period both in the presence and absence of selection. Correlation analysis on the HUES-2 40.2 FACS data revealed no statistically significant change in *GFP* expression of this clone either in the presence (p=0.203) or absence (p=0.258) of drug selection. Similar correlation analysis on the HUES-2 40.3 FACS data suggested a statistically significant increase in *GFP* expression of this clone in the presence (p=0.004), however not in the absence (p=0.081) of drug selection (p values calculated using two-tailed Pearson correlation analysis).

Table 6-4 FACS analysis of *GFP* expression of HUES-2 40.2 and HUES-2 40.3 clones on and off G418 selection for 90 days in culture

Clone	% *GFP* Positive Cells After X Days On & Off Selection			
	0 days	30 days	60 days	90 days
HUES-2 40.2 On Selection	83	84	89	87
HUES-2 40.2 Off Selection		81	88	87
HUES-2 40.3 On Selection	1.3	3.1	4.2	6.0
HUES-2 40.3 Off Selection		1.2	3.0	5.8

Data based on 1 replication. FACS runs and data analysis performed with the assistance of Dr Sally Cowley, Dunn School of Pathology at the University of Oxford.

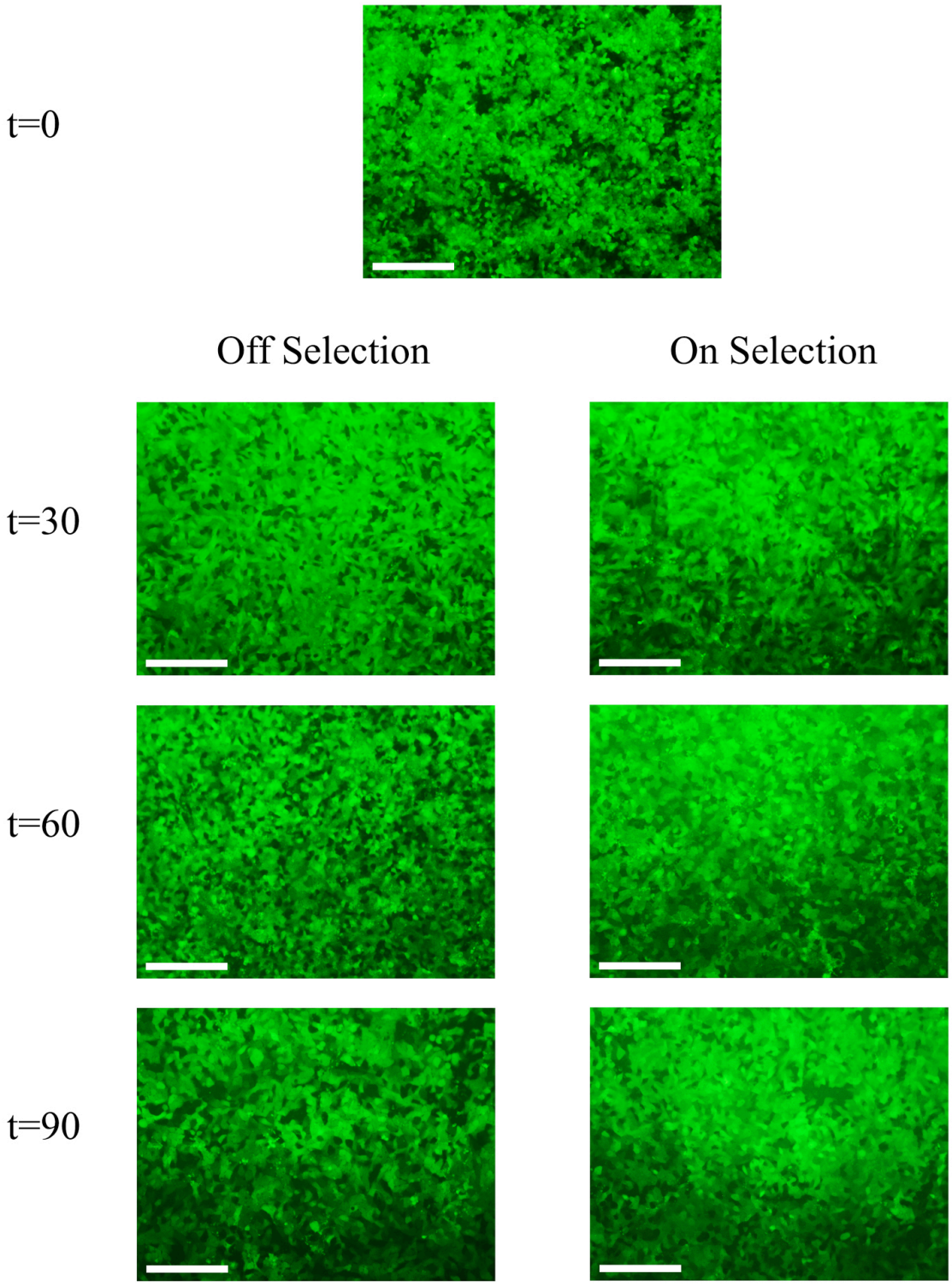

Figure 6-8 *GFP* expression in HUES-40.2 over a 90 day period on and off G418 selection.
The *GFP* expression of HUES-2 40.2 cells remained stable during this 90 day time period both on and off selection. Images were captured from samples at time points 0, 30, 60 and 90 days post initiation of passaging. Scale bar = 200μm.

Total RNA was also extracted from each clone in the presence and absence of selection at 30-day time intervals. Primers specific for *GFP* and *Neo* genes were used to quantify relative gene expression over the course of 90 days using the ubiquitously expressed glyceraldehyde-3-phosphate dehydrogenase (*GAPDH*) gene as reference (primers listed in Table 2-2). The efficiencies of these primer pairs were measured to be 2.0 (data not shown). The fold enrichment in *GFP* and *Neo* mRNA levels was quantified against that of *GAPDH* mRNA levels using the $2^{-\Delta\Delta Ct}$ method (Livak and Schmittgen 2001) as described in materials and methods section 2.31.

GFP and *Neo* mRNA levels were normalised against *GAPDH* mRNA levels in both HUES-2 40.2 and HUES-2 40.3 clones at time point 0 (Table 6-5). Quantification of *GFP* and *Neo* mRNA levels in both clones revealed that they were expressed in significantly lower amounts when compared to mRNA levels of the *GAPDH* housekeeping gene (all $p<0.001$). This result was expected as both *GFP* and *Neo* expression are driven by viral promoters, which are known to be downregulated in stable hESc clones (Strulovici et al. 2007). In both clones, *GFP* mRNA levels were significantly greater than *Neo* mRNA levels ($p_{HUES\text{-}2\ 40.2}<0.001$ and $p_{HUES\text{-}2\ 40.3}=0.009$). This result is probably due to promoter-specific differences between *GFP* and *Neo* expression (*GFP* is under the regulation of HSV-1 I/E promoter, while *Neo* is under the regulation of SV40). Furthermore, *GFP* and *Neo* mRNA levels in HUES-2 40.2 was also significantly higher than that of HUES-2 40.3 ($p_{GFP}<0.001$, $p_{Neo}=0.010$) (all p values calculated using one-way ANOVA). This result is partly explained by the lower HAC frequency of HUES-2 40.3 (~30%) as compared to HUES-2 40.2 (~70%). However, silencing processes such as DNA methylation and heterochromatinisation may have also contributed to this difference in HAC gene expression.

Table 6-5 Relative HAC gene expression normalised against *GAPDH* from samples at the initial time point.

Clone	Relative mRNA levels measured against *GAPDH* ± SE	
	GFP	***Neo***
HUES-2 40.2	$(3.08 \pm 0.19)\times10^{-2}$	$(6.88 \pm 0.14)\times10^{-4}$
HUES-2 40.3	$(8.99 \pm 0.63)\times10^{-4}$	$(1.51 \pm 0.09)\times10^{-4}$

Data based on 6 replications per group. SE, standard error of the mean.

To look at the trend of *GFP* and *Neo* expression during this 90-day, on and off selection period, mRNA levels in both clones were normalised relative to the sample at the initial time point. The results showed that in both HUES-2 40.2 and HUES-2 40.3 cells, *GFP* and *Neo* mRNA levels increased when compared to the initial starting point, both in the presence and absence of selection (Figure 6-9).

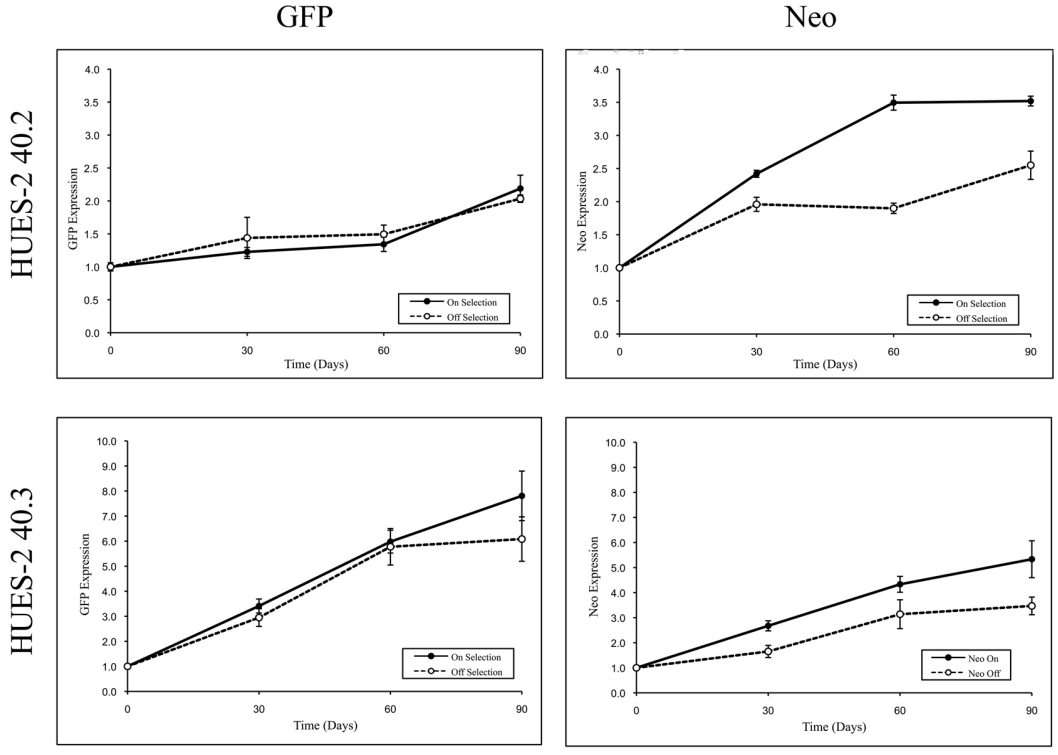

Figure 6-9 Relative gene expression of HUES-2 40.2 and HUES-2 40.3 over time. Real-Time qPCR was used to measure relative *GFP* and *Neo* gene expression (as measured by mRNA levels) against *GAPDH*, in the presence and absence of selection over a 90-day culturing period. Relative expression was then normalised against the sample at the initial time point. Data based on 6 replications per group. Error bars represent standard error of the mean. The solid and open circles represent data from on and off selection samples respectively.

In both clones, correlation analyses suggested a statistically significant increase in *GFP* and *Neo* expression (as indicated by mRNA levels) during this 90-day period (all $p<0.05$; two-tailed Pearson correlation analysis). However, it seems that gene expression may be reaching a plateau toward the end of this period. In HUES-2 40.2 cells, the *GFP* mRNA levels steadily increased over this 90-day period both in the presence and absence of selection to ~2× the initial amount of *GFP* mRNA levels, respectively. *Neo* mRNA levels in the presence and absence of selection increased to ~3.5× and ~2.5× the initial amount of *Neo* mRNA levels, respectively. Similarly, in HUES-2 40.3 cells, the *GFP* mRNA levels in the presence and absence of selection increased to ~7.5× and ~6× the initial *GFP* mRNA levels, respectively. *Neo* mRNA levels in the presence and absence of selection increased to 5.5× and 3.5× the initial amount of *Neo* mRNA levels, respectively (all $p<0.05$; one-way ANOVA).

At the end of the 90-day period, in both HUES-2 40.2 and HUES-2 40.3 clones, the *GFP* mRNA levels between the on and off selection samples were not significantly different ($p_{HUES\text{-}2\ 40.2}=0.713$; $p_{HUES\text{-}2\ 40.3}=0.212$; two-sample t-test). However, *Neo* mRNA levels were significantly higher after 90 days in the presence of selection in both clones as compared to the off selection sample ($p_{HUES\text{-}2\ 40.2}=0.011$, $p_{HUES\text{-}2\ 40.3}=0.025$; two-sample t-test). This difference in *Neo* mRNA levels is presumably due to the selection pressure, resulting in higher expression levels of *Neo* in the presence of G418 as compared to when selection pressure was not present.

To verify if the HAC were able to segregate correctly in the hESc clones, the HAC frequency in HUES-2 40.2 and HUES-2 40.3 cells was followed over 90 days in the absence of selection. The HAC frequency was scored using FISH as previously

described; 10 to 20 metaphases were scored for each sample (Table 6-6; FISH and HAC stability analysis performed by Dr Daniela Moralli).

Table 6-6 HAC Stability of HUES-2 40.2 and HUES-2 40.3 clones off G418 selection

Clone	HAC (%) After X Days Off Selection			
	0 days	30 days	60 days	90 days
HUES-2 40.2	70	70	70	65
HUES-2 40.3	30	35	22	40

10 to 20 metaphases were scored for each time point. FISH and HAC stability analysis performed by Dr Daniela Moralli.

Correlation analysis on the FISH results on both clones showed that there was no statistically significant trend (either loss or gain) in the HAC frequencies during this 90-day period ($p_{HUES\text{-}2\ 40.2} = 0.225$ and $p_{HUES\text{-}2\ 40.3} = 0.714$; p values calculated using two-tailed Pearson correlation analysis). This suggested that the HAC frequency remained stable in both clones, indicating that the established HAC segregated correctly during mitosis in human embryonic stem cells.

6.7 Karyotypic Analysis of HUES-2 Cells

To determine whether any chromosomal abnormalities resulted from the HSV-1 mediated amplicon transduction, the presence of HAC, or extensive passaging under feeder-free conditions, karyotypic analysis of HUES-2 parental and HAC-containing HUES-2 40.2 and HUES-2 40.3 cells was carried out.

Low passage HUES-2 cells (passage ~30), HUES-2 at the point of HSV-1 transduction (passage ~40), and the HAC-containing clones HUES-2 40.2 and HUES-2 40.3 (both passage ~70) were initially analysed by FISH using whole

chromosome 12 and 17 paints. Detailed analysis of at least 30 informative metaphases revealed that the low passage HUES-2 cells contained no trisomies 12 or 17 (Figure 6-10 A). However, the HUES-2 (passage ~40), and its derivative HAC-containing clones had trisomies of chromosomes 12 and 17 present at similar levels, as either an extra chromosome 12 or 17, or both were present in all scored metaphases (Figure 6-10, B, C & D). In the HUES-2 parental (passage ~40), 70% of the metaphases contained both chromosome 12 and 17 trisomies, and the remaining 30% of the cells had either one of the trisomies. In HUES-2 40.2 and HUES-2 40.3 cells, 66% and 68% of the metaphases contained both trisomies, respectively. These results are summarised in Table 6-7 (chromosome paint FISH were performed by Dr Mohammed Yusuf and analysed by Dr Emanuela Volpi, Molecular and Cytogenetics Core, WTCHG at the University of Oxford).

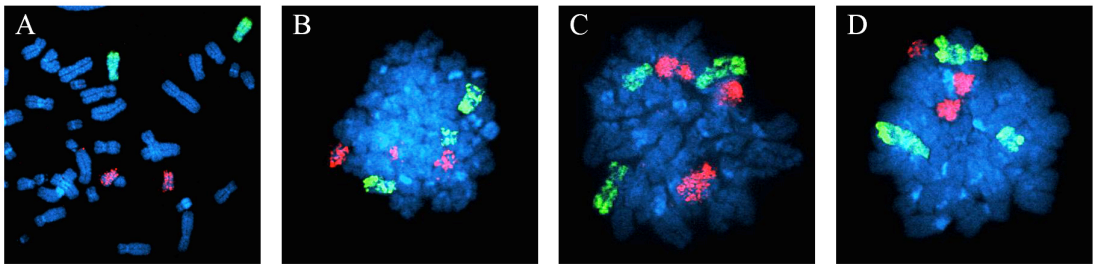

Figure 6-10 FISH analysis with chromosome 12 and 17 paints on HUES-2 parental and HAC-containing clones
Chromosome 12 (green) and chromosome 17 (red) paints were hybridised to HUES-2 at passage ~30 (A), HUES-2 at passage ~40 (B), HUES-2 40.2 at passage ~70 (C) and HUES-2 40.3 at passage ~70 (D). Chromosomes were stained with DAPI (blue). HUES-2 at passage ~30 contains 2 copies of chromosome 12 and 17, while HUES-2 at passage ~40 and its derivative HAC-containing clones (HUES-2 40.2 and HUES-2 40.3) contain trisomies for chromosomes 12 and 17. Chromosome spreads were prepared using the BHS hypotonic in A, while using standard 75mM KCl in B, C and D (FISH paints were performed by Dr Mohammed Yusuf and analysed by Dr Emanuela Volpi, WTCHG at the University of Oxford).

Table 6-7 Karyotypic analysis of HUES-2 cell lines and derivative HAC clones using chromosome 12 and 17 paints

Cell Line	Passage	Number of Metaphases Scored	% Metaphase Containing Both Trisomies (12&17)
HUES-2	~30	30	0
HUES-2	~40	33	70
HUES-2 40.2	~70	38	66
HUES-2 40.3	~70	38	68

FISH paints were performed by Dr Mohammed Yusuf and analysed by Dr Emanuela Volpi, WTCHG at the University of Oxford.

As previously mentioned in Chapter 1, under *in vitro* culture conditions, hESc harbouring trisomies 12 and 17 are known to exhibit a selective advantage over their wild-type counterparts. The karyotypic analysis of HUES-2 at passage ~30 and ~40 indicated that in approximately 10 passages, trisomies 12 and 17 were able to spread through the population starting from a small number of undetectable trisomies at passage ~30. Since these trisomies were present in HUES-2 at passage ~40, the derivative HAC-containing HUES-2 40.2 and HUES-2 40.3 clones also contained the same trisomies at similar levels.

Once it was determined that HUES-2 (passage ~40), and subsequently its derivative HAC-containing lines contained trisomies for both chromosome 12 and 17, further karyotypic characterisation was carried out through M-FISH analysis. The M-FISH was performed to determine the nature of the observed trisomies 12 and 17, and whether there were other chromosomal aberrations such as translocations, deletions or duplications. Detailed M-FISH analysis on 30 informative metaphases from HUES-2 cells at passage ~40 revealed that other than trisomies 12 and 17, this line contained a partial chromosome 1q trisomy, with the extra segment translocated onto

chromosome 18. The extra partial chromosome 17 was translocated onto chromosome 22 (Figure 6-11).

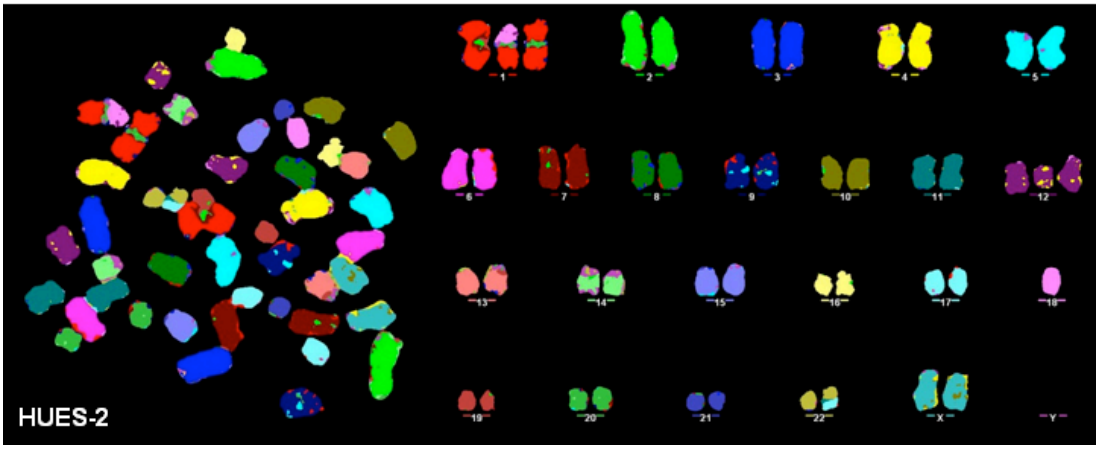

Figure 6-11 M-FISH analysis of HUES-2 at passage ~40
On the left is an image of a metaphase spread of HUES-2 pseudo-coloured with 24-colour paint. The karyotype of the same spread is shown on the right. This line has partial trisomies for chromosomes 1, 12 and 17. There is a translocation of the trisomic chromosome 1 onto chromosome 18 and a translocation of the trisomic section of chromosome 17 onto chromosome 22 (M-FISH performed by Dr Mohammed Yusuf and analysed by Dr Emanuela Volpi, WTCHG at the University of Oxford).

Similar to cancer cells, the presence of chromosomal abnormalities in cultured hESc is known to inhibit apoptosis and promote their self-renewal capacity (Baker et al. 2007). Chromosome 12 harbours the self-renewal gene *Nanog*. Similarly, chromosome 17 contains *Stat3* and *Grb2*, which promote self-renewal, while *Birc5* inhibits apoptotic pathways (Draper et al. 2004). The presence of extra copies of such anti-apoptotic and self-renewal genes is postulated to keep hESc "locked" in a pluripotent state. Thus, hESc carrying such abnormalities are known to be more difficult to differentiate into specific cell lineages (Draper et al. 2004; Baker et al. 2007; Spits et al. 2008).

6.8 Summary

In this chapter, the isolation, expansion and PCR screening for the presence of HAC DNA of putative HUES-2 stable clones was described. Detailed FISH analysis in HUES-2 cells revealed the presence of HAC in 13 out of 20 PCR positive clones with frequencies ranging from ~10-70% of the analysed metaphase spreads. Most significantly, no integrated HAC DNA was observed in hESc possibly due to the presence of molecular checkpoints which maintain genomic integrity, thus preventing large DNA integrations into the genome (Deng and Xu 2009). In turn, the presence of episomal or HAC elements would be favoured over integration events when large DNA is introduced into hESc. Similar to the HT1080 results described in Chapter 3, the pHSV17α40Neo HAC vector (containing ~40kb of 17α satellite DNA) showed the highest frequency of HAC formation in HUES-2 cells. Due to low stable clone formation efficiency in hESc, only HSV-1 amplicon transduction resulted in stable clone formation, while transfection only resulted in cell "pools". Immuno-FISH analysis using CENP-C antibody revealed the presence of an active centromere on the established HAC, and fibre-FISH suggested that the HAC consisted of several repeat units of input DNA. Established HAC were stable for over a 90-day time period off drug selection and maintained *GFP* and *Neo* expression during this period. Karyotypic analysis (using chromosome paints and M-FISH) revealed the presence of a number of abnormalities in the parental HUES-2 line that were also present in the derivative HAC-containing clones.

Chapter 7. Results and Discussion V: Differentiation of HUES-2 and Derivative HAC-Containing Clones

To demonstrate that the HAC-containing hESc clones (HUES-2 40.2, HUES-2 40.3), retained their pluripotent nature after genetic manipulation using HSV-1 amplicons and following prolonged culturing periods, several pluripotency assays were carried out. Initially, indirect-immunostaining of well-established pluripotency markers was tested, and once confirmed, embryoid bodies (EB) were successfully formed from the various hESc lines. The EB were then cultured either under undirected differentiation conditions to form the three embryonic germ layers or directed differentiation conditions toward neuronal lineages. Finally, teratoma formation was induced in severe combined immunodeficient (SCID) mice as the final and most comprehensive measure of pluripotency.

7.1 Indirect-Immunostaining of Pluripotency Markers

Four well-known hESc-specific pluripotency marker proteins (Oct4, Sox2, Nanog and Tra-1-60) were used in indirect-immunostaining experiments of the hESc lines. These hESc lines included the parental HUES-2 (passages ~30 and ~40), HUES-2 40.2 and HUES-2 40.3 (containing HAC) and HUES-2 Neo.4 (containing the control plasmid pHGNeo4). As previously discussed, HUES-2 at passage ~40 contained a number of chromosomal abnormalities, thus the parental with no chromosomal aberrations (HUES-2 at passage ~30), was also tested to ensure chromosomal aberrations did not influence the expression of pluripotency markers. Oct4 and Nanog are nuclear marker proteins, while Sox2 and Tra-1-60 are cell surface markers (Takahashi et al.

2007). Figure 7-1 shows indirect-immunostaining of the various hESc lines with the described antibodies. The HUES-2 parental (at passages ~30 and ~40) and derivative stable clones (HUES-2 40.2, HUES-2 40.3 and HUES-2 Neo.4) all express the described pluripotency markers. Mouse embryonic fibroblasts (MEF) were used as a negative control and were not stained with these antibodies (Figure 7-2).

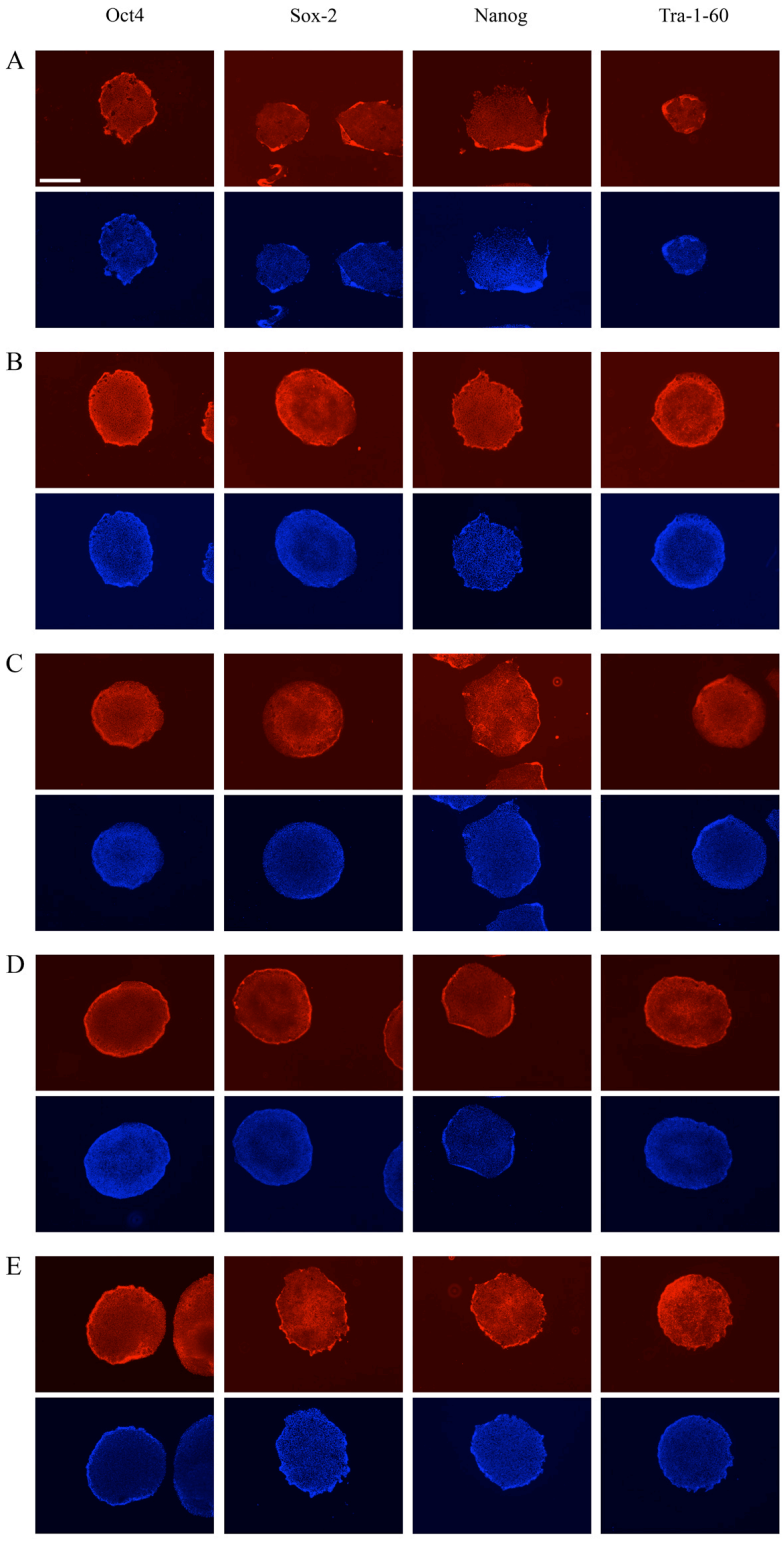

Figure 7-1 Indirect-Immunostaining of hESc lines using hESc-specific pluripotency markers

HUES-2 at passage ~30 (A), HUES-2 at passage ~40 (B), HUES-2 40.2 (C), HUES-2 40.3 (D) and HUES-2 Neo.4 (E) were stained with antibodies against Oct4, Sox2, Nanog and Tra-1-60 markers (in red). The nuclei were counterstained with DAPI in blue. Scale bar = 500µm.

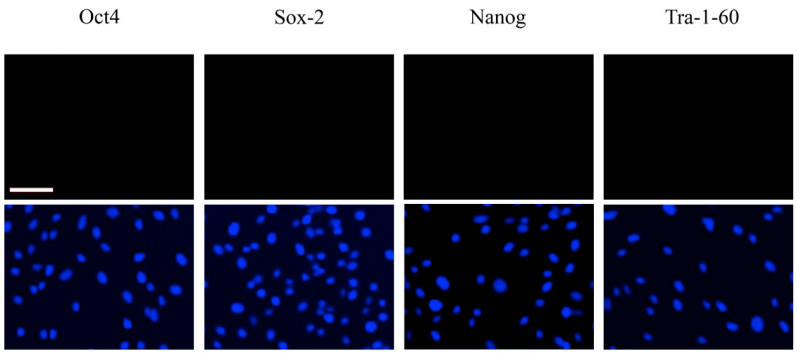

Figure 7-2 Indirect-Immunostaining of mouse embryonic fibroblasts (MEF) using hESc-specific pluripotency markers
MEF were used as a negative control to ensure that the antibodies for pluripotency markers (Oct4, Sox2, Nanog and Tra-1-60) did not stain non-pluripotent cells. The bottom panel shows the nuclei stained with DAPI in blue. Scale bar = 100μm.

7.2 Analysis of Long-Term Culture Effects on the Pluripotency of the HAC-Containing Clones

As described in the previous chapter, the HAC-containing clones, HUES-2 40.2 and HUES-2 40.3, were passaged in culture for 90 days both in the presence and absence of selection. To ensure that both clones retained their pluripotency during this period, RT-PCR analysis on pluripotency markers *Oct4*, *Sox2* and *Nanog*, was performed on cDNA obtained from RNA extracted from both clones (Figure 7-3) at definite time points. The three pluripotency markers were continuously expressed over this period of time in both clones. Due to an error prior to RNA extraction from HUES-2 40.3 at time point 60, the cells were left in culture longer than necessary, became over-confluent and started differentiating from a pluripotent state. Thus, the intensity of the RT-PCR bands of pluripotency markers appeared diminished in the HUES-2 40.3 time point 60 sample. However, as high intensity bands were still present at time point 90, off selection, this indicated that reduction in the pluripotency marker at time point 60 was most likely due to an error in sample preparation as opposed to loss of

pluripotency. Overall, the data suggested that both HUES-2 40.2 and HUES-2 40.3 clones retained their pluripotency during this 90-day period, indicating that prolonged presence and expression of HAC did not result in loss of pluripotency.

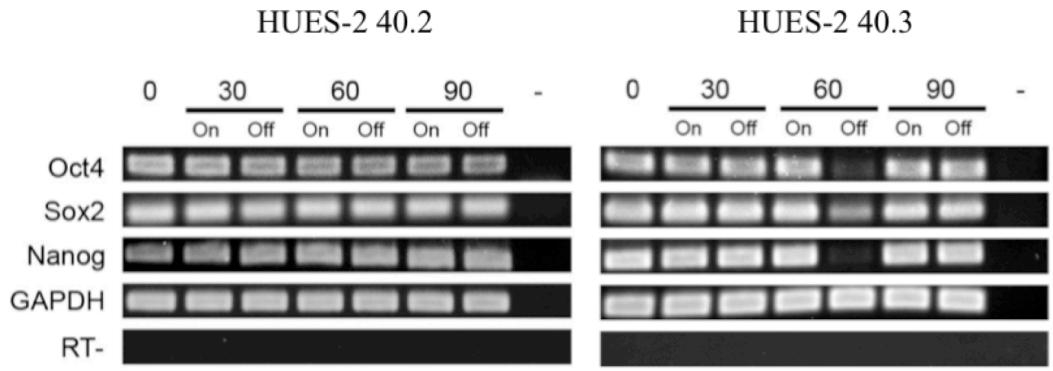

Figure 7-3 RT-PCR analysis of pluripotency markers in HUES-2 40.2 and HUES-2 40.3 cells over 90 days in culture
RT-PCR amplification with primers for the markers *Oct4*, *Sox2* and *Nanog* was used as an indicator of pluripotency in HUES-2 40.2 and HUES-2 40.3 cells, on and off selection at time points 0, 30, 60 and 90 days post initiation of passaging. Due to an error in RNA extraction from HUES-2 40.3 at time point 60 off selection, the presence of pluripotency markers was diminished, but were still present at day 90. *GAPDH* was used as a positive internal control. (RT-) primers for *GAPDH* were used on DNase treated RNA samples to ensure no contaminating DNA was present in the sample. (-) no template control. On, on selection. Off, off selection.

7.3 Embryoid Body Formation

Due to the pluripotent nature of hESc, they are capable of recapitulating embryogenesis *in vitro* by forming structures known as embryoid bodies (EBs). The EBs are formed by hESc aggregation, which mimics rudimentary embryonic development of the inner cell mass of an embryo at the blastocyst stage (Itskovitz-Eldor et al. 2000). Through successful EB formation, differentiation and subsequent culturing under specific conditions, the three embryonic germ layers are formed.

Embryoid bodies were formed from the parental HUES-2 (passages ~30 and ~40), and stable clones (HUES-2 40.2, HUES-2 40.3 and HUES-2 Neo.4) by forced cell

aggregation using either AggreWell or non-adherent 96-well V bottom plates. The hESc were left in AggreWell or non-adherent 96-well V bottom plates in mTeSR media supplemented with ROCK inhibitor Y-27632 for 2-3 days for successful EB formation. After complete EB formation (2-3 days), the mTeSR was removed, the EBs were washed and collected in PBS and transferred using a pipette to non-adherent 6-well plates. After this point, the EBs were left in suspension under differentiation media (DMEM F/12, 20% FBS, 1% P/S) for 5-10 days for the three germ layers to develop. Both AggreWell and non-adherent 96-well V bottom plates were similarly efficient at forming EB of homogeneous size through forced cell aggregation. AggreWell plates currently have an upper size limit of ~4,000 cells per EB (Figure 7-4 A), while 96-well V bottom plates can form EBs containing up to ~150,000 cells (Figure 7-4 B).

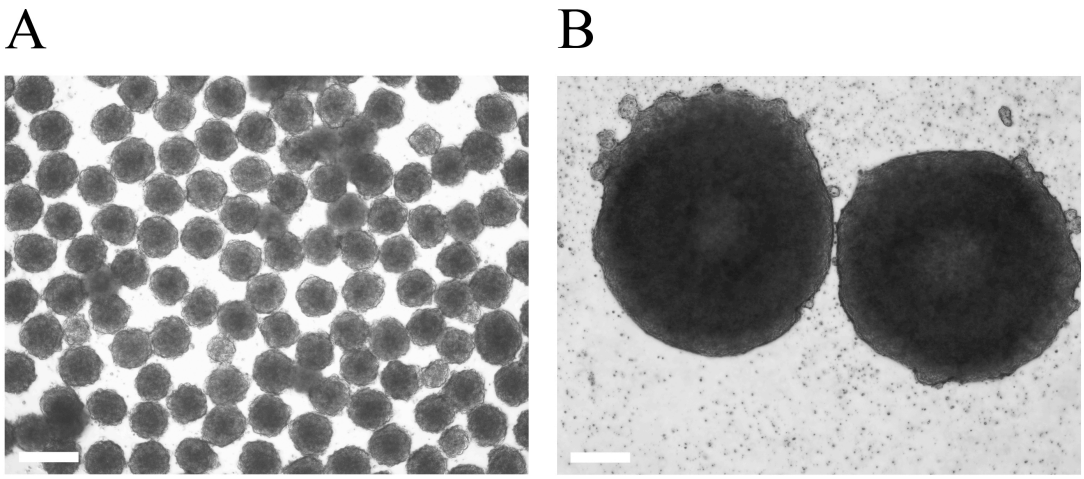

Figure 7-4 Bright field view of embryoid bodies formed using different forced cell aggregation methods
The HUES-2 40.2 cells were used to successfully form EB using AggreWell plates; ~1000 cells/EB (A) or 96-well V bottom; ~150,000 cells/EB (B). AggreWell and 96-well V bottom plates produced homogeneous EBs. Scale bar = 200µm.

Using AggreWell and 96-well V bottom plates, both small (~1000 cells/EB) and large (~150,000 cells/EB) embryoid bodies were successfully formed from HUES-2 (passages ~30 and ~40), HUES-2 40.2, HUES-2 40.3 and HUES-2 Neo.4 (all at

approximately passage 70). There were no observable differences in the EB formation potential among the various hESc lines. Figure 7-5 shows a representative sample of AggreWell formed EBs from the various lines. Up to ~95% of the cells were successfully incorporated within the structure of the EB, and up to ~98% of the formed EBs adhered to the Matrigel-coated plates after 1-2 days. These results validated the pluripotency of the described hESc lines through *in vitro* embryoid body formation.

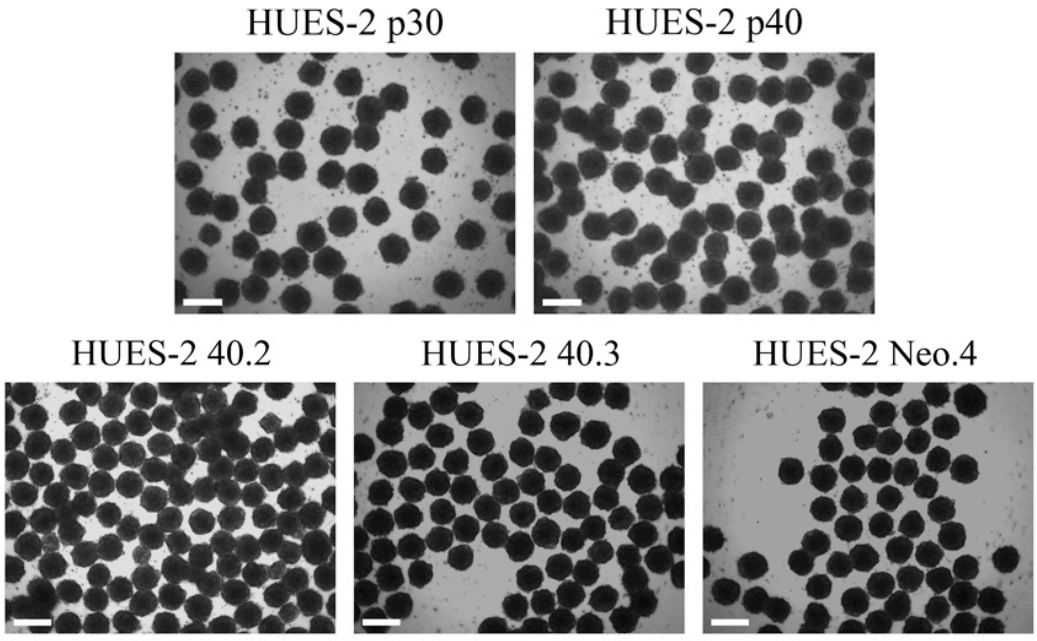

Figure 7-5 Embryoid bodies formed from various HUES-2 cell lines using AggreWell plates
Bright field view of embryoid bodies consisting of ~1000 cells/EB were formed from HUES-2 (passage ~30), HUES-2 (passage ~40), HUES-2 40.2, HUES-2 40.3 and HUES-2 Neo.4. There were no qualitative differences observed in EB formation potential among these lines. Scale bar = 200μm.

7.4 The Embryoid Body Size Affects its Differentiation Potential

The differentiation potential of small EB (~1,000 cells per EB using AggreWell plates) was qualitatively compared to large EB (~150,000 cells per EB using 96-well V bottom plates). The EBs from both methods were prepared and left in suspension

on non-adherent plates in differentiation media for 5 days to initiate differentiation. The differentiated EBs were then plated onto Matrigel-coated wells and allowed to adhere and grow outward onto the surface. After 7-10 days of cellular outward growth from the EBs, the morphology of the developed cells was qualitatively examined.

Differentiated cells were qualitatively assigned to a specific class based on their morphology. Fibroblast-like cells were identified as having a flat and slightly elongated outline, while cells with a hexagonal appearance were classed as epithelial-like cells. Neuronal-like cells were identified as forming an extensive network of axons and dendrites, while star-shaped cells with multiple cellular projections that did not extend as much as the axons and dendrites were defined as astrocyte-like cells. Small sized EBs released a limited range of cell types, mainly consisting of fibroblast-like cells (Figure 7-6), whereas large EBs released an array of differentiated cell types, such as fibroblast-like, epithelial-like and neuronal-like cells (Figure 7-7 and Figure 7-8).

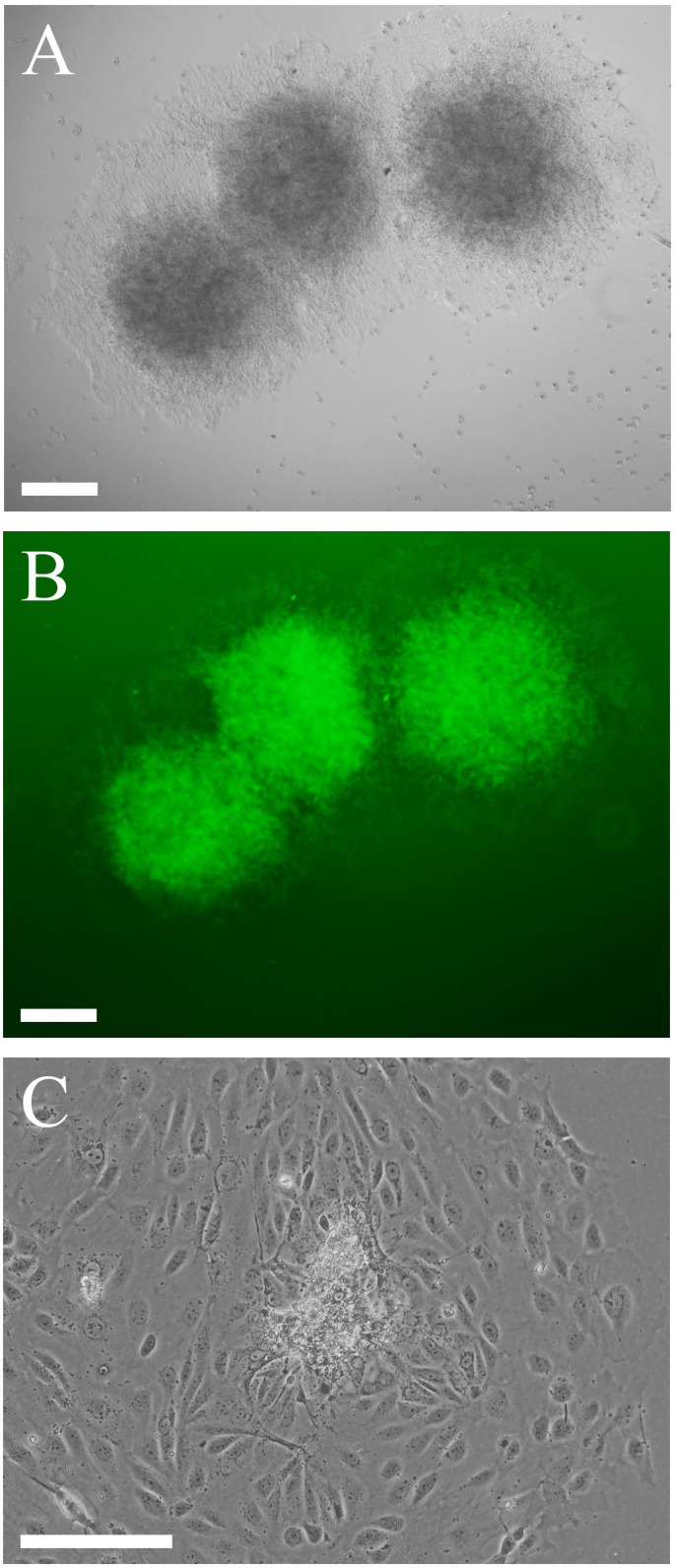

Figure 7-6 AggreWell formed embryoid bodies from HUES-2 40.2 cells
Embryoid bodies from HUES-2 40.2 cells plated onto Matrigel-coated wells. Bright field view of attached EBs on the surface of plate (A), the same field showing *GFP* expression (B). Smaller EBs released only a limited number of cell types post-differentiation (mainly fibroblast-like) (C). Scale bar = 200μm.

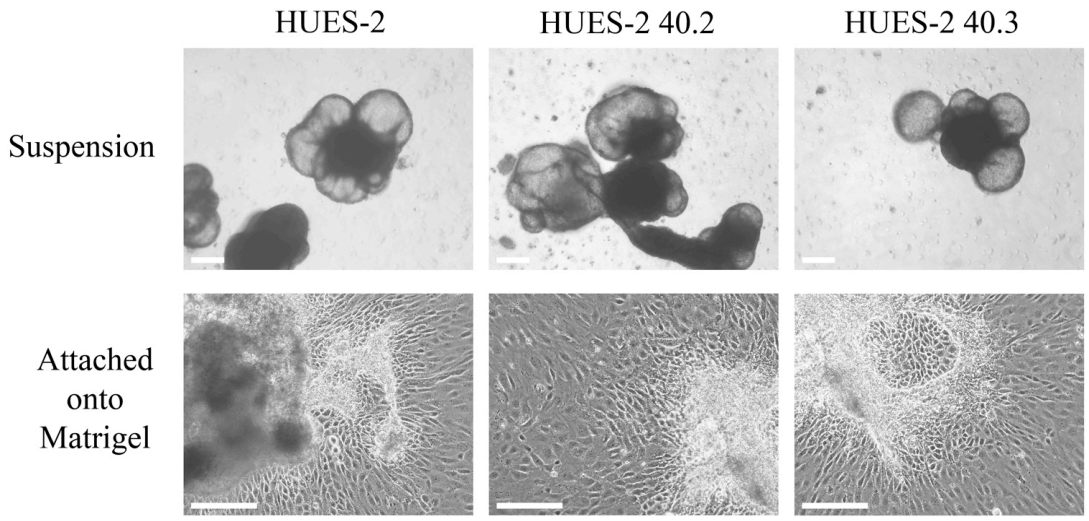

Figure 7-7 Large embryoid bodies of HUES-2 lines
Bright field view of EBs formed from HUES-2, HUES-2 40.2 and HUES-2 40.3 cells, 5 days after differentiation in differentiation media in non-adherent plates. Cellular outgrowth from inside the body of the EBs occurred when they were plated onto adherent plates. Attached EBs of HUES-2, HUES-2 40.2 and HUES-2 40.3 cells, 10 days post-adherence onto Matrigel-coated plates. Scale bar = 200μm.

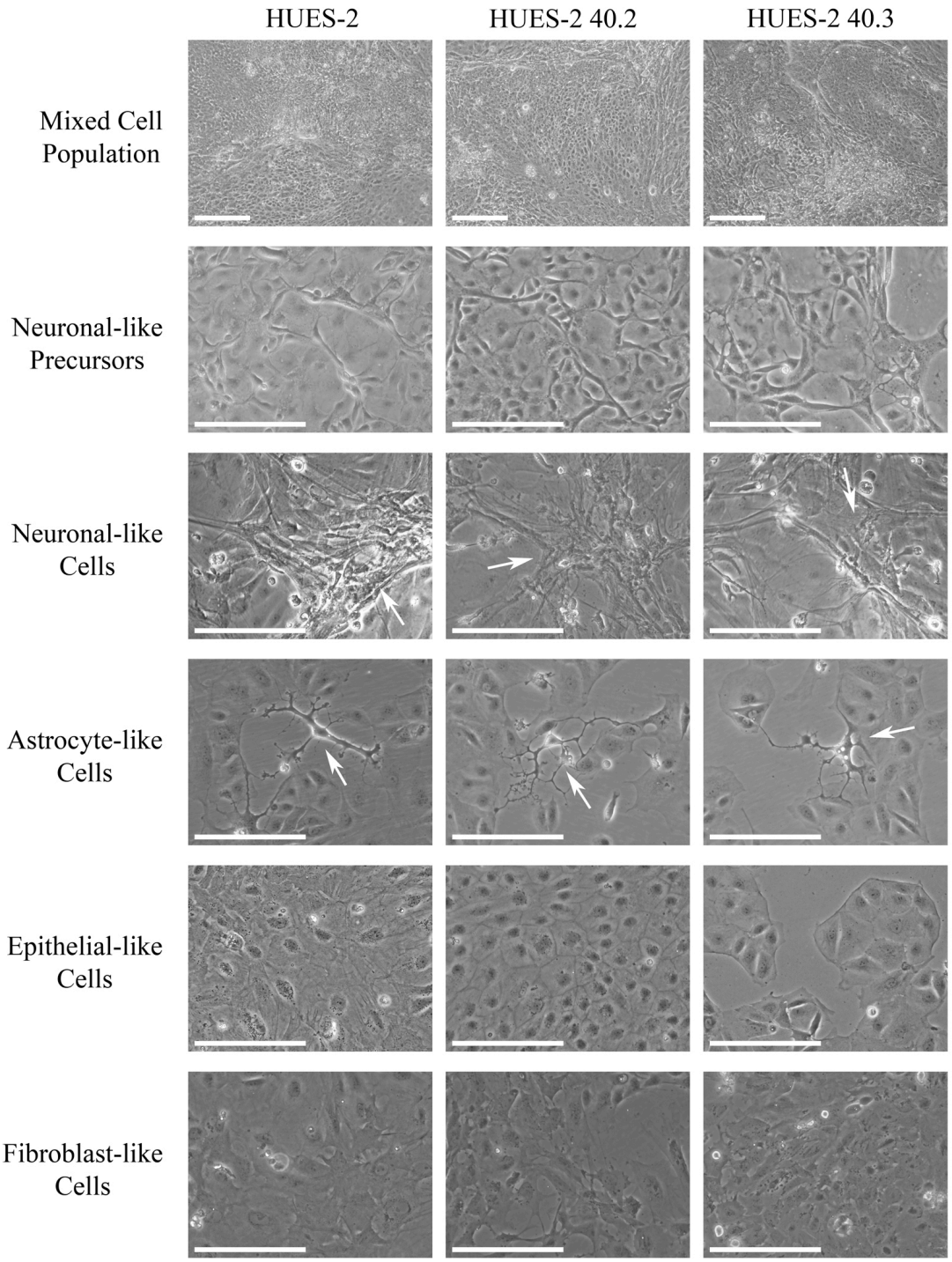

Figure 7-8 Different cell types developed after cellular release from large mature embryoid bodies from HUES-2 lines

Bright field view of differentiated cells derived from HUES-2, HUES-2 40.2 and HUES-2 40.3 embryoid bodies, 20 days following adherence to Matrigel-coated plates. Undirected differentiation of EBs resulted in the differentiation and appearance of various cell types in culture. Bright field images of mixed cell population, neuronal-like precursors, neuronal-like and astrocyte-like (indicated by arrows), epithelial-like and fibroblast-like cells were visualised from the differentiation of various HUES-2 lines. Scale bar = 200μm.

Qualitative analysis of differentiated cells from EB differentiation indicated that large EBs showed more differentiation potential as compared to small EBs. As preliminary observations suggested that large EBs were capable of developing various cells types, the differentiated cell populations were analysed for the expression of various germ layer markers through RT-PCR analysis.

7.5 Germ Layer Analysis of Embryoid Bodies

To further analyse the differentiation potential of the HAC-containing HUES-2 clones compared to the HUES-2 parental cells, total RNA was extracted from EBs and analysed by RT-PCR. Primers specific for genes expressed in the three embryonic germ layers and neuronal specific markers were used. Approximately 3.0×10^7 cells were used to make 200 EBs (~150,000 cells/EB) in 96-well V bottom plates from HUES-2 at passage ~30 (with normal karyotype), and passage ~40 (with partial trisomies of chromosomes 1, 12 and 17), HUES-2 40.2, HUES-2 40.3 and HUES-2 Neo.4. Various batches were prepared to look at how differences in EB formation affected the differentiation outcome. Table 7-1 summarises the formation history of each EB batch and the duration of incubation (days) in each differentiation phase. In phase I, the cells were in 96-well V bottom plates forming EBs in mTeSR medium. In phase II, the EBs were moved onto non-adherent plates and cultured in differentiation medium. Finally, in phase III, the EBs were moved onto Matrigel-coated plates and cultured under differentiation medium.

Table 7-1 Embryoid bodies formed from various HUES-2 lines

Phase	Incubation Period For Each Embryoid Body Batch (Days)								
	HUES-2 P30	HUES-2 P45	HUES-2 40.2 Batch 1	HUES-2 40.2 Batch 2	HUES-2 40.2 Batch 3	HUES-2 40.3 Batch 1	HUES-2 40.3 Batch 2	HUES-2 Neo.4 Batch 1	HUES-2 Neo.4 Batch 2
I	3	3	2	3	3	3	3	3	3
II	3	8	10	21	11	5	8	12	6
III	14	13	15	0	8	17	11	8	11
Total	20	24	27	24	22	25	22	23	20

These experiments showed that depending on the cell source, there were variations in how well EBs were able to maintain their structural integrity as an intact spherical mass post-formation. For example, EBs formed from HUES-2 at passage ~30 showed the least amount of structural integrity and cells started shedding away from the EBs after only 3 days in suspension (phase II), while EBs from HUES-2 40.2 cells maintained structural integrity up to 21 days in suspension (phase II). Variation in the structural integrity of EBs was also evident among different batches deriving from the same cell source. This variation suggested that differences in the initial EB formation conditions and other less defined stochastic events had a downstream effect on the differentiation potential of the formed EB.

At the end of the differentiation period, cells were harvested and total RNA was extracted from each EB batch. Samples were first treated with DNaseI and then converted to cDNA. RT-PCR was carried out on the cDNA using primers specific for genes expressed in the three embryonic germ layers and neuronal cells. For the endodermal layer, the expression of the following genes was verified: *αFP*, *HNF3α*, and *α-1 anti-trypsin*. *Mix-I*, *GATA-2* and *Kallikrein* were used as mesodermal markers and *CK-14*, *CK-5* and *High-sulphur Keratin* were used as epidermal markers. Finally, primers for *Pax-6* and *β-III-tubulin* were used as neuronal markers. *GAPDH* primers were used as an internal positive control and also as an RT negative control on the

DNaseI treated RNA to ensure no contaminating DNA was present in the samples. Figure 7-9 shows that the three embryonic germ layer markers are absent, or present only at low levels, in undifferentiated HUES-2 lines. However, after EB formation and an extended period of differentiation and culturing, a number of germ layer specific markers were expressed. Overall, the results suggested that all these hESc lines were capable of EB formation and successful germ layer differentiation.

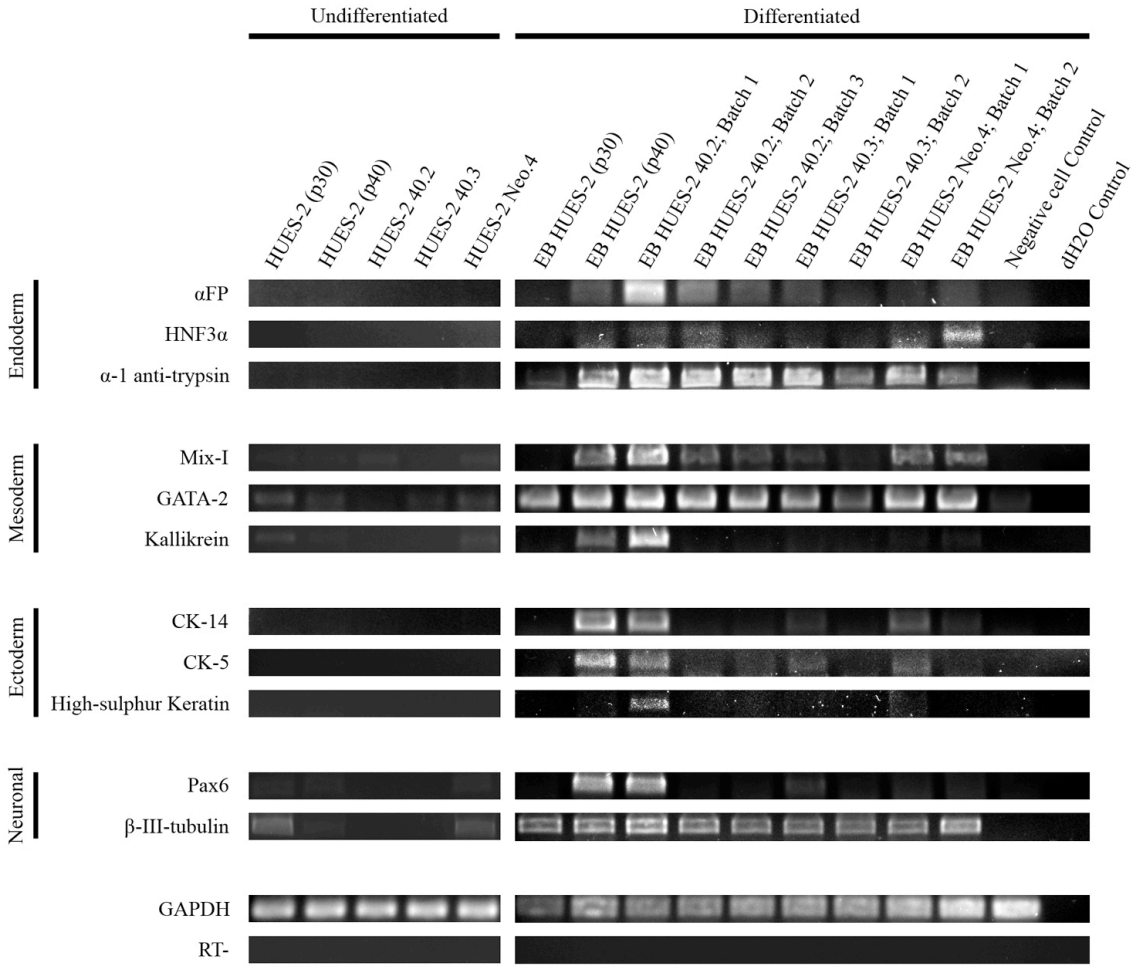

Figure 7-9 RT-PCR analysis of undifferentiated and differentiated HUES-2 and derivative clones
Undifferentiated and differentiated HUES-2 cells were analysed using RT-PCR. Primers specific for endoderm markers (*αFP*, *HFN3α*, *α-1 anti-trypsin*), mesoderm markers (*Mix-I*, *GATA-2*, *Kallikrein*), ectoderm markers (*CK-14*, *CK-5*, *High-sulphur Keratin*), and neuronal markers (*Pax6* and *β-III-tubulin*) were used. *GAPDH* was used as positive control. RT- control PCR was performed on RNA in the absence of the reverse transcription step using *GAPDH* primers.

Cells derived from EBs formed from HUES-2 (passage ~40) and HUES-2 40.2 batch 1, expressed at least 2 out of the 3 markers analysed for each of the embryonic germ layers. They also showed expression of the *Pax6* neuronal precursor at high levels compared to their undifferentiated parental cell line. No epidermal markers were detected in HUES-2 40.2 batch 2 as this sample was only kept in suspension and never cultured on Matrigel. Similarly, HUES-2 40.2 EB batch 3, that was kept on Matrigel for a short period of time (8 days), did not express any of the three epidermal markers. The results showed that the development of the epidermal and neuronal markers was highly dependent on both an extended period of differentiation in suspension, and also, an extended period of growth and culturing on Matrigel.

The HUES-2 cells at passage ~30 did not show a high differentiation potential compared to the differentiation of HUES-2 cells at passage ~40 and the HAC-containing derivative clones at higher passages (~70). This result is evident in Figure 7-9, as the majority of the embryonic germ layer markers were absent in the EBs derived from HUES-2 at passage ~30. This result was surprising and may be attributed to the lower adaptation of this line to the feeder-free culture conditions. The majority of the EBs formed from this line were structurally fragile and gradually fell apart in suspension; thus, it was only feasible to keep these EBs in suspension for a maximum of 3 days (see Table 7-1). As a result, the final number of deriving differentiated cells was dramatically reduced and the resulting EBs were less mature, leading to the development of only a few of the germ layer markers.

There are also other less defined stochastic events in play during the differentiation phase that may lead to differentiation of a particular cell line. An example is HUES-2

Neo.4 batch 2 that showed expression of the *HNF3α* endodermal marker, while all the other EB batches (including HUES-2 p40 and HUES-2 40.2 batch 1) were unsuccessful and did not show the expression of this marker. However, small quantities (<1ng) of amplified PCR product on the agarose gel may have gone undetected when using the UV transilluminator detection system.

Based on these results, the most suitable conditions for the development of the three embryonic germ layers were the following: ~2-3 days of formation (phase I), ~8-10 days of growth in suspension (phase II) and ~13-15 days of adherent growth on Matrigel (phase III). These conditions resulted in the formation of all three germ layers, in addition to the formation of neuronal precursors. RT-PCR products for the latter were amplified only when the ectodermal markers were present, as neuronal cells are derived from the ectoderm. After the establishment of optimal conditions for germ layer differentiation of various HUES-2 lines, the differentiation capacity of the HAC-containing HUES-2 40.2 cells was investigated. As this clone contains the highest HAC frequency amongst the various analysed stable clones, it was the suitable candidate to look at HAC stability and expression post-differentiation.

With the aim of characterising the HAC frequency in the differentiated cells, EB-derived HUES-2 40.2 cells were analysed by FISH using HAC-specific probes (pBeloBAC11 vector), coupled to antibodies staining the cytoskeleton (α and β-tubulin), to help identify the cells based on their morphology. The analysis of differentiated cells revealed that the EB-derived cell population consisted of ~40% fibroblasts, ~55% epithelial, and ~5% neuronal-like cells. The FISH analysis revealed the presence of HAC in ~65% of the fibroblast-like, ~50% of the epithelial-like and

present in all the remaining cells. The overall HAC frequency of the EB-derived differentiated cells was estimated at ~60% (FISH performed and analysed by Dr Daniela Moralli).

7.6 *GFP* Expression of HUES-2 40.2 Cells Post Embryoid Body Formation

To measure the effect of cell differentiation on the fraction of *GFP*-expressing population of the HAC-containing HUES-2 40.2 clone, EBs from this clone were prepared. EBs were harvested at four time points post-formation: 1, 5, 10 and 35 days. Cells were dissociated from the EBs using warm collagenase IV, fixed in 4% (v/v) formaldehyde, and analysed by FACS. Figure 7-10 shows the FACS results on the percentage of *GFP*-expressing cells from the differentiated (EB-derived) and undifferentiated HUES-2 40.2 at various time points. As expected, the fraction of *GFP*-expressing cells remained constant for the undifferentiated HUES-2 40.2 cell population (as previously discussed in Chapter 6). In contrast, the differentiated HUES-2 40.2 cells retained the percentage of *GFP*-expressing cells for up to 10 days post-differentiation, however there was a sharp decline in the fraction of *GFP*-expressing cells after an extend period of differentiation (35 days). The mean *GFP* expression after a 35-day differentiation period was significantly lower than the mean *GFP* expression of the non-differentiated sample ($p<0.001$; two-sample t-test).

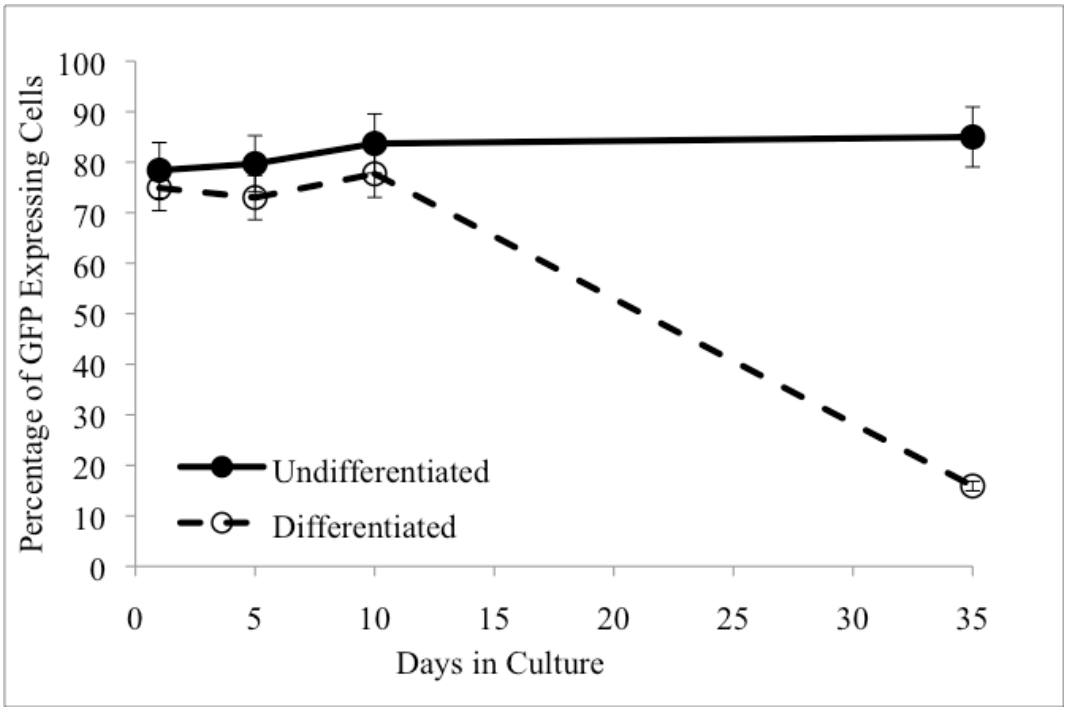

Figure 7-10 FACS analysis of *GFP*-expressing cells of HUES-2 40.2 clone after differentiation

Data based on 3 replications per group. The EBs from HUES-2 40.2 and HUES-2 cells (passage ~40) were formed and left in suspension for various amounts of time. After dissociation and fixation of cells, *GFP* expression was analysed using FACS. The HUES-2 cells were used as a negative control by setting the gate to less than 0.5% *GFP* positive. 100,000 events were captured for each time point (FACS runs and data analysis performed with the assistance of Dr Sally Cowley). Error bars represent standard error of the mean.

Visualisation using an epifluorescence microscope, after 35 days of undirected differentiation of HUES- 40.2 cells, revealed that the derivative differentiated cells exhibited a heterogeneous *GFP* expression. Some cell patches expressed *GFP*, while the majority of them had lost their *GFP* expression in their entirety. Variation in *GFP* expression was probably due to stochastic differentiation and silencing processes that may have occurred during the initial stages of EB formation, maturation and differentiation (Figure 7-11).

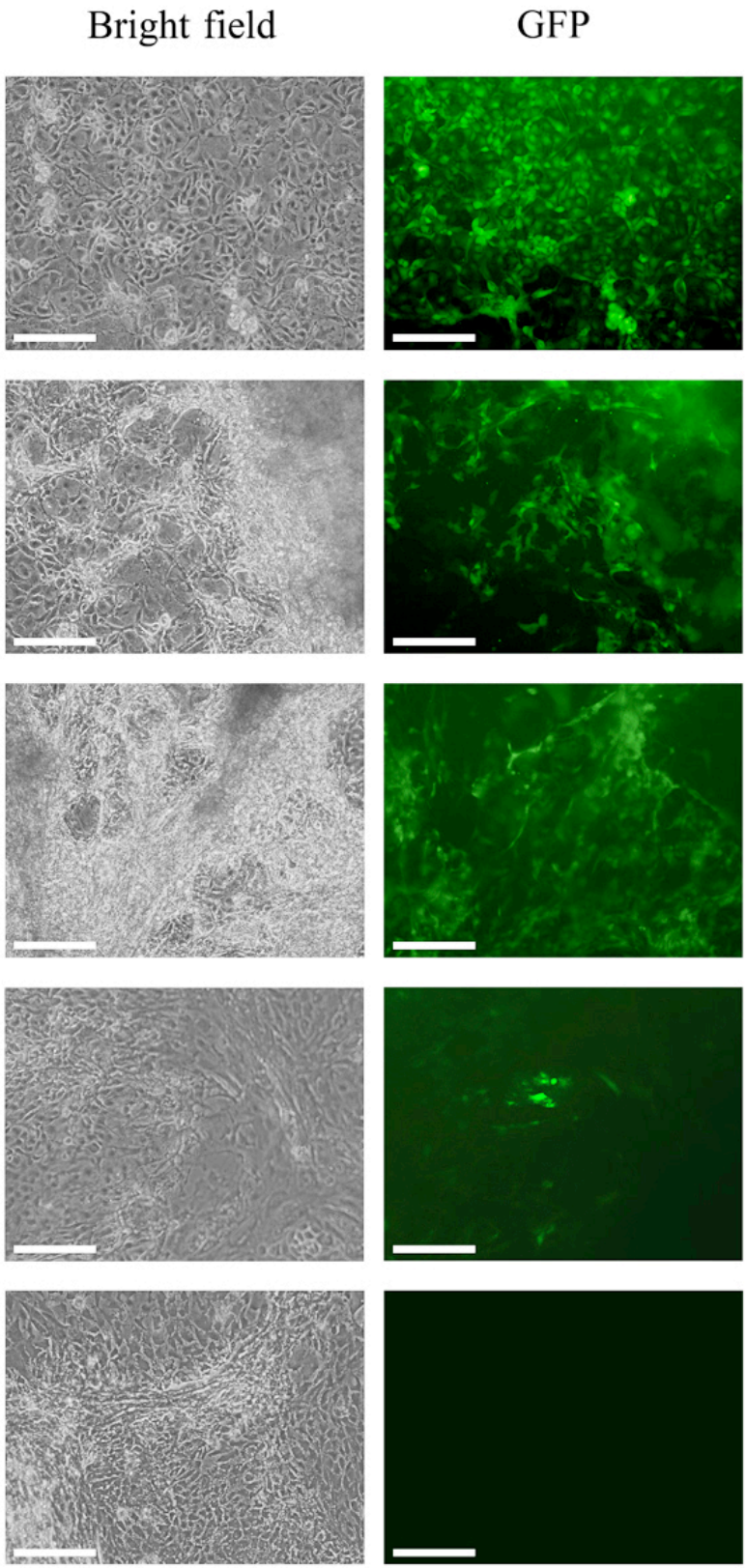

Figure 7-11 Variation in *GFP* expression of HUES-2 40.2 cells after 35 days of differentiation

After 35 days of differentiation of HUES-2 40.2 cells, a wide array of cell types was formed (see bright field images). After differentiation, the cells showed non-uniform *GFP* expression. Some fields showed patches of cells expressing *GFP*, while others contained no signal. Scale bar = 200μm.

These results indicated that extended differentiation of the HAC-containing HUES-2 40.2 cells led to a loss of *GFP* expression. DNA silencing and chromatin remodelling may have been the main contributing factors leading to this phenomenon (Macarthur et al. 2011). However, no further experiments were performed to elucidate the cause of loss of *GFP* expression.

7.7 Neuronal Differentiation of HUES-2 40.2 Cells

As previously described in Chapter 6, the HAC-containing HUES-2 40.2 cells showed HAC stability and stable gene expression during a 90-day period off drug selection. To further examine the pluripotent potential of this clone and more importantly, the HAC stability and gene expression post-differentiation, a directed differentiation pathway was chosen. *In vitro* neuronal differentiation of hESc was chosen as the differentiation procedure is relatively simple, is well characterised and yields high levels of neuronal cells. Furthermore, many research groups have proposed the use of hESc for treatment of neurological disorders such as Parkinson's disease (Thomson et al. 1998; Cowan et al. 2004; Kiskinis and Eggan 2010), and many groups are currently working on finding hESc-based treatments for neurological disorders (Kim et al. 2002; Li et al. 2008; Yang et al. 2008). Thus, neuronal differentiation was an ideal choice for the purpose of this study. Directed neuronal differentiation of HUES-2 40.2 cells was achieved through blocking bone morphogenetic protein (BMP) signalling pathways using noggin and fibronectin (Itsykson et al. 2005; Iacovitti et al. 2007), followed by the development of the ectodermal layer under N2 media, providing the conditions for neuronal growth and proliferation (Barker and McKelvy 1983).

EBs were formed from HUES-2 (passage ~40) and HUES-2 40.2 (passage ~70) cells by forced cell aggregation using AggreWell plates. Approximately 1200 EBs, of size ~4,000 cells/EB, were formed. After 2 days of formation inside AggreWell plates, the EBs were then released into non-adherent plates and left in suspension in neuronal differentiation media I (NDM-I) for 5 days. The EBs were then moved onto Matrigel-coated plates and grown under neuronal differentiation media II (NDM-II). Within 2 days of plating, approximately 99% of the EBs adhered onto the Matrigel surface. Subsequently, cellular release and outward growth was initiated from the EBs. As previously discussed, adherence and outward growth of cells within the EB was essential for the formation of the ectodermal germ layer. The development of the ectoderm precedes the formation of neuroectoderm, which consequently gives rise to neuronal cells. By the 10^{th} day of EB adherence and gradual outward cellular expansion under NDM-II, neuronal rosettes started to appear in culture. The development of neuronal rosettes preceded full neuronal maturation. Figure 7-12 outlines the presence of neuronal precursors in neuronal rosettes using β-III-tubulin, a commonly used marker to detect neuronal cell types (Iacovitti et al. 2007).

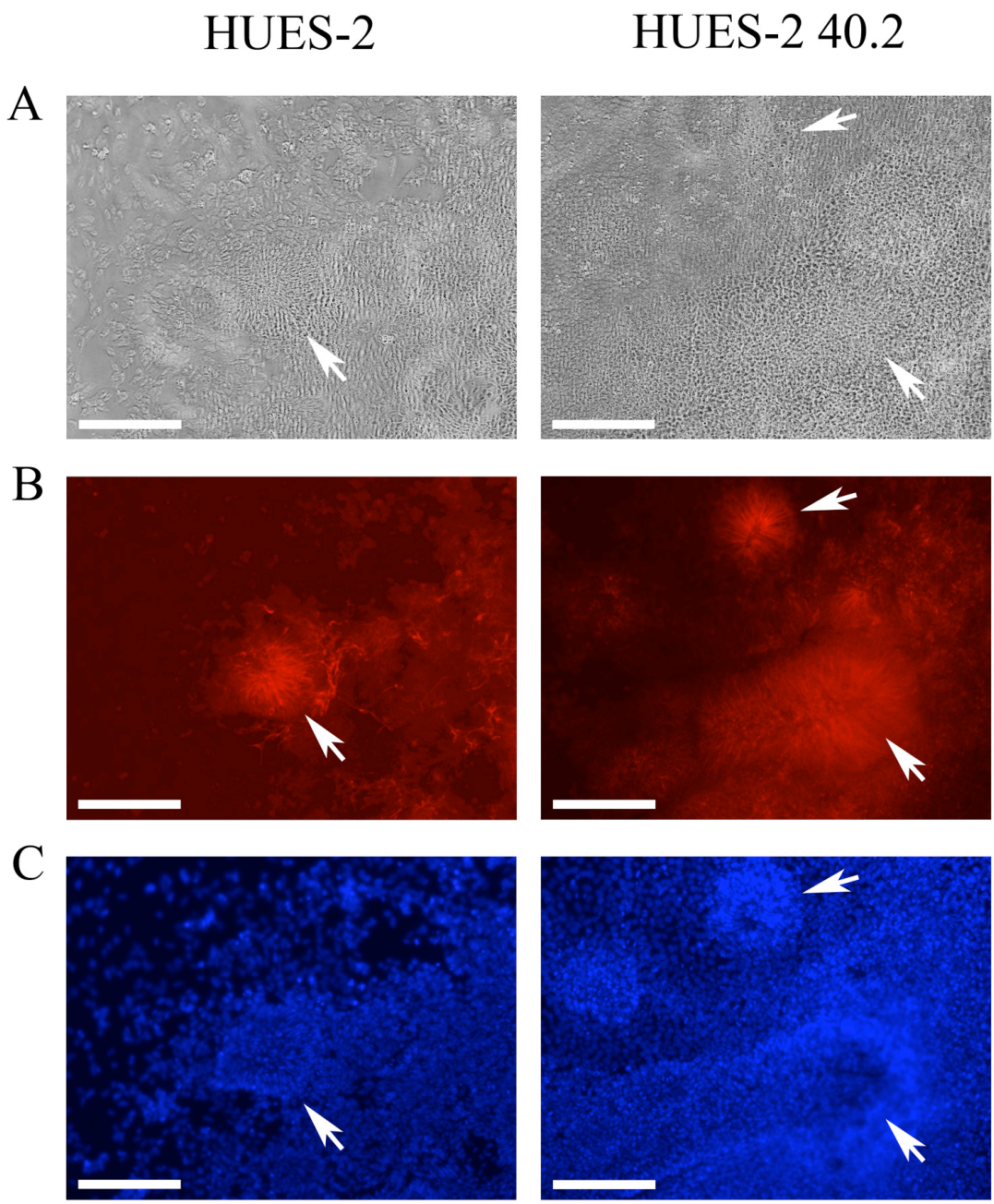

Figure 7-12 Neuronal rosettes stained with β-III-tubulin
Images taken from HUES-2 and HUES-2 40.2 cells, 10 days post-directed neuronal differentiation. Images show bright field (A), neuronal rosettes stained with β-III-tubulin antibody (in red) (B) and nuclei stained with DAPI (in blue) (C). The white arrows point to the location of neuronal rosettes. Scale bar = 200μm.

After 20 days of directed differentiation, neuronal cells started to emerge from "neuronal factories." Neuronal factories are surface-adhered, matured EBs harbouring hESc that are in the process of differentiation into neuronal cells. Figure 7-13 shows neuronal cells stained with β-III-tubulin antibody. The neuronal cells were gradually

released from the body of the "neuronal factory" and eventually adhered to the surface of the plate.

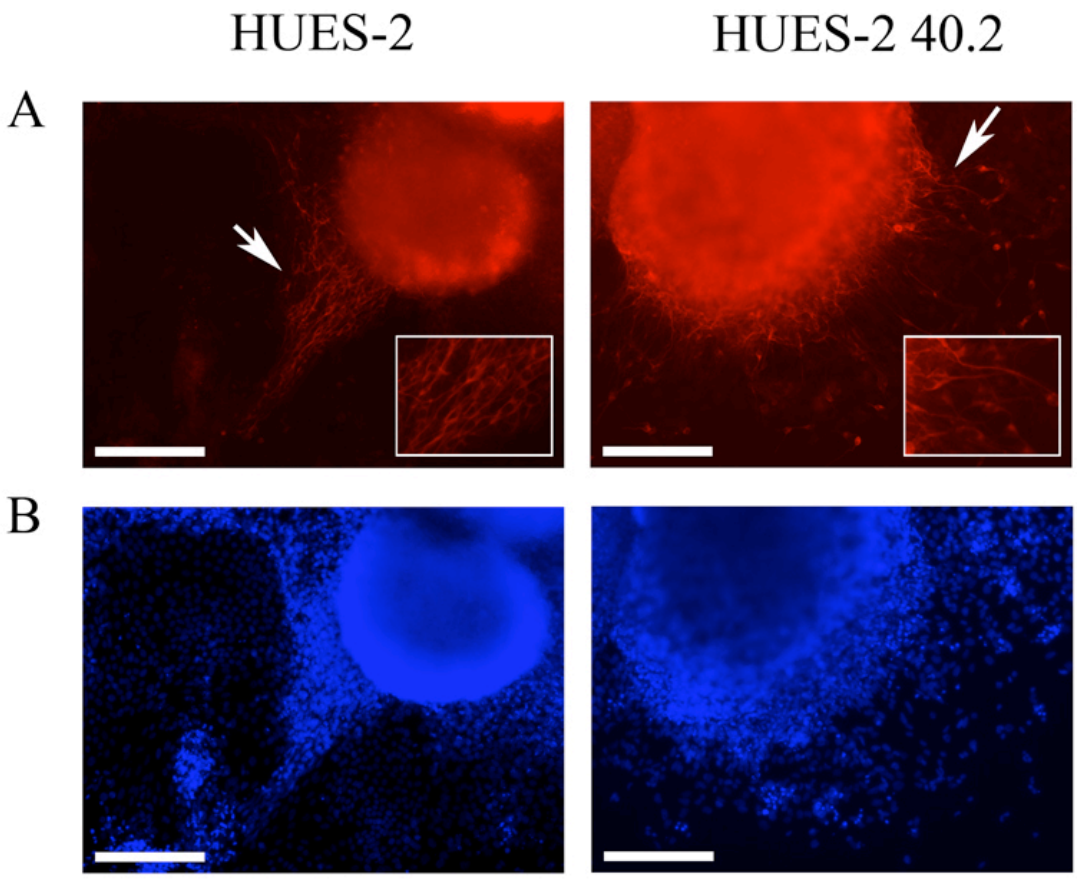

Figure 7-13 Neuronal cells released from neuronal factories
After 20 days of directed differentiation in neuronal differentiation media, HUES-2 and HUES-2 40.2 EBs formed neuronal factories. hESc within the EBs were gradually differentiated toward neuronal cells and released from the factory and adhered onto the surface of the plate. Arrows point to β-III-tubulin positive neuronal cells (in red) (A). The insets show a 2× enlargement of the area identified by the arrows. Nuclei are stained with DAPI (in blue) (B). Scale bar = 200μm.

Figure 7-14 shows neuronal-differentiated HUES-2 40.2 cells: both the bright field (A) and β-III-tubulin stained (B) images showed an extensive neuronal network consisting of axons and dendrites, as determined based on their morphology. The neuronal differentiation efficiency of HUES-2 40.2 was initially measured on the differentiating plate and was estimated at approximately 25% via indirect-immunostaining, using β-III-tubulin antibody. However, as seen in Figure 7-13, many of the differentiated neuronal cells were still present within the body of the "neuronal

factory"; thus, such an estimation may have been a misrepresentation of the differentiation efficiency. In an attempt to improve quantification of differentiation efficiency of the neuronal HUES-2 40.2, the cells were trypsinised and passaged onto Matrigel-coated slides. Of the cells that survived trypsinisation and reattached onto slides, approximately 20% were positively stained using β-III-tubulin antibody (Figure 7-14 C and D). During the process of trypsinisation and replating, the neuronal cells suffered from high cell loss and death; hence explaining the reduction in the fraction of neuronal cells after moving the cells onto slides. Immuno-FISH studies using a vector-specific probe (pBeloBAC11) on β-III-tubulin stained neuronal cells revealed that ~45% of cells contained a HAC signal (FISH performed and analysed by Dr Daniela Moralli). However, one limitation of HAC analysis in neuronal-differentiated cells was that these cells do not undergo mitotic division and thus can only be analysed during interphase. Furthermore, differentiated neuronal cells were difficult to maintain in culture and were short-lived, hence making the number and source of cells limited for downstream analysis.

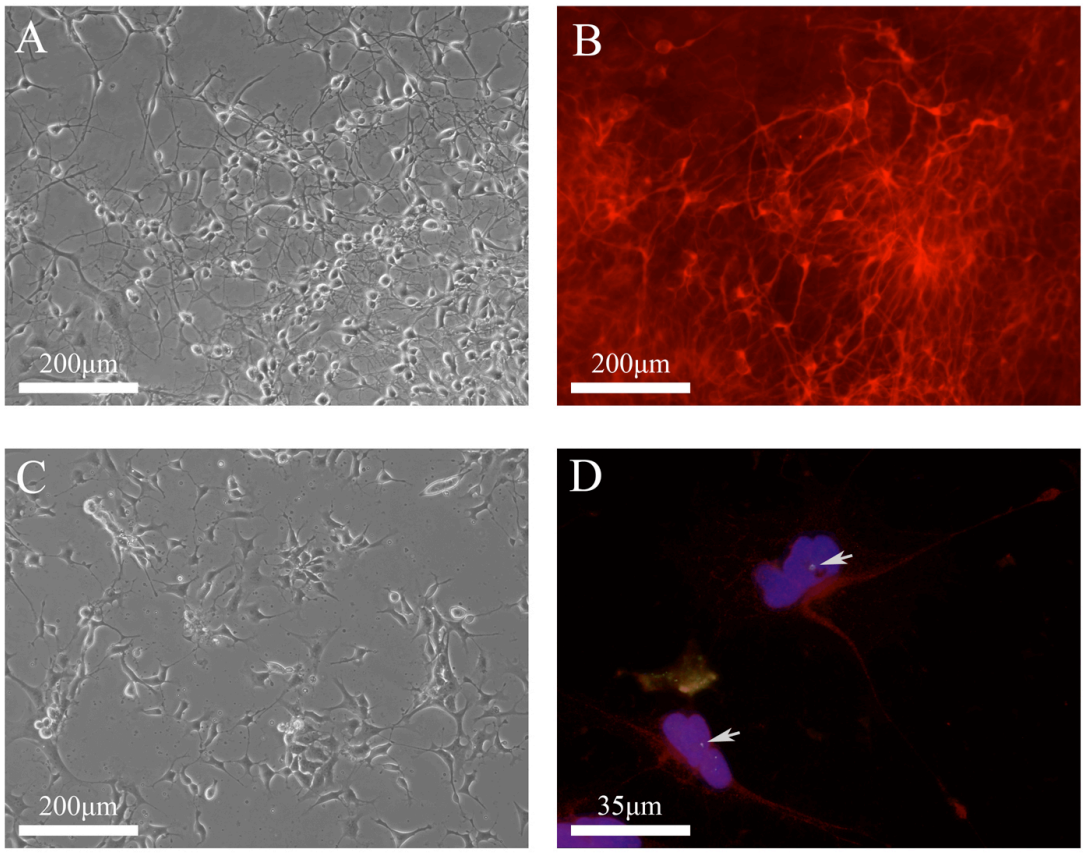

Figure 7-14 Neuronal-differentiated HUES-2 40.2 cells
Bright field image of differentiated neuronal HUES-2 40.2 cells displaying a network of axons and dendrites (A). A different field of HUES-2 40.2 neuronal cells showing an extensive neuronal network stained with β-III-tubulin antibody (in red), a neuronal-specific marker (B). Bright field images of HUES-2 40.2 derived neuronal cells after passaging onto Matrigel-coated slides at low densities for FISH analysis (C). Immuno-FISH performed on HUES-2 40.2 neuronal-differentiated cells using β-III-tubulin (in red) as a neuronal marker and vector probe (pBeloBAC11) to detect the presence of HAC (in green). Arrows point to a HAC-specific signal detected in β-III-tubulin stained cells. Nuclei were stained with DAPI (in blue) (D). Scale bar = 200µm except for D where scale bar =35µm.

7.8 Teratoma Formation of HUES-2 40.2 Cells

To date, the most comprehensive test of pluripotency, in human cells, is the teratoma formation assay (Loh et al. 2009). Thus, as the final test of pluripotency of the HAC-containing HUES-2 40.2 clone, the teratoma formation capacity was investigated. Approximately 2×10^6 cells from HUES-2 40.2 clone at passage ~70 were harvested and resuspended in RPMI media and Matrigel (1:1 v/v). The cell suspension mix was

then subcutaneously injected into the hind leg of severe combined immunodeficient (SCID) triple knockout mice; *IL2rg*, *Rag2*, and *C5* all -/- (The cells were prepared with the help of Dr Sayandip Mukharjee. Injections performed by Dr Michael Blundell at the Institute of Child Health, University College London).

After ~5-7 weeks post-injection, the mice developed tumours of approximately 10mm in diameter, the mice were sacrificed and tumours were extracted. The tumours were then sectioned, stained with haematoxylin/eosin or with antibodies for the following germ layer specific markers: β-III-tubulin (ectoderm), α-actinin (mesoderm) and α-feto protein (endoderm). The slides were then analysed with a Zeiss LSM 710 inverted confocal microscope. Histological and immunophenotypic analyses were carried out to validate the presence of the three embryonic germ layers (tumour extraction performed by Dr Michael Blundell; sectioning, staining and analysis performed by Dr Sayandip Mukharjee). Figure 7-15 shows the analysis of teratoma-derived sections confirming the presence of the three embryonic germ layers. Furthermore, haematoxylin/eosin staining of sections reveals the development of tissues such as neuronal tube (ectoderm), blood vessel and muscle (mesoderm), gut, gland, and alveoli (endoderm). The results confirmed the pluripotent nature of the HAC-containing HUES-2 40.2 clone, indicating that neither the HSV-1 amplicon transduction, nor the presence of HAC interfered with the pluripotent nature of hESc.

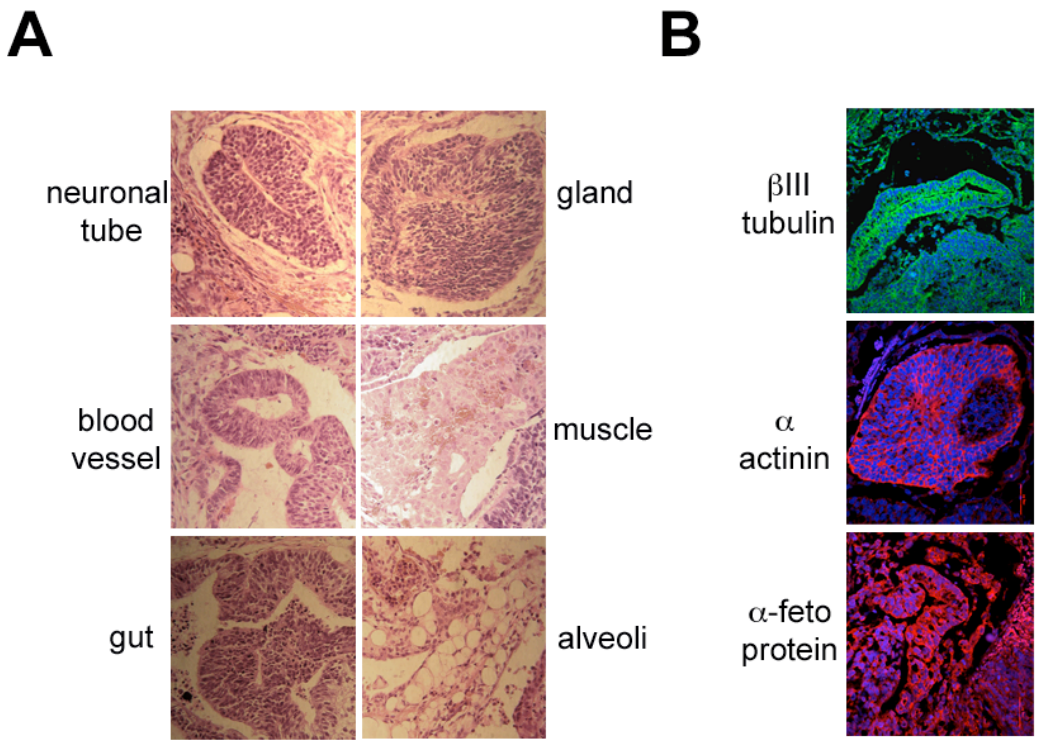

Figure 7-15 Germ layer analysis of teratoma-derived sections
Haematoxylin/eosin stained sections showed the presence of neuronal tube, blood vessel, gut, gland, muscle and alveoli (A). Indirect-immunostaining of HUES-2 40.2 teratoma-derived sections with antibodies for β-III-tubulin (ectoderm, in green), α-actinin (mesoderm, in red) and α-feto protein (endoderm, in red). Nuclei are stained with DAPI in blue (B) (samples prepared and images captured by Dr Sayandip Mukharjee).

In parallel to germ layer characterisation, an *in vitro* cell culture was established from cells dissociated from the teratoma for further analysis (see materials and methods section 2.38) (Figure 7-16). After passaging the teratoma-derived cells 4 times in culture, chromosome metaphase spreads were prepared from the HUES-2 40.2 teratoma cells and hybridised with HAC-specific probes and analysed using FISH. The analysis showed that HAC were present in approximately 20% of the scored metaphases. In approximately 30% of the cells, the HAC DNA had integrated into one of the host chromosomes (FISH experiments and analysis performed by Dr Daniela Moralli).

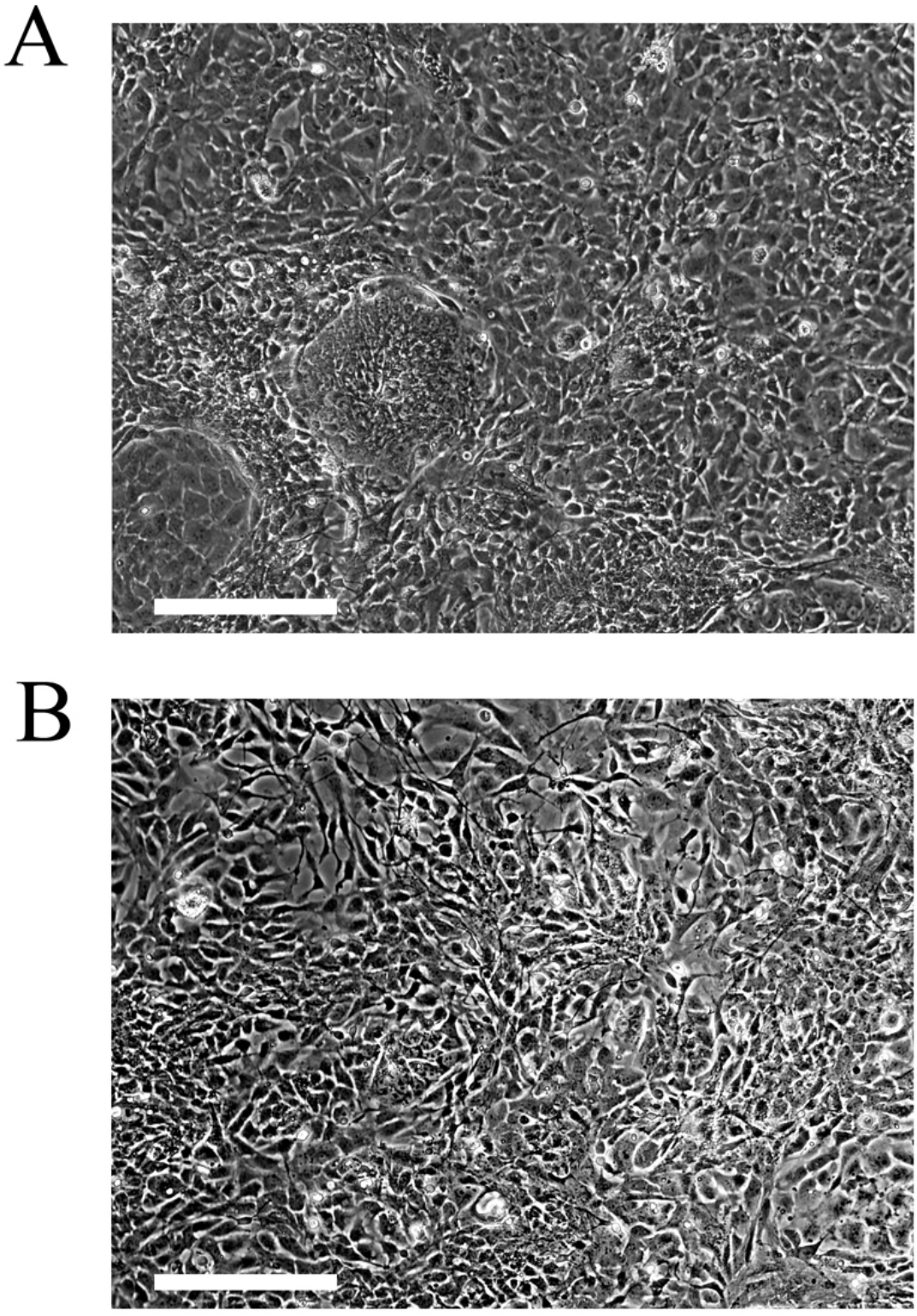

Figure 7-16 *In vitro* teratoma-derived cells at passages 2 and 4 post-establishment
Bright field images taken from *in vivo* teratoma-derived cells at passage 2 (A) and passage 4 (B) post-establishment. Scale bar = 200μm.

7.9 HAC Stability Post-Differentiation

Figure 7-17 summarises the HAC frequency in HUES-2 40.2 cells before and after differentiation. As previously reported, HAC frequency before differentiation was ~70%. HAC frequency was estimated at ~60% in EB-derived cells (mostly consisting of fibroblast-like and epithelial-like cells), ~45% in neuronal cells and ~20% (with the addition of ~30% integration events) in the *in vitro*-derived teratoma cells (FISH experiments performed and analysed by Dr Daniela Moralli).

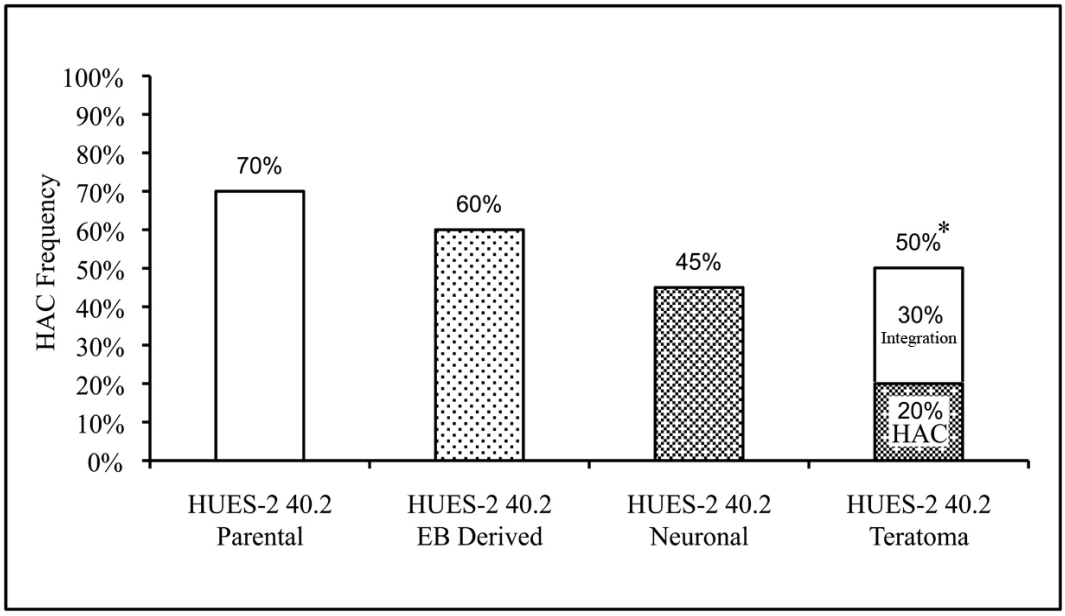

Figure 7-17 HAC stability of HUES-2 40.2 and differentiated cells
FISH analysis of HAC frequency in parental HUES-2 40.2 and differentiated cell types. 15-20 metaphases were scored per group. In this graph, for ease of comparison, the frequency of HAC and integrations in the teratoma cells are combined as marked with an asterisk (FISH experiments performed and analysed by Dr Daniela Moralli).

As other groups have reported extra chromosomal abnormalities in teratoma-derived cells (Yu et al. 1995; Andrews et al. 2005), the overall genomic instability of the teratoma-derived cells was investigated by looking at aberrations in the number of chromosome 12. The teratoma-derived cells were hybridised to whole chromosome 12 specific paints (60 metaphases were scored; experiments performed and analysed

by Dr Daniela Moralli). Figure 7-18 shows a histogram of the copy number of chromosome 12 present per cell in the *in vitro*-derived teratoma cell culture. Similar to the pre-injection HUES-2 40.2 cell population, ~30% of the teratoma cells had 2 copies of chromosome 12. However, the teratoma-derived cells appeared to show more instability as a number of metaphases were scored with 4-8 copies of chromosome 12.

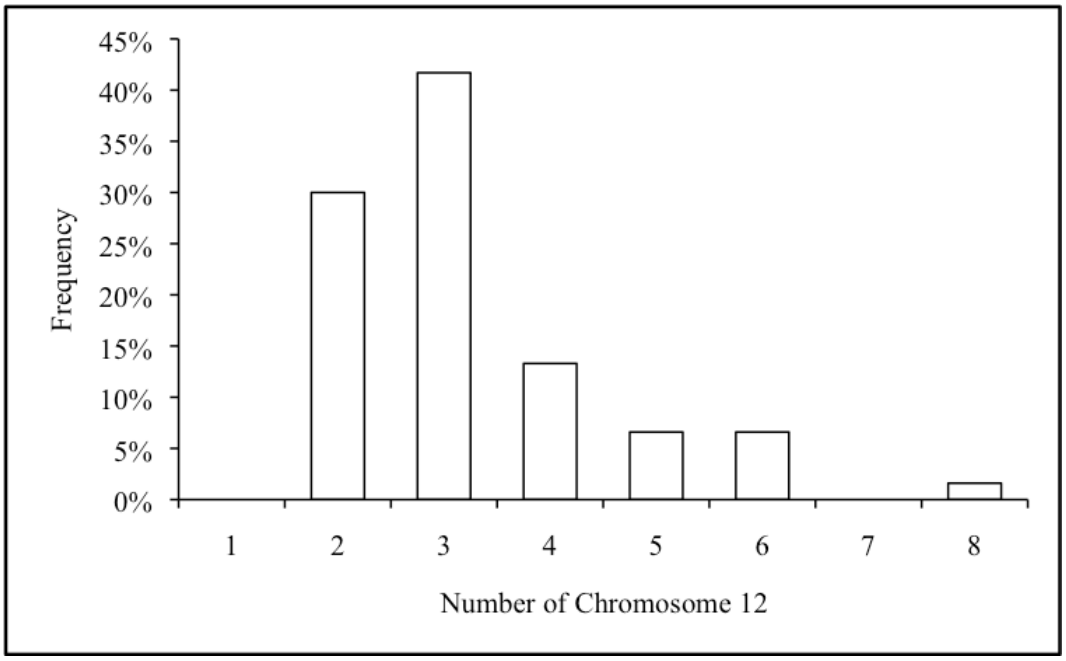

Figure 7-18 Analysis of number of chromosome 12 in the teratoma-derived cells
FISH using chromosome 12 paints were performed on teratoma-derived cells, suggesting the development of extra chromosomal aberrations during teratoma formation and development (FISH performed and analysed by Dr Daniela Moralli).

As extra copies of chromosome 12 are known to provide cells with a growth advantage, it is possible that after injecting the HUES-2 40.2 cell population into nude mice, cells with extra chromosome 12 aberrations were favoured and selected for rapid proliferation. These results suggested that the teratoma-derived cells have an increased level of genomic instability, which may be the leading cause of HAC instability as demonstrated by a reduction in HAC frequency and high frequency of

integration events, since it was previously shown that HAC were not stable in cell lines with high basal level of instability (Moralli et al. 2006).

7.10 Real-Time qPCR Quantification of HAC DNA Content Post-Differentiation

Sybr-green Real-Time qPCR on genomic DNA extracted from undifferentiated and differentiated (EB, neuronal and teratoma-derived) HUES-2 40.2 cells was performed to confirm the FISH results. HAC-specific primers for *GFP* and *Neo* genes were used and normalised against *GAPDH* to quantify HAC copy number per cell. Real-Time qPCR on genomic DNA from each sample resulted in a 1:1 ratio of *GFP* to *Neo* copy number. Normalisation of HAC DNA content (using *GFP* and *Neo*) against *GAPDH* (endogenous internal control) was performed using the $2^{-\Delta\Delta ct}$ method (Livak and Schmittgen 2001) as described in materials and methods section 2.31. The results suggested that the relative HAC DNA content in the differentiated cells to the undifferentiated parental was in general agreement to the reported FISH data (Figure 7-19).

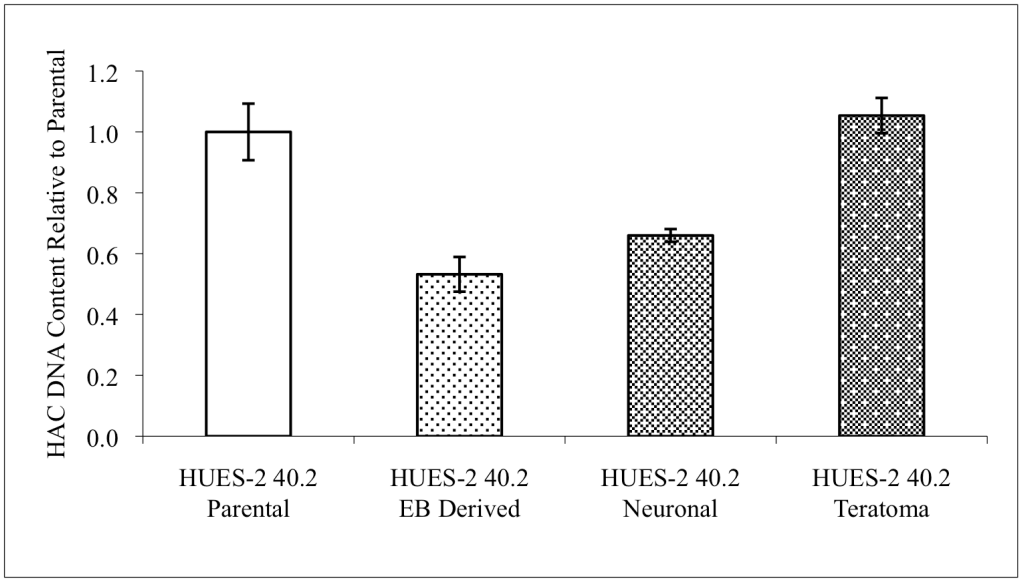

Figure 7-19 Real-Time qPCR quantification of HAC DNA content in HUES-2 40.2 and differentiated cell types
Data based on 4 replications per group. HAC-specific primers for *Neo* and *GFP* were used and normalised against an endogenous internal control, *GAPDH*. HAC DNA content in the differentiated cells types was then normalised against undifferentiated HUES-2 40.2 cells. Error bars represent standard error of the mean.

For comparative purposes, the HAC DNA content of HUES-2 40.2 pre differentiation was normalised to a value of 1.00±0.09, and the EB, neuronal and teratoma-derived cells had a HAC-specific DNA content of 0.53±0.06, 0.66±0.02 and 1.05±0.06, respectively. Based on the Real-Time qPCR results, the HAC DNA contents of EB and neuronal-differentiated cells were statistically lower than the undifferentiated parental, while this was not the case for the teratoma-derived cells (p_{EB}=0.001, $p_{Neuronal}$=0.010, $p_{Teratoma}$=0.968; one-way ANOVA; see Table 7-2). However, as Real-Time qPCR does not distinguish between independent versus integrated HAC DNA content, the HAC DNA content in the teratoma-derived cells represents a combination of both integrated and non-integrated HAC DNA.

Table 7-2 Statistical comparisons of the HAC DNA content of undifferentiated and differentiated HUES-2 40.2 cells

	EB	Neuronal	Teratoma
Parental	p=0.001	p=0.010	p=0.968
EB		p=0.441	p<0.001
Neuronal			p=0.004

One-way ANOVA was used to calculate statistical significance.

7.11 Real-Time qPCR Quantification of Gene Expression Post-Differentiation

For HAC gene expression studies, extracted RNA from undifferentiated and various differentiated HUES-2 40.2 cell types (EB, neuronal and teratoma-derived) was initially DNase treated, and converted to cDNA. Real-Time qPCR analysis using primers for *GFP* and *Neo* was performed and normalised against an internal housekeeping control, *GAPDH*. Figure 7-20 shows relative HAC gene expression, *GFP* and *Neo*, compared to the undifferentiated parental HUES-2 40.2 cells. There was a statistically significant reduction in *GFP* expression (under regulation of the HSV-1 I/E promoter) in differentiated cell types compared to the undifferentiated parental (all $p<0.001$; one-way ANOVA; see Table 7-3). On the contrary, there was a statistically significant increase in *Neo* expression (under regulation of the SV40 promoter) in differentiated cell types compared to the undifferentiated parental (all $p<0.01$; one-way ANOVA; see Table 7-3). The results indicated that differences in gene expression were promoter-specific and may be due to chromatin remodeling and silencing processes that take place during differentiation (Muller and Leutz 2001; de la Serna et al. 2006; Macarthur et al. 2011).

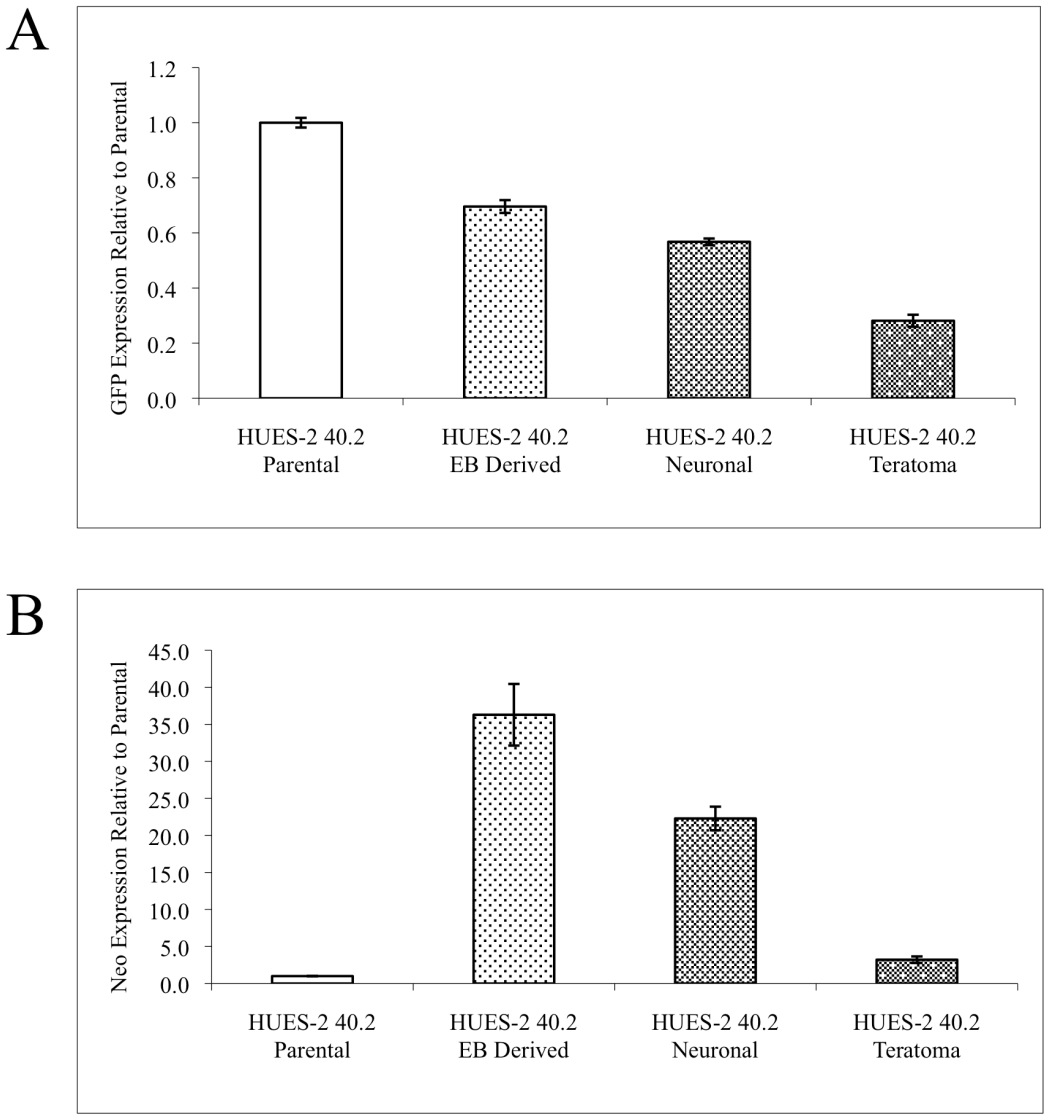

Figure 7-20 HAC gene expression of HUES-2 40.2 and differentiated cells
Data based on 3 replications per group. Gene expression of various derivative differentiated cells types relative to the undifferentiated HUES-2 40.2 parental. Primers for *GFP* (A) and *Neo* (B) were used to normalise gene expression using an internal housekeeping control *GAPDH*, relative to the undifferentiated parental population. Error bars represent standard error of the mean.

Table 7-3 Statistical comparisons of the relative *GFP* and *Neo* expression of undifferentiated and differentiated HUES-2 40.2 cells

Gene		EB	Neuronal	Teratoma
GFP	**Parental**	p<0.001	p<0.001	p<0.001
	EB		p=0.008	p<0.001
	Neuronal			p<0.001
Neo	**Parental**	p<0.001	p=0.001	p=0.008
	EB		p=0.009	p<0.001
	Neuronal			p=0.001

One-way ANOVA was used to calculate statistical significance.

7.12 Summary

In this chapter the pluripotent nature of stable HAC-containing HUES-2 cells was analysed using indirect-immunostaining and RT-PCR detection of well-known hESc markers. Once detection of pluripotent markers was confirmed in these clones, embryoid bodies (EBs) were formed to test the differentiation potential of these hESc lines. Qualitative morphological analysis of EB-derived cells revealed the presence of various cell types (fibroblast-like, epithelial-like, astrocyte-like and neuronal-like), and RT-PCR analysis confirmed the presence of the three embryonic germ layers (endoderm, mesoderm and ectoderm). Neuronal differentiation and *in vivo* teratoma formation were induced in the HUES-2 40.2 clone. High neuronal differentiation efficiency and teratoma formation in SCID mice strongly confirmed the pluripotent nature of this HAC-containing clone, suggesting that HSV-1 amplicon transduction, presence and expression of the HAC did not result in loss of pluripotency. FISH and Real-Time qPCR analyses suggested *in vitro* and *in vivo* differentiation events had led to HAC instability in the various differentiated cell types. Furthermore, Real-Time qPCR analysis revealed cell-type specific differences in gene expression following differentiation: *GFP* expression was reduced, while *Neo* expression was increased relative to the undifferentiated HUES-2 40.2 parental cells.

Chapter 8. Discussion

Human artificial chromosomes (HAC) have been constructed using either the "top-down" (engineered chromosomes) or "bottom-up" (*de novo* artificial chromosome) approach. HAC offer a number of theoretical advantages over conventional gene delivery vectors: they do not integrate into the host genome and can encompass large genomic regions for the delivery of multiple genes, under the regulation of endogenous promoters (Harrington et al. 1997; Saffery and Choo 2002; Basu and Willard 2005; Moralli et al. 2006; Ren et al. 2006; Hoshiya et al. 2009). Indeed, various groups have demonstrated successful stable gene expression under the regulation of endogenous promoters in various HAC studies. In HT1080 cells, sustained transgene expression and complementation of various genetic deficiencies has been achieved using *de novo* HAC vectors containing ~140kb of the hypoxanthine phosphoribosyltransferase (*HPRT*) genomic locus (Grimes et al. 2001; Mejía et al. 2001; Kotzamanis et al. 2005), ~180kb of genomic DNA carrying the guanosine triphosphate cyclohydrolase 1 (*GCH1*) (Ikeno et al. 2002), ~150kb of the human globin cluster (Suzuki et al. 2006b) and the *HPRT* minigene (Moralli et al. 2006). Using a top-down engineered chromosome, derived from human chromosome 21, successful Erythropoietin (*EPO*) expression has been achieved in primary fibroblasts (Kakeda et al. 2005), immortalised mesenchymal stem cells (Ren et al. 2005) and haematopoietic cells (Yamada et al. 2006). In more recent studies by the same group, expression of the human *p53* tumour suppressor gene has been reported in wild-type mESc and mouse germ stem cells (Kazuki et al. 2008). In addition, dystrophin expression has been achieved in mESc, human immortalised mesenchymal stem cells

(Hoshiya et al. 2009), mouse iPSc and patient-specific fibroblasts (Kazuki et al. 2010).

Despite the advantages HAC offer, in human studies, their use has been limited to human immortalised cell lines, predominantly due to the challenges with introducing large vectors into cells. Using lipofection, successful *de novo* HAC generation, from input vector DNA, has been obtained mainly in the tumour-derived mesenchymal human fibrosarcoma HT1080 cell line (Harrington et al. 1997; Mejía et al. 2001; Mejía et al. 2002). Use of microcell mediated chromosome transfer (MMCT) has enabled HAC delivery to human immortalised mesenchymal stem cells (Ren et al. 2005; Hoshiya et al. 2009; Kurosaki et al. 2011) and patient-specific human fibroblasts, which were subsequently reprogrammed into a pluripotent state (Kazuki et al. 2010). However, to date, *de novo* HAC generation in human primary cell lines, specifically in pluripotent cells such as hESc and iPSc, has been unsuccessful due to low delivery efficiency of large vectors and difficulties in stable clone selection (Ludwig et al. 2006; Yates and Daley 2006; Ardehali et al. 2011; Moore et al. 2011).

To overcome the difficulties of delivering large vectors into cells, our group took advantage of the ability of the HSV-1 amplicons to deliver large DNA constructs at high frequencies into cells. This approach proved successful at *de novo* HAC formation in a range of different human cell types (G16-9, 293, BeFA, MRC-5V2 and MRC5) (Moralli et al. 2006). As the delivery of HAC vectors using transfection and MMCT into pluripotent cells is extremely inefficient, and has been unattainable to date (Kazuki et al. 2010), the HSV-1 amplicon system was used in this study to deliver HAC vectors into hESc at high efficiencies. The purpose of this study was to

develop an efficient, non-integrating gene-expressing system in pluripotent hESc using HSV-HAC vectors, with the aim of genetically manipulating hESc for expression studies and ultimately translating this technology toward patient-specific *ex vivo* gene therapy applications. The utilisation of the HSV-HAC system enabled, for the first time, the establishment of mitotically stable, gene-expressing HAC in hESc.

8.1 Drug Selection Conditions for hESc

One of the major challenges of the project was determining the appropriate conditions for selection, isolation and expansion of stable hESc clones without loss of pluripotency. As hESc grow in tightly packed colonies and favour high-cell density growth conditions (Thomson et al. 1998), their stable clone isolation has proven to be difficult (Yates and Daley 2006; Ardehali et al. 2011; Moore et al. 2011). Recent studies have shown that increasing cell mobility (through inhibition of Rho-associated kinase) leads to an increase in isolation of false positive colonies. Conversely, enhancing clonogenicity (through upregulation of E-cadherin) leads to improvement of stable clone selection (Li et al. 2010b).

Indeed, the results presented in this thesis are in accordance with such findings. As previously described, hESc growing at low densities on Matrigel were highly mobile and actively sought neighbouring cells to further establish cell-to-cell contact. As a result, stable clone selection on Matrigel proved to be difficult and after repeated attempts, only false positive colonies were recovered. Instead, hESc growing on a feeder layer tended be less motile, and thus aggregated into highly packed colonies. Thus, use of *Neo*^{R} MEFi as a feeder layer provided extra cellular support for single

human embryonic stem cells under selection. With more robust cell types, selection is usually maintained throughout the duration of clonal expansion; however, due to the sensitive nature of hESc to selection-induced stress, selection was performed using relatively low concentrations of G418 and maintained for only a short period. Therefore, using this strategy enabled the recovery of a number of putative stable clones, out of which approximately half were shown to be PCR positive.

8.2 Preparation of High Quality Chromosome Spreads from hESc

Generating high quality chromosome spreads was of vital importance for the analysis of *de novo* HAC in hESc. Standard methods used for human cultured cells did not yield sufficient quantities of high quality spreads suitable for FISH analysis (Catalina et al. 2008). Improvement of both the quantity and quality of hESc metaphase spreads was achieved through replacing Colcemid with nocodazole, extending the incubation period and using the buffered hypotonic solution (Genial Genetics). These modifications resulted in a significant increase in the number of cells arrested in metaphase and a significant reduction in the number of chromosomal overlaps in the metaphases obtained. Improvements to the quality and quantity of chromosome spreads were not only instrumental in drastically improving the detection of a small-sized HAC signal, but also, ensured that no HAC-specific signal went undetected, confirming the presence of no genomic integration events in any of the analysed hESc clones.

Increasing the incubation period with a mitotic arresting agent seemed an obvious choice in improving the quantity of the metaphase spreads. However, extended incubation periods in Colcemid was not as effective at improving the percentage of

metaphase spreads when compared to nocodazole. In addition, chromosome lengths were shortened during extended exposure to Colcemid (Moralli et al. 2011). The difference between the potency of Colcemid and nocodazole may be attributed to their different modes of action on arresting the cell cycle. Another determining factor in the percentage of acquired metaphase spreads could be due to differential cell toxicity of these compounds (Parry et al. 2002).

The high metabolic rate of rapidly dividing hESc resulted in the hESc media (mTeSR) to become acidic (pH ~6.5-6.8 vs. cytoplasmic pH ~7.2-7.4) after an overnight incubation period. Residual presence of acidic media during the hypotonic treatment and chromosome fixation may have lead to poorly spread metaphases observed when unbuffered hypotonic solution was used. As changes in the pH of a solution may alter protein structures, a reduction in the pH of the hypotonic solution may have resulted in a clustering effect of chromosomes, preventing their separation during the hypotonic treatment. Thus, the reduction in the number of chromosomal overlaps was probably achieved as the buffered hypotonic solution maintained its pH at 7.4 using HEPES.

8.3 HSV-1 Amplicon Transduction versus Transfection

Based on the limited data-set presented in this study, transduction efficiencies of HSV-1 amplicons appeared to be higher than transfection in both HT1080 and HUES-2 cells. In general, the higher the multiplicity of infection (MOI), the higher the HSV-1 transduction efficiency, and spinoculation improved the transduction efficiency at lower MOIs, prior to approaching the maximal transduction threshold. The transfection efficiency of the delivered vectors was generally lower than that of

HSV-1 transduction, especially for the larger vectors (>55kb). Additionally, HSV-1 amplicon transduction was more efficient at producing stable clones in HT1080 cells, when compared to transfection. However, additional experiments using different sized vectors with more replications would be necessary to provide further support for these hypotheses.

As previously described, due to low delivery efficiency of large vectors and low cloning efficiency, stable clone selection of hESc has proved to be difficult; as such, *de novo* HAC formation in pluripotent cells has been unattainable to date (Kazuki et al. 2010). Based on the hypothesis that HSV-1 amplicons were more efficient at large DNA delivery into cells and produced more stable clones, HSV-1 amplicon transduction was used to deliver HAC vectors into hESc. The HSV-1 amplicon system allowed for improved transduction efficiencies in the order of ~100 times that of transfection for the delivery of large DNA vectors in hESc. As a result, the HSV-1 amplicons were preferentially used to deliver large HAC vectors into hESc and were successful at generating a number of stable clones. However, using transfection, the recovery of stable hESc clones proved unsuccessful, and only pools of cells were recovered. HSV-1 amplicon transduction of hESc did not impose an adverse effect on their viability or growth rate. In addition, there were no qualitative signs showing that the morphology of the transduced hESc differed from that of the non-transduced cells. These results were significant as they suggested that HSV-1 amplicon transduction was not only an ideal system for delivery of large DNA vectors into hESc at high efficiencies, but also, HSV-1 amplicons did not cause any observable adverse effects on the growth rate and morphology of pluripotent hESc.

8.4 *De novo* HAC Formation

Using HSV-1 amplicon transduction, the three newly constructed HAC vectors (pHSV17α40Neo, pHSV17α60Neo and pHSV17α100Neo) were capable of HAC formation in HT1080 cells, present in ~5-30% of the metaphases. In addition to the presence of HAC, integration events were observed in all stable HT1080 clones ranging from ~10-35%, even in clones where HAC were not present. Most significantly, the described vectors were capable of HAC formation in pluripotent hESc. Stable HUES-2 clones contained HAC in ~10-70% of the analysed metaphases. Another important finding in this study was the lack of integration events in the stable HUES-2 clones. The absence of integration events in hESc may be due to the nature of pluripotent cells where DNA replication and cell division checkpoint pathways maintain genomic integrity (Shiloh 2003), and thus prevent large DNA integrations into the genome (Deng and Xu 2009). This finding suggested that the formation of an episomal element from the delivered vector would have been favoured over integration events when introducing large DNA elements into hESc. Based on this hypothesis, it is possible that small sized HAC, which failed to show DAPI staining, may have gone undetected by FISH analysis; thus, resulting in an underestimation of the HAC frequency in the analysed stable clones.

The HAC formation results in both HT1080 and HUES-2 cells indicated that the composition of 17α satellite DNA array of hBAC495J24 vector was efficient at HAC formation at reasonable frequencies. These results solidified the notion that 17α satellite DNA was an ideal candidate for construction of HAC vectors (Grimes et al. 2002; Mejía et al. 2002). Some studies have estimated the minimal amount of alpha

satellite DNA length necessary for successful centromere formation and function to range from ~60-80kb (Lo et al. 1999; Yang et al. 2000). Others have reported that reducing the length of input 17α satellite DNA from ~80 to 35kb decreased HAC formation efficiency (Grimes et al. 2002). In contrast, Okamoto et al. (2007) reported successful HAC formation using as little as 30kb of alphoid DNA, which showed comparable stability to HAC with longer alphoid satellite sequences. The findings presented in this thesis are in accordance with the latter study, suggesting that *de novo* HAC formation can be achieved using vectors containing as little as ~40 to 100kb of 17α satellite DNA in both immortalised HT1080 and pluripotent hESc.

The pHSV17α40Neo vector (containing ~40kb 17α satellite DNA) appeared to have the highest HAC formation efficiency, amongst the other studied vectors, in both HT1080 and HUES-2 cells. Furthermore, pHSV17α40Neo (~55kb) was not only the most efficient vector at HAC formation, but also, potentially the most useful in accommodating multiple genes of interest with their regulatory elements (up to ~95kb) for HSV-1 amplicon mediated delivery into pluripotent cells for both scientific and clinical purposes.

8.5 HAC Stability and Gene Expression

Two of the HAC-containing HUES-2 clones (HUES-2 40.2 and HUES-2 40.3, with ~70% and ~30% HAC frequency, respectively) were shown to stably retain their HAC during a 90-day period in the absence of selection, without integration into the host genome. In addition, CENP-C analysis, indicated the presence of an active centromere on the *de novo* HAC, highlighting that the established HAC were behaving similarly to endogenous chromosomes.

Fibre-FISH analysis of the HUES-2 40.2 cells showed that the HAC was composed of an alternating pattern of 17α satellite and vector DNA sequences. This pattern suggested that the HAC consisted of concatemeric repeat units from the input HAC vector. Similar to other established HAC in HT1080 cells (Mejía et al. 2001; Grimes et al. 2002), HAC in HUES-2 cells showed a similar pattern of concatemerisation, thus suggesting that comparable HAC establishment processes take place in pluripotent cells. Concatemerisation results in the presence of multiple copies of the transgene on the HAC, which may increase the overall expression levels by allowing the genes of interest to escape possible heterochromatinisation events due to proximity to the centromere. However, concatemerisation could also lead to truncation of the genes of interest, potentially resulting in unwanted features such as reduced expression levels.

The percentage of *GFP*-expressing HUES-2 40.2 cells remained stable over the 90-day passaging period, as demonstrated by FACS analysis (~85%). However, Real-Time qPCR results suggested that the *GFP* and *Neo* mRNA levels steadily increased over this period. While *GFP* mRNA levels in both the presence and absence of selection increased at a similar rate, *Neo* mRNA levels increased at a greater rate in the presence of selection pressure. Although the fraction of *GFP*-expressing cells in the HUES-2 40.3 clone was very low (~5%), comparable patterns of increased *GFP* and *Neo* mRNA levels were observed during this period. Similar to HUES-2 40.2, *GFP* mRNA levels increased at a similar rate both in the presence and absence of selection, while *Neo* mRNA levels increased at a greater rate in the presence of selection.

The rise of *GFP* and *Neo* mRNA levels in the absence of selection pressure over this 90-day period could be attributed to the amplification of HAC concatemers throughout this time frame. However, no visible difference in the HAC size was detected over this 90-day period. Furthermore, in the presence of selection, only *Neo* mRNA levels increased at a greater rate compared to when selection was absent. This result suggested that the continuous presence of low concentrations of G418, enabled the selection of cells containing HAC with a more active SV40 promoter, driving *Neo* expression. A more active promoter state may have been achieved through the presence of an open chromatin state (Kim et al. 2009b; Sims and Reinberg 2009), as also suggested by some preliminary results from our laboratory (unpublished data), or low levels of CpG methylation (Chen et al. 2008; Bergbauer et al. 2010). Alternatively, the SV40 promoter may have been subjected to epigenetic remodelling events, possibly in the form of chromatin and DNA methylation in the presence of selection pressure (Sollars et al. 2003).

8.6 Implications of Karyotypic Abnormalities for HAC Formation

Many studies have reported that long-term culturing and passaging of hESc leads to the development of chromosomal abnormalities, such as trisomies of chromosomes 12, 17 and X (Draper et al. 2004; Baker et al. 2007; Spits et al. 2008). Karyotypic analyses of the HAC-containing HUES-2 40.2 and HUES-2 40.3 cells showed that both clones were trisomic for either chromosome 12 or 17, while approximately 70% of the analysed metaphases contained both trisomies. These abnormalities were also present in the HUES-2 parental cell line at the point of transduction (passage ~40), but not at passage ~30. Detailed analysis using M-FISH on the HUES-2 parental cell

line at passage ~40 further revealed the presence of an extra partial chromosome 1 that was translocated onto chromosome 18. These results indicated that partial trisomies of chromosomes 1, 12 and 17 had developed as a result of long-term culturing under feeder-free conditions prior to HSV-1 amplicon transduction and HAC formation. Abnormalities such as trisomies of chromosomes 12 and 17, which provide cells with a net growth advantage (either through promoting self-renewal or suppressing apoptosis) over karyotypically normal cells, spread rapidly in a population (Draper et al. 2004). As this case demonstrated, trisomies of chromosomes 12 and 17 were undetectable, or possibly absent, at passage ~30, while both trisomies were present in ~70% of the population at passage ~40. This finding indicated that such chromosomal abnormalities provided cells with a significant growth advantage, thus enabling their rapid population spread in as little as 10 passages.

In this case, the machinery responsible for safeguarding genomic integrity (such as tumour suppression signal transduction pathways) must have been compromised prior to the development of the described chromosomal abnormalities (Shiloh 2003). In addition, hESc harbouring extra chromosomes 12 and 17 are known to be more prolific and resistant to apoptosis (Draper et al. 2004). Altogether, these conditions may have supported *de novo* HAC formation and its retention in a chromosomally compromised hESc line. Recent studies carried out by our group have confirmed the feasibility of HAC formation and expression in a karyotypically normal pluripotent hESc line. However, the reported efficiencies of HAC formation appeared to be lower than the karyotypically abnormal HUES-2 line. These findings indicated that HAC formation was not only exclusive to chromosomally abnormal cell lines but can also be achieved in a karyotypically normal pluripotent hESc line (Mandegar et al. 2011).

8.7 Retention of Pluripotency

Ensuring the retention of pluripotency in stable hESc clones was essential in realising the efficacy of introducing HAC vectors via HSV-1 amplicons into pluripotent hESc. Indirect-immunostaining and RT-PCR analysis using pluripotency markers suggested the pluripotent nature of the HAC-containing clones was retained after prolonged periods of culturing. Derivation of multiple *in vitro* cell types and the three embryonic germ layers was successfully achieved through embryoid body formation followed by an extended differentiation period. In addition, successful *in vitro* neuronal differentiation and *in vivo* teratoma formation assays conclusively demonstrated the pluripotent nature of the HAC-containing HUES-2 clones. Taken together, the various pluripotency assays indicated that prolonged presence and expression of HAC did not compromise the pluripotent nature of the HAC-containing hESc clones.

The presence of chromosomal abnormalities in pluripotent cells is thought to reduce their differentiation capacity. This phenomenon is thought to be because many of the developed karyotypic abnormalities promote self-renewal and thus "lock" karyotypically abnormal cells in a stem cell state, diminishing their differentiation potential. For example, chromosome 12 harbours the *Nanog* gene, which is involved in maintaining self-renewal and a stem cell state (Draper et al. 2004). Thus, the presence of an extra chromosome 12 can result in a reduction of the differentiation potential of the cells carrying it. Indeed, a comparable example to hESc is the tumour-derived embryonal carcinoma cells that share many characteristics with hESc, however are chromosomally abnormal and have a limited differentiation potential (Andrews et al. 2005). However, based on the various differentiation assays

performed on the HUES-2 parental and HUES-2 40.2 cells, there were no indications that their differentiation capacity was impaired due to the presence of chromosomal abnormalities.

8.8 HAC Stability Post-Differentiation

FISH analysis on EB-derived and neuronal-differentiated HUES-2 40.2 cells suggested that HAC were still present after differentiation as compared to the undifferentiated parental cells (~70% HAC). EB-derived and neuronal-differentiated cells contained HAC in ~60% and ~45% of the analysed nuclei, respectively. However, as FISH analysis on EB-derived and neuronal-differentiated cells was only performed on interphase nuclei, the assay would not have been able to discriminate between non-integrated and integrated DNA content. FISH analysis on the *in vitro* teratoma-derived cells showed the presence of HAC in ~20% of the metaphases, in addition to ~30% integration events. This finding suggested loss of HAC stability due to teratoma formation. The karyotype of the teratoma-derived cells exhibited a high increase in chromosome instability, with cells having up to 8 copies of chromosome 12 present. This suggested that after injection of the HUES-2 40.2 cell population into mice, *in vivo* conditions have selected for cells exhibiting extra chromosomal abnormalities. Indeed, other groups have also reported extra chromosomal abnormalities in the teratoma-derived cells (Yu et al. 1995; Andrews et al. 2005). Furthermore, artificial chromosome loss has been reported in teratoma-derived cells from HAC-containing mouse germ cells (Kazuki et al. 2008) and human iPSc (Kazuki et al. 2010). Therefore, global chromosomal abnormalities in teratoma-derived cells may have been the leading cause of HAC instability and integration events during the

teratoma formation process, as it is known that HAC are rapidly lost in cells exhibiting high levels of genomic instability (Moralli et al. 2006).

Compared to FISH studies, Real-Time qPCR analysis revealed a slightly different picture of the HAC content of the undifferentiated and differentiated HUES-2 40.2 cell population: the EB-derived cells and neuronal-differentiated cells had lost ~45% and ~35% of their HAC DNA content, respectively. However, the teratoma-derived cells had similar HAC DNA content relative to the starting population. As Real-Time qPCR does not distinguish between independent and integrated HAC DNA, the measured content using this method represents a combination of both integrated and non-integrated DNA content. Furthermore, as HAC detection on EB-derived and neuronal-differentiated cells was performed using 2D FISH on interphase nuclei, it is possible that the position of the HAC in the nucleus may have compromised its detection, thus leading to an underestimation of HAC frequencies. Another reason for the discrepancy observed between the FISH and Real-Time qPCR results could be due to a discriminatory cell loss when the differentiated cells were transferred onto slides for FISH analysis. Indeed we observed significant neuronal loss when cells were being passaged onto slides for FISH analysis. On the other hand, Real-Time qPCR analyses a representative sample from the entire population. However, one limitation of Real-Time qPCR analysis is its dependency on requiring comparisons of DNA content to a reference gene; any change in the copy number of the reference gene would compromise the analysis.

Together, FISH and Real-Time qPCR results on HUES-2 40.2 cells indicated that although the HAC was stable for up to 90-days in culture, differentiation events have

led to some level of HAC instability in the various differentiated cell types. It is hypothesised that HSV-HAC vectors are packaged into HSV-1 amplicons as a linear structure, and upon infection tend to re-circularise. However, if the HAC vector fails to re-circularise in pluripotent hESc, due to high telomerase expression, the linear HAC should still remain stable in the absence of telomeric sequences (Moralli et al. 2006). However, after induction of differentiation, telomerase expression would be downregulated and thus may be a contributing factor in the observed HAC instability. In addition, chemically-induced *in vitro* differentiation may have led to the down regulation of pathways safeguarding hESc genomic integrity (Deng and Xu 2009), thus leading to HAC instability post-differentiation. Furthermore, recent findings by our group have suggested that established HAC in a chromosomally normal hESc line showed more stability following neuronal differentiation (unpublished data). Thus, it is possible that established HAC in a karyotypically-compromised pluripotent line may be prone to instability upon induction of *in vitro* differentiation. Such findings might shed light on reasons driving HAC instability in the differentiated cell types. As such, studies using HAC vectors with and without telomeric sequences would be necessary in karyotypically normal hESc to elucidate factors driving differentiation-induced HAC instability.

8.9 Gene Expression Post-Differentiation

Real-Time qPCR gene expression analysis from HUES-2 40.2 cells and the differentiated cell types confirmed the presence of gene expression post-differentiation. However, depending on the cell type and transgene promoter, the levels of gene expression were variable. *GFP* (under regulation of the HSV-1 I/E promoter) expression in EB, neuronal and teratoma-derived cells was statistically

lower, in comparison to the undifferentiated HUES-2 40.2 cell population. However, *Neo* (under regulation of the SV40 promoter) expression in EB, neuronal and teratoma-derived cells showed a statistically significant increase compared to the starting HUES-2 40.2 cells. Quantification of *GFP* and *Neo* mRNA levels in hESc revealed that they were expressed ~30× and ~1000× less than the mRNA levels of the *GAPDH* housekeeping gene, respectively. As both *GFP* and *Neo* are under the regulation of viral promoters (HSV-1 I/E and SV40 respectively), down regulation and silencing of viral-driven transgenes by hESc is probably the main driving factor resulting in their low expression levels. Indeed, studies have suggested low transgene expression levels in hESc under the regulation of viral promoters, including SV40, when compared to mammalian promoters such as hEF1α, CHEF1α, R26 and UbC (Ma et al. 2003; Liu et al. 2004b; Xiong et al. 2005; Liew et al. 2007; Chan et al. 2008; Macarthur et al. 2011). Thus, differences in gene expression pre and post-differentiation are most likely promoter-specific and may be attributed to silencing and epigenetic processes, such as CpG methylation and heterochromatinisation through histone modifications, that occur during cell differentiation (Sollars et al. 2003; Cho et al. 2004; Riu et al. 2007; Macarthur et al. 2011).

As the percentage of the HAC-containing and *GFP*-expressing HUES-2 40.2 cells was approximately 70% and 85% respectively, it is important to acknowledge the limitations of Real-Time qPCR analysis. The Real-Time qPCR data is an average representation of the entire population, where a fraction of the cells does not contain HAC and subsequently does not express the genes of interest. Furthermore, heterogeneous *GFP* and *Neo* expression is possible from the HAC-containing cells, where some cells express these genes at high levels, while other cells express them at

lower levels. However, taken together, the expression results suggested that the HSV-HAC vector was a potentially promising gene expression system in both pluripotent hESc and derivative differentiated cell types. However, in future studies, it would be necessary to include the genes of interest under the regulation of ubiquitous mammalian (e.g hEF1α, R26) (Liew et al. 2007; Chan et al. 2008) or tissue-specific (e.g CK6, hAAT) (Bertoni et al. 2006; Keravala et al. 2011) promoters to investigate whether long-term transgene expression can be achieved in the desired cell types.

8.10 Future Directions: Basic Research

As previous reports have studied HAC composition in immortalised human cells (Harrington et al. 1997; Mejía et al. 2001; Ren et al. 2005; Moralli et al. 2006; Hoshiya et al. 2009), it is necessary to characterise the structure of HAC, their mitotic stability, gene expression and epigenetic composition in karyotypically normal pluripotent and multipotent human lines such as hESc, iPSc and adult stem cells. Furthermore, targeted mutations in specific sequences involved in centromere formation (such as CENP-B boxes) or centromere specific proteins (such as CENP-A) can elucidate the processes involved in successful HAC formation in stem cells.

To obtain reliable disease-specific hESc models, which are capable of recapitulating disease pathophysiology in the desired cell types, a system must be implemented that enables stable expression of the gene of interest in various differentiated cell types (Irion et al. 2007). As the HSV-HAC in hESc is non-integrating and capable of gene expression after differentiation, this technology could serve as a suitable system for the creation of disease-specific hESc models. For example, overexpression of a particular gene, such as the Swedish-type β-amyloid precursor protein (*β-APP*) for the

study of Alzheimer's disease, can be achieved using the HSV-HAC system (Haass et al. 1995; Li et al. 2010a). However, as some loss of reporter expression was observed in various differentiated cell types, strategies can be implemented to prevent loss of transgene expression by incorporating the gene of interest in a region that resists gene silencing (Macarthur et al. 2011). A good candidate region is the *ROSA26* locus which is well-known to escape silencing and is thus ubiquitously expressed in various mouse (Zambrowicz et al. 1997; Soriano 1999; Hohenstein et al. 2008) and human (Irion et al. 2007) cell types. The *hROSA26* locus can be cloned onto the HAC vector, then the transgene of interest can be targeted into the first intron of the *hROSA26* on the HAC construct. Using this strategy, the HAC-*hROSA26* can be used as a non-integrating, transgene delivery construct, which resists gene silencing for applications in both basic and clinical research. Additionally, by flanking the gene of interest and its regulatory elements between genetic insulator sequences such as chicken hypersensitive site-4 (cHS4) (Chen et al. 2008) or gamma satellite DNA arrays (Kim et al. 2009b), silencing of the transgene of interest may be prevented through maintenance of an open chromatin state and prevention of heterochromatinisation.

To elucidate factors necessary to drive various differentiation pathways, hESc can be genetically modified using the HSV-HAC system where different reporter genes are placed under the regulation of lineage-specific promoters for lineage tracing and cell-fate determination (Livesey and Cepko 2001; Stern and Fraser 2001; Dontu et al. 2004). By using a high-throughput screening method (Stegmaier et al. 2004; Bushway and Mercola 2006), a combination of transcription factors and small molecules can be tested to identify factors that are necessary for cell lineage commitment as identified by the expression of a reporter gene driven by a lineage-specific promoter.

The derivation of integration-free iPSc, devoid of retroviral transgene integrations, from fibroblast (Takahashi et al. 2007; Yu et al. 2009; Okita et al. 2011) or other cell types (Ye et al. 2009; Jia et al. 2010) can also be achieved using the HSV-HAC system, as it is capable of delivering multiple transcription factors at high efficiencies into target cells, without integrating into the host genome. The same system can be implemented to deliver the necessary transcription factors for transdifferentiation of fibroblasts directly into neuronal (Vierbuchen et al. 2010; Kim et al. 2011) or cardiomyocyte progenitors (Efe et al. 2011) without the requirement of an intermediate iPSc derivation step. HSV-1 mediated RNAi silencing can be used for loss of function studies in various cell types (Saydam et al. 2005), and the induction of directed differentiation in hESc (Ma et al. 2010). In addition, recent findings in our laboratory have demonstrated potential for using a double HSV-1 amplicon transduction strategy in HT1080 cells. Using this strategy, the HSV-HAC mediated delivery capacity can theoretically be doubled where one amplicon subtype delivers alphoid DNA sequences, while the other delivers the transgene of interest. Preliminary double infection experiments have shown co-localisation of independently delivered DNA vectors as a single episomal element in stable HT1080 clones, albeit at low frequencies (Chan 2011). Further studies would be necessary to investigate whether such findings would be applicable to human stem and pluripotent cells.

8.11 Future Directions: Potential Clinical Applications

As this study is the first to report the establishment of HSV-1 delivered HAC into pluripotent hESc, the HAC have not yet been studied extensively and are not well defined. To date, this system has only been studied in two pluripotent hESc lines:

HUES-2 and HUES-10 (Mandegar et al. 2011). In addition, the efficacy of the HSV-HAC vector has not yet been demonstrated in the mouse model (Chan 2011). Thus, the HAC expression system in pluripotent cells is still in the research and development phase and far from the clinic. However, measures can be taken to advance this system to meet good manufacturing practice (GMP) standards and potentially closer to a clinical setting. At first, it is essential to demonstrate the feasibility and success of the HSV-HAC gene delivery approach in animal models prior to advancing to human studies. As the focus of this thesis has been on human pluripotent cells, potential clinical applications of the HSV-HAC system will be described below, in the context of human studies.

To ensure the safety and efficacy of HAC for clinical purposes, further rigorous HAC studies would need to be conducted on additional pluripotent hESc, patient-specific iPSc, and multipotent adult stem cells. Characterisation of the long-term mitotic stability and gene expression profile of HAC in various stem cell lines is important to fulfill the necessary requirements for GMP guidelines (Hewitt et al. 2007). To this end, it would be essential to implement high-throughput mechanisms for both passaging and subsequent screening of any deriving stable clones. The efficiencies of stable clone formation and HAC generation would need to be measured and optimised to satisfy GMP guidelines if this system is to be used in the clinic for the purposes of gene and cell therapy. Furthermore, as indicated by some preliminary evidence in this study, the established HAC in hESc might have been smaller than the current resolution of FISH techniques. Therefore, refinements to current FISH methods, such as utilisation of fluorophores developed from quantum dot technology (Ioannou et al. 2009), might improve the sensitivity and detection resolution of small HAC signals.

Alternatively, the development of indirect detection assays, such as the splinkerette-PCR based method (Uren et al. 2009) or strategies based on deep sequencing (Hager 2009) could enable a high-throughput screening method for the identification and elimination of any clones containing possible integration events.

The success of a gene therapy system is dependent on its safety, efficiency of transgene delivery and duration of expression at physiological amounts (Basu and Willard 2005; Kazuki et al. 2008; Hoshiya et al. 2009; Kazuki et al. 2010). As HAC can accommodate the therapeutic gene of interest under a tissue-specific promoter in the targeted stem cells, gene expression can be achieved at physiologically relevant levels post-differentiation as demonstrated by recent HAC studies expressing the dystrophin gene in mice (Hoshiya et al. 2009; Kazuki et al. 2010). Thus, the HSV-HAC system developed in pluripotent hESc can be potentially implemented for use in a patient-specific *ex vivo* gene therapy based approach. For example, while retroviral vectors need to resort to independent delivery of the heavy and light chain of Factor VIII cDNA (9kb) in clinical studies aimed at the treatment of haemophilia A (Murphy and High 2008), the HSV-HAC system can deliver Factor VIII accompanied by liver-specific promoters (e.g. hAAT) (Keravala et al. 2011) into either patient-specific iPSc or adult liver stem cells. Modified cells expressing the required levels of Factor VIII can be expanded *ex vivo*, differentiated into specific functional Factor VIII secreting liver cells and administered into patients for treatment.

8.11.1 HAC-based Gene Therapy for the Treatment of DMD

Due to the size of the dystrophin gene (2.4Mb total size; 14kb of cDNA), the treatment of Duchenne muscular dystrophy (DMD) using HAC-based gene therapies

has been discussed as the delivery of the entire dystrophin locus into cells is unattainable unless delivered as part of a HAC vector (Wang et al. 2000; Murakami et al. 2003; Ren et al. 2006; Kazuki et al. 2010). As previously described, using MMCT-delivered DYS-HAC, Kazuki et al. (2010) demonstrated successful genetic complementation of the dystrophin gene in mouse iPSc derived from the *mdx* dystrophic mouse model and human fibroblasts derived from a DMD patient, which were subsequently reprogrammed into a pluripotent state. Tissue-specific expression of human dystrophin was observed and the presence of HAC did not interfere with differentiation processes. However, as the efficiency of MMCT is extremely low, the transfer of the DYS-HAC into pluripotent hESc and hiPSc was unsuccessful (Kazuki et al. 2010). Thus, utilisation of MMCT-delivered HAC may not be the most efficient and practical method for gene therapy purposes. Furthermore, rearrangement events can occur in the MMCT-delivered HAC, which has raised safety concerns for clinical applications (Marschall et al. 1999; Kazuki et al. 2008).

Other *in vivo* studies have used physical methods of delivering dystrophin cDNA (Murakami et al. 2003; Bertoni et al. 2006) or adeno-associated viruses to deliver the mini-dystrophin gene (<4.2kb) (Wang et al. 2000) into the *mdx* dystrophic mouse model to alleviate symptoms of the disease. However, both methods suffered from low delivery efficiencies and transgene expression was short-lived. Furthermore, most commonly used viral methods have a size restriction, limiting their capacity delivery to the mini-dystrophin gene, which is ineffective for many patients who carry larger deletions in their dystrophin gene (Koppanati et al. 2010).

Alternatively, an *ex vivo* gene therapy system based on the HSV-HAC vector delivery can be implemented for the treatment of DMD. However, prior to initiating any human studies, it is essential to first test the safety and efficacy of the HSV-HAC gene delivery approach for the treatment of DMD in animal models. The *mdx* mouse model has been widely used to study gene therapy based approaches for the treatment of DMD (Wang et al. 2000; Murakami et al. 2003; Bertoni et al. 2006; Kazuki et al. 2010). However, possibly due to the small size of the animal, the *mdx* model does not recapitulate the human DMD phenotype (Collins and Morgan 2003). Instead, the golden retriever muscular dystrophy canine model (Howell et al. 1997), and more recently the *mdx*/mTR mouse model (an *mdx* mouse lacking the RNA component of telomerase) (Sacco et al. 2011) have been proposed for use in animal gene therapy trials, as they closely resemble the human DMD phenotype. Below, some of the difficulties of implementing a combination of a cell and gene therapy approach will be further discussed in describing potential strategies for the treatment of DMD in human trails (Kuang et al. 2008; Park 2010).

The HSV-HAC vector carrying the dystrophin cDNA, under the regulation of a muscle-specific promoter (e.g. CK6), can be used to genetically modify either patient-specific iPSc or satellite cells (muscle stem cells) *ex vivo*. The silencing of the dystrophin gene (either due to the presence of bacterial backbone DNA or heterochromatinisation of nearby sequences to the alpha satellite DNA) may be prevented by flanking the therapeutic gene and its regulatory elements between genetic insulator sequences such as cHS4 (Chen et al. 2008), *hROSA26* locus (Irion et al. 2007) or gamma satellite DNA arrays (Kim et al. 2009b). Next, genetically modified patient-specific iPSc or satellite cells can then be screened for quality

assurance, assessed for their differentiation potential, expanded *ex vivo* and differentiated into functional myogenic progenitors and skeletal muscle cells (Kuang and Rudnicki 2008). Finally, these cells can be administered directly into the desired sites (Skuk and Tremblay 2003) or through blood circulation (Peault et al. 2007) to provide a functional, genetically corrected autologous cell source (Kuang et al. 2008; Park 2010).

The differentiation of patient-specific iPSc or satellite cells toward functional myogenic cell types consists of a two-step process: the identification of small molecules (Borowiak et al. 2009) or transcription factors (e.g *Pax3* and *Pax7*) (Peault et al. 2007; Park 2010) required for efficient induction of differentiation toward a myogenic fate, and identification of cell surface markers for isolation and characterisation of functional myogenic cell types. Examples of myogenic precursor cells and their corresponding cell surface markers include: side-population cells ($CD34^+$) (Asakura et al. 2002), muscle-derived stem cells (Alessandri et al. 2004), bone marrow derived stem cells (Dezawa et al. 2005), mesoangioblasts ($NG2^+$) (Sampaolesi et al. 2006), pericytes ($CD146^+$, $PDGFR\beta^+$) (Dellavalle et al. 2007), $CD133^+$ stem cells (Benchaouir et al. 2007) and myoendothelial cells ($CD34^+$, $CD114^+$) (Kuang and Rudnicki 2008).

Utilisation of a combined gene and patient-specific cell therapy strategy for the treatment of DMD, would not only require the development of high-capacity, efficacious, safe and GMP-certified gene therapy vectors, but also, high-throughput differentiation and sorting assays to isolate the desired myogenic cell types. Furthermore, sufficient quantities of genetically corrected patient-specific functional

cell types would be required for administration to restore skeletal muscle function in the degenerated sites. Finally, identification of effective cellular administration methods for proper homing, engraftment and survival of the cells into the desired sites would be necessary to ultimately achieve long-term functional restoration of the genetic deficiency in DMD patients (Kuang et al. 2008; Park 2010). However, as the HSV-HAC vector system and patient-specific skeletal muscle-based cell therapies are both in their preliminary research and development stages, it will be several years before any real clinical benefits would be seen from a combination of these technologies.

8.12 Conclusions

The clonogenic, self-renewal and pluripotent nature of hESc, in conjunction with the notion that HAC can carry large genomic loci, has made HAC vector delivery into hESc a candidate system for studying an *ex vivo* gene delivery approach. However, due to low cloning and delivery efficiencies of large DNA vectors into human cells, utilisation of such a system in pluripotent cells has been unattainable thus far. In this thesis, for the first time, input HAC vectors were transduced into hESc using HSV-1 amplicons at high efficiencies. HAC were generated in hESc and showed high mitotic stability for an extended period, in the absence of selection. No integrated HAC DNA was detected in the host genome and reporter genes were also stably expressed from the HAC. Following differentiation of HAC-containing hESc, gene-expressing HAC were present at reasonable frequencies, thus demonstrating the potential use of HAC in pluripotent cells for developing experimental gene therapy systems. These findings constitute a proof of principle study that hold potential for delivering high-capacity genomic constructs safely and efficiently into pluripotent cells using HSV-1

amplicons for the purpose of genetic manipulation, and ultimately experimental and patient-specific clinical gene therapy.

Chapter 9. References

Abranches, E., M. Silva, L. Pradier, H. Schulz, O. Hummel, D. Henrique, and E. Bekman. 2009. Neural differentiation of embryonic stem cells in vitro: a road map to neurogenesis in the embryo. PLoS One 4:e6286.

Acsadi, G., D. O'Hagan, H. Lochmuller, S. Prescott, N. Larochelle, J. Nalbantoglu, A. Jani, and G. Karpati. 1998. Interferons impair early transgene expression by adenovirus-mediated gene transfer in muscle cells. J Mol Med (Berl) 76:442-450.

Aiuti, A., and M. G. Roncarolo. 2009. Ten years of gene therapy for primary immune deficiencies. Hematology Am Soc Hematol Educ Program:682-689.

Alessandri, G., S. Pagano, A. Bez, A. Benetti, S. Pozzi, G. Iannolo, M. Baronio, G. Invernici, A. Caruso, C. Muneretto, G. Bisleri, and E. Parati. 2004. Isolation and culture of human muscle-derived stem cells able to differentiate into myogenic and neurogenic cell lineages. Lancet 364:1872-1883.

Allegrucci, C., and L. E. Young. 2007. Differences between human embryonic stem cell lines. Hum Reprod Update 13:103-120.

Allsopp, R. C., E. Chang, M. Kashefi-Aazam, E. I. Rogaev, M. A. Piatyszek, J. W. Shay, and C. B. Harley. 1995. Telomere shortening is associated with cell division in vitro and in vivo. Exp Cell Res 220:194-200.

Amit, M., J. Chebath, V. Margulets, I. Laevsky, Y. Miropolsky, K. Shariki, M. Peri, I. Blais, G. Slutsky, M. Revel, and J. Itskovitz-Eldor. 2010. Suspension culture of undifferentiated human embryonic and induced pluripotent stem cells. Stem Cell Rev 6:248-259.

Amor, D. J., K. Bentley, J. Ryan, J. Perry, L. Wong, H. Slater, and K. H. Choo. 2004. Human centromere repositioning "in progress". Proc Natl Acad Sci U S A 101:6542-6547.

Amor, D. J., and K. H. Choo. 2002. Neocentromeres: role in human disease, evolution, and centromere study. Am J Hum Genet 71:695-714.

Anak, S., E. T. Saribeyoglu, H. Bilgen, A. Unuvar, Z. Karakas, O. Devecioglu, L. Agaoglu, and G. Gedikoglu. 2005. Allogeneic versus autologous versus peripheral stem cell transplantation in CR1 pediatric AML patients: a single center experience. Pediatr Blood Cancer 44:654-659.

Anderson, D., T. Self, I. R. Mellor, G. Goh, S. J. Hill, and C. Denning. 2007. Transgenic enrichment of cardiomyocytes from human embryonic stem cells. Mol Ther 15:2027-2036.

Andrews, P. W., M. M. Matin, A. R. Bahrami, I. Damjanov, P. Gokhale, and J. S. Draper. 2005. Embryonic stem (ES) cells and embryonal carcinoma (EC) cells: opposite sides of the same coin. Biochem Soc Trans 33:1526-1530.

Ardehali, R., M. A. Inlay, S. R. Ali, C. Tang, M. Drukker, and I. L. Weissman. 2011. Overexpression of BCL2 enhances survival of human embryonic stem cells during stress and obviates the requirement for serum factors. Proc Natl Acad Sci U S A 108:3282-3287.

Argyros, O., S. P. Wong, and R. P. Harbottle. 2011. Non-viral episomal modification of cells using S/MAR elements. Expert Opin Biol Ther 11:1177-1191.

Argyros, O., S. P. Wong, M. Niceta, S. N. Waddington, S. J. Howe, C. Coutelle, A. D. Miller, and R. P. Harbottle. 2008. Persistent episomal transgene expression

in liver following delivery of a scaffold/matrix attachment region containing non-viral vector. Gene Ther 15:1593-1605.

Arvidson, K., B. M. Abdallah, L. A. Applegate, N. Baldini, E. Cenni, E. Gomez-Barrena, D. Granchi, M. Kassem, Y. T. Konttinen, K. Mustafa, D. P. Pioletti, T. Sillat, and A. Finne-Wistrand. 2011. Bone regeneration and stem cells. J Cell Mol Med 15:718-746.

Asakura, A., P. Seale, A. Girgis-Gabardo, and M. A. Rudnicki. 2002. Myogenic specification of side population cells in skeletal muscle. J Cell Biol 159:123-134.

Assmus, B., J. Honold, V. Schachinger, M. B. Britten, U. Fischer-Rasokat, R. Lehmann, C. Teupe, K. Pistorius, H. Martin, N. D. Abolmaali, T. Tonn, S. Dimmeler, and A. M. Zeiher. 2006. Transcoronary transplantation of progenitor cells after myocardial infarction. N Engl J Med 355:1222-1232.

Auriche, C., D. Carpani, M. Conese, E. Caci, O. Zegarra-Moran, P. Donini, and F. Ascenzioni. 2002. Functional human CFTR produced by a stable minichromosome. EMBO Rep 3:862-868.

Auriche, C., E. G. Di Domenico, S. Pierandrei, M. Lucarelli, S. Castellani, M. Conese, R. Melani, O. Zegarra-Moran, and F. Ascenzioni. 2010. CFTR expression and activity from the human CFTR locus in BAC vectors, with regulatory regions, isolated by a single-step procedure. Gene Ther 17:1341-1354.

Bach, F. H., R. J. Albertini, P. Joo, J. L. Anderson, and M. M. Bortin. 1968. Bone-marrow transplantation in a patient with the Wiskott-Aldrich syndrome. Lancet 2:1364-1366.

Baird, D. M., and C. J. Farr. 2006. The organization and function of chromosomes. EMBO Rep 7:372-376.

Baker, D. E., N. J. Harrison, E. Maltby, K. Smith, H. D. Moore, P. J. Shaw, P. R. Heath, H. Holden, and P. W. Andrews. 2007. Adaptation to culture of human embryonic stem cells and oncogenesis in vivo. Nat Biotechnol 25:207-215.

Barker, J. L., and J. F. McKelvy. 1983. Current Methods in Cellular Neurobiology, Vol. I, Anatomical Techniques. Wiley, New York Volume 4.

Barnett, M. A., V. J. Buckle, E. P. Evans, A. C. Porter, D. Rout, A. G. Smith, and W. R. Brown. 1993. Telomere directed fragmentation of mammalian chromosomes. Nucleic Acids Res 21:27-36.

Barry, A. E., E. V. Howman, M. R. Cancilla, R. Saffery, and K. H. Choo. 1999. Sequence analysis of an 80 kb human neocentromere. Hum Mol Genet 8:217-227.

Basu, J., G. Stromberg, G. Compitello, H. F. Willard, and G. Van Bokkelen. 2005. Rapid creation of BAC-based human artificial chromosome vectors by transposition with synthetic alpha-satellite arrays. Nucleic Acids Res 33:587-596.

Basu, J., and H. F. Willard. 2005. Artificial and engineered chromosomes: non-integrating vectors for gene therapy. Trends Mol Med 11:251-258.

Basu, J., and H. F. Willard. 2006. Human artificial chromosomes: potential applications and clinical considerations. Pediatr Clin North Am 53:843-853, viii.

Belmont, A. S. 2002. Mitotic chromosome scaffold structure: new approaches to an old controversy. Proc Natl Acad Sci U S A 99:15855-15857.

Benchaouir, R., M. Meregalli, A. Farini, G. D'Antona, M. Belicchi, A. Goyenvalle, M. Battistelli, N. Bresolin, R. Bottinelli, L. Garcia, and Y. Torrente. 2007.

Restoration of human dystrophin following transplantation of exon-skipping-engineered DMD patient stem cells into dystrophic mice. Cell Stem Cell 1:646-657.

Bendich, A. J., and K. Drlica. 2000. Prokaryotic and eukaryotic chromosomes: what's the difference? Bioessays 22:481-486.

Bergbauer, M., M. Kalla, A. Schmeinck, C. Gobel, U. Rothbauer, S. Eck, A. Benet-Pages, T. M. Strom, and W. Hammerschmidt. 2010. CpG-methylation regulates a class of Epstein-Barr virus promoters. PLoS Pathog 6.

Bertoni, C., S. Jarrahian, T. M. Wheeler, Y. Li, E. C. Olivares, M. P. Calos, and T. A. Rando. 2006. Enhancement of plasmid-mediated gene therapy for muscular dystrophy by directed plasmid integration. Proc Natl Acad Sci U S A 103:419-424.

Bjorklund, L. M., R. Sanchez-Pernaute, S. Chung, T. Andersson, I. Y. Chen, K. S. McNaught, A. L. Brownell, B. G. Jenkins, C. Wahlestedt, K. S. Kim, and O. Isacson. 2002. Embryonic stem cells develop into functional dopaminergic neurons after transplantation in a Parkinson rat model. Proc Natl Acad Sci U S A 99:2344-2349.

Blaese, R. M., K. W. Culver, A. D. Miller, C. S. Carter, T. Fleisher, M. Clerici, G. Shearer, L. Chang, Y. Chiang, P. Tolstoshev, J. J. Greenblatt, S. A. Rosenberg, H. Klein, M. Berger, C. A. Mullen, W. J. Ramsey, L. Muul, R. A. Morgan, and W. F. Anderson. 1995. T lymphocyte-directed gene therapy for ADA- SCID: initial trial results after 4 years. Science 270:475-480.

Blelloch, R., Z. Wang, A. Meissner, S. Pollard, A. Smith, and R. Jaenisch. 2006. Reprogramming efficiency following somatic cell nuclear transfer is influenced by the differentiation and methylation state of the donor nucleus. Stem Cells 24:2007-2013.

Blow, J. J., P. J. Gillespie, D. Francis, and D. A. Jackson. 2001. Replication origins in Xenopus egg extract Are 5-15 kilobases apart and are activated in clusters that fire at different times. J Cell Biol 152:15-25.

Blower, M. D., B. A. Sullivan, and G. H. Karpen. 2002. Conserved organization of centromeric chromatin in flies and humans. Dev Cell 2:319-330.

Bock, C., E. Kiskinis, G. Verstappen, H. Gu, G. Boulting, Z. D. Smith, M. Ziller, G. F. Croft, M. W. Amoroso, D. H. Oakley, A. Gnirke, K. Eggan, and A. Meissner. 2011. Reference Maps of human ES and iPS cell variation enable high-throughput characterization of pluripotent cell lines. Cell 144:439-452.

Boddingius, J., H. Dijkman, W. van der Meijden, P. Schmitz, T. van Joost, and E. Stolz. 1987. Replication characteristics and core size of intranuclear herpes simplex virus (HSV-1) in genital skin lesions: electronmicroscopy studies of a biopsy from a female patient. J Med Microbiol 24:93-103.

Bode, J., C. Benham, A. Knopp, and C. Mielke. 2000. Transcriptional augmentation: modulation of gene expression by scaffold/matrix-attached regions (S/MAR elements). Crit Rev Eukaryot Gene Expr 10:73-90.

Borowiak, M., R. Maehr, S. Chen, A. E. Chen, W. Tang, J. L. Fox, S. L. Schreiber, and D. A. Melton. 2009. Small molecules efficiently direct endodermal differentiation of mouse and human embryonic stem cells. Cell Stem Cell 4:348-358.

Boyer, L. A., T. I. Lee, M. F. Cole, S. E. Johnstone, S. S. Levine, J. P. Zucker, M. G. Guenther, R. M. Kumar, H. L. Murray, R. G. Jenner, D. K. Gifford, D. A. Melton, R. Jaenisch, and R. A. Young. 2005. Core transcriptional regulatory circuitry in human embryonic stem cells. Cell 122:947-956.

Braam, S. R., C. Denning, E. Matsa, L. E. Young, R. Passier, and C. L. Mummery. 2008a. Feeder-free culture of human embryonic stem cells in conditioned medium for efficient genetic modification. Nat Protoc 3:1435-1443.

Braam, S. R., C. Denning, S. van den Brink, P. Kats, R. Hochstenbach, R. Passier, and C. L. Mummery. 2008b. Improved genetic manipulation of human embryonic stem cells. Nat Methods 5:389-392.

Brokhman, I., O. Pomp, L. Fishman, T. Tennenbaum, M. Amit, J. Itzkovitz-Eldor, and R. S. Goldstein. 2009. Genetic modification of human embryonic stem cells with adenoviral vectors: differences of infectability between lines and correlation of infectability with expression of the coxsackie and adenovirus receptor. Stem Cells Dev 18:447-456.

Brunetti-Pierri, N., T. C. Nichols, S. McCorquodale, E. Merricks, D. J. Palmer, A. L. Beaudet, and P. Ng. 2005. Sustained phenotypic correction of canine hemophilia B after systemic administration of helper-dependent adenoviral vector. Hum Gene Ther 16:811-820.

Buckley, R. H. 2004. A historical review of bone marrow transplantation for immunodeficiencies. J Allergy Clin Immunol 113:793-800.

Burge, S., G. N. Parkinson, P. Hazel, A. K. Todd, and S. Neidle. 2006. Quadruplex DNA: sequence, topology and structure. Nucleic Acids Res 34:5402-5415.

Burton, E. A., J. C. Glorioso, and D. J. Fink. 2003. Gene therapy progress and prospects: Parkinson's disease. Gene Ther 10:1721-1727.

Bushway, P. J., and M. Mercola. 2006. High-throughput screening for modulators of stem cell differentiation. Methods Enzymol 414:300-316.

Bzymek, M., and S. T. Lovett. 2001. Instability of repetitive DNA sequences: the role of replication in multiple mechanisms. Proc Natl Acad Sci U S A 98:8319-8325.

Campbell, M. S., and G. J. Gorbsky. 1995. Microinjection of mitotic cells with the 3F3/2 anti-phosphoepitope antibody delays the onset of anaphase. J Cell Biol 129:1195-1204.

Caplan, A. I. 2005. Review: mesenchymal stem cells: cell-based reconstructive therapy in orthopedics. Tissue Eng 11:1198-1211.

Carpenter, M. K., J. Frey-Vasconcells, and M. S. Rao. 2009. Developing safe therapies from human pluripotent stem cells. Nat Biotechnol 27:606-613.

Carroll, C. W., and A. F. Straight. 2006. Centromere formation: from epigenetics to self-assembly. Trends Cell Biol 16:70-78.

Catalina, P., R. Montes, G. Ligero, L. Sanchez, T. de la Cueva, C. Bueno, P. E. Leone, and P. Menendez. 2008. Human ESCs predisposition to karyotypic instability: Is a matter of culture adaptation or differential vulnerability among hESC lines due to inherent properties? Mol Cancer 7:76.

Caulfield, T., C. Scott, I. Hyun, R. Lovell-Badge, K. Kato, and A. Zarzeczny. 2010. Stem cell research policy and iPS cells. Nat Methods 7:28-33.

Cerni, C. 2000. Telomeres, telomerase, and myc. An update. Mutat Res 462:31-47.

Chan, D. Y. L. 2011. Development of novel artificial chromosomes in murine cultured and embryonic stem cells. DPhil Thesis. University of Oxford.

Chan, G. K., S. T. Liu, and T. J. Yen. 2005. Kinetochore structure and function. Trends Cell Biol 15:589-598.

Chan, K. K., S. M. Wu, P. M. Nissom, S. K. Oh, and A. B. Choo. 2008. Generation of high-level stable transgene expressing human embryonic stem cell lines using Chinese hamster elongation factor-1 alpha promoter system. Stem Cells Dev 17:825-836.

Chen, H. F., H. C. Kuo, C. L. Chien, C. T. Shun, Y. L. Yao, P. L. Ip, C. Y. Chuang, C. C. Wang, Y. S. Yang, and H. N. Ho. 2007. Derivation, characterization and differentiation of human embryonic stem cells: comparing serum-containing versus serum-free media and evidence of germ cell differentiation. Hum Reprod 22:567-577.

Chen, S. L., W. W. Fang, F. Ye, Y. H. Liu, J. Qian, S. J. Shan, J. J. Zhang, R. Z. Chunhua, L. M. Liao, S. Lin, and J. P. Sun. 2004a. Effect on left ventricular function of intracoronary transplantation of autologous bone marrow mesenchymal stem cell in patients with acute myocardial infarction. Am J Cardiol 94:92-95.

Chen, Z. Y., C. Y. He, A. Ehrhardt, and M. A. Kay. 2003. Minicircle DNA vectors devoid of bacterial DNA result in persistent and high-level transgene expression in vivo. Mol Ther 8:495-500.

Chen, Z. Y., C. Y. He, L. Meuse, and M. A. Kay. 2004b. Silencing of episomal transgene expression by plasmid bacterial DNA elements in vivo. Gene Ther 11:856-864.

Chen, Z. Y., E. Riu, C. Y. He, H. Xu, and M. A. Kay. 2008. Silencing of episomal transgene expression in liver by plasmid bacterial backbone DNA is independent of CpG methylation. Mol Ther 16:548-556.

Cheng, L., H. Hammond, Z. Ye, X. Zhan, and G. Dravid. 2003. Human adult marrow cells support prolonged expansion of human embryonic stem cells in culture. Stem Cells 21:131-142.

Cho, K. S., L. I. Elizondo, and C. F. Boerkoel. 2004. Advances in chromatin remodeling and human disease. Curr Opin Genet Dev 14:308-315.

Clarke, L., and J. Carbon. 1980. Isolation of the centromere-linked CDC10 gene by complementation in yeast. Proc Natl Acad Sci U S A 77:2173-2177.

Cleveland, D. W., Y. Mao, and K. F. Sullivan. 2003. Centromeres and kinetochores: from epigenetics to mitotic checkpoint signaling. Cell 112:407-421.

Collins, C. A., and J. E. Morgan. 2003. Duchenne's muscular dystrophy: animal models used to investigate pathogenesis and develop therapeutic strategies. Int J Exp Pathol 84:165-172.

Cooke, C. A., R. L. Bernat, and W. C. Earnshaw. 1990. CENP-B: a major human centromere protein located beneath the kinetochore. J Cell Biol 110:1475-1488.

Cooper, S., G. Iyer, M. Tarquini, and P. Bissett. 2006. Nocodazole does not synchronize cells: implications for cell-cycle control and whole-culture synchronization. Cell Tissue Res 324:237-242.

Costa, M., M. Dottori, K. Sourris, P. Jamshidi, T. Hatzistavrou, R. Davis, L. Azzola, S. Jackson, S. M. Lim, M. Pera, A. G. Elefanty, and E. G. Stanley. 2007. A method for genetic modification of human embryonic stem cells using electroporation. Nat Protoc 2:792-796.

Costantini, L. C., D. R. Jacoby, S. Wang, C. Fraefel, X. O. Breakefield, and O. Isacson. 1999. Gene transfer to the nigrostriatal system by hybrid herpes simplex virus/adeno-associated virus amplicon vectors. Hum Gene Ther 10:2481-2494.

Cowan, C. A., I. Klimanskaya, J. McMahon, J. Atienza, J. Witmyer, J. P. Zucker, S. Wang, C. C. Morton, A. P. McMahon, D. Powers, and D. A. Melton. 2004. Derivation of embryonic stem-cell lines from human blastocysts. N Engl J Med 350:1353-1356.

Crook, J. M., T. T. Peura, L. Kravets, A. G. Bosman, J. J. Buzzard, R. Horne, H. Hentze, N. R. Dunn, R. Zweigerdt, F. Chua, A. Upshall, and A. Colman. 2007. The Generation of Six Clinical-Grade Human Embryonic Stem Cell Lines. Cell Stem Cell 1:490-494.

Csonka, E., I. Cserpan, K. Fodor, G. Hollo, R. Katona, J. Kereso, T. Praznovszky, B. Szakal, A. Telenius, G. deJong, A. Udvardy, and G. Hadlaczky. 2000. Novel generation of human satellite DNA-based artificial chromosomes in mammalian cells. J Cell Sci 113 (Pt 18):3207-3216.

Dan, Y. Y., and G. C. Yeoh. 2008. Liver stem cells: a scientific and clinical perspective. J Gastroenterol Hepatol 23:687-698.

Dawe, R. K., and S. Henikoff. 2006. Centromeres put epigenetics in the driver's seat. Trends Biochem Sci 31:662-669.

de la Serna, I. L., Y. Ohkawa, and A. N. Imbalzano. 2006. Chromatin remodelling in mammalian differentiation: lessons from ATP-dependent remodellers. Nat Rev Genet 7:461-473.

deJong, G., A. H. Telenius, H. Telenius, C. F. Perez, J. I. Drayer, and G. Hadlaczky. 1999. Mammalian artificial chromosome pilot production facility: large-scale isolation of functional satellite DNA-based artificial chromosomes. Cytometry 35:129-133.

Dellavalle, A., M. Sampaolesi, R. Tonlorenzi, E. Tagliafico, B. Sacchetti, L. Perani, A. Innocenzi, B. G. Galvez, G. Messina, R. Morosetti, S. Li, M. Belicchi, G. Peretti, J. S. Chamberlain, W. E. Wright, Y. Torrente, S. Ferrari, P. Bianco, and G. Cossu. 2007. Pericytes of human skeletal muscle are myogenic precursors distinct from satellite cells. Nat Cell Biol 9:255-267.

Deng, W., and Y. Xu. 2009. Genome integrity: linking pluripotency and tumorgenicity. Trends Genet 25:425-427.

Denker, H. W. 2006. Potentiality of embryonic stem cells: an ethical problem even with alternative stem cell sources. J Med Ethics 32:665-671.

Depinet, T. W., J. L. Zackowski, W. C. Earnshaw, S. Kaffe, G. S. Sekhon, R. Stallard, B. A. Sullivan, G. H. Vance, D. L. Van Dyke, H. F. Willard, A. B. Zinn, and S. Schwartz. 1997. Characterization of neo-centromeres in marker chromosomes lacking detectable alpha-satellite DNA. Hum Mol Genet 6:1195-1204.

Deshmane, S. L., B. Raengsakulrach, J. F. Berson, and N. W. Fraser. 1995. The replicating intermediates of herpes simplex virus type 1 DNA are relatively short. J Neurovirol 1:165-176.

Dezawa, M., H. Ishikawa, Y. Itokazu, T. Yoshihara, M. Hoshino, S. Takeda, C. Ide, and Y. Nabeshima. 2005. Bone marrow stromal cells generate muscle cells and repair muscle degeneration. Science 309:314-317.

Dontu, G., K. W. Jackson, E. McNicholas, M. J. Kawamura, W. M. Abdallah, and M. S. Wicha. 2004. Role of Notch signaling in cell-fate determination of human mammary stem/progenitor cells. Breast Cancer Res 6:R605-615.

Draper, J. S., K. Smith, P. Gokhale, H. D. Moore, E. Maltby, J. Johnson, L. Meisner, T. P. Zwaka, J. A. Thomson, and P. W. Andrews. 2004. Recurrent gain of chromosomes 17q and 12 in cultured human embryonic stem cells. Nat Biotechnol 22:53-54.

Drexler, H., G. P. Meyer, and K. C. Wollert. 2006. Bone-marrow-derived cell transfer after ST-elevation myocardial infarction: lessons from the BOOST trial. Nat Clin Pract Cardiovasc Med 3 Suppl 1:S65-68.

Earnshaw, W. C., H. Ratrie, 3rd, and G. Stetten. 1989. Visualization of centromere proteins CENP-B and CENP-C on a stable dicentric chromosome in cytological spreads. Chromosoma 98:1-12.

Ebersole, T. A., A. Ross, E. Clark, N. McGill, D. Schindelhauer, H. Cooke, and B. Grimes. 2000. Mammalian artificial chromosome formation from circular alphoid input DNA does not require telomere repeats. Hum Mol Genet 9:1623-1631.

Edelstein, M. L., M. R. Abedi, and J. Wixon. 2007. Gene therapy clinical trials worldwide to 2007--an update. J Gene Med 9:833-842.

Edelstein, M. L., M. R. Abedi, J. Wixon, and R. M. Edelstein. 2004. Gene therapy clinical trials worldwide 1989-2004-an overview. J Gene Med 6:597-602.

Efe, J. A., S. Hilcove, J. Kim, H. Zhou, K. Ouyang, G. Wang, J. Chen, and S. Ding. 2011. Conversion of mouse fibroblasts into cardiomyocytes using a direct reprogramming strategy. Nat Cell Biol 13:215-222.

Eiges, R., M. Schuldiner, M. Drukker, O. Yanuka, J. Itskovitz-Eldor, and N. Benvenisty. 2001. Establishment of human embryonic stem cell-transfected clones carrying a marker for undifferentiated cells. Curr Biol 11:514-518.

El-Sherbini, Y. M. 2010. Genetic modification human mesenchymal stem cells using HSV-1 amplicons for therapeutic purposes. DPhil Thesis. University of Oxford.

Farr, C., J. Fantes, P. Goodfellow, and H. Cooke. 1991. Functional reintroduction of human telomeres into mammalian cells. Proc Natl Acad Sci U S A 88:7006-7010.

Farr, C. J., R. A. Bayne, D. Kipling, W. Mills, R. Critcher, and H. J. Cooke. 1995. Generation of a human X-derived minichromosome using telomere-associated chromosome fragmentation. EMBO J 14:5444-5454.

Farr, C. J., M. Stevanovic, E. J. Thomson, P. N. Goodfellow, and H. J. Cooke. 1992. Telomere-associated chromosome fragmentation: applications in genome manipulation and analysis. Nat Genet 2:275-282.

Feng, J., H. Huang, and T. J. Yen. 2006. CENP-F is a novel microtubule-binding protein that is essential for kinetochore attachments and affects the duration of the mitotic checkpoint delay. Chromosoma 115:320-329.

Fischbach, G. D., and R. L. Fischbach. 2004. Stem cells: science, policy, and ethics. J Clin Invest 114:1364-1370.

Forbes, S. J., R. Poulsom, and N. A. Wright. 2002. Hepatic and renal differentiation from blood-borne stem cells. Gene Ther 9:625-630.

Fowler, K. J., L. H. Wong, B. K. Griffiths, M. C. Sibson, S. Reed, and K. H. Choo. 2004. Centromere protein b-null mice display decreasing reproductive performance through successive generations of breeding due to diminishing endometrial glands. Reproduction 127:367-377.

Fox, J. L. 2011. Human iPSC and ESC translation potential debated. Nat Biotechnol 29:375-376.

Friedmann, T., and R. Roblin. 1972. Gene therapy for human genetic disease? Science 175:949-955.

Fukagawa, T., Y. Mikami, A. Nishihashi, V. Regnier, T. Haraguchi, Y. Hiraoka, N. Sugata, K. Todokoro, W. Brown, and T. Ikemura. 2001. CENP-H, a constitutive centromere component, is required for centromere targeting of CENP-C in vertebrate cells. Embo J 20:4603-4617.

Garber, D. A., S. M. Beverley, and D. M. Coen. 1993. Demonstration of circularization of herpes simplex virus DNA following infection using pulsed field gel electrophoresis. Virology 197:459-462.

Gassmann, R., S. L. Kline, A. Carvalho, and A. Desai. 2007. Analysis of kinetochore assembly and function in Caenorhabditis elegans embryos and human cells. Methods 41:177-189.

Geens, M., I. Mateizel, K. Sermon, M. De Rycke, C. Spits, G. Cauffman, P. Devroey, H. Tournaye, I. Liebaers, and H. Van de Velde. 2009. Human embryonic stem cell lines derived from single blastomeres of two 4-cell stage embryos. Hum Reprod 24:2709-2717.

Genbacev, O., A. Krtolica, T. Zdravkovic, E. Brunette, S. Powell, A. Nath, E. Caceres, M. McMaster, S. McDonagh, Y. Li, R. Mandalam, J. Lebkowski, and S. J. Fisher. 2005. Serum-free derivation of human embryonic stem cell lines on human placental fibroblast feeders. Fertil Steril 83:1517-1529.

Gerbi, S. A., and A. K. Bielinsky. 2002. DNA replication and chromatin. Curr Opin Genet Dev 12:243-248.

Gharwan, H., R. K. Hirata, P. Wang, R. E. Richard, L. Wang, E. Olson, J. Allen, C. B. Ware, and D. W. Russell. 2007. Transduction of human embryonic stem cells by foamy virus vectors. Mol Ther 15:1827-1833.

Gilbert, D. M. 2001. Making sense of eukaryotic DNA replication origins. Science 294:96-100.

Gill, D. R., S. E. Smyth, C. A. Goddard, I. A. Pringle, C. F. Higgins, W. H. Colledge, and S. C. Hyde. 2001. Increased persistence of lung gene expression using plasmids containing the ubiquitin C or elongation factor 1alpha promoter. Gene Ther 8:1539-1546.

Gilson, E., and V. Geli. 2007. How telomeres are replicated. Nat Rev Mol Cell Biol 8:825-838.

Gimelli, G., O. Zuffardi, S. Giglio, C. Zeng, and D. He. 2000. CENP-G in neocentromeres and inactive centromeres. Chromosoma 109:328-333.

Girdler, F., K. E. Gascoigne, P. A. Eyers, S. Hartmuth, C. Crafter, K. M. Foote, N. J. Keen, and S. S. Taylor. 2006. Validating Aurora B as an anti-cancer drug target. J Cell Sci 119:3664-3675.

Glorioso, J. C., and D. J. Fink. 2009. Herpes vector-mediated gene transfer in the treatment of chronic pain. Mol Ther 17:13-18.

Goss, J. R., M. Mata, W. F. Goins, H. H. Wu, J. C. Glorioso, and D. J. Fink. 2001. Antinociceptive effect of a genomic herpes simplex virus-based vector expressing human proenkephalin in rat dorsal root ganglion. Gene Ther 8:551-556.

Grassi, G., P. Maccaroni, R. Meyer, H. Kaiser, E. D'Ambrosio, E. Pascale, M. Grassi, A. Kuhn, P. Di Nardo, R. Kandolf, and J. H. Kupper. 2003. Inhibitors of DNA methylation and histone deacetylation activate cytomegalovirus promoter-controlled reporter gene expression in human glioblastoma cell line U87. Carcinogenesis 24:1625-1635.

Gray, S. J., J. Gerhardt, W. Doerfler, L. E. Small, and E. Fanning. 2007. An origin of DNA replication in the promoter region of the human fragile X mental retardation (FMR1) gene. Mol Cell Biol 27:426-437.

Grewal, S. I., and S. Jia. 2007. Heterochromatin revisited. Nat Rev Genet 8:35-46.

Grewal, S. I., and D. Moazed. 2003. Heterochromatin and epigenetic control of gene expression. Science 301:798-802.

Grimes, B. R., and Z. L. Monaco. 2005. Artificial and engineered chromosomes: developments and prospects for gene therapy. Chromosoma 114:230-241.

Grimes, B. R., A. A. Rhoades, and H. F. Willard. 2002. Alpha-satellite DNA and vector composition influence rates of human artificial chromosome formation. Mol Ther 5:798-805.

Grimes, B. R., D. Schindelhauer, N. I. McGill, A. Ross, T. A. Ebersole, and H. J. Cooke. 2001. Stable gene expression from a mammalian artificial chromosome. EMBO Rep 2:910-914.

Gropp, M., P. Itsykson, O. Singer, T. Ben-Hur, E. Reinhartz, E. Galun, and B. E. Reubinoff. 2003. Stable genetic modification of human embryonic stem cells by lentiviral vectors. Mol Ther 7:281-287.

Guiducci, C., F. Ascenzioni, C. Auriche, E. Piccolella, A. M. Guerrini, and P. Donini. 1999. Use of a human minichromosome as a cloning and expression vector for mammalian cells. Hum Mol Genet 8:1417-1424.

Gutierrez-Aranda, I., V. Ramos-Mejia, C. Bueno, M. Munoz-Lopez, P. J. Real, A. Macia, L. Sanchez, G. Ligero, J. L. Garcia-Parez, and P. Menendez. 2010. Human induced pluripotent stem cells develop teratoma more efficiently and faster than human embryonic stem cells regardless the site of injection. Stem Cells 28:1568-1570.

Haass, C., C. A. Lemere, A. Capell, M. Citron, P. Seubert, D. Schenk, L. Lannfelt, and D. J. Selkoe. 1995. The Swedish mutation causes early-onset Alzheimer's disease by beta-secretase cleavage within the secretory pathway. Nat Med 1:1291-1296.

Hacein-Bey-Abina, S., C. Von Kalle, M. Schmidt, M. P. McCormack, N. Wulffraat, P. Leboulch, A. Lim, C. S. Osborne, R. Pawliuk, E. Morillon, R. Sorensen, A. Forster, P. Fraser, J. I. Cohen, G. de Saint Basile, I. Alexander, U. Wintergerst, T. Frebourg, A. Aurias, D. Stoppa-Lyonnet, S. Romana, I. Radford-Weiss, F. Gross, F. Valensi, E. Delabesse, E. Macintyre, F. Sigaux, J. Soulier, L. E. Leiva, M. Wissler, C. Prinz, T. H. Rabbitts, F. Le Deist, A. Fischer, and M. Cavazzana-Calvo. 2003. LMO2-associated clonal T cell proliferation in two patients after gene therapy for SCID-X1. Science 302:415-419.

Hager, G. 2009. Footprints by deep sequencing. Nat Methods 6:254-255.

Hansson, G. K., and K. Edfeldt. 2005. Toll to be paid at the gateway to the vessel wall. Arterioscler Thromb Vasc Biol 25:1085-1087.

Harrington, J. J., G. Van Bokkelen, R. W. Mays, K. Gustashaw, and H. F. Willard. 1997. Formation of de novo centromeres and construction of first-generation human artificial microchromosomes. Nat Genet 15:345-355.

Hay, D. C., D. Zhao, J. Fletcher, Z. A. Hewitt, D. McLean, A. Urruticoechea-Uriguen, J. R. Black, C. Elcombe, J. A. Ross, R. Wolf, and W. Cui. 2008. Efficient differentiation of hepatocytes from human embryonic stem cells exhibiting markers recapitulating liver development in vivo. Stem Cells 26:894-902.

He, D., C. Zeng, K. Woods, L. Zhong, D. Turner, R. K. Busch, B. R. Brinkley, and H. Busch. 1998. CENP-G: a new centromeric protein that is associated with the alpha-1 satellite DNA subfamily. Chromosoma 107:189-197.

Heinzel, S. S., P. J. Krysan, C. T. Tran, and M. P. Calos. 1991. Autonomous DNA replication in human cells is affected by the size and the source of the DNA. Mol Cell Biol 11:2263-2272.

Heller, R., K. E. Brown, C. Burgtorf, and W. R. Brown. 1996. Mini-chromosomes derived from the human Y chromosome by telomere directed chromosome breakage. Proc Natl Acad Sci U S A 93:7125-7130.

Hemmi, H., O. Takeuchi, T. Kawai, T. Kaisho, S. Sato, H. Sanjo, M. Matsumoto, K. Hoshino, H. Wagner, K. Takeda, and S. Akira. 2000. A Toll-like receptor recognizes bacterial DNA. Nature 408:740-745.

Heng, B. C., K. J. Vinoth, H. Liu, M. P. Hande, and T. Cao. 2006. Low temperature tolerance of human embryonic stem cells. Int J Med Sci 3:124-129.

Henikoff, S., K. Ahmad, and H. S. Malik. 2001. The centromere paradox: stable inheritance with rapidly evolving DNA. Science 293:1098-1102.

Henning, K. A., E. A. Novotny, S. T. Compton, X. Y. Guan, P. P. Liu, and M. A. Ashlock. 1999. Human artificial chromosomes generated by modification of a yeast artificial chromosome containing both human alpha satellite and single-copy DNA sequences. Proc Natl Acad Sci U S A 96:592-597.

Hentze, H., R. Graichen, and A. Colman. 2007. Cell therapy and the safety of embryonic stem cell-derived grafts. Trends Biotechnol 25:24-32.

Herzog, R. W., E. Y. Yang, L. B. Couto, J. N. Hagstrom, D. Elwell, P. A. Fields, M. Burton, D. A. Bellinger, M. S. Read, K. M. Brinkhous, G. M. Podsakoff, T. C. Nichols, G. J. Kurtzman, and K. A. High. 1999. Long-term correction of canine hemophilia B by gene transfer of blood coagulation factor IX mediated by adeno-associated viral vector. Nat Med 5:56-63.

Hewitt, Z. A., K. J. Amps, and H. D. Moore. 2007. Derivation of GMP raw materials for use in regenerative medicine: hESC-based therapies, progress toward clinical application. Clin Pharmacol Ther 82:448-452.

Hibbitt, O. C., and R. Wade-Martins. 2006. Delivery of large genomic DNA inserts >100 kb using HSV-1 amplicons. Curr Gene Ther 6:325-336.

Hirota, T., D. Gerlich, B. Koch, J. Ellenberg, and J. M. Peters. 2004. Distinct functions of condensin I and II in mitotic chromosome assembly. J Cell Sci 117:6435-6445.

Hochedlinger, K., and R. Jaenisch. 2003. Nuclear transplantation, embryonic stem cells, and the potential for cell therapy. N Engl J Med 349:275-286.

Hodges, B. L., K. M. Taylor, M. F. Joseph, S. A. Bourgeois, and R. K. Scheule. 2004. Long-term transgene expression from plasmid DNA gene therapy vectors is negatively affected by CpG dinucleotides. Mol Ther 10:269-278.

Hohenstein, P., J. Slight, D. D. Ozdemir, S. F. Burn, R. Berry, and N. D. Hastie. 2008. High-efficiency Rosa26 knock-in vector construction for Cre-regulated overexpression and RNAi. Pathogenetics 1:3.

Hoki, Y., N. Kimura, M. Kanbayashi, Y. Amakawa, T. Ohhata, H. Sasaki, and T. Sado. 2009. A proximal conserved repeat in the Xist gene is essential as a genomic element for X-inactivation in mouse. Development 136:139-146.

Hollon, T. 2000. Researchers and regulators reflect on first gene therapy death. Nat Med 6:6.

Hoshiya, H., Y. Kazuki, S. Abe, M. Takiguchi, N. Kajitani, Y. Watanabe, T. Yoshino, Y. Shirayoshi, K. Higaki, G. Messina, G. Cossu, and M. Oshimura. 2009. A highly stable and nonintegrated human artificial chromosome (HAC) containing the 2.4 Mb entire human dystrophin gene. Mol Ther 17:309-317.

Howell, J. M., S. Fletcher, B. A. Kakulas, M. O'Hara, H. Lochmuller, and G. Karpati. 1997. Use of the dog model for Duchenne muscular dystrophy in gene therapy trials. Neuromuscul Disord 7:325-328.

Howman, E. V., K. J. Fowler, A. J. Newson, S. Redward, A. C. MacDonald, P. Kalitsis, and K. H. Choo. 2000. Early disruption of centromeric chromatin organization in centromere protein A (Cenpa) null mice. Proc Natl Acad Sci U S A 97:1148-1153.

Hudson, D. F., K. J. Fowler, E. Earle, R. Saffery, P. Kalitsis, H. Trowell, J. Hill, N. G. Wreford, D. M. de Kretser, M. R. Cancilla, E. Howman, L. Hii, S. M. Cutts, D. V. Irvine, and K. H. Choo. 1998. Centromere protein B null mice are mitotically and meiotically normal but have lower body and testis weights. J Cell Biol 141:309-319.

Hyde, S. C., I. A. Pringle, S. Abdullah, A. E. Lawton, L. A. Davies, A. Varathalingam, G. Nunez-Alonso, A. M. Green, R. P. Bazzani, S. G. Sumner-Jones, M. Chan, H. Li, N. S. Yew, S. H. Cheng, A. C. Boyd, J. C. Davies, U. Griesenbach, D. J. Porteous, D. N. Sheppard, F. M. Munkonge, E. W. Alton, and D. R. Gill. 2008. CpG-free plasmids confer reduced inflammation and sustained pulmonary gene expression. Nat Biotechnol 26:549-551.

Iacovitti, L., A. E. Donaldson, C. E. Marshall, S. Suon, and M. Yang. 2007. A protocol for the differentiation of human embryonic stem cells into dopaminergic neurons using only chemically defined human additives: Studies in vitro and in vivo. Brain Res 1127:19-25.

Ikeno, M., B. Grimes, T. Okazaki, M. Nakano, K. Saitoh, H. Hoshino, N. I. McGill, H. Cooke, and H. Masumoto. 1998. Construction of YAC-based mammalian artificial chromosomes. Nat Biotechnol 16:431-439.

Ikeno, M., H. Inagaki, K. Nagata, M. Morita, H. Ichinose, and T. Okazaki. 2002. Generation of human artificial chromosomes expressing naturally controlled guanosine triphosphate cyclohydrolase I gene. Genes Cells 7:1021-1032.

Ikeno, M., H. Masumoto, and T. Okazaki. 1994. Distribution of CENP-B boxes reflected in CREST centromere antigenic sites on long-range alpha-satellite DNA arrays of human chromosome 21. Hum Mol Genet 3:1245-1257.

Imber, R., R. L. Low, and D. S. Ray. 1983. Identification of a primosome assembly site in the region of the ori 2 replication origin of the Escherichia coli mini-F plasmid. Proc Natl Acad Sci U S A 80:7132-7136.

Ioannou, D., H. G. Tempest, B. M. Skinner, A. R. Thornhill, M. Ellis, and D. K. Griffin. 2009. Quantum dots as new-generation fluorochromes for FISH: an appraisal. Chromosome Res 17:519-530.

Ioannou, P. A., C. T. Amemiya, J. Garnes, P. M. Kroisel, H. Shizuya, C. Chen, M. A. Batzer, and P. J. de Jong. 1994. A new bacteriophage P1-derived vector for the propagation of large human DNA fragments. Nat Genet 6:84-89.

Irion, S., H. Luche, P. Gadue, H. J. Fehling, M. Kennedy, and G. Keller. 2007. Identification and targeting of the ROSA26 locus in human embryonic stem cells. Nat Biotechnol 25:1477-1482.

Irvine, D. V., D. J. Amor, J. Perry, N. Sirvent, F. Pedeutour, K. H. Choo, and R. Saffery. 2004. Chromosome size and origin as determinants of the level of CENP-A incorporation into human centromeres. Chromosome Res 12:805-815.

Itskovitz-Eldor, J., M. Schuldiner, D. Karsenti, A. Eden, O. Yanuka, M. Amit, H. Soreq, and N. Benvenisty. 2000. Differentiation of human embryonic stem cells into embryoid bodies compromising the three embryonic germ layers. Mol Med 6:88-95.

Itsykson, P., N. Ilouz, T. Turetsky, R. S. Goldstein, M. F. Pera, I. Fishbein, M. Segal, and B. E. Reubinoff. 2005. Derivation of neural precursors from human embryonic stem cells in the presence of noggin. Mol Cell Neurosci 30:24-36.

Itzhaki, J. E., M. A. Barnett, A. B. MacCarthy, V. J. Buckle, W. R. Brown, and A. C. Porter. 1992. Targeted breakage of a human chromosome mediated by cloned human telomeric DNA. Nat Genet 2:283-287.

Jacobs, A., X. O. Breakefield, and C. Fraefel. 1999a. HSV-1-based vectors for gene therapy of neurological diseases and brain tumors: part I. HSV-1 structure, replication and pathogenesis. Neoplasia 1:387-401.

Jacobs, A., X. O. Breakefield, and C. Fraefel. 1999b. HSV-1-based vectors for gene therapy of neurological diseases and brain tumors: part II. Vector systems and applications. Neoplasia 1:402-416.

Jain, K. K. 2005. Ethical and regulatory aspects of embryonic stem cell research. Expert Opin Biol Ther 5:153-162.

Jang, J. E., K. Shaw, X. J. Yu, D. Petersen, K. Pepper, C. Lutzko, and D. B. Kohn. 2006. Specific and stable gene transfer to human embryonic stem cells using pseudotyped lentiviral vectors. Stem Cells Dev 15:109-117.

Jia, F., K. D. Wilson, N. Sun, D. M. Gupta, M. Huang, Z. Li, N. J. Panetta, Z. Y. Chen, R. C. Robbins, M. A. Kay, M. T. Longaker, and J. C. Wu. 2010. A nonviral minicircle vector for deriving human iPS cells. Nat Methods 7:197-199.

Jordan, M. A., D. Thrower, and L. Wilson. 1992. Effects of vinblastine, podophyllotoxin and nocodazole on mitotic spindles. Implications for the role of microtubule dynamics in mitosis. J Cell Sci 102 (Pt 3):401-416.

Kakeda, M., M. Hiratsuka, K. Nagata, Y. Kuroiwa, M. Kakitani, M. Katoh, M. Oshimura, and K. Tomizuka. 2005. Human artificial chromosome (HAC) vector provides long-term therapeutic transgene expression in normal human primary fibroblasts. Gene Ther 12:852-856.

Kameda, T., K. Smuga-Otto, and J. A. Thomson. 2006. A severe de novo methylation of episomal vectors by human ES cells. Biochem Biophys Res Commun 349:1269-1277.

Kastenberg, Z. J., and J. S. Odorico. 2008. Alternative sources of pluripotency: science, ethics, and stem cells. Transplant Rev (Orlando) 22:215-222.

Katoh, M., F. Ayabe, S. Norikane, T. Okada, H. Masumoto, S. Horike, Y. Shirayoshi, and M. Oshimura. 2004. Construction of a novel human artificial chromosome vector for gene delivery. Biochem Biophys Res Commun 321:280-290.

Kay, M. A. 2011. State-of-the-art gene-based therapies: the road ahead. Nat Rev Genet 12:316-328.

Kay, M. A., C. Y. He, and Z. Y. Chen. 2010. A robust system for production of minicircle DNA vectors. Nat Biotechnol 28:1287-1289.

Kazuki, Y., M. Hiratsuka, M. Takiguchi, M. Osaki, N. Kajitani, H. Hoshiya, K. Hiramatsu, T. Yoshino, K. Kazuki, C. Ishihara, S. Takehara, K. Higaki, M. Nakagawa, K. Takahashi, S. Yamanaka, and M. Oshimura. 2010. Complete genetic correction of ips cells from Duchenne muscular dystrophy. Mol Ther 18:386-393.

Kazuki, Y., H. Hoshiya, Y. Kai, S. Abe, M. Takiguchi, M. Osaki, S. Kawazoe, M. Katoh, M. Kanatsu-Shinohara, K. Inoue, N. Kajitani, T. Yoshino, Y. Shirayoshi, A. Ogura, T. Shinohara, J. C. Barrett, and M. Oshimura. 2008. Correction of a genetic defect in multipotent germline stem cells using a human artificial chromosome. Gene Ther 15:617-624.

Keravala, A., C. L. Chavez, G. Hu, L. E. Woodard, P. E. Monahan, and M. P. Calos. 2011. Long-term phenotypic correction in factor IX knockout mice by using phiC31 integrase-mediated gene therapy. Gene Ther.

Kim, D., C. H. Kim, J. I. Moon, Y. G. Chung, M. Y. Chang, B. S. Han, S. Ko, E. Yang, K. Y. Cha, R. Lanza, and K. S. Kim. 2009a. Generation of human induced pluripotent stem cells by direct delivery of reprogramming proteins. Cell Stem Cell 4:472-476.

Kim, J., J. A. Efe, S. Zhu, M. Talantova, X. Yuan, S. Wang, S. A. Lipton, K. Zhang, and S. Ding. 2011. Direct reprogramming of mouse fibroblasts to neural progenitors. Proc Natl Acad Sci U S A 108:7838-7843.

Kim, J. H., J. M. Auerbach, J. A. Rodriguez-Gomez, I. Velasco, D. Gavin, N. Lumelsky, S. H. Lee, J. Nguyen, R. Sanchez-Pernaute, K. Bankiewicz, and R. McKay. 2002. Dopamine neurons derived from embryonic stem cells function in an animal model of Parkinson's disease. Nature 418:50-56.

Kim, J. H., T. Ebersole, N. Kouprina, V. N. Noskov, J. Ohzeki, H. Masumoto, B. Mravinac, B. A. Sullivan, A. Pavlicek, S. Dovat, S. D. Pack, Y. W. Kwon, P. T. Flanagan, D. Loukinov, V. Lobanenkov, and V. Larionov. 2009b. Human gamma-satellite DNA maintains open chromatin structure and protects a transgene from epigenetic silencing. Genome Res 19:533-544.

Kim, U. J., B. W. Birren, T. Slepak, V. Mancino, C. Boysen, H. L. Kang, M. I. Simon, and H. Shizuya. 1996. Construction and characterization of a human bacterial artificial chromosome library. Genomics 34:213-218.

Kiskinis, E., and K. Eggan. 2010. Progress toward the clinical application of patient-specific pluripotent stem cells. J Clin Invest 120:51-59.

Klimanskaya, I., Y. Chung, S. Becker, S. J. Lu, and R. Lanza. 2006. Human embryonic stem cell lines derived from single blastomeres. Nature 444:481-485.

Klose, R. J., and A. P. Bird. 2006. Genomic DNA methylation: the mark and its mediators. Trends Biochem Sci 31:89-97.

Kohn, D. B. 2010. Update on gene therapy for immunodeficiencies. Clin Immunol 135:247-254.

Kohno, S. I., C. Luo, A. Nawa, Y. Fujimoto, D. Watanabe, F. Goshima, T. Tsurumi, and Y. Nishiyama. 2007. Oncolytic virotherapy with an HSV amplicon vector expressing granulocyte-macrophage colony-stimulating factor using the replication-competent HSV type 1 mutant HF10 as a helper virus. Cancer Gene Ther 14:918-926.

Koppanati, B. M., J. Li, D. P. Reay, B. Wang, M. Daood, H. Zheng, X. Xiao, J. F. Watchko, and P. R. Clemens. 2010. Improvement of the mdx mouse dystrophic phenotype by systemic in utero AAV8 delivery of a minidystrophin gene. Gene Ther 17:1355-1362.

Korbling, M., and Z. Estrov. 2003. Adult stem cells for tissue repair - a new therapeutic concept? N Engl J Med 349:570-582.

Kornberg, R. D. 1974. Chromatin structure: a repeating unit of histones and DNA. Science 184:868-871.

Kotin, R. M., M. Siniscalco, R. J. Samulski, X. D. Zhu, L. Hunter, C. A. Laughlin, S. McLaughlin, N. Muzyczka, M. Rocchi, and K. I. Berns. 1990. Site-specific integration by adeno-associated virus. Proc Natl Acad Sci U S A 87:2211-2215.

Kotzamanis, G., W. Cheung, H. Abdulrazzak, S. Perez-Luz, S. Howe, H. Cooke, and C. Huxley. 2005. Construction of human artificial chromosome vectors by recombineering. Gene 351:29-38.

Kouprina, N., T. Ebersole, M. Koriabine, E. Pak, I. B. Rogozin, M. Katoh, M. Oshimura, K. Ogi, M. Peredelchuk, G. Solomon, W. Brown, J. C. Barrett, and V. Larionov. 2003. Cloning of human centromeres by transformation-associated recombination in yeast and generation of functional human artificial chromosomes. Nucleic Acids Res 31:922-934.

Krieg, A. M. 1996. Lymphocyte activation by CpG dinucleotide motifs in prokaryotic DNA. Trends Microbiol 4:73-76.

Krysan, P. J., J. G. Smith, and M. P. Calos. 1993. Autonomous replication in human cells of multimers of specific human and bacterial DNA sequences. Mol Cell Biol 13:2688-2696.

Kuang, S., M. A. Gillespie, and M. A. Rudnicki. 2008. Niche regulation of muscle satellite cell self-renewal and differentiation. Cell Stem Cell 2:22-31.

Kuang, S., and M. A. Rudnicki. 2008. The emerging biology of satellite cells and their therapeutic potential. Trends Mol Med 14:82-91.

Kubo, S., Y. Saeki, E. A. Chiocca, and K. Mitani. 2003. An HSV amplicon-based helper system for helper-dependent adenoviral vectors. Biochem Biophys Res Commun 307:826-830.

Kurosaki, H., M. Hiratsuka, N. Imaoka, Y. Iida, N. Uno, Y. Kazuki, C. Ishihara, Y. Yakura, J. Mimuro, Y. Sakata, H. Takeya, and M. Oshimura. 2011. Integration-free and stable expression of FVIII using a human artificial chromosome. J Hum Genet.

Lakshmipathy, U., B. Pelacho, K. Sudo, J. L. Linehan, E. Coucouvanis, D. S. Kaufman, and C. M. Verfaillie. 2004. Efficient transfection of embryonic and adult stem cells. Stem Cells 22:531-543.

Lamba, D. A., J. Gust, and T. A. Reh. 2009. Transplantation of human embryonic stem cell-derived photoreceptors restores some visual function in Crx-deficient mice. Cell Stem Cell 4:73-79.

Larin, Z., and J. E. Mejía. 2002. Advances in human artificial chromosome technology. Trends Genet 18:313-319.

Larin, Z., A. P. Monaco, and H. Lehrach. 1991. Yeast artificial chromosome libraries containing large inserts from mouse and human DNA. Proc Natl Acad Sci U S A 88:4123-4127.

Laslett, A. L., A. A. Filipczyk, and M. F. Pera. 2003. Characterization and culture of human embryonic stem cells. Trends Cardiovasc Med 13:295-301.

Lebkowski, J. S., J. Gold, C. Xu, W. Funk, C. P. Chiu, and M. K. Carpenter. 2001. Human embryonic stem cells: culture, differentiation, and genetic modification for regenerative medicine applications. Cancer J 7 Suppl 2:S83-93.

Levy, M. Z., R. C. Allsopp, A. B. Futcher, C. W. Greider, and C. B. Harley. 1992. Telomere end-replication problem and cell aging. J Mol Biol 225:951-960.

Li, H., B. Wang, Z. Wang, Q. Guo, K. Tabuchi, R. E. Hammer, T. C. Sudhof, and H. Zheng. 2010a. Soluble amyloid precursor protein (APP) regulates transthyretin and Klotho gene expression without rescuing the essential function of APP. Proc Natl Acad Sci U S A 107:17362-17367.

Li, J. Y., N. S. Christophersen, V. Hall, D. Soulet, and P. Brundin. 2008. Critical issues of clinical human embryonic stem cell therapy for brain repair. Trends Neurosci 31:146-153.

Li, L., B. H. Wang, S. Wang, L. Moalim-Nour, K. Mohib, D. Lohnes, and L. Wang. 2010b. Individual cell movement, asymmetric colony expansion, rho-associated kinase, and E-cadherin impact the clonogenicity of human embryonic stem cells. Biophys J 98:2442-2451.

Li, Z., C. S. Yang, K. Nakashima, and T. M. Rana. 2011. Small RNA-mediated regulation of iPS cell generation. EMBO J 30:823-834.

Liao, H., R. J. Winkfein, G. Mack, J. B. Rattner, and T. J. Yen. 1995. CENP-F is a protein of the nuclear matrix that assembles onto kinetochores at late G2 and is rapidly degraded after mitosis. J Cell Biol 130:507-518.

Liew, C. G., J. S. Draper, J. Walsh, H. Moore, and P. W. Andrews. 2007. Transient and stable transgene expression in human embryonic stem cells. Stem Cells 25:1521-1528.

Lin, T., R. Ambasudhan, X. Yuan, W. Li, S. Hilcove, R. Abujarour, X. Lin, H. S. Hahm, E. Hao, A. Hayek, and S. Ding. 2009. A chemical platform for improved induction of human iPSCs. Nat Methods 6:805-808.

Lipford, G. B., K. Heeg, and H. Wagner. 1998. Bacterial DNA as immune cell activator. Trends Microbiol 6:496-500.

Liu, J., D. Wolfe, S. Hao, S. Huang, J. C. Glorioso, M. Mata, and D. J. Fink. 2004a. Peripherally delivered glutamic acid decarboxylase gene therapy for spinal cord injury pain. Mol Ther 10:57-66.

Liu, Y. P., O. V. Dovzhenko, M. A. Garthwaite, S. V. Dambaeva, M. Durning, L. M. Pollastrini, and T. G. Golos. 2004b. Maintenance of pluripotency in human embryonic stem cells stably over-expressing enhanced green fluorescent protein. Stem Cells Dev 13:636-645.

Livak, K. J., and T. D. Schmittgen. 2001. Analysis of relative gene expression data using real-time quantitative PCR and the 2(-Delta Delta C(T)) Method. Methods 25:402-408.

Livesey, F. J., and C. L. Cepko. 2001. Vertebrate neural cell-fate determination: lessons from the retina. Nat Rev Neurosci 2:109-118.

Lo, A. W., J. M. Craig, R. Saffery, P. Kalitsis, D. V. Irvine, E. Earle, D. J. Magliano, and K. H. Choo. 2001a. A 330 kb CENP-A binding domain and altered replication timing at a human neocentromere. Embo J 20:2087-2096.

Lo, A. W., G. C. Liao, M. Rocchi, and K. H. Choo. 1999. Extreme reduction of chromosome-specific alpha-satellite array is unusually common in human chromosome 21. Genome Res 9:895-908.

Lo, A. W., D. J. Magliano, M. C. Sibson, P. Kalitsis, J. M. Craig, and K. H. Choo. 2001b. A novel chromatin immunoprecipitation and array (CIA) analysis identifies a 460-kb CENP-A-binding neocentromere DNA. Genome Res 11:448-457.

Logan, A. C., C. Lutzko, and D. B. Kohn. 2002. Advances in lentiviral vector design for gene-modification of hematopoietic stem cells. Curr Opin Biotechnol 13:429-436.

Loh, Y. H., S. Agarwal, I. H. Park, A. Urbach, H. Huo, G. C. Heffner, K. Kim, J. D. Miller, K. Ng, and G. Q. Daley. 2009. Generation of induced pluripotent stem cells from human blood. Blood 113:5476-5479.

Ludwig, T. E., M. E. Levenstein, J. M. Jones, W. T. Berggren, E. R. Mitchen, J. L. Frane, L. J. Crandall, C. A. Daigh, K. R. Conard, M. S. Piekarczyk, R. A. Llanas, and J. A. Thomson. 2006. Derivation of human embryonic stem cells in defined conditions. Nat Biotechnol 24:185-187.

Luger, K., A. W. Mader, R. K. Richmond, D. F. Sargent, and T. J. Richmond. 1997. Crystal structure of the nucleosome core particle at 2.8 A resolution. Nature 389:251-260.

Ma, Y., J. Jin, C. Dong, E. C. Cheng, H. Lin, Y. Huang, and C. Qiu. 2010. High-efficiency siRNA-based gene knockdown in human embryonic stem cells. RNA 16:2564-2569.

Ma, Y., A. Ramezani, R. Lewis, R. G. Hawley, and J. A. Thomson. 2003. High-level sustained transgene expression in human embryonic stem cells using lentiviral vectors. Stem Cells 21:111-117.

Macarthur, C., H. Xue, D. Van Hoof, P. T. Lieu, M. Dudas, A. Fontes, A. Swistowski, T. Touboul, R. Seerke, L. C. Laurent, J. F. Loring, M. S. German, X. Zeng, M. S. Rao, U. Lakshmipathy, J. D. Chesnut, and Y. Liu. 2011. Chromatin Insulator Elements Block Transgene Silencing in Engineered hESC Lines at a Defined Chromosome 13 Locus. Stem Cells Dev doi:10.1089/scd.2011.0163.

Mackay, A. M., A. M. Ainsztein, D. M. Eckley, and W. C. Earnshaw. 1998. A dominant mutant of inner centromere protein (INCENP), a chromosomal protein, disrupts prometaphase congression and cytokinesis. J Cell Biol 140:991-1002.

Maekawa, M., K. Yamaguchi, T. Nakamura, R. Shibukawa, I. Kodanaka, T. Ichisaka, Y. Kawamura, H. Mochizuki, N. Goshima, and S. Yamanaka. 2011. Direct reprogramming of somatic cells is promoted by maternal transcription factor Glis1. Nature 474:225-229.

Magnus, D., and M. K. Cho. 2005. Ethics. Issues in oocyte donation for stem cell research. Science 308:1747-1748.

Maguire, A. M., F. Simonelli, E. A. Pierce, E. N. Pugh, Jr., F. Mingozzi, J. Bennicelli, S. Banfi, K. A. Marshall, F. Testa, E. M. Surace, S. Rossi, A. Lyubarsky, V. R. Arruda, B. Konkle, E. Stone, J. Sun, J. Jacobs, L. Dell'Osso, R. Hertle, J. X. Ma, T. M. Redmond, X. Zhu, B. Hauck, O. Zelenaia, K. S. Shindler, M. G. Maguire, J. F. Wright, N. J. Volpe, J. W. McDonnell, A. Auricchio, K. A. High, and J. Bennett. 2008. Safety and efficacy of gene transfer for Leber's congenital amaurosis. N Engl J Med 358:2240-2248.

Maione, D., C. Della Rocca, P. Giannetti, R. D'Arrigo, L. Liberatoscioli, L. L. Franlin, V. Sandig, G. Ciliberto, N. La Monica, and R. Savino. 2001. An improved helper-dependent adenoviral vector allows persistent gene expression after intramuscular delivery and overcomes preexisting immunity to adenovirus. Proc Natl Acad Sci U S A 98:5986-5991.

Mallon, B. S., K. Y. Park, K. G. Chen, R. S. Hamilton, and R. D. McKay. 2006. Toward xeno-free culture of human embryonic stem cells. Int J Biochem Cell Biol 38:1063-1075.

Mandegar, M. A., D. Moralli, S. Khoja, S. Cowley, M. Yusuf, D. Chan, S. Mukherjee, M. Blundell, A. Thrasher, E. Volpi, W. James, and Z. Monaco. 2011. Functional human artificial chromosomes are generated and stably maintained in human embryonic stem cells. Human Molecular Genetics. doi: 10.1093/hmg/ddr144.

Mao, Y., A. Abrieu, and D. W. Cleveland. 2003. Activating and silencing the mitotic checkpoint through CENP-E-dependent activation/inactivation of BubR1. Cell 114:87-98.

Marschall, P., N. Malik, and Z. Larin. 1999. Transfer of YACs up to 2.3 Mb intact into human cells with polyethylenimine. Gene Ther 6:1634-1637.

Marshall, E. 1999. Gene therapy death prompts review of adenovirus vector. Science 286:2244-2245.
Marshall, O. J., and K. H. Choo. 2009. Neocentromeres come of age. PLoS Genet 5:e1000370.
Marshall, O. J., A. C. Chueh, L. H. Wong, and K. H. Choo. 2008a. Neocentromeres: new insights into centromere structure, disease development, and karyotype evolution. Am J Hum Genet 82:261-282.
Marshall, O. J., A. T. Marshall, and K. H. Choo. 2008b. Three-dimensional localization of CENP-A suggests a complex higher order structure of centromeric chromatin. J Cell Biol 183:1193-1202.
Martin, D. W., S. P. Deb, J. S. Klauer, and S. Deb. 1991. Analysis of the herpes simplex virus type 1 OriS sequence: mapping of functional domains. J Virol 65:4359-4369.
Masumoto, H., H. Masukata, Y. Muro, N. Nozaki, and T. Okazaki. 1989. A human centromere antigen (CENP-B) interacts with a short specific sequence in alphoid DNA, a human centromeric satellite. J Cell Biol 109:1963-1973.
Masumoto, H., M. Nakano, and J. Ohzeki. 2004. The role of CENP-B and alpha-satellite DNA: de novo assembly and epigenetic maintenance of human centromeres. Chromosome Res 12:543-556.
Matzke, M. A., M. F. Mette, W. Aufsatz, J. Jakowitsch, and A. J. Matzke. 1999. Host defenses to parasitic sequences and the evolution of epigenetic control mechanisms. Genetica 107:271-287.
Matzke, M. A., M. F. Mette, and A. J. Matzke. 2000. Transgene silencing by the host genome defense: implications for the evolution of epigenetic control mechanisms in plants and vertebrates. Plant Mol Biol 43:401-415.
McDonald, J. W., X. Z. Liu, Y. Qu, S. Liu, S. K. Mickey, D. Turetsky, D. I. Gottlieb, and D. W. Choi. 1999. Transplanted embryonic stem cells survive, differentiate and promote recovery in injured rat spinal cord. Nat Med 5:1410-1412.
McEwen, B. F., G. K. Chan, B. Zubrowski, M. S. Savoian, M. T. Sauer, and T. J. Yen. 2001. CENP-E is essential for reliable bioriented spindle attachment, but chromosome alignment can be achieved via redundant mechanisms in mammalian cells. Mol Biol Cell 12:2776-2789.
Mejía, J. E., A. Alazami, A. Willmott, P. Marschall, E. Levy, W. C. Earnshaw, and Z. Larin. 2002. Efficiency of de novo centromere formation in human artificial chromosomes. Genomics 79:297-304.
Mejía, J. E., A. Willmott, E. Levy, W. C. Earnshaw, and Z. Larin. 2001. Functional complementation of a genetic deficiency with human artificial chromosomes. Am J Hum Genet 69:315-326.
Menendez, P., L. Wang, and M. Bhatia. 2005. Genetic manipulation of human embryonic stem cells: a system to study early human development and potential therapeutic applications. Curr Gene Ther 5:375-385.
Miller, O. J., and E. Therman. 2001. Human Chromosomes (Fourth Edition). Springer-Verlag, New York.
Mills, W., R. Critcher, C. Lee, and C. J. Farr. 1999. Generation of an approximately 2.4 Mb human X centromere-based minichromosome by targeted telomere-associated chromosome fragmentation in DT40. Hum Mol Genet 8:751-761.
Mimeault, M., R. Hauke, and S. K. Batra. 2007. Stem cells: a revolution in therapeutics-recent advances in stem cell biology and their therapeutic

applications in regenerative medicine and cancer therapies. Clin Pharmacol Ther 82:252-264.
Mitsui, K., K. Suzuki, E. Aizawa, E. Kawase, H. Suemori, N. Nakatsuji, and K. Mitani. 2009. Gene targeting in human pluripotent stem cells with adeno-associated virus vectors. Biochem Biophys Res Commun 388:711-717.
Miura, K., Y. Okada, T. Aoi, A. Okada, K. Takahashi, K. Okita, M. Nakagawa, M. Koyanagi, K. Tanabe, M. Ohnuki, D. Ogawa, E. Ikeda, H. Okano, and S. Yamanaka. 2009. Variation in the safety of induced pluripotent stem cell lines. Nat Biotechnol 27:743-745.
Moore, J. C., K. Atze, P. L. Yeung, A. J. Toro-Ramos, C. Camarillo, K. Thompson, C. L. Ricupero, M. A. Brenneman, R. I. Cohen, and R. P. Hart. 2011. Efficient, high-throughput transfection of human embryonic stem cells. Stem Cell Res Ther 1:23.
Moralli, D., K. M. Simpson, R. Wade-Martins, and Z. L. Monaco. 2006. A novel human artificial chromosome gene expression system using herpes simplex virus type 1 vectors. EMBO Rep 7:911-918.
Moralli, D., M. Yusuf, M. A. Mandegar, S. Khoja, Z. L. Monaco, and E. V. Volpi. 2011. An Improved Technique for Chromosomal Analysis of Human ES and iPS Cells. Stem Cell Rev doi:10.1007/s12015-010-9224-4.
Mori, H., A. Kondo, A. Ohshima, T. Ogura, and S. Hiraga. 1986. Structure and function of the F plasmid genes essential for partitioning. J Mol Biol 192:1-15.
Mountain, A. 2000. Gene therapy: the first decade. Trends Biotechnol 18:119-128.
Moyzis, R. K., J. M. Buckingham, L. S. Cram, M. Dani, L. L. Deaven, M. D. Jones, J. Meyne, R. L. Ratliff, and J. R. Wu. 1988. A highly conserved repetitive DNA sequence, (TTAGGG)n, present at the telomeres of human chromosomes. Proc Natl Acad Sci U S A 85:6622-6626.
Muller, C., and A. Leutz. 2001. Chromatin remodeling in development and differentiation. Curr Opin Genet Dev 11:167-174.
Muller-Sieburg, C. E., R. H. Cho, M. Thoman, B. Adkins, and H. B. Sieburg. 2002. Deterministic regulation of hematopoietic stem cell self-renewal and differentiation. Blood 100:1302-1309.
Murakami, T., T. Nishi, E. Kimura, T. Goto, Y. Maeda, Y. Ushio, M. Uchino, and Y. Sunada. 2003. Full-length dystrophin cDNA transfer into skeletal muscle of adult mdx mice by electroporation. Muscle Nerve 27:237-241.
Murphy, S. L., and K. A. High. 2008. Gene therapy for haemophilia. Br J Haematol 140:479-487.
Murray, A. W., and J. W. Szostak. 1983. Construction of artificial chromosomes in yeast. Nature 305:189-193.
Musacchio, A., and E. D. Salmon. 2007. The spindle-assembly checkpoint in space and time. Nat Rev Mol Cell Biol 8:379-393.
Nagy, A., M. Gertsenstein, K. Vintersten, and R. Behringer. 2003. Manipulating the Mouse Embryo: A Laboratory Manual (Third Edition). Cold Spring Harbor Laboratory Press.
Nakagawa, M., N. Takizawa, M. Narita, T. Ichisaka, and S. Yamanaka. 2010. Promotion of direct reprogramming by transformation-deficient Myc. Proc Natl Acad Sci U S A 107:14152-14157.
Naldini, L. 2011. Ex vivo gene transfer and correction for cell-based therapies. Nat Rev Genet 12:301-315.
Nawa, A., C. Luo, L. Zhang, Y. Ushjima, D. Ishida, M. Kamakura, Y. Fujimoto, F. Goshima, F. Kikkawa, and Y. Nishiyama. 2008. Non-engineered, naturally

oncolytic herpes simplex virus HSV1 HF-10: applications for cancer gene therapy. Curr Gene Ther 8:208-221.
Neidle, S., and G. N. Parkinson. 2003. The structure of telomeric DNA. Curr Opin Struct Biol 13:275-283.
Ng, K., D. Pullirsch, M. Leeb, and A. Wutz. 2007. Xist and the order of silencing. EMBO Rep 8:34-39.
Nishihashi, A., T. Haraguchi, Y. Hiraoka, T. Ikemura, V. Regnier, H. Dodson, W. C. Earnshaw, and T. Fukagawa. 2002. CENP-I is essential for centromere function in vertebrate cells. Dev Cell 2:463-476.
Nishikawa, S., R. A. Goldstein, and C. R. Nierras. 2008. The promise of human induced pluripotent stem cells for research and therapy. Nat Rev Mol Cell Biol 9:725-729.
Norio, P. 2006. DNA replication: the unbearable lightness of origins. EMBO Rep 7:779-781.
O'Doherty, U., W. J. Swiggard, and M. H. Malim. 2000. Human immunodeficiency virus type 1 spinoculation enhances infection through virus binding. J Virol 74:10074-10080.
Oh, S. K., A. K. Chen, Y. Mok, X. Chen, U. M. Lim, A. Chin, A. B. Choo, and S. Reuveny. 2009. Long-term microcarrier suspension cultures of human embryonic stem cells. Stem Cell Res 2:219-230.
Ohzeki, J., M. Nakano, T. Okada, and H. Masumoto. 2002. CENP-B box is required for de novo centromere chromatin assembly on human alphoid DNA. J Cell Biol 159:765-775.
Okamoto, Y., M. Nakano, J. Ohzeki, V. Larionov, and H. Masumoto. 2007. A minimal CENP-A core is required for nucleation and maintenance of a functional human centromere. Embo J 26:1279-1291.
Okita, K., Y. Matsumura, Y. Sato, A. Okada, A. Morizane, S. Okamoto, H. Hong, M. Nakagawa, K. Tanabe, K. Tezuka, T. Shibata, T. Kunisada, M. Takahashi, J. Takahashi, H. Saji, and S. Yamanaka. 2011. A more efficient method to generate integration-free human iPS cells. Nat Methods 8:409-412.
Olschowka, J. A., W. J. Bowers, S. D. Hurley, M. A. Mastrangelo, and H. J. Federoff. 2003. Helper-free HSV-1 amplicons elicit a markedly less robust innate immune response in the CNS. Mol Ther 7:218-227.
OMIM. 2011. Online Mendelian Inheritance in Man, OMIM®. McKusick-Nathans Institute of Genetic Medicine, Johns Hopkins University (Baltimore, MD), [cited Sunday, July 31, 2011]. World Wide Web URL: http://omim.org/.
Orthaus, S., S. Ohndorf, and S. Diekmann. 2006. RNAi knockdown of human kinetochore protein CENP-H. Biochem Biophys Res Commun 348:36-46.
Oshimura, M., and M. Katoh. 2008. Transfer of human artificial chromosome vectors into stem cells. Reprod Biomed Online 16:57-69.
Otto, S. P., and T. Day. 2007. A Biologist's Guide to Mathematical Modeling in Ecology and Evolution Princeton University Press.
Palmer, D. J., and P. Ng. 2005. Helper-dependent adenoviral vectors for gene therapy. Hum Gene Ther 16:1-16.
Palmer, D. K., K. O'Day, H. L. Trong, H. Charbonneau, and R. L. Margolis. 1991. Purification of the centromere-specific protein CENP-A and demonstration that it is a distinctive histone. Proc Natl Acad Sci U S A 88:3734-3738.
Papadakis, E. D., S. A. Nicklin, A. H. Baker, and S. J. White. 2004. Promoters and control elements: designing expression cassettes for gene therapy. Curr Gene Ther 4:89-113.

Park, I. H. 2010. DYS-HAC-iPS cells: the combination of gene and cell therapy to treat duchenne muscular dystrophy. Mol Ther 18:238-240.

Parry, E. M., J. M. Parry, C. Corso, A. Doherty, F. Haddad, T. F. Hermine, G. Johnson, M. Kayani, E. Quick, T. Warr, and J. Williamson. 2002. Detection and characterization of mechanisms of action of aneugenic chemicals. Mutagenesis 17:509-521.

Parson, A. 2006. The long journey from stem cells to medical product. Cell 125:9-11.

Paterson, H., B. Reeves, R. Brown, A. Hall, M. Furth, J. Bos, P. Jones, and C. Marshall. 1987. Activated N-ras controls the transformed phenotype of HT1080 human fibrosarcoma cells. Cell 51:803-812.

Paulis, M., M. Bensi, D. Orioli, C. Mondello, G. Mazzini, M. D'Incalci, C. Falcioni, E. Radaelli, E. Erba, E. Raimondi, and L. De Carli. 2007. Transfer of a human chromosomal vector from a hamster cell line to a mouse embryonic stem cell line. Stem Cells 25:2543-2550.

Peault, B., M. Rudnicki, Y. Torrente, G. Cossu, J. P. Tremblay, T. Partridge, E. Gussoni, L. M. Kunkel, and J. Huard. 2007. Stem and progenitor cells in skeletal muscle development, maintenance, and therapy. Mol Ther 15:867-877.

Penny, G. D., G. F. Kay, S. A. Sheardown, S. Rastan, and N. Brockdorff. 1996. Requirement for Xist in X chromosome inactivation. Nature 379:131-137.

Pfeifer, A., and I. M. Verma. 2001. Gene therapy: promises and problems. Annu Rev Genomics Hum Genet 2:177-211.

Pidoux, A. L., and R. C. Allshire. 2000. Centromeres: getting a grip of chromosomes. Curr Opin Cell Biol 12:308-319.

Pierce, J. C., B. Sauer, and N. Sternberg. 1992. A positive selection vector for cloning high molecular weight DNA by the bacteriophage P1 system: improved cloning efficacy. Proc Natl Acad Sci U S A 89:2056-2060.

Pohl, C., and S. Jentsch. 2008. Final stages of cytokinesis and midbody ring formation are controlled by BRUCE. Cell 132:832-845.

Poirier, M. G., and J. F. Marko. 2002. Mitotic chromosomes are chromatin networks without a mechanically contiguous protein scaffold. Proc Natl Acad Sci U S A 99:15393-15397.

Poleshko, A., M. B. Einarson, N. Shalginskikh, R. Zhang, P. D. Adams, A. M. Skalka, and R. A. Katz. 2010. Identification of a functional network of human epigenetic silencing factors. J Biol Chem 285:422-433.

Poleshko, A., I. Palagin, R. Zhang, P. Boimel, C. Castagna, P. D. Adams, A. M. Skalka, and R. A. Katz. 2008. Identification of cellular proteins that maintain retroviral epigenetic silencing: evidence for an antiviral response. J Virol 82:2313-2323.

Politi, V., G. Perini, S. Trazzi, A. Pliss, I. Raska, W. C. Earnshaw, and G. Della Valle. 2002. CENP-C binds the alpha-satellite DNA in vivo at specific centromere domains. J Cell Sci 115:2317-2327.

Prokhorova, T. A., L. M. Harkness, U. Frandsen, N. Ditzel, H. D. Schroder, J. S. Burns, and M. Kassem. 2009. Teratoma formation by human embryonic stem cells is site dependent and enhanced by the presence of Matrigel. Stem Cells Dev 18:47-54.

Przewloka, M. R., Z. Venkei, V. M. Bolanos-Garcia, J. Debski, M. Dadlez, and D. M. Glover. 2011. CENP-C Is a Structural Platform for Kinetochore Assembly. Curr Biol 21:399-405.

Qin, L., Y. Ding, D. R. Pahud, E. Chang, M. J. Imperiale, and J. S. Bromberg. 1997. Promoter attenuation in gene therapy: interferon-gamma and tumor necrosis factor-alpha inhibit transgene expression. Hum Gene Ther 8:2019-2029.

Quesenberry, P., and L. Levitt. 1979. Hematopoietic stem cells. N Engl J Med 301:755-761.

Raikwar, S. P., T. Mueller, and N. Zavazava. 2006. Strategies for developing therapeutic application of human embryonic stem cells. Physiology (Bethesda) 21:19-28.

Rajcani, J., V. Andrea, and R. Ingeborg. 2004. Peculiarities of herpes simplex virus (HSV) transcription: an overview. Virus Genes 28:293-310.

Rasheed, S., W. A. Nelson-Rees, E. M. Toth, P. Arnstein, and M. B. Gardner. 1974. Characterization of a newly derived human sarcoma cell line (HT-1080). Cancer 33:1027-1033.

Rattner, J. B., A. Rao, M. J. Fritzler, D. W. Valencia, and T. J. Yen. 1993. CENP-F is a .ca 400 kDa kinetochore protein that exhibits a cell-cycle dependent localization. Cell Motil Cytoskeleton 26:214-226.

Reddy, P. S., K. Sakhuja, S. Ganesh, L. Yang, D. Kayda, T. Brann, S. Pattison, D. Golightly, N. Idamakanti, A. Pinkstaff, M. Kaloss, C. Barjot, J. S. Chamberlain, M. Kaleko, and S. Connelly. 2002. Sustained human factor VIII expression in hemophilia A mice following systemic delivery of a gutless adenoviral vector. Mol Ther 5:63-73.

Ren, X., M. Katoh, H. Hoshiya, A. Kurimasa, T. Inoue, F. Ayabe, K. Shibata, J. Toguchida, and M. Oshimura. 2005. A novel human artificial chromosome vector provides effective cell lineage-specific transgene expression in human mesenchymal stem cells. Stem Cells 23:1608-1616.

Ren, X., C. G. Tahimic, M. Katoh, A. Kurimasa, T. Inoue, and M. Oshimura. 2006. Human artificial chromosome vectors meet stem cells: new prospects for gene delivery. Stem Cell Rev 2:43-50.

Reubinoff, B. E., M. F. Pera, C. Y. Fong, A. Trounson, and A. Bongso. 2000. Embryonic stem cell lines from human blastocysts: somatic differentiation in vitro. Nat Biotechnol 18:399-404.

Reynolds, B. A., and S. Weiss. 1992. Generation of neurons and astrocytes from isolated cells of the adult mammalian central nervous system. Science 255:1707-1710.

Ribeiro, S. A., P. Vagnarelli, Y. Dong, T. Hori, B. F. McEwen, T. Fukagawa, C. Flors, and W. C. Earnshaw. 2010. A super-resolution map of the vertebrate kinetochore. Proc Natl Acad Sci U S A 107:10484-10489.

Richards, M., C. Y. Fong, W. K. Chan, P. C. Wong, and A. Bongso. 2002. Human feeders support prolonged undifferentiated growth of human inner cell masses and embryonic stem cells. Nat Biotechnol 20:933-936.

Rideout, W. M., 3rd, K. Hochedlinger, M. Kyba, G. Q. Daley, and R. Jaenisch. 2002. Correction of a genetic defect by nuclear transplantation and combined cell and gene therapy. Cell 109:17-27.

Riu, E., Z. Y. Chen, H. Xu, C. Y. He, and M. A. Kay. 2007. Histone modifications are associated with the persistence or silencing of vector-mediated transgene expression in vivo. Mol Ther 15:1348-1355.

Riu, E., D. Grimm, Z. Huang, and M. A. Kay. 2005. Increased maintenance and persistence of transgenes by excision of expression cassettes from plasmid sequences in vivo. Hum Gene Ther 16:558-570.

Rivero-Muller, A., S. Lajic, and I. Huhtaniemi. 2007. Assisted large fragment insertion by Red/ET-recombination (ALFIRE)--an alternative and enhanced method for large fragment recombineering. Nucleic Acids Res 35:e78.

Robinson, A. J., A. C. Meedeniya, K. M. Hemsley, D. Auclair, A. C. Crawley, and J. J. Hopwood. 2005. Survival and engraftment of mouse embryonic stem cell-derived implants in the guinea pig brain. Neurosci Res 53:161-168.

Robinson, P. J., and D. Rhodes. 2006. Structure of the '30 nm' chromatin fibre: a key role for the linker histone. Curr Opin Struct Biol 16:336-343.

Rocha, V., J. E. Wagner, Jr., K. A. Sobocinski, J. P. Klein, M. J. Zhang, M. M. Horowitz, and E. Gluckman. 2000. Graft-versus-host disease in children who have received a cord-blood or bone marrow transplant from an HLA-identical sibling. Eurocord and International Bone Marrow Transplant Registry Working Committee on Alternative Donor and Stem Cell Sources. N Engl J Med 342:1846-1854.

Rosenthal, N. 2003. Prometheus's vulture and the stem-cell promise. N Engl J Med 349:267-274.

Ross, P. J., M. A. Kennedy, C. Christou, M. Risco Quiroz, K. L. Poulin, and R. J. Parks. 2011. Assembly of helper-dependent adenovirus DNA into chromatin promotes efficient gene expression. J Virol 85:3950-3958.

Rudd, M. K., and H. F. Willard. 2004. Analysis of the centromeric regions of the human genome assembly. Trends Genet 20:529-533.

Sacco, A., F. Mourkioti, R. Tran, J. Choi, M. Llewellyn, P. Kraft, M. Shkreli, S. Delp, J. H. Pomerantz, S. E. Artandi, and H. M. Blau. 2011. Short telomeres and stem cell exhaustion model Duchenne muscular dystrophy in mdx/mTR mice. Cell 143:1059-1071.

Saeki, Y., X. O. Breakefield, and E. A. Chiocca. 2003. Improved HSV-1 amplicon packaging system using ICP27-deleted, oversized HSV-1 BAC DNA. Methods Mol Med 76:51-60.

Saeki, Y., C. Fraefel, T. Ichikawa, X. O. Breakefield, and E. A. Chiocca. 2001. Improved helper virus-free packaging system for HSV amplicon vectors using an ICP27-deleted, oversized HSV-1 DNA in a bacterial artificial chromosome. Mol Ther 3:591-601.

Saffery, R., and K. H. Choo. 2002. Strategies for engineering human chromosomes with therapeutic potential. J Gene Med 4:5-13.

Saffery, R., D. V. Irvine, B. Griffiths, P. Kalitsis, L. Wordeman, and K. H. Choo. 2000. Human centromeres and neocentromeres show identical distribution patterns of >20 functionally important kinetochore-associated proteins. Hum Mol Genet 9:175-185.

Saffery, R., L. H. Wong, D. V. Irvine, M. A. Bateman, B. Griffiths, S. M. Cutts, M. R. Cancilla, A. C. Cendron, A. J. Stafford, and K. H. Choo. 2001. Construction of neocentromere-based human minichromosomes by telomere-associated chromosomal truncation. Proc Natl Acad Sci U S A 98:5705-5710.

Saitoh, H., J. Tomkiel, C. A. Cooke, H. Ratrie, 3rd, M. Maurer, N. F. Rothfield, and W. C. Earnshaw. 1992. CENP-C, an autoantigen in scleroderma, is a component of the human inner kinetochore plate. Cell 70:115-125.

Sampaolesi, M., S. Blot, G. D'Antona, N. Granger, R. Tonlorenzi, A. Innocenzi, P. Mognol, J. L. Thibaud, B. G. Galvez, I. Barthelemy, L. Perani, S. Mantero, M. Guttinger, O. Pansarasa, C. Rinaldi, M. G. Cusella De Angelis, Y. Torrente, C. Bordignon, R. Bottinelli, and G. Cossu. 2006. Mesoangioblast stem cells ameliorate muscle function in dystrophic dogs. Nature 444:574-579.

Samson, F., J. A. Donoso, I. Heller-Bettinger, D. Watson, and R. H. Himes. 1979. Nocodazole action on tubulin assembly, axonal ultrastructure and fast axoplasmic transport. J Pharmacol Exp Ther 208:411-417.

Sandri-Goldin, R. M. 2003. Replication of the herpes simplex virus genome: does it really go around in circles? Proc Natl Acad Sci U S A 100:7428-7429.

Saydam, O., D. L. Glauser, I. Heid, G. Turkeri, M. Hilbe, A. H. Jacobs, M. Ackermann, and C. Fraefel. 2005. Herpes simplex virus 1 amplicon vector-mediated siRNA targeting epidermal growth factor receptor inhibits growth of human glioma cells in vivo. Mol Ther 12:803-812.

Schmidt, M., P. Zickler, G. Hoffmann, S. Haas, M. Wissler, A. Muessig, J. F. Tisdale, K. Kuramoto, R. G. Andrews, T. Wu, H. P. Kiem, C. E. Dunbar, and C. von Kalle. 2002. Polyclonal long-term repopulating stem cell clones in a primate model. Blood 100:2737-2743.

Schueler, M. G., A. W. Higgins, M. K. Rudd, K. Gustashaw, and H. F. Willard. 2001. Genomic and genetic definition of a functional human centromere. Science 294:109-115.

Schulz, T. C., G. M. Palmarini, S. A. Noggle, D. A. Weiler, M. M. Mitalipova, and B. G. Condie. 2003. Directed neuronal differentiation of human embryonic stem cells. BMC Neurosci 4:27.

Schulz, T. F., and S. Cordes. 2009. Is the Epstein-Barr virus EBNA-1 protein an oncogen? Proc Natl Acad Sci U S A 106:2091-2092.

Sena-Esteves, M., Y. Saeki, C. Fraefel, and X. O. Breakefield. 2000. HSV-1 amplicon vectors--simplicity and versatility. Mol Ther 2:9-15.

Shay, J. W. 1999. At the end of the millennium, a view of the end. Nat Genet 23:382-383.

Shen, M. H., P. J. Mee, J. Nichols, J. Yang, F. Brook, R. L. Gardner, A. G. Smith, and W. R. Brown. 2000. A structurally defined mini-chromosome vector for the mouse germ line. Curr Biol 10:31-34.

Shen, M. H., J. Yang, M. L. Loupart, A. Smith, and W. Brown. 1997. Human mini-chromosomes in mouse embryonal stem cells. Hum Mol Genet 6:1375-1382.

Shen, Y., J. Chow, Z. Wang, and G. Fan. 2006. Abnormal CpG island methylation occurs during in vitro differentiation of human embryonic stem cells. Hum Mol Genet 15:2623-2635.

Sheridan, C. 2011. Gene therapy finds its niche. Nat Biotechnol 29:121-128.

Shiloh, Y. 2003. ATM and related protein kinases: safeguarding genome integrity. Nat Rev Cancer 3:155-168.

Shizuya, H., B. Birren, U. J. Kim, V. Mancino, T. Slepak, Y. Tachiiri, and M. Simon. 1992. Cloning and stable maintenance of 300-kilobase-pair fragments of human DNA in Escherichia coli using an F-factor-based vector. Proc Natl Acad Sci U S A 89:8794-8797.

Siemen, H., M. Nix, E. Endl, P. Koch, J. Itskovitz-Eldor, and O. Brustle. 2005. Nucleofection of human embryonic stem cells. Stem Cells Dev 14:378-383.

Siemen, H., L. Nolden, S. Terstegge, P. Koch, and O. Brustle. 2008. Nucleofection of human embryonic stem cells. Methods Mol Biol 423:131-138.

Sims, R. J., 3rd, and D. Reinberg. 2009. Stem cells: Escaping fates with open states. Nature 460:802-803.

Singec, I., R. Jandial, A. Crain, G. Nikkhah, and E. Y. Snyder. 2007. The leading edge of stem cell therapeutics. Annu Rev Med 58:313-328.

Skuk, D., and J. P. Tremblay. 2003. Myoblast transplantation: the current status of a potential therapeutic tool for myopathies. J Muscle Res Cell Motil 24:285-300.

Slack, J. M. 2000. Stem cells in epithelial tissues. Science 287:1431-1433.
Smith-Arica, J. R., A. J. Thomson, R. Ansell, J. Chiorini, B. Davidson, and J. McWhir. 2003. Infection efficiency of human and mouse embryonic stem cells using adenoviral and adeno-associated viral vectors. Cloning Stem Cells 5:51-62.
Snyder, R. O., C. Miao, L. Meuse, J. Tubb, B. A. Donahue, H. F. Lin, D. W. Stafford, S. Patel, A. R. Thompson, T. Nichols, M. S. Read, D. A. Bellinger, K. M. Brinkhous, and M. A. Kay. 1999. Correction of hemophilia B in canine and murine models using recombinant adeno-associated viral vectors. Nat Med 5:64-70.
Sollars, V., X. Lu, L. Xiao, X. Wang, M. D. Garfinkel, and D. M. Ruden. 2003. Evidence for an epigenetic mechanism by which Hsp90 acts as a capacitor for morphological evolution. Nat Genet 33:70-74.
Soriano, P. 1999. Generalized lacZ expression with the ROSA26 Cre reporter strain. Nat Genet 21:70-71.
Spits, C., I. Mateizel, M. Geens, A. Mertzanidou, C. Staessen, Y. Vandeskelde, J. Van der Elst, I. Liebaers, and K. Sermon. 2008. Recurrent chromosomal abnormalities in human embryonic stem cells. Nat Biotechnol 26:1361-1363.
Srinivasan, R., D. J. Fink, and J. C. Glorioso. 2008. HSV vectors for gene therapy of chronic pain. Curr Opin Mol Ther 10:449-455.
Stack, S. M., and L. K. Anderson. 2001. A model for chromosome structure during the mitotic and meiotic cell cycles. Chromosome Res 9:175-198.
Stegmaier, K., K. N. Ross, S. A. Colavito, S. O'Malley, B. R. Stockwell, and T. R. Golub. 2004. Gene expression-based high-throughput screening(GE-HTS) and application to leukemia differentiation. Nat Genet 36:257-263.
StemCells&Diseases. 2011. In Stem Cell Information [World Wide Web site]. Bethesda, MD: National Institutes of Health, U.S. Department of Health and Human Services, 2011 [cited Sunday, July 31, 2011] Available at <http://stemcells.nih.gov/info/health>
Stern, C. D., and S. E. Fraser. 2001. Tracing the lineage of tracing cell lineages. Nat Cell Biol 3:E216-218.
Stinchcomb, D. T., K. Struhl, and R. W. Davis. 1979. Isolation and characterisation of a yeast chromosomal replicator. Nature 282:39-43.
Strelchenko, N., O. Verlinsky, V. Kukharenko, and Y. Verlinsky. 2004. Morula-derived human embryonic stem cells. Reprod Biomed Online 9:623-629.
Strulovici, Y., P. L. Leopold, T. P. O'Connor, R. G. Pergolizzi, and R. G. Crystal. 2007. Human embryonic stem cells and gene therapy. Mol Ther 15:850-866.
Sugata, N., S. Li, W. C. Earnshaw, T. J. Yen, K. Yoda, H. Masumoto, E. Munekata, P. E. Warburton, and K. Todokoro. 2000. Human CENP-H multimers colocalize with CENP-A and CENP-C at active centromere--kinetochore complexes. Hum Mol Genet 9:2919-2926.
Sugimoto, K., H. Yata, Y. Muro, and M. Himeno. 1994. Human centromere protein C (CENP-C) is a DNA-binding protein which possesses a novel DNA-binding motif. J Biochem (Tokyo) 116:877-881.
Sullivan, B. A., M. D. Blower, and G. H. Karpen. 2001. Determining centromere identity: cyclical stories and forking paths. Nat Rev Genet 2:584-596.
Sullivan, B. A., and S. Schwartz. 1995. Identification of centromeric antigens in dicentric Robertsonian translocations: CENP-C and CENP-E are necessary components of functional centromeres. Hum Mol Genet 4:2189-2197.

Sumner, A. T. 2003. Chromosomes : organization and function. Blackwell, Malden, Mass. ; Oxford.

Sung, R. S., L. Qin, and J. S. Bromberg. 2001. TNFalpha and IFNgamma induced by innate anti-adenoviral immune responses inhibit adenovirus-mediated transgene expression. Mol Ther 3:757-767.

Suzuki, K., K. Mitsui, E. Aizawa, K. Hasegawa, E. Kawase, T. Yamagishi, Y. Shimizu, H. Suemori, N. Nakatsuji, and K. Mitani. 2008. Highly efficient transient gene expression and gene targeting in primate embryonic stem cells with helper-dependent adenoviral vectors. Proc Natl Acad Sci U S A 105:13781-13786.

Suzuki, M., E. A. Chiocca, and Y. Saeki. 2007. Early STAT1 activation after systemic delivery of HSV amplicon vectors suppresses transcription of the vector-encoded transgene. Mol Ther 15:2017-2026.

Suzuki, M., K. Kasai, and Y. Saeki. 2006a. Plasmid DNA sequences present in conventional herpes simplex virus amplicon vectors cause rapid transgene silencing by forming inactive chromatin. J Virol 80:3293-3300.

Suzuki, N., K. Nishii, T. Okazaki, and M. Ikeno. 2006b. Human artificial chromosomes constructed using the bottom-up strategy are stably maintained in mitosis and efficiently transmissible to progeny mice. J Biol Chem 281:26615-26623.

Takahashi, K., K. Tanabe, M. Ohnuki, M. Narita, T. Ichisaka, K. Tomoda, and S. Yamanaka. 2007. Induction of pluripotent stem cells from adult human fibroblasts by defined factors. Cell 131:861-872.

Takahashi, K., and S. Yamanaka. 2006. Induction of pluripotent stem cells from mouse embryonic and adult fibroblast cultures by defined factors. Cell 126:663-676.

Tan, S. M., and P. Droge. 2005. Comparative analysis of sequence-specific DNA recombination systems in human embryonic stem cells. Stem Cells 23:868-873.

Tang, C., and M. Drukker. 2011. Potential barriers to therapeutics utilizing pluripotent cell derivatives: intrinsic immunogenicity of in vitro maintained and matured populations. Semin Immunopathol doi: 10.1007/s00281-011-0269-5.

Tang, C., A. S. Lee, J. P. Volkmer, D. Sahoo, D. Nag, A. R. Mosley, M. A. Inlay, R. Ardehali, S. L. Chavez, R. R. Pera, B. Behr, J. C. Wu, I. L. Weissman, and M. Drukker. 2011. An antibody against SSEA-5 glycan on human pluripotent stem cells enables removal of teratoma-forming cells. Nat Biotechnol 29:829-834.

Teramoto, K., K. Asahina, Y. Kumashiro, S. Kakinuma, R. Chinzei, K. Shimizu-Saito, Y. Tanaka, H. Teraoka, and S. Arii. 2005. Hepatocyte differentiation from embryonic stem cells and umbilical cord blood cells. J Hepatobiliary Pancreat Surg 12:196-202.

Thomson, J. A., J. Itskovitz-Eldor, S. S. Shapiro, M. A. Waknitz, J. J. Swiergiel, V. S. Marshall, and J. M. Jones. 1998. Embryonic stem cell lines derived from human blastocysts. Science 282:1145-1147.

Tomkiel, J., C. A. Cooke, H. Saitoh, R. L. Bernat, and W. C. Earnshaw. 1994. CENP-C is required for maintaining proper kinetochore size and for a timely transition to anaphase. J Cell Biol 125:531-545.

Turek-Plewa, J., and P. P. Jagodzinski. 2005. The role of mammalian DNA methyltransferases in the regulation of gene expression. Cell Mol Biol Lett 10:631-647.

Uhlmann, F., F. Lottspeich, and K. Nasmyth. 1999. Sister-chromatid separation at anaphase onset is promoted by cleavage of the cohesin subunit Scc1. Nature 400:37-42.

Unger, C., S. Gao, M. Cohen, M. Jaconi, R. Bergstrom, F. Holm, A. Galan, E. Sanchez, O. Irion, J. B. Dubuisson, M. Giry-Laterriere, P. Salmon, C. Simon, O. Hovatta, and A. Feki. 2009. Immortalized human skin fibroblast feeder cells support growth and maintenance of both human embryonic and induced pluripotent stem cells. Hum Reprod 24:2567-2581.

Uren, A. G., H. Mikkers, J. Kool, L. van der Weyden, A. H. Lund, C. H. Wilson, R. Rance, J. Jonkers, M. van Lohuizen, A. Berns, and D. J. Adams. 2009. A high-throughput splinkerette-PCR method for the isolation and sequencing of retroviral insertion sites. Nat Protoc 4:789-798.

Vagnarelli, P., and W. C. Earnshaw. 2004. Chromosomal passengers: the four-dimensional regulation of mitotic events. Chromosoma 113:211-222.

Vaillancourt, C., and J. Lafond. 2009. Human embryogenesis: overview. Methods Mol Biol 550:3-7.

Van Hooser, A. A., Ouspenski, II, H. C. Gregson, D. A. Starr, T. J. Yen, M. L. Goldberg, K. Yokomori, W. C. Earnshaw, K. F. Sullivan, and B. R. Brinkley. 2001. Specification of kinetochore-forming chromatin by the histone H3 variant CENP-A. J Cell Sci 114:3529-3542.

VandenDriessche, T., V. Vanslembrouck, I. Goovaerts, H. Zwinnen, M. L. Vanderhaeghen, D. Collen, and M. K. Chuah. 1999. Long-term expression of human coagulation factor VIII and correction of hemophilia A after in vivo retroviral gene transfer in factor VIII-deficient mice. Proc Natl Acad Sci U S A 96:10379-10384.

Vanderbyl, S., G. N. MacDonald, S. Sidhu, L. Gung, A. Telenius, C. Perez, and E. Perkins. 2004. Transfer and stable transgene expression of a mammalian artificial chromosome into bone marrow-derived human mesenchymal stem cells. Stem Cells 22:324-333.

Vasquez, R. J., B. Howell, A. M. Yvon, P. Wadsworth, and L. Cassimeris. 1997. Nanomolar concentrations of nocodazole alter microtubule dynamic instability in vivo and in vitro. Mol Biol Cell 8:973-985.

Vierbuchen, T., A. Ostermeier, Z. P. Pang, Y. Kokubu, T. C. Sudhof, and M. Wernig. 2010. Direct conversion of fibroblasts to functional neurons by defined factors. Nature 463:1035-1041.

Voet, T., J. Vermeesch, A. Carens, J. Durr, C. Labaere, H. Duhamel, G. David, and P. Marynen. 2001. Efficient male and female germline transmission of a human chromosomal vector in mice. Genome Res 11:124-136.

Vogel, G. 1999. Breakthrough of the year. Capturing the promise of youth. Science 286:2238-2239.

Vogel, G. 2005. Cell biology. Ready or not? Human ES cells head toward the clinic. Science 308:1534-1538.

Vukicevic, S., H. K. Kleinman, F. P. Luyten, A. B. Roberts, N. S. Roche, and A. H. Reddi. 1992. Identification of multiple active growth factors in basement membrane Matrigel suggests caution in interpretation of cellular activity related to extracellular matrix components. Exp Cell Res 202:1-8.

Wade-Martins, R., Y. Saeki, and E. A. Chiocca. 2003. Infectious delivery of a 135-kb LDLR genomic locus leads to regulated complementation of low-density lipoprotein receptor deficiency in human cells. Mol Ther 7:604-612.

Wade-Martins, R., E. R. Smith, E. Tyminski, E. A. Chiocca, and Y. Saeki. 2001. An infectious transfer and expression system for genomic DNA loci in human and mouse cells. Nat Biotechnol 19:1067-1070.

Wang, B., J. Li, and X. Xiao. 2000. Adeno-associated virus vector carrying human minidystrophin genes effectively ameliorates muscular dystrophy in mdx mouse model. Proc Natl Acad Sci U S A 97:13714-13719.

Wang, I. I., and I. I. Huang. 2000. Adenovirus technology for gene manipulation and functional studies. Drug Discov Today 5:10-16.

Warburton, P. E. 2004. Chromosomal dynamics of human neocentromere formation. Chromosome Res 12:617-626.

Warburton, P. E., C. A. Cooke, S. Bourassa, O. Vafa, B. A. Sullivan, G. Stetten, G. Gimelli, D. Warburton, C. Tyler-Smith, K. F. Sullivan, G. G. Poirier, and W. C. Earnshaw. 1997. Immunolocalization of CENP-A suggests a distinct nucleosome structure at the inner kinetochore plate of active centromeres. Curr Biol 7:901-904.

Warburton, P. E., J. S. Waye, and H. F. Willard. 1993. Nonrandom localization of recombination events in human alpha satellite repeat unit variants: implications for higher-order structural characteristics within centromeric heterochromatin. Mol Cell Biol 13:6520-6529.

Watanabe, K., M. Ueno, D. Kamiya, A. Nishiyama, M. Matsumura, T. Wataya, J. B. Takahashi, S. Nishikawa, K. Muguruma, and Y. Sasai. 2007. A ROCK inhibitor permits survival of dissociated human embryonic stem cells. Nat Biotechnol 25:681-686.

Watt, F. M., and B. L. Hogan. 2000. Out of Eden: stem cells and their niches. Science 287:1427-1430.

Waye, J. S., and H. F. Willard. 1986. Structure, organization, and sequence of alpha satellite DNA from human chromosome 17: evidence for evolution by unequal crossing-over and an ancestral pentamer repeat shared with the human X chromosome. Mol Cell Biol 6:3156-3165.

Wells, D. J. 2004. Gene therapy progress and prospects: electroporation and other physical methods. Gene Ther 11:1363-1369.

Willard, H. F. 2001. Neocentromeres and human artificial chromosomes: an unnatural act. Proc Natl Acad Sci U S A 98:5374-5376.

Wollert, K. C., G. P. Meyer, J. Lotz, S. Ringes-Lichtenberg, P. Lippolt, C. Breidenbach, S. Fichtner, T. Korte, B. Hornig, D. Messinger, L. Arseniev, B. Hertenstein, A. Ganser, and H. Drexler. 2004. Intracoronary autologous bone-marrow cell transfer after myocardial infarction: the BOOST randomised controlled clinical trial. Lancet 364:141-148.

Wong, S. P., O. Argyros, C. Coutelle, and R. P. Harbottle. 2010. Non-viral S/MAR vectors replicate episomally in vivo when provided with a selective advantage. Gene Ther 18:82-87.

Wu, F., I. Levchenko, and M. Filutowicz. 1995. A DNA segment conferring stable maintenance on R6K gamma-origin core replicons. J Bacteriol 177:6338-6345.

Wu, Z., H. Yang, and P. Colosi. 2009. Effect of genome size on AAV vector packaging. Mol Ther 18:80-86.

Xiong, C., D. Q. Tang, C. Q. Xie, L. Zhang, K. F. Xu, W. E. Thompson, W. Chou, G. H. Gibbons, L. J. Chang, L. J. Yang, and Y. E. Chen. 2005. Genetic engineering of human embryonic stem cells with lentiviral vectors. Stem Cells Dev 14:367-377.

Xu, Y., X. Zhu, H. S. Hahm, W. Wei, E. Hao, A. Hayek, and S. Ding. 2010. Revealing a core signaling regulatory mechanism for pluripotent stem cell survival and self-renewal by small molecules. Proc Natl Acad Sci U S A 107:8129-8134.

Yamada, H., A. Kunisato, M. Kawahara, C. G. Tahimic, X. Ren, H. Ueda, T. Nagamune, M. Katoh, T. Inoue, M. Nishikawa, and M. Oshimura. 2006. Exogenous gene expression and growth regulation of hematopoietic cells via a novel human artificial chromosome. J Hum Genet 51:147-150.

Yan, Y., D. Yang, E. D. Zarnowska, Z. Du, B. Werbel, C. Valliere, R. A. Pearce, J. A. Thomson, and S. C. Zhang. 2005. Directed differentiation of dopaminergic neuronal subtypes from human embryonic stem cells. Stem Cells 23:781-790.

Yang, C. H., J. Tomkiel, H. Saitoh, D. H. Johnson, and W. C. Earnshaw. 1996. Identification of overlapping DNA-binding and centromere-targeting domains in the human kinetochore protein CENP-C. Mol Cell Biol 16:3576-3586.

Yang, D., Z. J. Zhang, M. Oldenburg, M. Ayala, and S. C. Zhang. 2008. Human embryonic stem cell-derived dopaminergic neurons reverse functional deficit in parkinsonian rats. Stem Cells 26:55-63.

Yang, J. W., C. Pendon, J. Yang, N. Haywood, A. Chand, and W. R. Brown. 2000. Human mini-chromosomes with minimal centromeres. Hum Mol Genet 9:1891-1902.

Yang, Z., J. Guo, Q. Chen, C. Ding, J. Du, and X. Zhu. 2005. Silencing mitosin induces misaligned chromosomes, premature chromosome decondensation before anaphase onset, and mitotic cell death. Mol Cell Biol 25:4062-4074.

Yates, F., and G. Q. Daley. 2006. Progress and prospects: gene transfer into embryonic stem cells. Gene Ther 13:1431-1439.

Ye, Z., H. Zhan, P. Mali, S. Dowey, D. M. Williams, Y. Y. Jang, C. V. Dang, J. L. Spivak, A. R. Moliterno, and L. Cheng. 2009. Human-induced pluripotent stem cells from blood cells of healthy donors and patients with acquired blood disorders. Blood 114:5473-5480.

Yen, T. J., G. Li, B. T. Schaar, I. Szilak, and D. W. Cleveland. 1992. CENP-E is a putative kinetochore motor that accumulates just before mitosis. Nature 359:536-539.

Yeomans, D. C., and S. P. Wilson. 2009. Herpes virus-based recombinant herpes vectors: gene therapy for pain and molecular tool for pain science. Gene Ther 16:502-508.

Yew, N. S., and S. H. Cheng. 2004. Reducing the immunostimulatory activity of CpG-containing plasmid DNA vectors for non-viral gene therapy. Expert Opin Drug Deliv 1:115-125.

Yew, N. S., H. Zhao, M. Przybylska, I. H. Wu, J. D. Tousignant, R. K. Scheule, and S. H. Cheng. 2002. CpG-depleted plasmid DNA vectors with enhanced safety and long-term gene expression in vivo. Mol Ther 5:731-738.

Yoda, K., S. Ando, A. Okuda, A. Kikuchi, and T. Okazaki. 1998. In vitro assembly of the CENP-B/alpha-satellite DNA/core histone complex: CENP-B causes nucleosome positioning. Genes Cells 3:533-548.

Young, H. E., C. Duplaa, M. Romero-Ramos, M. F. Chesselet, P. Vourc'h, M. J. Yost, K. Ericson, L. Terracio, T. Asahara, H. Masuda, S. Tamura-Ninomiya, K. Detmer, R. A. Bray, T. A. Steele, D. Hixson, M. el-Kalay, B. W. Tobin, R. D. Russ, M. N. Horst, J. A. Floyd, N. L. Henson, K. C. Hawkins, J. Groom, A. Parikh, L. Blake, L. J. Bland, A. J. Thompson, A. Kirincich, C. Moreau, J. Hudson, F. P. Bowyer, 3rd, T. J. Lin, and A. C. Black, Jr. 2004. Adult reserve

stem cells and their potential for tissue engineering. Cell Biochem Biophys 40:1-80.

Yu, G., J. R. Wu, and D. M. Gilbert. 1998. Analysis of mammalian origin specification in ORC-depleted Xenopus egg extracts. Genes Cells 3:709-720.

Yu, I. T., C. A. Griffin, P. C. Phillips, L. C. Strauss, and E. J. Perlman. 1995. Numerical sex chromosomal abnormalities in pineal teratomas by cytogenetic analysis and fluorescence in situ hybridization. Lab Invest 72:419-423.

Yu, J., K. Hu, K. Smuga-Otto, S. Tian, R. Stewart, Slukvin, II, and J. A. Thomson. 2009. Human induced pluripotent stem cells free of vector and transgene sequences. Science 324:797-801.

Yu, J., M. A. Vodyanik, K. Smuga-Otto, J. Antosiewicz-Bourget, J. L. Frane, S. Tian, J. Nie, G. A. Jonsdottir, V. Ruotti, R. Stewart, Slukvin, II, and J. A. Thomson. 2007. Induced pluripotent stem cell lines derived from human somatic cells. Science 318:1917-1920.

Zambrowicz, B. P., A. Imamoto, S. Fiering, L. A. Herzenberg, W. G. Kerr, and P. Soriano. 1997. Disruption of overlapping transcripts in the ROSA beta geo 26 gene trap strain leads to widespread expression of beta-galactosidase in mouse embryos and hematopoietic cells. Proc Natl Acad Sci U S A 94:3789-3794.

Zhang, X., P. Stojkovic, S. Przyborski, M. Cooke, L. Armstrong, M. Lako, and M. Stojkovic. 2006. Derivation of human embryonic stem cells from developing and arrested embryos. Stem Cells 24:2669-2676.

Zhao, T., Z. N. Zhang, Z. Rong, and Y. Xu. 2011. Immunogenicity of induced pluripotent stem cells. Nature 474:212-215.

Zheng, C., and B. J. Baum. 2005. Evaluation of viral and mammalian promoters for use in gene delivery to salivary glands. Mol Ther 12:528-536.

Zhong, B., K. L. Watts, J. L. Gori, M. E. Wohlfahrt, J. Enssle, J. E. Adair, and H. P. Kiem. 2011. Safeguarding Nonhuman Primate iPS Cells With Suicide Genes. Mol Ther doi:10.1038/mt.2011.51.

Zittoun, R. A., F. Mandelli, R. Willemze, T. de Witte, B. Labar, L. Resegotti, F. Leoni, E. Damasio, G. Visani, G. Papa, and et al. 1995. Autologous or allogeneic bone marrow transplantation compared with intensive chemotherapy in acute myelogenous leukemia. European Organization for Research and Treatment of Cancer (EORTC) and the Gruppo Italiano Malattie Ematologiche Maligne dell'Adulto (GIMEMA) Leukemia Cooperative Groups. N Engl J Med 332:217-223.

Chapter 10. Appendix

10.1.1 ***Mandegar MA****, Moralli D, Khoja S, Cowley S, Yusuf M, Chan DYL, Mukherjee S, Blundell MP, Thrasher AJ, Volpi EV, James WS, Monaco ZL (2011). Functional Human Artificial Chromosomes are Generated and Stably Maintained in Human Embryonic Stem Cells. Human Molecular Genetics. First published online: May 18 2011. doi: 10.1093/hmg/ddr144.*

10.1.2 Moralli D, Yusuf M, ***Mandegar MA****, Khoja S, Monaco ZL, Volpi EV (2010). An Improved Technique for Chromosomal Analysis of Human ES and iPS Cells. Stem Cell Reviews and Reports. First published on 29 December 2010. doi:10.1007/s12015-010-9224-4.*

Human Molecular Genetics, 2011, Vol. 20, No. 15 **2905–2913**
doi:10.1093/hmg/ddr144
Advance Access published on May 18, 2011

Functional human artificial chromosomes are generated and stably maintained in human embryonic stem cells

Mohammad A. Mandegar[1], Daniela Moralli[1], Suhail Khoja[1], Sally Cowley[2], David Y.L. Chan[1], Mohammed Yusuf[1], Sayandip Mukherjee[3], Michael P. Blundell[3], Emanuela V. Volpi[1], Adrian J. Thrasher[3], William James[2] and Zoia L. Monaco[1,*]

[1]Wellcome Trust Centre for Human Genetics, University of Oxford, Roosevelt Drive, Oxford OX3 7BN, UK, [2]Sir William Dunn School of Pathology, University of Oxford, South Parks Road, Oxford OX1 3RE, UK and [3]Institute of Child Health, University College London, 30 Guilford Street, London WC1N 1EH, UK

Received February 8, 2011; Revised and Accepted March 28, 2011

We present a novel and efficient non-integrating gene expression system in human embryonic stem cells (hESc) utilizing human artificial chromosomes (HAC), which behave as autonomous endogenous host chromosomes and segregate correctly during cell division. HAC are important vectors for investigating the organization and structure of the kinetochore, and gene complementation. HAC have so far been obtained in immortalized or tumour-derived cell lines, but never in stem cells, thus limiting their potential therapeutic application. In this work, we modified the herpes simplex virus type 1 amplicon system for efficient transfer of HAC DNA into two hESc. The deriving stable clones generated green fluorescent protein gene-expressing HAC at high frequency, which were stably maintained without selection for 3 months. Importantly, no integration of the HAC DNA was observed in the hESc lines, compared with the fibrosarcoma-derived control cells, where the exogenous DNA frequently integrated in the host genome. The hESc retained pluripotency, differentiation and teratoma formation capabilities. This is the first report of successfully generating gene expressing *de novo* HAC in hESc, and is a significant step towards the genetic manipulation of stem cells and potential therapeutic applications.

INTRODUCTION

Human embryonic stem cells (hESc) are an important tool in clinical and basic research. Due to their high replicative lifespan and ability to differentiate into the three different germ layers, they are used for human developmental biology, tissue regeneration, transplant therapies and drug discovery studies (1). Safe and efficient *in vitro* genetic manipulation of hESc is an essential step in realizing their full potential for clinical applications (2).

Most gene expression studies in hESc utilize lentiviral, adenoviral and adeno-associated viral (AAV) vectors for gene delivery (3–5). However, lentiviral vectors integrate randomly at multiple sites within the host genome leading to insertional mutagenesis (6), and although adenoviral vectors remain episomal, silencing post-transduction may occur. Another disadvantage is that the capacity of AAV and lentiviral vectors is limited to ~5 and 10 kb of DNA, respectively (7).

An alternative vector type is represented by human artificial chromosomes (HAC), which are autonomous functional chromosomal elements that behave as normal chromosomes. Gene-expressing HAC are generated in cells following delivery of vectors with centromeric alpha-satellite (alphoid, α) DNA, appropriate markers and genes. The maintenance of the HAC does not require integration into the host genome, and they are suitable for the delivery of large gene loci.

Previously, we introduced input HAC DNA (404 kb) containing the hypoxanthine–guanine phosphoribosyl transferase (*HPRT*) gene into human HPRT-deficient HT1080 fibrosarcoma cells, and the HAC generated successfully complemented the deficiency (8). The input HAC DNA was delivered by standard transfection, but we found this method inefficient for

*To whom correspondence should be addressed. Tel: +44 1865287502/287523; Fax: +44 1865287650; Email: zoia@well.ox.ac.uk

routine large DNA transfer. In more recent studies, we utilized the highly efficient herpes simplex virus-1 (HSV-1) amplicon technology for delivery of the input HAC DNA using infectious amplicons (9). The advantage of this system is that HSV-1 amplicons have a high capacity for large DNA delivery (up to 150 kb) to efficiently introduce HAC input DNA into immortalized cell lines. Following transduction, we observed that the efficiency of input HAC DNA delivery into HT1080 and other cell lines was significantly greater than transfection (by a factor of 10^4) (9).

In this study, input HAC DNA vectors (ranging from 55 to 115 kb) containing the marker gene for green fluorescent protein (*GFP*) were delivered into HUES-2 and HUES-10 hESc lines (10) following transduction with HSV-1 amplicons. Mitotically stable, gene-expressing, functional HAC were generated. The HAC were present in up to 70% of the hESc, and gene expression was maintained in the absence of selection over a period of 60 days and following cell differentiation. No DNA integrated into the hESc genome, in contrast to HT1080 cells, where the HAC DNA frequently integrated into the host chromosomes. More importantly, the HSV-1 HAC hESc retained their pluripotency and differentiation capabilities.

This is the first successful study to establish non-integrating, stable, gene-expressing HAC using HSV-1 amplicons in hESc, and is a significant step forward for HAC in gene therapy studies.

RESULTS

Vector construction

To generate HSV-1-based input HAC DNA vectors that were highly proficient at HAC formation, the BAC hBAC495J24 (containing 220 kb of chromosome 17 core α DNA) used in a previous study to construct an efficient input HAC DNA vector (pJM2256) (11) was modified. As hBAC495J24 was ~70 kb larger than the 150 kb packaging limit of HSV-1, we aimed to reduce it while retaining its HAC-forming properties. Three derivatives of the BAC hBAC495J24 were generated, two of which arose spontaneously (containing 40 and 100 kb of 17α DNA) during culture, and the third derivative (containing 60 kb of 17α DNA) by utilizing the RED/ET recombination system (12). All three derivatives were modified by LoxP–Cre recombination with pHGNeo4 to include the essential HSV-1 elements, and reporter genes (*GFP*), thereby generating pα40 (55 kb, including 40 kb of 17α DNA), pα60 (75 kb, including 60 kb of 17α DNA) and pα100 (115 kb, including 100 kb of 17α DNA) (Fig. 1A, and Supplementary Material, Fig. S1A).

Introduction of input HAC DNA vectors into hES cells

Among the three HSV-1 HAC input DNA vectors we generated, pα40 (40 kb of 17α DNA) was the most useful, as its size allowed up to 100 kb of transgenic DNA to be accommodated within the vector for packaging into HSV-1 amplicons (limit capacity of 150 kb). For this reason, we investigated its HAC-forming efficiency, by delivering pα40 to HUES-2 (at passage 40) or HUES-10 (at passage 29) by HSV-1 amplicon transduction at multiplicity of infection (MOI) 2. In a parallel control experiment, pHGNeo4 amplicons were also delivered to both cell lines. The other 17α input HAC DNA vectors, pα60 and pα100, were delivered only to the HUES-2 line, in the same conditions described above.

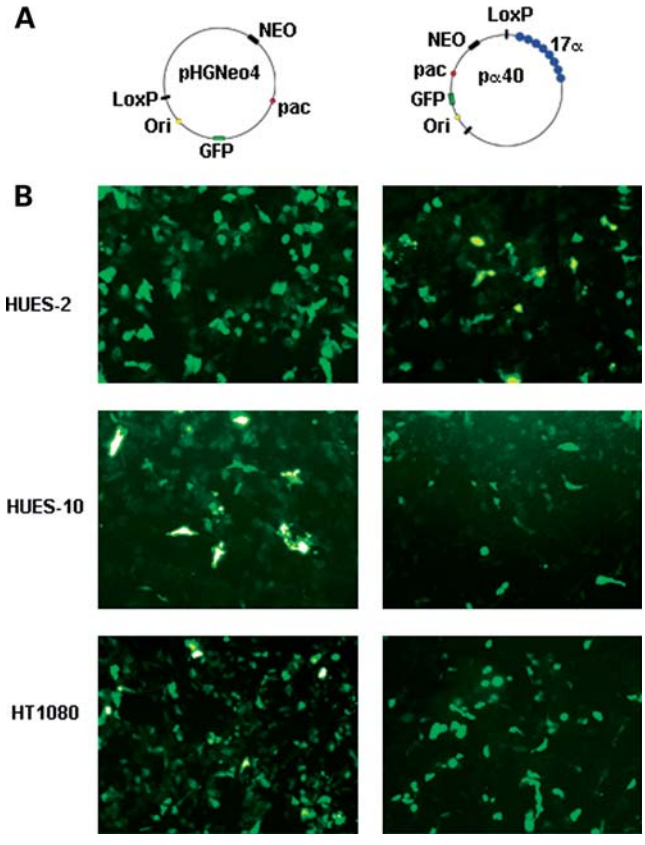

Figure 1. (**A**) Schematic representation of the vectors used in this study, not drawn to scale. (**B**) GFP expression in HUES-2, HUES-10 and HT1080 cells 24 h after transduction with pHGNeo4 (left) and pα40 (right) amplicons.

The efficiency (%) of transduction, summarized in Table 1, was determined after 24 h by fluorescence-activated cell sorting (FACS) or counting *GFP* expressing cells. The results are also shown in Figure 1B and Supplementary Material, Figure S1B. In HUES-2, the average transduction efficiency was ~40% for both pα40 and the control vector pHGNeo4. The two larger vectors, pα100 and pα60, were delivered to HUES-2 with an efficiency of 16 and 20%, respectively (Table 1, Supplementary Material, Fig. S1B). In HUES-10, the delivery efficiency was 27% for both pHGNeo4 and pα40 (Table 1, Fig. 1B).

In parallel control experiments, the input HAC DNA amplicon vectors were delivered by HSV-1-mediated transduction to HT1080 cells, which efficiently form HAC (8,9,11). The delivery efficiency of the input HAC DNA vectors was similar to that observed in hESc (Table 1, Fig. 1B, Supplementary Material, Fig. S1A).

Viability of hESc following transduction with HSV-1 amplicons

In addition to the experiments outlined above, to determine whether the HSV-1 amplicon transduction-affected hESc

Table 1. Average efficiency of HSV-1 amplicon transduction at MOI 2, and HAC formation in HUES-2, HUES-10 and HT1080 cells

Cell line	Input HAC DNA vector	Efficiency of transduction (%)	No. of clones analysed	HAC positive clones	% of HAC/ cells
HUES-2	pα40	40	10	5	10–70
	pα60	20	9	5	10–25
	pα100	16	7	3	10–20
	pHGNeo4	40	5	NA	NA
HUES-10	pα40	27	5	5	35–50
	pHGNeo4	27	1	NA	NA
HT1080	pα40	19	10	6	5–30
	pα60	34	3	1	20
	pα100	25	4	1	15
	pHGNeo4	28	3	NA	NA

NA, not applicable.

viability, 2.5×10^5 HUES-2 cells were transduced with pHGNeo4 amplicons at MOI 1, 2 and 5. The average efficiency of transduction was determined after 24 h by FACS or counting *GFP* expressing cells, and found to be ~27% for MOI 1, 42% for MOI 2 and 48% for MOI 5. Since transduction efficiencies were similar at MOI 2 and 5, the HUES-2 cell lines probably reached transduction saturation in this range.

The cells were monitored for 6 days post-transduction, and the average growth rate was calculated by measuring the rate of population increase divided by the initial number of cells, and compared with that of an untreated control. The growth rate and morphology of HUES-2 were not affected post-HSV-1 amplicon transduction, with a 5% reduction in viability, detected only for MOI 1.

Generation and analysis of stable clones in hES cells

Overall, 10 HUES-2 and 5 HUES-10 clones were isolated following G418 selection, derived from the pα40 transduction (Table 1). In addition, we also isolated 9 and 7 clones from pα60 and pα100, respectively, following transduction into HUES-2 cells. The stable clone formation efficiency of HSV-1 transduction was relatively high for both hESc lines, at 10^{-4}, as calculated by the ratio between the number of stable clones and GFP-positive cells 24 h post-transduction. Chromosome metaphase spreads were prepared from stable clones, and analysed by two colour fluorescence *in situ* hybridization (FISH) with vector and 17α DNA probes (Table 1 and Fig. 2A, Supplementary Material, Fig. S1B). Following HSV-1 transduction with pα40, HAC were detected in 5 of the 10 stable clones obtained in HUES-2 cells, and in all 5 clones isolated in HUES-10. The HAC were present in up to 70% of the cells from each clone. In the HUES-2 cells transduced with either pα60 or pα100, HAC were detected in approximately half of the clones, with a frequency of up to 25% of the cells of each clone (Supplementary Material, Fig. S1B). The lower HAC frequency per cell observed with pα60 or pα100 indicated that the pα40 vector was the most efficient at HAC formation in HUES-2 following HSV-1 transduction. Most importantly, in none of the 31 clones (HUES-2 or HUES-10) analysed, the HAC DNA had integrated into the host genome. However, in all of the analysed hESc clones derived from the HSV-1 delivery of the control vector pHGNeo4, the exogenous DNA had integrated into the host genome.

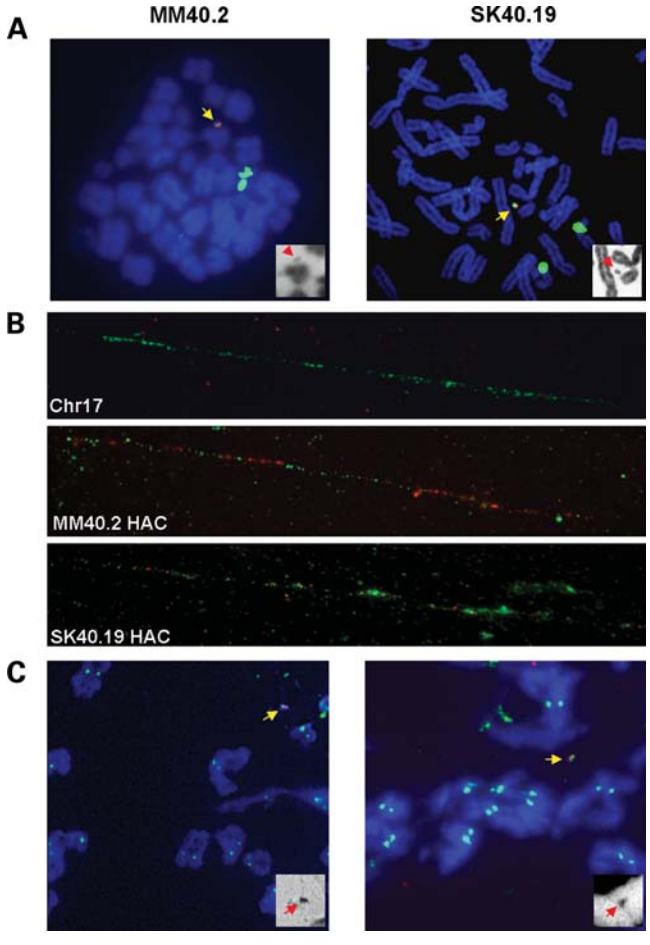

Figure 2. HAC analysis. (**A**) FISH with a 17α DNA probe (green), and a vector probe (red). The chromosomes are counterstained in DAPI, blue. The HAC are identified by yellow arrows. The insets show DAPI staining only (HAC, red arrows), in black and white. (**B**) Fibre FISH on HAC clones, with 17α DNA (green) and vector DNA (red) probes. (**C**) ImmunoFISH with anti-CENP C antibody (green), and 17α HAC probe (red).

In HT1080, the HSV-1 amplicon transduction successfully generated several hundred clones from each of the 17α HSV-1 HAC input DNA vectors, and several clones were selected for analysis from pα40, pα60 and pα100 (Table 1). The stable clone formation efficiency of HSV-1 transduction was 5×10^{-3}. Positive clones were analysed by two colour FISH with vector and 17α DNA probes (Table 1). The HSV-17α input DNA vectors generated HAC in most of the clones following transduction, but were present at a lower frequency in cells (up to 30%), and concomitant integrations in the HT1080 genome were found in all of the clones.

Karyotypic analysis of hESc HAC clones

Two hESc HAC clones were chosen for further studies. Clone MM40.2 derived from the HSV-1-mediated delivery of pα40 into HUES-2, and contained a HAC in 70% of the cells

(Fig. 2A). Clone SK40.19 was generated by the transduction of pα40 in HUES-10 cells and contained HAC in 50% of the analysed metaphases (Fig. 2A). The structure of the HAC present in both clones was analysed further by FISH on extended chromatin fibres. The HAC contained repeat units of input DNA, arranged in an alternate fashion as seen in previous studies (8), but the vector backbone DNA was less abundant in clone SK40.19 (Fig. 2B).

The percentage of GFP-positive cells in the two HAC clones was established by FACS analysis, and found to be 33% for SK40.19 and 83% for MM40.2. These values are in concordance with the estimated HAC frequency.

The chromosomal content of the two HAC clones was characterized by chromosome painting for two of the most frequently described chromosomal numerical aberrations in hESc, chromosome 12 and 17 trisomy. In clone MM40.2 (analysed at passage 70), 66% of the cells presented both an extra chromosome 12 and 17. The remaining 34% contained either a chromosome 12 or 17 trisomy.

To investigate whether the HSV-1 transduction and HAC formation processes could have caused the chromosomal instability observed in clone MM40.2, the karyotype of the parental HUES-2 cell line was analysed by chromosome painting at low passage (passage 28) and at the passage when the transduction was undertaken (passage 40). While no extra chromosome 12 or 17 were identified in the parental HUES-2 at passage 28, a double trisomy for chromosome 12 and 17 was detected in 70% of the cells at passage 40, while 30% of cells had either an extra chromosome 12 or 17. These data suggested that the numerical aberration occurred in the parental HUES-2 late passage 40 before the HAC formation and was not the result of the HSV-1 transduction.

In contrast, a similar analysis on clone SK40.19 (at passage 60) showed no extra chromosome 12 or 17. The clone chromosome number was 46 + HAC, and furthermore, the analysis of G-banding pattern indicated that no major rearrangements were present, indicating that SK40.19 was karyotypically normal. The parental HUES-10 line was analysed by whole-genome cytogenetic microarrays. The karyotype of the cell line was found to be completely normal (confidence 0.9, 200 markers).

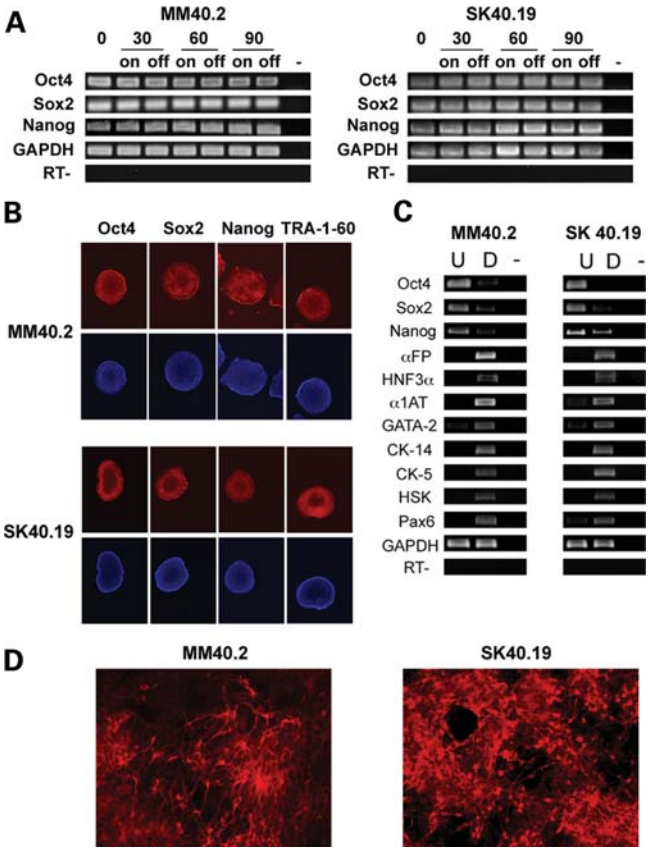

Figure 3. Pluripotency analysis. (**A**) RT–PCR with primers specific for pluripotency genes at time points 0, 30, 60 and 90 days in culture (0, 30, 60, 90) in the presence (on) or absence (off) of selection. (RT-) control PCR performed in the absence of the reverse transcriptase, using *GAPDH* primers, (-) no template control. (**B**) Immunostaining with pluripotency marker antibodies (red). The cells are counterstained with DAPI, blue. (**C**) RT–PCR analysis of germinal layer transcripts on cDNA from *in vitro* differentiated MM40.2 and SK40.19 cells, with primers specific for pluripotency (*Oct4*, *Sox2*, *Nanog*), endoderm (*αFP*, *HFN3α*, *α1AT*), mesoderm (*GATA-2*), epidermis (*CK-14*, *CK-5*, *HSK*) and neuronal markers (*Pax6*). U: undifferentiated cells, D: differentiated cells. (RT-): control PCR performed in the absence of the reverse transcriptase, using *GAPDH* primers. (-) no template control. (**D**) Neuronal differentiated cells stained with anti-βIII tubulin antibody (red).

HAC stability and centromere protein C staining

The mitotic stability of the HAC in MM40.2 and SK40.19 was monitored by FISH for 90 days (corresponding to ∼30 passages) in the absence of selection. In both clones, the HAC frequency did not change significantly over this period, with a daily loss rate of 0.03% for MM40.2 and 0.24% for SK40.19 (calculated by the formula $N_n = N_0 \times (1 - R)^n$, where N_0 is the number of metaphase chromosome spreads showing HAC in the cells cultured under selection, N_n the number of HAC-containing metaphase chromosome spreads after n days of culture in the absence of selection and R the daily rate of loss).

To confirm that an active centromere was present on the HAC, cells from the MM40.2 and SK40.19 clones were stained with anti-centromere protein C (CENP C) antibody, coupled to FISH with HAC-specific probes. A positive CENP C signal was identified on the HAC in both clones at a similar intensity of those observed on endogenous chromosomes (Fig. 2C), thus confirming that an active centromere was present, similar to the HSV-1 HAC in HT1080 cells (9).

Pluripotency studies

To determine whether the MM40.2 and SK40.19 cells expressed pluripotency epitopes compared with the parental lines, cells from each clone (at approximately passages 70 and 60, respectively) were stained with antibodies against the embryonic stem cell markers Oct4, Sox2, Nanog and TRA-1-60 (Fig. 3B). The HAC clones and the parental lines were stained similarly by the antibodies, while HT1080 and mouse embryonic fibroblast (MEF) control cells were completely negative. The result indicated that the HAC-containing hESc clones expressed embryonic stem cell markers.

The hESc markers expression was sustained over time in both HAC clones, as confirmed by reverse transcription

polymerase chain reaction (RT–PCR) analysis on RNA extracted from the MM40.2 and SK40.19 cells, over a period of 90 days, cultivated in the presence and absence of selection (Fig. 3A).

To confirm that the HAC-containing clones were pluripotent, we induced differentiation of the three embryonic germ layers through embryoid body (EB) formation of MM40.2 and SK40.19. Total RNA was extracted from the pool of differentiated cells and analysed for the presence of endoderm (α *Feto-protein*, *HNF3*α, α1 *anti-trypsin*), mesoderm (*GATA-2*) and ectoderm (*CK-5*, *CK-14*, *high sulphur keratin*, *Pax6*) specific transcripts. RT–PCR experiments revealed that mRNAs for all the markers were present (Fig. 3C), indicating that both HAC clones retained pluripotency.

HAC clones directed differentiation

Furthermore, neuronal differentiation was induced in clones MM40.2 and SK40.19 by treatment with medium containing noggin and fibronectin (13). After 25 days of directed differentiation, the cells were fixed in formaldehyde and stained with anti-βIII-tubulin antibody, a neuronal cell marker. We detected neuronal cells, highly positive for βIII-tubulin staining, in both HAC clones, ranging approximately between 18 and 40% of the treated cells (Fig. 3D). On average, the SK40.19 was up to two times more efficient at forming neuronal cells, compared with MM40.2. The control cells (untreated MM40.2 and SK40.19; HT1080; MEF) never displayed positive cells. To determine whether the HAC was still present in the cells following neuronal differentiation, we conducted FISH experiments on the interphasic cells stained with the anti-βIII-tubulin antibody. In clone SK40.19, the HAC frequency remained the same (50%), while a positive HAC signal was detected in 44% of the MM40.2 cells (Supplementary Material, Fig. S2).

Teratoma formation assay

Since the MM40.2 cells contained the highest HAC frequency, teratomas were generated using these cells in immunodeficient mice, as this constituted the most rigorous test of pluripotency for human ES cells. Sub-cutaneous injection into immunodeficient mice generated tumours between the 5th and 7th week post-treatment. The subsequent histological analysis of haematoxylin/eosin-stained tumour sections revealed the presence of ectodermal (neural tube), mesodermal (muscle and blood vessels) and endodermal (gut epithelium, alveoli and glandular epithelium) structures (Fig. 4A). Moreover, immunostaining using suitable antibodies confirmed the presence of all three germinal layers in these sections (Fig. 4B) thereby confirming the tumour growth as a teratoma.

As the sections prepared for the immunological staining were not suitable for FISH experiments, we confirmed the presence of HAC in the teratoma cells by real-time qPCR on total genomic DNA extracted from the teratoma mass. HAC-specific primers (*Neo* and *GFP*) were used, and the HAC DNA content in the teratoma cells was normalized against that of the undifferentiated MM40.2 cells (Supplementary Material, Fig. S3). We detected no difference in the abundance of HAC sequences between the undifferentiated MM40.2 and

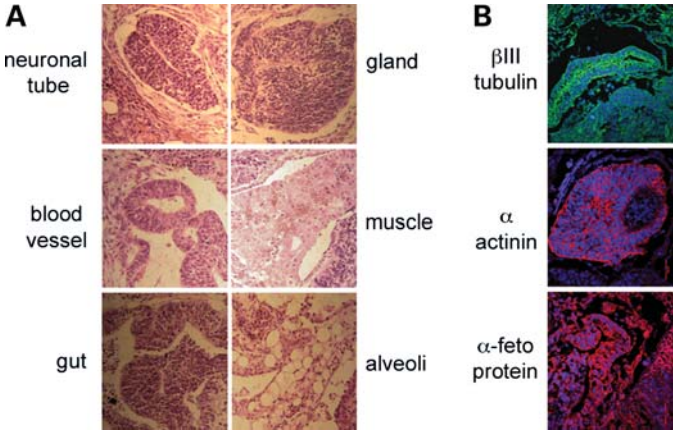

Figure 4. Teratoma assay. (**A**) Haematoxylin/eosin-stained MM40.2-teratoma derived sections. (**B**) immunostaining with antibodies for ectoderm (βIII-tubulin, green), mesoderm (α-actinin, red) and endoderm(α-feto protein, red) markers.

teratoma cells, suggesting that the HAC had not been lost during the *in vivo* cell replications. A similar analysis was conducted on the neuronal-differentiated MM40.2 cells, previously analysed by FISH. The qPCR results closely reflected the FISH quantification of HAC distribution (Supplementary Material, Fig. S3).

HAC gene expression analysis

The expression level of the reporter gene for *GFP* from the MM40.2 and SK40.19 HAC was investigated by real-time qPCR experiments on cDNA, in cells grown either on or off selection. The HAC gene expression was compared with that of a ubiquitously expressed gene glyceraldehyde 3-phosphate dehydrogenase (*GAPDH*). In SK40.19, the *GFP* expression was found to be decreased by about 50% after ∼40 days on or off selection (Table 2). In contrast, in MM40.2, the *GFP* gene expression level remained constant for a prolonged period of time (60 days) on or off selection (Table 2). To further analyse the reporter gene expression clonal variability, the *GFP* relative amount in three pHGNeo4 stable clones was measured by real-time qPCR. Compared with the MM40.2, one clone had approximately five times lower levels of *GFP*, and two had 5 and 10 times more *GFP*, respectively (Supplementary Material, Table S1). Taken together, these data suggested that stochastic events may have affected the level of expression of the reporter gene in different clones. To confirm that the MM40.2 clone had very stable levels of reporter gene expression, GFP presence was further monitored by FACS over the course of 90 days. The percentage of *GFP*-expressing cells remained relatively constant and ranged from 81 to 89%. The fold increase in the geometric mean of fluorescence intensity compared with the untreated control ranged from ∼8 to 12, indicating that the average *GFP* expression per cell also remained relatively constant.

Furthermore, the *GFP* reporter gene expression levels of the MM40.2 clone were characterized by qPCR following differentiation, and compared with the levels present in the undifferentiated MM40.2 parental. The *GFP* gene was still expressed in both EB-derived, and neuronal-differentiated

Table 2. Analysis by qPCR of the *GFP* reporter gene expression in clones MM40.2 and SK40.19, in the presence or absence of selection

		Day 0 (SD)	Day 30 (SD)	Day 60 (SD)
MM40.2	On selection	1.00 (0.03)	1.23 (0.03)	1.34 (0.05)
	Off selection	1.00 (0.03)	1.43 (0.15)	1.49 (0.07)
SK40.19	On selection	1.00 (0.02)	0.40[a] (0.01)	NA
	Off selection	1.00 (0.02)	0.52[a] (0.02)	NA

The qPCR-fold difference values are expressed in reference to the day 0 time point, using *GAPDH* as internal control. SD, standard deviation. NA, not analysed.
[a]37 days.

Table 3. Analysis by qPCR of the *GFP* reporter gene expression, in differentiated MM40.2 cells

	Undifferentiated hESc (SD)	EB-derived cells (SD)	Neuronal cells (SD)
GFP expression	1.00 (0.03)	0.70 (0.04)	0.60 (0.02)

The values are expressed in reference to the undifferentiated parental, using *GAPDH* as internal control. SD, standard deviation.

cells, at ~60–70% of the level present in the undifferentiated parental (Table 3). The level of *GFP* expression was consistent with the HAC frequency observed in the neuronal-differentiated MM40.2 cells. Based on direct microscopic observation of the EB-derived and neuronal cells, the derivative differentiated cells exhibited a heterogeneous *GFP* expression: while some cells were still highly GFP positive, in others the GFP fluorescence appeared reduced or absent (Supplementary Material, Fig. S4). This suggested that stochastic events in the early stages of hESc differentiation had an effect in the level of expression of the reporter gene during the later stages.

DISCUSSION

hESc have been hailed as an ideal model to study cell differentiation into organ-specific lineages, gene expression, and to eventually establish patient-specific/gene therapy applications (1). Several techniques utilizing viral and non-viral vectors have been used to deliver transgenes to hESc. Most viral vectors are highly efficient at introducing the DNA into the cells, but they are usually limited by the size of the gene they can accommodate and they may randomly integrate into the host genome, possibly resulting in deleterious mutagenic effects (6).

In this study, we describe an alternative efficient approach, based on direct HAC formation in two hESc lines utilizing HSV-1 amplicons for delivery. HAC can accommodate large genomic regions containing potentially therapeutic genes along with their regulatory sequences, and have successfully been used as gene transfer vectors to complement genetic deficiencies in human-cultured cells (8). HAC are also composed of heterochromatic and euchromatic regions in a similar pattern to endogenous chromosomes. While the presence of heterochromatin is necessary for the correct segregation of HAC (14,15), the euchromatin potentially ensures the prolonged transgene expression.

We delivered input HAC DNA vectors to the HUES-2, HUES-10 and HT1080 cells, using HSV-1 amplicon-mediated transduction. This technique is up to 10^4 times more efficient at delivering large DNA than chemical transfection, in several different cell types (9).

The FISH analysis revealed that HAC were formed in both HUES-2 and HUES-10. This is the first report of *de novo* HAC formation in a karyotypically normal primary human cell line, and is highly significant for developing HAC as gene expression vectors for gene therapy applications. Most importantly, the input HAC DNA vectors never integrated in the hESc genome, compared with HT1080, where integrations were found in most of the clones. It is possible that the presence in hESc of systems actively guarding genome integrity (16) may prevent or reduce the frequency of large vector integration events, thus giving an advantage to cells where the exogenous DNA forms episomal HAC, in the presence of selective pressure. In this scenario, the smaller vector pHGNeo4 integrated in hES cells, because no other outcome would have allowed the cells to survive selection, as pHGNeo4 is incapable of forming HAC. On the other hand, HT1080 cells are tumour derived, and lack an efficient control of genome integrity, thus explaining why we observed both HAC formation and integration events. Future studies with hESc lines mutant for genome guarding proteins, such as p53, may help clarify this issue.

The hESc HAC were fully stable, and formed an active centromere. This showed that although the HAC were not detected in 100% of the cells, it was not the result of instability. It is possible that the cloning procedure for hESc did not produce pure clones [hESc have a low survival rate as single cells, even when rho-associated kinase (ROCK) inhibitor Y-27632 is used], and hence the HAC frequency in the cells was $<100\%$, as different sublines may have been present within the clones.

The analysis of HAC gene expression showed that the RNA levels of the *GFP* reporter gene on or off selection were different in the clones characterized, containing either HAC or integrated pHGNeo4 DNA. This confirmed the existence of clonal variability between different lines, possibly due to epigenetic effects. In one of the clones, MM40.2, *GFP* expression was highly stable, and did not change over prolonged time in culture, both on and off selection. Furthermore, the reporter gene expression was maintained following MM40.2 *in vitro* differentiation, although we observed heterogeneity in the GFP levels among the differentiated cells. The process of *de novo* HAC formation generally results in the multimerization of the input DNA, as shown by the alternate pattern of vector and alpha-satellite signals observed in the FISH on chromatin fibres, and the possibility that more than one copy of the transgene is present on the HAC. This ensures that copies of the transgene will be localized away from the centromeric heterochromatic area, and thus escape potential silencing. The spreading of heterochromatin, which is a stochastic event, may explain the variability observed in the *GFP* reporter gene expression following differentiation in clone MM40.2, and in the prolonged culture in clone

SK40.19. Expression studies where the gene on the HAC is under the control of its appropriate promoter and regulatory sequences will verify if physiological expression levels can be achieved. It may also be interesting to study the possibility of loading the transgenes on the HAC via an *in vivo* LoxP-based system as shown by other reports (17,18), and screening clones where only one copy has been acquired by the HAC.

Importantly, neither the HSV-1 transduction nor the HAC formation led to a loss of pluripotency in the HUES-2 or HUES-10 cells, as suggested by the staining with hESc-specific markers, expression of three germinal layer markers in EB-derived cells, by the differentiation into neuronal types and by MM40.2 teratoma formation. The HAC were present in the neuronal-differentiated cells in both MM40.2 and SK40.19. The HAC frequency in MM40.2 neuronal cells was slightly lower than in the undifferentiated cells, yet the frequency in SK40.19 remained unchanged following differentiation.

The HSV-1 amplicon particles package DNAs up to 150 kb (19). This is far larger than the size which can be accommodated in lentiviral, AAV or adenovirus-based vectors. In this study, the pα40 containing the shortest tract of 17 alpha-satellite DNA (40 kb) was the most efficient vector at HAC formation in hESc, and since its total size is ∼55 kb, it can accommodate a large genomic region containing gene loci of up to 100 kb. HSV-1 HAC replicate at the same rate as the endogenous chromosome, making the gene dosage level more easily controllable.

In summary, we obtained high-capacity, gene-expressing HAC formation in two hES cell lines, using a high-efficiency delivery method based on the HSV-1 amplicon technology. The HAC were stable and sustained long-term gene expression. The lack of integrated DNA in hESc is an important and exciting finding, prompting further work to understand the mechanism in HAC generation. This is the first report of direct *de novo* HAC formation in human stem cell lines, and shows HAC vectors as a viable alternative to other gene delivery systems in hESc. Our findings are not exclusive to the field of hESc, but may also be relevant for induced pluripotent stem cells.

MATERIALS AND METHODS

Input HAC DNA vector assembly

The pHGNeo4 vector was released from pHSV21αNeo (9) by *Bst*BI digestion, and re-circularized by treatment with T4 DNA ligase. The pHGNeo4 vector carries the HSV-1 amplicon origin of replication (*Ori*) and packaging signal (*pac*), the reporter *GFP* gene, under the control of the I/E promoter from HSV-1, and the G418 resistance gene (*Neo*), controlled by the SV40 promoter.

Vectors BAC17α40 and BAC17α100, containing, respectively, 40 kb and 100 kb of a satellite DNA from human chromosome 17 (17α), were derived by spontaneous deletions of hBAC495J24 (11,20). PAC17α60 was obtained by RED/ET recombination (12), which transferred 60 kb of 17α DNA from hBAC495J24 to pCYPAC2 vector. Briefly, the pCYPAC2 vector was used as a template to generate a 9.5 kb PCR fragment, using primers containing 50 bp homologous tails to the alpha 17 satellite DNA consensus (Supplementary Material, Table S2). The linear 9.5 kb pCYPAC2 PCR product was then transformed into *Escherichia coli* cells containing hBAC495J24, and expressing the RED/ET system proteins.

The BAC17α40, PAC17α60 and BAC17α100 constructs were then retrofitted with pHGNeo4 by LoxP-Cre recombination (9), to generate three new HSV-1-based HAC vectors: pα40, pα60 and pα100, respectively.

Cell culture

The hESc lines HUES-2 and HUES-10 (10) were obtained from Douglas Melton (Harvard University, Cambridge, MA, USA) and grown under license from the UK Stem Cell Steering Committee as described previously (10,21), on mitomycin C-inactivated MEFs or SNL76/7 cells. Feeder-independent HUES-2 and HUES-10 cells were grown on Matrigel (BD Biosciences) coated wells using the mTeSR medium (STEMCELL Technologies). TrypLE Express (Invitrogen) was used to enzymatically passage the hESc. Cells were maintained and passaged at high densities on Matrigel. To increase single-cell survival, ROCK inhibitor Y-27632 (Merck Biosciences) was added during each passaging step, at a final concentration of 10 μM. The HT1080 (ATCC-CCL-121) cells were grown using standard techniques in Dulbecco's modified eagle medium (DMEM) medium (Invitrogen), supplemented with 10% foetal bovine serum (FBS) and 1% penicillin/streptomycin.

HSV-1 amplicon preparation

HSV-1 amplicons were prepared as described (9,22). Briefly, the packaging cell line Vero 2-2 was transfected with each input HAC vector DNA, fHSVΔpacΔ270 0+ and pEBHICP27 by Lipofectamine (Invitrogen) and Plus Reagent (Invitrogen). The cells were harvested, sonicated and then amplicons concentrated as described. The pellet was resuspended in 500 μl of phosphate buffered saline (PBS). The titre of the HSV-1 amplicon preparation was determined by transducing the glioma cell line G16-9 (9).

HSV-1 amplicon transduction

Transduction of HUES-2 (passage 40), HUES-10 (passage 29) and HT1080 cells with HSV-1 HAC amplicons was carried out as described (9,22). The HUES-2 and HUES-10 on Matrigel-coated plates, and the HT1080 cells were seeded at 2.5×10^5 cells per 24 well plates the day before transduction. On the day of transduction, HSV-1 HAC amplicons were inoculated at a MOI of 1, 2 or 5 in 250 μl of media (mTeSR or DMEM).

To improve the transduction efficiency, upon addition of the HSV-1 amplicons, the cells were centrifuged under low gravitational forces. The plates were covered with sterile adhesive films, to avoid aerosol escape during centrifugation, and centrifuged at 750*g* for 45 min (23). Transient expression was monitored at 24 h post-transduction either under the microscope or by flow cytometry. Three days after HSV-1 HAC transduction, the HUES-2 cells were transferred onto G418 resistant-inactivated MEF or SNL-76/7 cells. Two days later,

50 μg/ml of G418 (Invitrogen) was added as selection. After 7 days, individual hESc clones were observed and cells were removed from selection. The clones were allowed to grow for an extra 7 days, then each clone was isolated and expanded on inactivated MEF. Upon reaching confluency in a 24-well dish, the cells were transferred to feeder-free growing conditions on Matrigel and mTeSR. The HT1080 cells were selected with 350 μg/ml of G418.

EB formation and germ layer differentiation

For germ layer differentiation of each hESc line, $\sim 3 \times 10^7$ cells were used to form 192 uniform-sized EBs of size $\sim 1.5 \times 10^5$ cells/EB. The hESc were seeded in non-adherent 96-well V-Bottom plates (Nunc) in mTeSR and 10 μM ROCK inhibitor Y-27632. After 3 days, the EBs were released into suspension on non-adherent plates for 8–10 days in DMEM, 20% FBS. The EBs were then plated on Matrigel-coated plates and left to adhere and expand for a further 15–20 days.

Neuronal differentiation

Neuronal differentiation was carried out as described previously (13) with minor modifications. Uniform-sized EBs composed of ~4000 cells were formed using Aggrewell™400 plates (STEMCELL Technologies) as described by the manufacturer. After 2 days, the EBs were released and left in suspension in non-adherent plates for 5 days in DMEM F/12 (Invitrogen), 1% N2 supplement (Invitrogen), containing human plasma fibronectin (5 μg/ml) (Sigma) and recombinant human noggin (200 μg/ml) (RDI/Fitzgerald Industries). The EBs were then transferred onto Matrigel-coated plates under the same medium for further 8 days. Recombinant human bFGF (20 ng/ml) (BD Biosciences) was then added to the medium, and the cells were incubated for further 8–10 days for expansion of neuronal rosettes. Neuronal rosettes were lifted using TrypLE Express (Invitrogen) and plated on Matrigel-coated slides with the addition of ROCK Y-27632 inhibitor.

Teratoma formation assay

For the teratoma formation assay, 1×10^6 Matrigel-grown MM40.2 cells were injected subcutaneously into immunodeficient mice (common gamma-chain−/−, RAG2−/−, C5−/−). The mice were sacrificed between 5 and 7 weeks after injection and the teratoma was dissected and processed for haematoxylin/eosin staining and immunostaining with the following primary antibodies: anti-tubulin beta III isoform (Tuj1) (ectodermal derivatives), anti-alpha-actinin (mesodermal derivatives) and anti-alpha fetoprotein (endodermal derivatives) (all from Millipore).

Total genomic DNA was prepared from the teratoma mass by phenol/chloroform extraction. The HAC abundance was estimated by real-time qPCR analysis of the DNA, using the *GFP* and *GAPDH* primers listed in Supplementary Material, Table S2, with the kit SYBR Green Supermix IQ (Quanta Biosciences), on an ICycler (Bio-Rad) machine. The DNA relative amount was measured using the $2^{-\Delta\Delta Ct}$ method.

Fluorescence-activated cell sorting (FACS)

Cells were fixed in 4% formaldehyde in PBS. Samples were then run through a FACS Calibur and a minimum of 10 000 events was captured for each sample. Acquired data were analysed using FlowJo 7.6 software. The percentage of GFP-expressing cells was calculated by setting the gate at 0.5% for the negative control.

FISH and immuno-FISH

Chromosome preparation and FISH analyses were carried out as described previously (9,24,25). For each experiment, up to 40 metaphases were scored, and the number of HAC-containing cells was recorded. For HUES-2 karyotype analysis, metaphase spreads were subjected to FISH with whole chromosomes paint probes for chromosomes 12 and 17 (Aquarius Whole Chromosome Paint Probes, Cytocell), according to the manufacturer instructions. The HUES-10 karyotype was analysed on Affymetrix Cytogenetics Whole-Genome 2.7M Arrays, following the manufacturer instructions.

The binding of CENP C to chromosome metaphase spreads was carried out by immuno-FISH as previously described (9), using an anti-CENP C primary antibody.

Cytological preparations were analysed with an Olympus BX-51 epifluorescence microscope coupled to a JAI CVM4 + CCD camera, with CytoVysion software system (Genetix).

Immunofluorescence staining of fixed cells

Actively growing cells were fixed in 2% formaldehyde in PBS. After permeabilization in PBS, 0.1% Triton X-100 the following antibodies were used: mouse-anti-TRA-1-60 (Abcam); rabbit-anti-Oct4 (Abcam); rabbit-anti-Nanog (Abcam); rabbit-anti-Sox2 (Abcam); mouse-anti-βIII tubulin (R&D Systems), followed by TRITC-conjugated anti-rabbit or anti-mouse antibodies (Molecular Probes, Invitrogen).

The cells were analysed with a wide-field-inverted Nikon TE2000U fluorescence microscope. Images were acquired using the IPLab software, and pseudo-coloured using Adobe Photoshop.

RNA preparation and analysis

Total RNA was extracted from $\sim 6 \times 10^6$ cells using the RNeasy kit (Qiagen), following the manufacturer's instructions. The RNA was treated with DNase I (Qiagen) and reverse transcribed into cDNA, using the RETROScript system (Ambion), with random decamer primers. Gene expression levels were quantified by real-time qPCR analysis of the cDNA, using the *GFP* and *GAPDH* primers listed in Supplementary Material, Table S2, as described for the genomic DNA analysis. The RNA relative amount was measured using the $2^{-\Delta\Delta Ct}$ method.

SUPPLEMENTARY MATERIAL

Supplementary Material is available at *HMG* online.

ACKNOWLEDGEMENTS

We thank Richard Wade-Martins, Sara Ahmadi and Elizabeth Hartfield for invaluable technical advice, use of equipment and discussions. We also thank Cathy Browne for technical assistance with the hESc work. We are grateful to Ben Davies for providing the G418 resistant MEF, Allan Bradley for the SNL-76/7 feeder line and William Earnshaw for the kind gift of anti-CENP C antibody. Confocal images of teratoma sections were taken at the Confocal facility, UCL ICH.

Conflict of Interest statement. None declared.

FUNDING

This work was supported by the Wellcome Trust (075491/Z/04 to Z.L.M. and E.V.V., 082260/Z/07/Z to S.C., 090233/Z/09/Z to A.J.T. and M.P.B.); M.A.M. is a recipient of the PGSD NSERC and EPA Cephalosporin studentship; S.K. is a recipient of the Clarendon Fund/ Keble Sloane Robinson Scholarship; S.C. is a recipient of a Wellcome Career Re-entry Fellowship; D.Y.L.C. is funded by the Clarendon Fund and Oxford China Scholarship; S.M. is supported by a European Union grant (222878).

REFERENCES

1. Thomson, J.A., Itskovitz-Eldor, J., Shapiro, S.S., Waknitz, M.A., Swiergiel, J.J., Marshall, V.S. and Jones, J.M. (1998) Embryonic stem cell lines derived from human blastocysts. *Science*, **282**, 1145–1147.
2. Strulovici, Y., Leopold, P.L., O'Connor, T.P., Pergolizzi, R.G. and Crystal, R.G. (2007) Human embryonic stem cells and gene therapy. *Mol. Ther.*, **15**, 850–866.
3. Mátrai, J., Chuah, M.K. and VandenDriessche, T. (2010) Recent advances in lentiviral vector development and applications. *Mol. Ther.*, **18**, 477–490.
4. Giudice, A. and Trounson, A. (2008) Genetic modification of human embryonic stem cells for derivation of target cells. *Cell Stem Cell*, **2**, 422–433.
5. Gray, S.J. and Samulski, R.J. (2008) Optimizing gene delivery vectors for the treatment of heart disease. *Expert Opin. Biol. Ther.*, **8**, 911–922.
6. Baum, C. (2007) Insertional mutagenesis in gene therapy and stem cell biology. *Curr. Opin. Hematol.*, **14**, 337–342.
7. Wu, Z., Yang, H. and Colosi, P. (2010) Effect of genome size on AAV vector packaging. *Mol. Ther.*, **18**, 80–86.
8. Mejía, J.E., Willmott, A., Levy, E., Earnshaw, W.C. and Larin, Z. (2001) Functional complementation of a genetic deficiency with human artificial chromosomes. *Am. J. Hum. Genet.*, **69**, 315–326.
9. Moralli, D., Simpson, K.M., Wade-Martins, R. and Monaco, Z.L. (2006) A novel human artificial chromosome gene expression system using herpes simplex virus type 1 vectors. *EMBO Rep.*, **7**, 911–918.
10. Cowan, C.A., Klimanskaya, I., McMahon, J., Atienza, J., Witmyer, J., Zucker, J.P., Wang, S., Morton, C.C., McMahon, A.P., Powers, D. *et al.* (2004) Derivation of embryonic stem-cell lines from human blastocysts. *N. Engl. J. Med.*, **350**, 1353–1366.
11. Mejía, J.E., Alazami, A., Willmott, A., Marschall, P., Levy, E., Earnshaw, W.C. and Larin, Z. (2002) Efficiency of de novo centromere formation in human artificial chromosomes. *Genomics*, **79**, 297–304.
12. Rivero-Müller, A., Lajić, S. and Huhtaniemi, I. (2007) Assisted large fragment insertion by Red/ET-recombination (ALFIRE)—an alternative and enhanced method for large fragment recombineering. *Nucleic Acids Res.*, **35**, e78. doi:10.1093/nar/gkm250.
13. Iacovitti, L., Donaldson, A.E., Marshall, C.E., Suon, S. and Yang, M. (2007) A protocol for the differentiation of human embryonic stem cells into dopaminergic neurons using only chemically defined human additives: studies *in vitro* and *in vivo*. *Brain Res.*, **1127**, 19–25.
14. Nakano, M., Cardinale, S., Noskov, V.N., Gassmann, R., Vagnarelli, P., Kandels-Lewis, S., Larionov, V., Earnshaw, W.C. and Masumoto, H. (2008) Inactivation of a human kinetochore by specific targeting of chromatin modifiers. *Dev. Cell*, **14**, 507–522.
15. Spence, J.M., Mills, W., Mann, K., Huxley, C. and Farr, C.J. (2006) Increased missegregation and chromosome loss with decreasing chromosome size in vertebrate cells. *Chromosoma*, **115**, 60–74.
16. Deng, W. and Xu, Y. (2009) Genome integrity: linking pluripotency and tumorigenicity. *Trends Genet.*, **10**, 425–427.
17. Kazuki, Y., Hoshiya, H., Takiguchi, M., Abe, S., Iida, Y., Osaki, M., Katoh, M., Hiratsuka, M., Shirayoshi, Y., Hiramatsu, K. *et al.* (2010) Refined human artificial chromosome vectors for gene therapy and animal transgenesis. *Gene Ther.*, First published on 18 November 2010, doi:10.1038/gt.2010.147.
18. Iida, Y., Kim, J.H., Kazuki, Y., Hoshiya, H., Takiguchi, M., Hayashi, M., Erliandri, I., Lee, H.S., Samoshkin, A., Masumoto, H. *et al.* (2010) Human artificial chromosome with a conditional centromere for gene delivery and gene expression. *DNA Res.*, **17**, 293–301.
19. Saeki, Y., Breakefield, X.O. and Chiocca, E.A. (2003) Improved HSV-1 amplicon packaging system using ICP27-deleted, oversized HSV-1 BAC DNA. *Methods Mol. Med.*, **76**, 51–60.
20. Kim, U.J., Birren, B.W., Slepak, T., Mancino, V., Boysen, C., Kang, H.L., Simon, M.I. and Shizuya, H. (1996) Construction and characterization of a human bacterial artificial chromosome library. *Genomics*, **34**, 213–218.
21. Karlsson, K.R., Cowley, S., Martinez, F.O., Shaw, M., Minger, S.L. and James, W. (2008) Homogeneous monocytes and macrophages from human embryonic stem cells following coculture-free differentiation in m-csf and il-3. *Exp. Hematol.*, **36**, 1167–1175.
22. Wade-Martins, R., Smith, E.R., Tyminski, E., Chiocca, E.A. and Saeki, Y. (2001) An infectious transfer and expression system for genomic DNA loci in human and mouse cells. *Nat. Biotechnol.*, **19**, 1067–1070.
23. El-Sherbini, Y.M., Stevenson, M.M., Seymour, L.W. and Wade-Martins, R. (2009) Quantitative characterization of cell transduction by HSV-1 amplicons using flow cytometry and real-time PCR. *J. Virol. Methods*, **159**, 160–166.
24. Moralli, D. and Monaco, Z.L. (2009) Simultaneous detection of FISH signals and bromo-deoxyuridine incorporation in fixed tissue cultured cells. *PLoS ONE*, **4**, e4483. doi:10.1371/journal.pone.0004483.
25. Moralli, D., Yusuf, M., Mandegar, M.A., Khoja, S., Monaco, Z.L. and Volpi, E.V. (2010) An improved technique for chromosomal analysis of human ES and iPS cells. *Stem Cell Rev.*, First published on 29 December 2010. doi:10.1007/s12015-010-9224-4.

Stem Cell Rev and Rep (2011) 7:471–477
DOI 10.1007/s12015-010-9224-4

An Improved Technique for Chromosomal Analysis of Human ES and iPS Cells

Daniela Moralli · Mohammed Yusuf · Mohammad A. Mandegar · Suhail Khoja · Zoia L. Monaco · Emanuela V. Volpi

Published online: 29 December 2010

Abstract Prolonged in vitro culture of human embryonic stem (hES) cells can result in chromosomal abnormalities believed to confer a selective advantage. This potential occurrence has crucial implications for the appropriate use of hES cells for research and therapeutic purposes. In view of this, time-point karyotypic evaluation to assess genetic stability is recommended as a necessary control test to be carried out during extensive 'passaging'. Standard techniques currently used for the cytogenetic assessment of ES cells include G-banding and/or Fluorescence in situ Hybridization (FISH)-based protocols for karyotype analysis, including M-FISH and SKY. Critical for both banding and FISH techniques are the number and quality of metaphase spreads available for analysis at the microscope. Protocols for chromosome preparation from hES and human induced pluripotent stem (hiPS) cells published so far appear to differ considerably from one laboratory to another. Here we present an optimized technique, in which both the number and the quality of chromosome metaphase spreads were substantially improved when compared to current standard techniques for chromosome preparations. We believe our protocol represents a significant advancement in this line of work, and has the required attributes of simplicity and consistency to be widely accepted as a reference method for high quality, fast chromosomal analysis of human ES and iPS cells.

Keywords Human embryonic stem cells · Induced pluripotent stem cells · Chromosomal analysis · Fluorescence in situ hybridization · M-FISH

Introduction

A euploid karyotype is one of the defining characteristics of hES cells [1]. Once established, hES cell lines are expected to be chromosomally stable. However, karyotypic abnormalities of hES cells in long term cultures have been repeatedly reported by independent laboratories [2]. Some of the recurring abnormalities, for instance trisomy 12 and trisomy 17, appear to provide a selective advantage, with cells carrying such chromosomal extra copies being able to replace the cell population in 5–10 passages [3]. The duration of culture, conditions (presence or absence of feeders) and replace-by-passaging methods (mechanical versus enzymatic) have been pointed at as possible contributing factors to chromosomal changes in hES cells [4, 5]. However, recent evidence seems to support the notion that regardless of culture conditions, some hES cell lines are inherently more inclined to karyotypic instability [6]. To which extent differences in the chromosomal complement affect their ability to differentiate, as well as their proliferative capacity, is still being investigated [7, 8]. In the meantime, while establishing and/or maintaining hES cell lines, time-point karyotypic analysis is widely recommended as one of the important steps in the quality control process [3, 9–11]. There have been a few reports underscoring an increasing interest in the possible use of

Daniela Moralli and Mohammed Yusuf have contributed equally to this paper.

D. Moralli · M. Yusuf · M. A. Mandegar · S. Khoja · Z. L. Monaco · E. V. Volpi (✉)
Wellcome Trust Centre for Human Genetics,
University of Oxford,
Roosevelt Drive,
OX3 7BN Oxford, UK
e-mail: emanuela.volpi@well.ox.ac.uk
URL: http://www.well.ox.ac.uk/volpi

microarray-based techniques—such as Comparative Genomic Hybridization (CGH), single nucleotide polymorphism (SNP) analysis and transcriptional profiling—to monitor the chromosomal stability of hES and hiPS cells in culture [12–14]. However, classical and molecular cytogenetic protocols are still considered the default approach for routine karyotypic assessment. The analysis at the microscope that classical cytogenetic protocols—such as G-banding—entail is extremely laborious and requires highly specialized training. More modern and user-friendly Fluorescence in situ Hybridization (FISH)-based protocols for karyotyping, such as Multiplex FISH (M-FISH) and Spectral Karyotyping (SKY), or simple "target analysis" protocols to detect recurring aneuplodies by means of chromosome specific probes, provide a suitable alternative, and are increasingly used by different laboratories for in-house, rapid chromosomal assessment of ES cells. Crucial for both banding and FISH techniques are the number and quality of metaphase 'spreads' available for analysis at the microscope. Protocols for chromosome preparation (or 'harvesting') from hES cells published so far appear to vary considerably from one laboratory to another. In this paper we describe an optimized technique for chromosome preparation from hES and hiPS cells, in which both the number and the quality of metaphase spreads were substantially improved when compared to current standard techniques.

Materials

Cell Culture

1. hES cells or iPS cells
2. 1×Phosphate Buffered Saline (PBS)
3. Matrigel (BD, U.K.)
4. mTeSR™1 (STEMCELL Technologies Inc, France)
5. TrypLE Express 1× (Invitrogen, U.K.)
6. ROCK inhibitor Y-27632 (Merck Biosciences, Germany)
7. Penicillin at 10,000 units ml^{-1} and Streptomycin at 10 mg ml^{-1}
8. 6-well culture dish(es)
9. 15 ml conical centrifuge tubes
10. Access to a hemocytometer
11. Access to a Class II microbiological cabinet
12. Access to an incubator at 37°C with 5% CO_2
13. Access to an inverted microscope
14. Access to a bench-top centrifuge

Chromosome Harvest

1. Nocodazole (Sigma Aldrich, U.K., http://www.sigmaaldrich.com), 2.5 mg/ml stock solution in dimethyl sulfoxide, (DMSO) (Sigma Aldrich, U.K) (Note 1). Aliquot and store at −20°C
2. "Buffered" hypotonic solution (0.4% KCl with HEPES) (Genial Genetics, U.K., http://www.genialgenetics.com)
3. Carnoy's fixative solution: 3:1 (v/v) methanol/glacial acetic acid, freshly prepared
4. Pre-cleaned microscope slides (VWR International)
5. 1 mL disposable plastic Pasteur pipettes
6. Slide storage boxes (VWR International)
7. Access to a water-bath at 37°C
8. Access to a phase-contrast microscope with a 10× or 20× objective

Chromosome Quality Assessment

1. Vectashield mounting medium with 4′,6-diamidino-2-phenylindole (DAPI) (Vector Laboratories, UK)
2. 24XCyte mFISH probe kit (MetaSystems, Germany, http://www.metasystems-international.com)
3. Access to an epifluorescent light microscope with a 63× and/or a 100× oil immersion objective equipped with a charge-coupled device (CCD) camera and appropriate operating software for digital image capturing and analysis (e.g. CytoVysion system), consisting of an Olympus BX-51 epifluorescence microscope coupled to a JAI CVM4+ CCD camera (Genetix, U.K., http://www.genetix.com)

Methods

Cell Culture

1. Cells are grown in a feeder free system in a 6-well dish (Note 2).
2. Two days before the chromosome harvest procedure, remove the spent medium from a well of confluent cells.
3. Add 1 ml of sterile PBS, at 37°C, to wash the cells, and remove.
4. Add 0.5 ml of sterile TrypLE Express, warmed at 37°C. Place the dish in a 37°C incubator, for 5 min. Using an inverted microscope, confirm that all the cells have detached from the tissue culture dish.
5. Resuspend the cells in 10 ml of warm PBS, at 37°C, and transfer to a 15 ml conical centrifuge tube.
6. Count the cell number using a hemocytometer cell counter.
7. Centrifuge the cell suspension at 365 g for 10 min, and resuspend $1–2\times10^6$ cells in 2 ml of mTeSR™1 medium.
8. Add ROCK inhibitor Y-27632 to a final concentration of 10 μM, and plate on a fresh well, coated in Matrigel.
9. Place in the CO_2 thermostatic incubator.

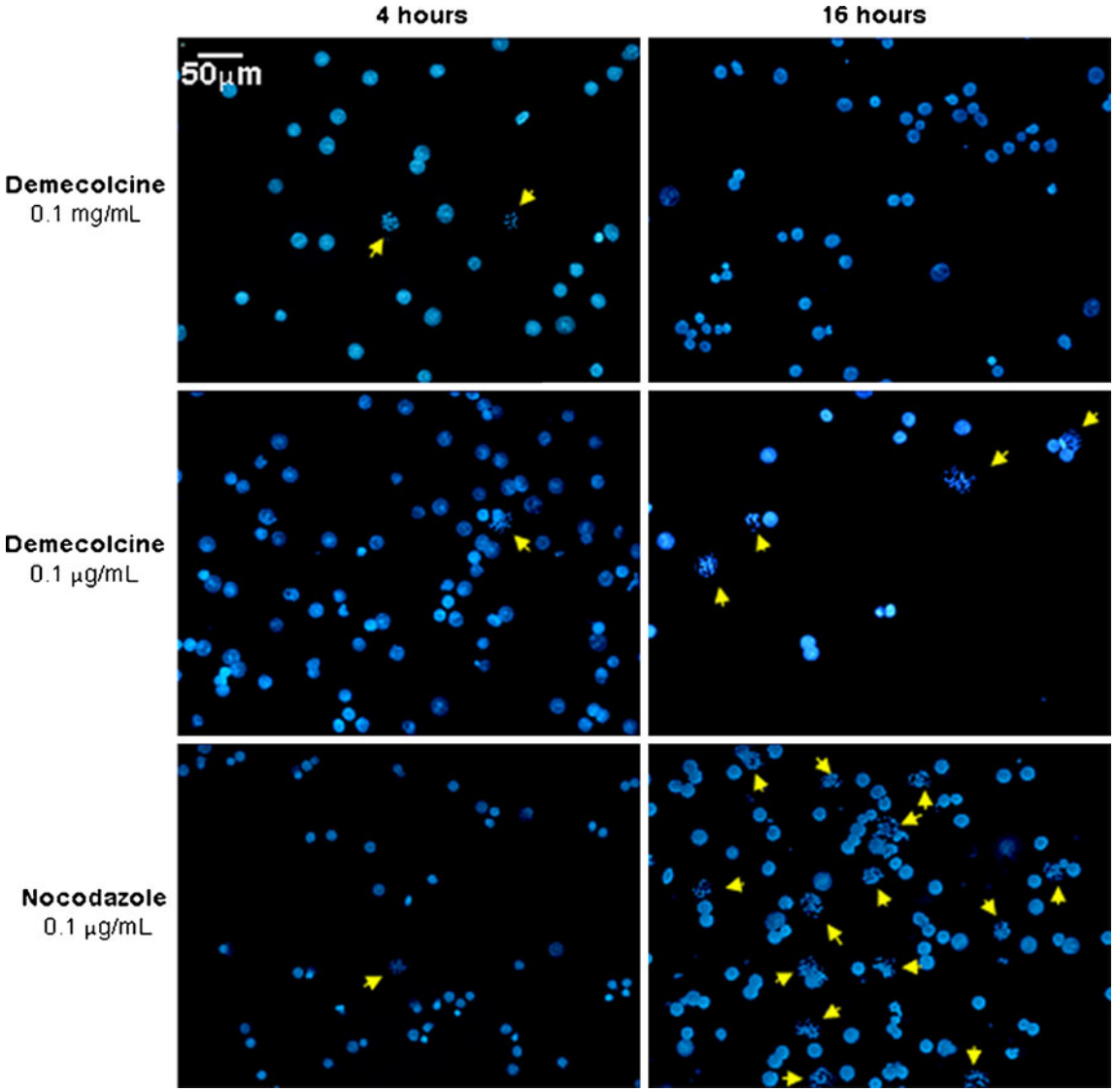

Fig. 1 Efficiency of mitotic arrest following treatment with either demecolcine or nocodazole. Different concentrations and incubation times were compared. After fixation the cells were stained with DAPI, and analyzed at the microscope. Ten random fields from each of the slides prepared under different conditions were captured with Genus on the CytoVision system. The yellow arrows identify metaphasic cells

Chromosome Harvest and Quality Assessment

1. The day after, change medium and add nocodazole at a final concentration of 0.1 µg/ml, and incubate for 16 h in the CO_2 thermostatic incubator (Note 3).
2. Following incubation with the mitotic synchronizing agent, trypsinize the cells as described above, collect

Table 1 Mitotic arrest efficacy

	Percentage of metaphase cells	Total number of cells scored
Demecolcine 0.1 mg/ml, 4 h	1.5%	471
Demecolcine 0.1 µg/ml, 4 h	0.5%	854
Demecolcine 0.1 mg/ml, 16 h	3.2%	279
Demecolcine 0.1 µg/ml, 16 h	8%	249
Nocodazole 0.1 µg/ml, 4 h	2.6%	1,254
Nocodazole 0.1 µg/ml, 16 h	15.2%	788

Table 2 Statistical comparisons of the differences between treatments (2×2 contingency table, analysed with Fisher exact test, 2-tailed)

	Demecolcine 0.1 μg/ml, 4 h	Demecolcine 0.1 mg/ml, 16 h	Demecolcine 0.1 μg/ml, 16 h	Nocodazole 0.1 μg/ml, 4 h	Nocodazole 0.1 μg/ml, 16 h
Demecolcine 0.1 mg/ml, 4 h	$p=0.062$	$p=0.1265$	$p<0.0001$	$p=0.2083$	$p<0.0001$
Demecolcine 0.1 μg/ml, 4 h		$p=0.0010$	$p<0.0001$	$p<0.0001$	$p<0.0001$
Demecolcine 0.1 mg/ml, 16 h			$p=0.0341$	$p=0.4163$	$p<0.0001$
Demecolcine 0.1 μg/ml, 16 h				$p=0.0003$	$p=0.0098$
Nocodazole 0.1 μg/ml, 4 h					$p<0.0001$

in the culture medium, and centrifuge at 365 g, for 10 min.

3. Remove the supernatant by pipetting it out of the tube, and fully resuspend the cell pellet by gently flicking the tube.
4. Add 5 ml of "Buffered" hypotonic solution (Notes 4 and 5), and pipette delicately the cell suspension, to evenly disperse the cells. Incubate for 30 min at 37°C.
5. Centrifuge the cells as before.
6. Gently resuspend the cell pellet, and quickly add about 500 μl of cold Carnoy's fixative solution.
7. Mix by pipetting, then bring the total volume up to 10 ml with fresh cold fixative. Incubate for 30 min at room temperature.
8. Centrifuge the cells as before and wash in fixative for a second time. Incubate for 10 min.
9. Following a final spin, resuspend the cell pellet in 200–300 μl of fresh fixative, and drop 30–50 μl of the cell suspensions onto clean slides.
10. Places the slides on a warm plate, 37°C, and allow to air-dry.
11. Check the cell suspension quality by observing the slide with a phase contrast microscope, 10× objective. There should be a good number of metaphases, and no cytoplasmic halo should be visible (Note 6).

Notes

1. It is important to use a very concentrated nocodazole stock solution, so that a minimal volume of DMSO is

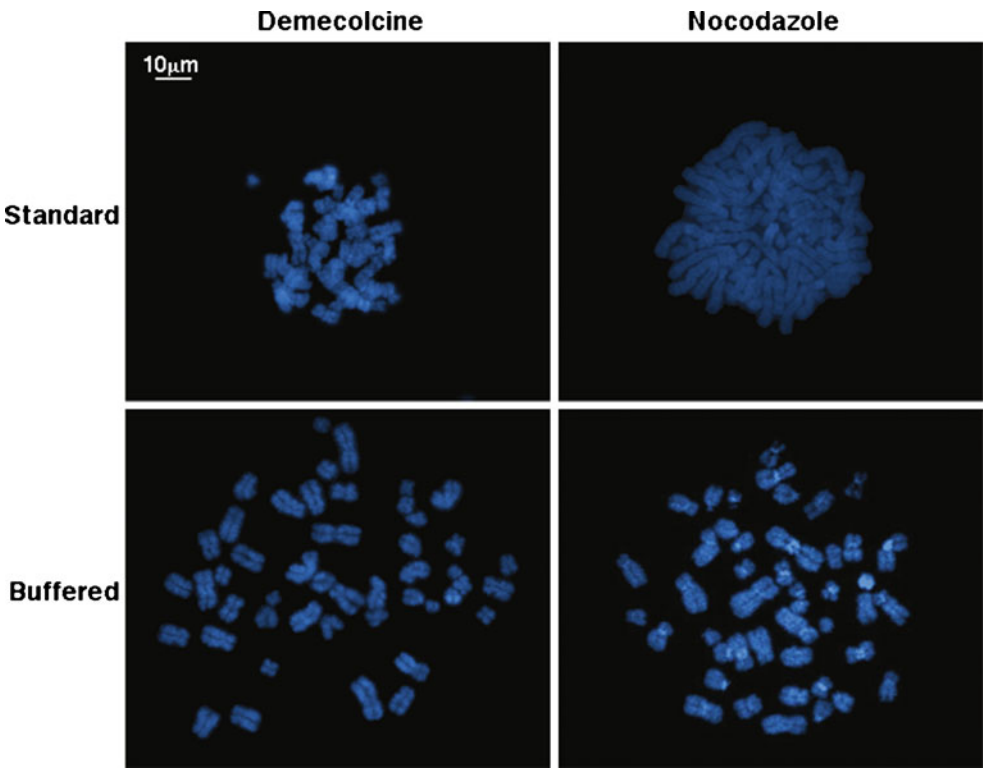

Fig. 2 Assessment of chromosome overlaps following different mitotic and hypotonic treatments. The number of chromosome overlaps per metaphase was compared in four different 'harvest' conditions. Where the metaphase quality was poor, we assigned an arbitrary number of 23 overlaps per metaphase, meaning that all the chromosomes were involved in at least one overlapping event

Table 3 Metaphase spread quality assessment: chromosome overlaps

	Mean number of chromosome overlaps/metaphase	Range of chromosome overlaps/metaphase	Standard deviation	Significance of the difference (*t*-student)
Nocodazole/standard hypotonic	12.8	5–23	5.988	$p<0.001$
Nocodazole/buffered hypotonic	4.8	0–16	4.5	
Demecolcine/standard hypotonic	12.6	4–23	6.3369	$p<0.001$
Demecolcine/buffered hypotonic	4.3	0–10	3.9636	

added to the cell culture, as an excess of DMSO might be toxic to the hES/hiPS cells. The stock solution may be diluted in PBS immediately prior to use, but discard any unused diluted material as nocodazole is not stable for prolonged periods when diluted in a water-based buffer.

2. For our study we used two human embryonic stem cell lines—HUES-2 and HUES-10 [15]—cultured under license from the UK Stem Cell Steering Committee—and one human induced pluripotent stem cell line—iPS-DF19-9-11T.H [16]—grown as in Karlsson et al. [17]. Briefly, cells were seeded onto wells coated with Matrigel and cultured in mTeSR™1 medium with the addition of 10 μM ROCK inhibitor Y-27632. The protocol for chromosome preparation here presented works equally well with hES and hiPS cells grown on a mouse embryonic fibroblasts (MEF) feeder layer.
3. Standard protocols for chromosome preparation in stem cells normally make use of Colcemid® (a synonym of demecolcine in solution), a well known and widely used mitotic spindle inhibitor. Oddly, concentrations of demecolcine used and published so far by different research groups appear to vary strikingly, the most frequently used concentration being either 0.1 μg/ml or 0.1 mg/ml. Accordingly, we set up parallel cultures of HUES-2 cells testing two different concentrations of demecolcine (0.1 μg/ml and 0.1 mg/ml), and compared them to HUES-2 cell cultures treated with nocodazole, an alternative anti-mitotic agent, at the final concentration of 0.1 μg/ml. The cultures were incubated with the mitotic agents for either 4 h or 16 h (effectively an overnight incubation). After fixation, the cells were stained with 4′,6-diamidino-2-phenylindole (DAPI), and analyzed at the microscope (Fig. 1). Ten random fields from each of the slides prepared under different conditions were collected. The efficacy of the mitotic arrest treatment was assessed dividing the total number of metaphases observed by the total number of cells analyzed (Tables 1 and 2). The statistical significance of the differences between the various treatments was measured using a 2×2 contingency table, with Fisher exact test. Comparison between the cultures revealed a sustained incubation (16 h) with a low dose of nocodazole (0.1 μg/ml) as the optimal mitotic arrest treatment able to provide the highest yield of metaphases (15.2%). A sustained incubation (16 h) with a low dose of demecolcine (0.1 μg/ml) provided the second highest yield of metaphases (8%).
4. With the aim of optimizing the quality of metaphase spreading, we tested two different hypotonic treatments. We set as first parameter for our quality analysis the average number of chromosome overlaps per metaphase. A high number of overlaps makes chromosome identification laborious and can ultimately hinder high-quality karyotypic analysis. The average number of chromosome overlaps was measured and compared in HUES-2 cells treated with either demecolcine or nocodazole, both at 0.1 μg/ml for 16 h, and harvested with either a standard hypotonic solution (0.075 M KCl) or a buffered hypotonic solution (0.4% KCl with

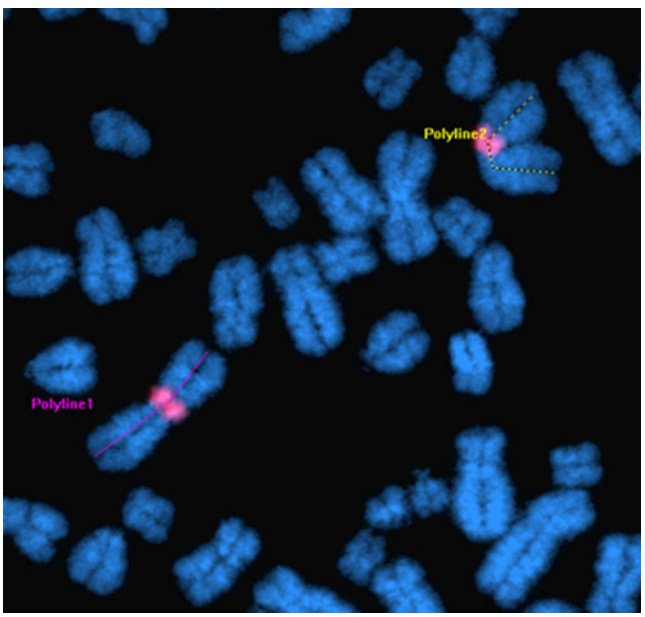

Fig. 3 Chromosome length as a parameter for metaphase spread quality for karyotype analysis. The average length of chromosome 1 (here with the centromeric region marked in red) was measured using the image analysis package MetaMorph v7.6 (example above), and compared between the nocodazole 16 h/buffered hypotonic harvest and the demecolcine 16 h/buffered hypotonic harvest

HEPES), obtained commercially. We randomly acquired and analyzed twenty-five metaphases from each of the four different harvesting conditions (Fig. 2). We initially scored the number of overlaps between chromosomes per metaphase (Table 3). In some cases, where the metaphase quality was poor and it was impossible to distinguish individual chromosomes, we assigned an arbitrary maximum overlap number of 23, meaning that all the chromosomes were involved in at least one overlapping event. When the different harvests were compared, the number of overlaps in chromosomes harvested with the buffered hypotonic solution—following either nocodazole or demecolcine treatment—was significantly lower than in chromosomes harvested with the standard hypotonic solution ($p<0.001$, Student's *T*-test for independent samples). In contrast, neither the difference between nocodazole and demecolcine harvests after buffered hypotonic ($p=0.335$) nor the difference between nocodazole and demecolcine harvests after standard hypotonic ($p=0.47$) was significant. The pH of the cell preparations resuspended in the standard hypotonic solution was slightly acidic (pH 6.5–6.7), similar to the pH of the spent tissue culture medium, while the buffered hypotonic solution maintained a pH of 7.4. The chromosome suspensions obtained by "acidified" KCl were consistently of poor quality, in comparison to the preparation obtained with the buffered hypotonic treatment. However, the addition of a PBS wash, before resuspending the cells in hypotonic, lead to a slight improvement in the KCl-prepared metaphase quality, but decreased their overall number.

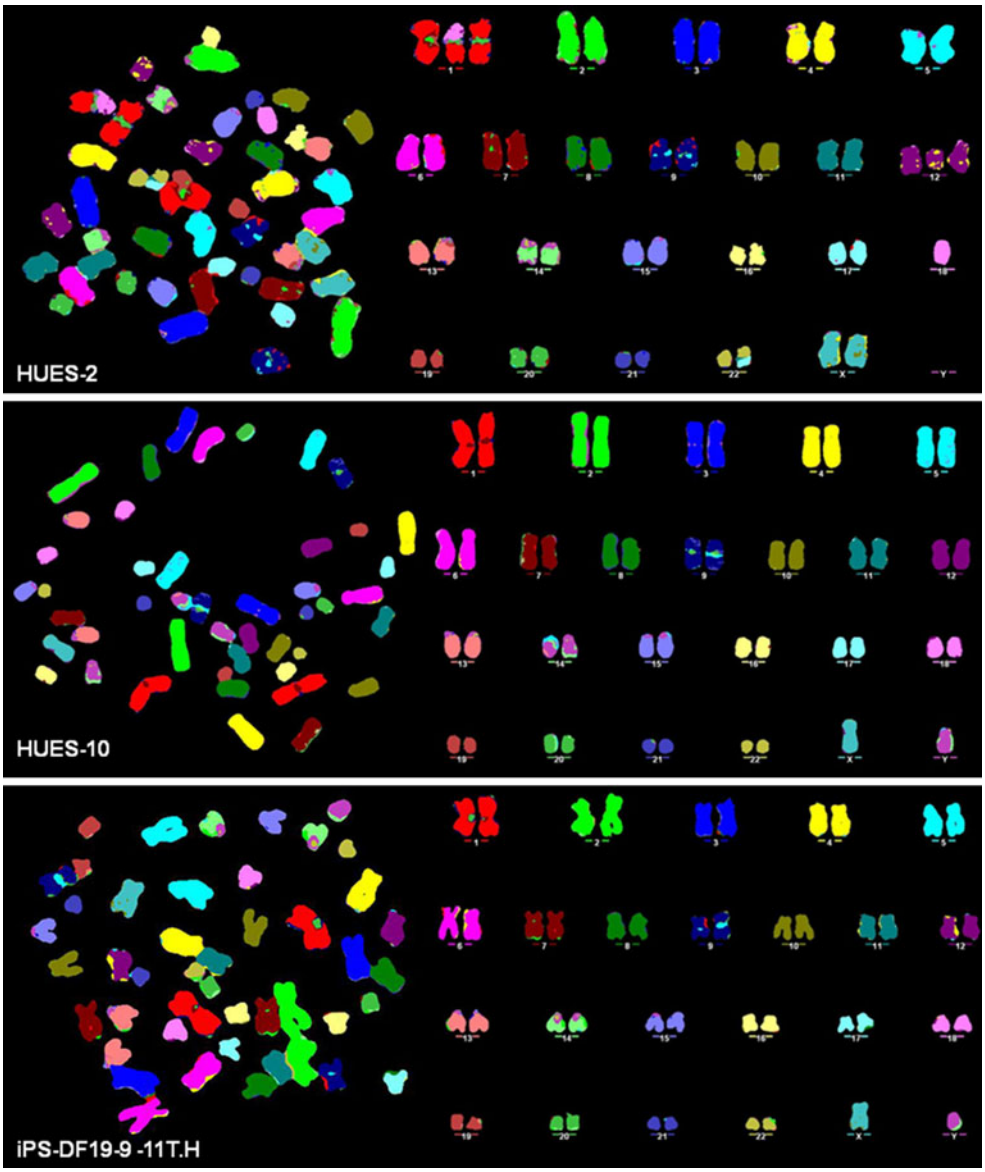

Fig. 4 Twenty-four color karyotyping of hES cells (HUES-2 and HUES-10) and iPS-DF19-9-11T.H by M-FISH. The high standard and improved speed of the M-FISH analysis have together confirmed the newly identified optimal mitotic arrest and hypotonic conditions to provide a significant technical breakthrough for chromosomal analysis of hES and hiPS cells. While HUES-10 (passage 37) and iPS-DF19-9-11T.H (passage 29) presented a normal karyotype, M-FISH analysis on HUES-2 at passage 40 revealed, as well as chromosome 12 partial trisomy, a couple of structural abnormalities to include a translocation involving an extra copy of chromosome 1q and chromosome 18, and an unbalanced translocation involving chromosomes 17 and 22

5. The average chromosome length was set as the second parameter for metaphase spread quality. Increased chromosome length means improved chromosomal morphology and, most importantly, improved longitudinal resolution for karyotyping purposes. For our analysis we chose chromosome 1—the longest chromosome—to reduce the% error during measurements. The length of the two chromosome 1 homologues was measured in μm using the image analysis package MetaMorph v7.6 (Molecular Devices Inc, Danaher Corporation, U.S.A.) in twenty-five randomly captured metaphases from chromosome harvests prepared using the buffered hypotonic, which had given the best results in the previous assay (Fig. 3). The average length of chromosome 1 in the demecolcine 16 h/buffered hypotonic harvest was found to be 20% lower than the average length of chromosome 1 in the nocodazole 16 h/buffered hypotonic solution harvest (Student *t*-test for independent samples showing a two tailed *p* value of 0.01).
6. Having established—on the basis of the number and quality of metaphase spreads recovered- the '0.1 μg/ml nocodazole 16 h/buffered hypotonic solution' to be the best protocol combination for chromosome harvests of hES cells, we proceeded to further confirm its suitability for FISH-based karyotyping techniques by analyzing by M-FISH chromosome spreads obtained from the three different cell lines used in this study, namely HUES-2 (passage 40), HUES-10 (passage 37) and iPS-DF19-9-11T.H (passage 29) (Fig. 4). M-FISH was performed as recommended by the 24XCyte mFISH probe kit manufacturer. The high standard and improved speed of the M-FISH analysis together confirmed the newly identified mitotic arrest and hypotonic conditions as optimal.

Acknowledgements We thank Prof. William James and Dr. Sally Cowley (William Dunn School of Pathology, University of Oxford) for their assistance in setting up the hESc cultures, and the kind gift of the HUES-2 cells. We also thank Dr. Keith Morris (Molecular Cytogenetics and Microscopy Core, Wellcome Trust Centre for Human Genetics) for help with chromosome measurements. M.A.M is a recipient of the PGSD NSERC and EPA Cephalosporin studentships. S.K is a recipient of the Clarendon Fund/Keble Sloane Robinson Scholarship. This work was supported by The Wellcome Trust [075491/Z/04].

Conflict of interest The authors declare no potential conflicts of interest.

References

1. Hoffman, L. M., & Carpenter, M. K. (2005). Characterization and culture of human embryonic stem cells. *Nature Biotechnology, 23*, 699–708.
2. Baker, D. E., Harrison, N. J., Maltby, E., Smith, K., Moore, H. D., et al. (2007). Adaptation to culture of human embryonic stem cells and oncogenesis in vivo. *Nature Biotechnology, 25*, 207–215.
3. Meisner, L. F., & Johnson, J. A. (2008). Protocols for cytogenetic studies of human embryonic stem cells. *Methods, 45*, 133–141.
4. Caisander, G., Park, H., Frej, K., Lindqvist, J., Bergh, C., et al. (2006). Chromosomal integrity maintained in five human embryonic stem cell lines after prolonged in vitro culture. *Chromosome Research, 14*, 131–137.
5. Grandela, C., & Wolvetang, E. (2007). hESC adaptation, selection and stability. *Stem Cell Reviews, 3*, 183–191.
6. Catalina, P., Montes, R., Ligero, G., Sanchez, L., de la Cueva, T., et al. (2008). Human ESCs predisposition to karyotypic instability: is a matter of culture adaptation or differential vulnerability among hESC lines due to inherent properties? *Molecular Cancer, 7*, 76.
7. Yang, S., Lin, G., Tan, Y. Q., Deng, L. Y., Yuan, D., et al. (2010). Differences between karyotypically normal and abnormal human embryonic stem cells. *Cell Proliferation, 43*, 195–206.
8. Imreh, M. P., Gertow, K., Cedervall, J., Unger, C., Holmberg, K., et al. (2006). In vitro culture conditions favoring selection of chromosomal abnormalities in human ES cells. *Journal of Cellular Biochemistry, 99*, 508–516.
9. The International Stem Cell Banking Initiative. (2009). Consensus guidance for banking and supply of human embryonic stem cell lines for research purposes. *Stem Cell Reviews, 5*, 301–314.
10. Catalina, P., Cobo, F., Cortes, J. L., Nieto, A. I., Cabrera, C., et al. (2007). Conventional and molecular cytogenetic diagnostic methods in stem cell research: a concise review. *Cell Biology International, 31*, 861–869.
11. Nieto, A., Cobo, F., Barroso-Deljesus, A., Barnie, A. H., Catalina, P., et al. (2006). Embryonic stem cell bank: a work proposal. *Stem Cell Reviews, 2*, 117–126.
12. Elliott, A. M., Hohenstein Elliott, K. A., & Kammesheidt, A. (2010). High resolution array-CGH characterization of human stem cells using a stem cell focused microarray. *Molecular Biotechnology, 46*, 234–242.
13. Narva, E., Autio, R., Rahkonen, N., Kong, L., Harrison, N., et al. (2010). High-resolution DNA analysis of human embryonic stem cell lines reveals culture-induced copy number changes and loss of heterozygosity. *Nature Biotechnology, 28*, 371–377.
14. Mayshar, Y., Ben-David, U., Lavon, N., Biancotti, J. C., Yakir, B., et al. (2010). Identification and classification of chromosomal aberrations in human induced pluripotent stem cells. *Cell Stem Cell, 7*, 521–531.
15. Cowan, C. A., Klimanskaya, I., McMahon, J., Atienza, J., Witmyer, J., et al. (2004). Derivation of embryonic stem-cell lines from human blastocysts. *The New England Journal of Medicine, 350*, 1353–1356.
16. Yu, J., Hu, K., Smuga-Otto, K., Tian, S., Stewart, R., et al. (2009). Human induced pluripotent stem cells free of vector and transgene sequences. *Science, 324*, 797–801.
17. Karlsson, K. R., Cowley, S., Martinez, F. O., Shaw, M., Minger, S. L., et al. (2008). Homogeneous monocytes and macrophages from human embryonic stem cells following coculture-free differentiation in M-CSF and IL-3. *Experimental Hematology, 36*, 1167–1175.